ALMA MATER STUDIORUM – UNIVERSITÀ DI BOLOGNA

DIPARTIMENTO DI INGEGNERIA DELL'ENERGIA ELETTRICA
E DELL'INFORMAZIONE "GUGLIELMO MARCONI" – DEI

DOTTORATO DI RICERCA IN INGEGNERIA ELETTROTECNICA
XXIX ciclo

Settore Concorsuale: 09/E1
Settore Scientifico disciplinare: ING-IND/31

MATHEMATICAL APPROACH FOR AN ACCURATE SOLUTION OF THE CIRCUIT MODEL OF RESONATOR ARRAYS FOR INDUCTIVE POWER TRANSFER

Presentata da:
José Miguel Mamede Albuquerque Vieira Alberto

Coordinatore:
Prof. Domenico Casadei

Relatore:
Dr. Ing. Leonardo Sandrolini

Esame finale anno 2017

It always seems impossible until it’s done.” – Nelson Mandela

Acknowledgments

This entire thesis could not be possible without the support of my supervisor, Prof. Leonardo Sandrolini, who guided me through this thesis, assisting me with his help and providing me with the best work conditions so that I could develop my thesis at the University of Bologna. Also, I would like to thank my co-supervisors Prof. Ugo Reggiani, who through his advice made my work more scientifically accurate and Prof. Gabriele Grandi, for his help with the construction of the power inverter.

I would like to thank all my colleagues at the University of Bologna during these three years, specially Giovanni Pucetti, for transmitting me his passion for wireless power and giving me material to develop for my thesis, and my colleagues of "Office 32". Also, my deepest thanks to Fabiola, for simply standing by my side during these three years and thanks to all the amazing people I found during my stay in Bologna, especially my flatmates who always made me feel at home. Also I do not forget my old friends, who even at a distance made their presence and support felt.

Finally a very special appreciation to my mother for her precious guidance, helping me find the way when I was lost and for believing in me even when I didn't, and to my father for giving all his support by helping me write this thesis and always being available for any question.

Contents

List of Figures

List of Tables

1 Introduction

1.1 Inductive power transfer

Despite that wireless power transfer technologies are under intensive research lately, the idea of transmitting energy wirelessly was initially explored by Nikola Tesla in the beginning of the 20th century [6, 7]. Wireless power transfer (WPT) systems can be divided mainly in two categories: far-field (radiative) and near-field (non-radiative) systems. Far-field WPT or microwave power transfer (MPT) usually refers to systems that are capable to transmit power over long distances (up to tens of kms) and operate at frequencies from 1 to 300 GHz. On the other hand, near-field WPT systems use inductive coupling to transfer power through distances from from a few mm [8] to a few meters [9] and usually operate at frequencies from tens of kHz [2] up to a few MHz [10]. The amount of power transmitted by these WPT systems is in the range of a few mW [8] to tens of kW [2], depending on the type of applications. In fact, the reason why these inductive power transfer (IPT) systems have gained popularity recently is due to their wide range of applications: they can be used to power biomedical devices [8], charge small electronic devices [11] or large electrical vehicles [2]. Moreover, these systems have the advantage of being capable of transferring power even in harsh environments with water, dust or dirt and allow the bypass of electrical contact.

A typical IPT system, as described in [1] and depicted in Fig. 1.1, is composed of a power source, usually a power converter that picks power from the grid and converts it into a high frequency current (usually from tens to hundreds of kHz) that feeds the emitter (track) coil. The magnetic time varying near field produced by the emitter coil is then picked up by the receiver (pickup) coil and the current induced in the pickup coil can be used to feed a load and, if needed, converted to DC or to another frequency. Moreover, the emitter and receiver coils are compensated and tuned to a certain resonant frequency. The type of compensation depends on whether the resonance of the RLC circuit of the emitter and receiver coils is a parallel or series one, as shown in Fig. 1.2.

1.2 Resonator arrays

Usually, one of the drawbacks of these systems is that in situations of misalignment or large distances between the emitter and receiver coils, the efficiency and the power transmitted to the receiver drop abruptly. Larger distances between the transmitter and receiver were achieved for wireless power transfer using strongly coupled resonances as in [9], where a transmission distance of 2m is achieved using a system of four coils, with the transmitter and receiver coils in self-resonance; however, the efficiency is low (about 15% [12]). Besides using strongly coupled resonances, another method to transfer power over long distances or with significant misalignment of the emitter and receiver coils is the utilization of arrays of resonators. These arrays of

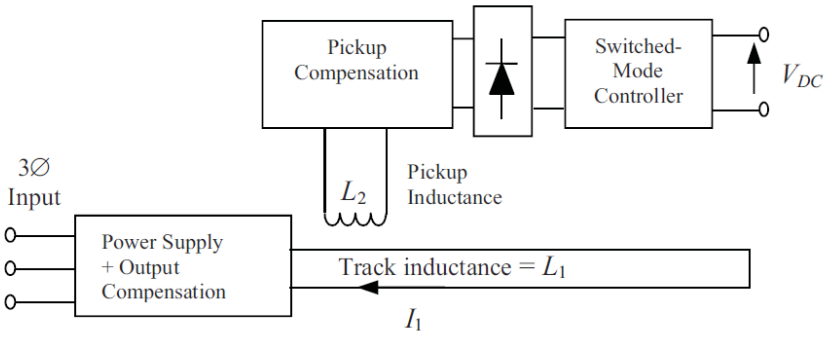

Figure 1.1: Example of a typical IPT system [1].

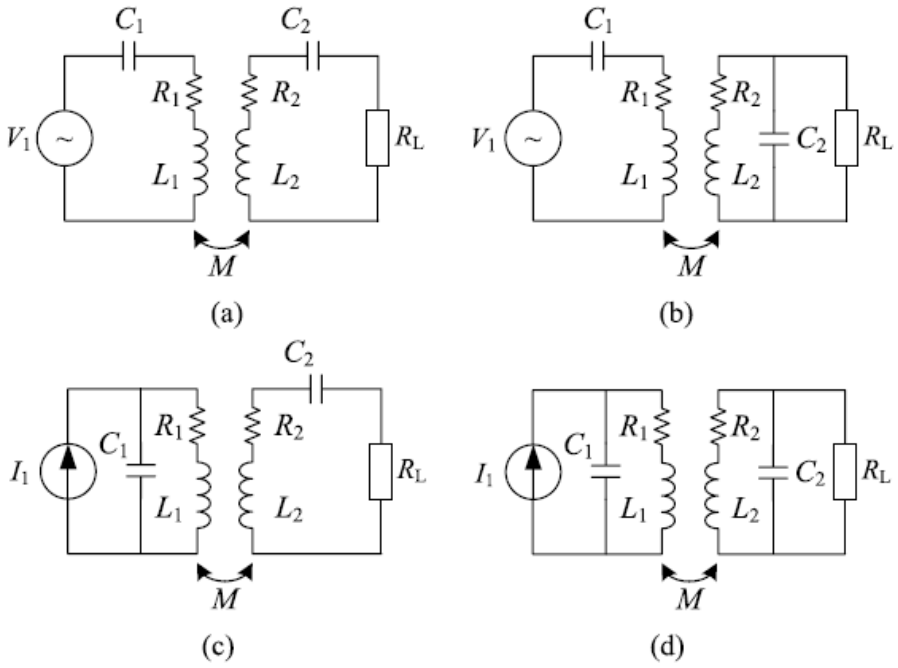

Figure 1.2: Four types of compensation for the transmitter and receiver coils depending on the type of resonance of the RLC circuit of each inductor: (a) Series-Series, (b) Series-Parallel, (c) Parallel-Series and (d) Parallel-Parallel [2].

(a) (b)

Figure 1.3: Example of two types of 1D resonator arrays: (a) domino resonator array with a load at then end of the array [3] and (b) a planar resonator array with a receiver over the array.

resonators can be placed along one direction arranged in a line (1D) [3, 13–16] or over a plane in two directions (2D) [17, 18].

Regarding the 1D resonator arrays, we can have two types of arrays depending on the orientation of the resonators: we can place the resonators facing each other with their axes aligned, referred in literature as domino resonators ([3, 13, 15], Fig. 1.3 (a)), that can transfer power to a load at the end of the array, or they can be placed in a plane with their axes parallel as in [14, 16, 19], where the power can be transferred to a receiver coil that is over the array, as shown in Fig. 1.3 (b).

Many works in literature use magnetoinductive wave theory to study and analyse resonator arrays, that are seen as metamaterials [16, 20, 21]. Magnetoinductive wave theory considers resonator arrays as transmission lines and by analysing the reflected and traveling waves propagating through the array and the matching of the resonator array, it is possible to study the power delivered to a receiver over the array or the efficiency of the system [14]. However, this type of analysis, despite being scientifically accurate, fails to give a full understanding of the behaviour of a system composed of an array of magnetically coupled resonators, specially for varying conditions of the system, as for example different operating frequencies, position of the receiver, multiple receivers or value of the termination impedance.

Eventually, a way to perform an accurate study on the power transferred by an array of resonators and its performance with the variation of the parameters of the array, could be to carry out a circuit analysis of the equivalent circuit of the array, as done in [3, 15]. Nevertheless, numerical analyses on the equivalent circuit of a resonator array refers to particular situations and case studies, not allowing one to make generalizations for different types of arrays, parameters of the system or operating conditions.

For these reasons, in this thesis an analytical and general study is conducted on the equivalent circuit model of a resonator array. In this way, it is possible to have a broad understanding of these systems, by predicting their behaviour with the variation of their parameters or operating conditions, even for different types of resonator arrays. Moreover, with this analysis it is possible to develop closed-form expressions for the equivalent impedance of an array of resonators and for the current in each resonator of the array. These expressions allow one to quickly obtain the power transfer characteristics of the array for varying conditions and therefore can be a useful tool to design this type of arrays. Thus, after the present introductive chapter, it is presented the

mathematical approach based on the theory of the linear homogeneous difference equations used to obtain the general term of the recursive sequence representing the continued fraction that defines the equivalent impedance of a resonator array. Afterwards, in the third chapter of this thesis, a mathematical analysis is performed on the impedance matrix that represents the equivalent circuit of the array, by analysing the inverse of a tridiagonal matrix with one or two different elements of the diagonal. This analysis allows the currents in each resonator to be obtained as closed form expressions, which can then be used to calculate the power delivered to a load (or to one or two receivers over the array) and the efficiency of the system. Then, in the following chapter a study of the variation of the magnetic near field generated by an array of resonators with respect to the termination impedance is carried out with simulations executed using a finite-element software and measurements made with a circular probe. Furthermore, in the fifth chapter, the experimental setup used to verify the theoretical and numerical results obtained in the precedent chapters is described, along with its construction and design. Finally, the thesis is concluded commenting the main results and outlining not only the original contribution of this thesis but also the potential future work that can be further carried out.

1.3 Aim of the thesis

The aim of this thesis is the improvement of the performance of an IPT system composed of an array of magnetically coupled resonators. This is achieved through the development of a mathematical approach for the study of the circuit model of resonator arrays, that allows analytical expressions for the equivalent impedance and for the currents in the resonators to be obtained. With this approach it is possible to achieve a wide understanding of the power transfer behaviour for different types of array, different parameters and operating conditions. More specifically, with this approach, for an array of resonators with given electrical parameters, it is possible to find the conditions of the system which give maximum efficiency or maximum power transfer to a load, or to one or two receivers.

Moreover, among the aims of this thesis there was the fabrication of an IPT system composed of an array of stranded-wire resonators fed by a power inverter operating at a frequency around hundred kHz and capable of delivering 100W to a load. Nevertheless, this IPT system was used to validate all the theoretical results obtained throughout this thesis, thus showing a practical application for the developed expressions and the possible utilization of resonator arrays with power converters which have higher power transfer capability.

2 Mathematical modelling of the equivalent impedance of an array of resonators

2.1 Introduction

Resonator arrays can be modeled using a circuital approach as in [3, 14, 22, 23]. The circuit that describes a resonator array can be simplified by representing all the resonators of the array after the one connected to the voltage source (and possible receivers sliding over the array) by an equivalent impedance, as seen in [14].

The equivalent impedance of a resonator array can be described by a continued fraction ([14, 16]). Several types of continued fractions [24] are applied in a variety of branches of engineering and applied sciences, as in [25, 26]. It is possible to determine numerically the value of the continued fraction by using a computing environment, for given conditions of the system. However, a closed-form expression for the equivalent impedance of the resonator array has not been given yet; it is simply acknowledged that an analytical study of this fraction seems not to be possible [16].

By representing the continued fraction as a term of a complex sequence defined by recurrence, it is possible to develop a closed-form expression of the equivalent impedance of the resonator array for any condition of the system. This closed-form expression is found by determining the general term of the recursive sequence using the theory of linear homogeneous equations. Moreover, with the obtained analytical expressions it is also possible to analyse the convergence and monotonicity of the continuous fraction. In this way, we can achieve a better insight of the behaviour of the system with respect to the variation of its geometrical and electrical parameters. In fact, the study of the equivalent impedance allows one to analyse the power delivered by the source to the array terminated in a load or facing a receiver. In addition, it allows one to examine a possible matching of the source to the input impedance of the loaded resonator array.

Furthermore, the developed formulas can be useful for the design of the array and its power source as they allow one to determine the equivalent impedance for several conditions of the system (different circuit parameters, number of resonators, number of perturbations) and predict the behaviour of the system with the variation of its parameters (for example: change of termination impedance, change of impedance or position of the receiver). Therefore, with the closed-form expressions designers can save time and increase the calculation accuracy compared with using a numerical or electromagnetic simulation software.

In this chapter, after a short description of the examined circuit in section 2.2, a mathematical study on the continued fraction is performed by developing a closed-form expression and studying

its convergence in section 2.3. After, in section 2.4, the results obtained with the mathematical approach are then applied to the circuit of a resonator array and then several examples are made in order to illustrate the theoretical results and show possible applications of the closed-form expressions. The examples, carried out with the computing environment MATLAB, for different parameters of the system, concern the equivalent impedance of an array with no receiver over it, one or two receivers and also in the case that the resonator is connected to the source in series or in parallel resonance. In section 2.5, a verification of the theoretical results is accomplished with the simulation software Simulink. Finally in the last section, an experimental validation of the closed-form expressions is achieved using the experimental setup described in Chapter 5 and an example of practical application of the expressions is made regarding the variation of the input power with the variation of the equivalent impedance of the resonator array.

2.2 Description of the circuit - representation of the equivalent impedance as a continued fraction

In this chapter we perform an analysis on the circuit of a system that consists of an array of $n+1$ identical resonators (cells) as represented in Fig. 2.1. Each cell can be described as an R-L-C series circuit [27], with R representing the intrinsic resistance of the resonator cell, L its self-inductance and C the additional capacitance needed to tune the resonant frequency of the cell, given by $f_0 = 1/(2\pi\sqrt{LC})$. Considering that the impedance of each cell is given by $\hat{Z} = R + j\omega L + 1/(j\omega C)$ (being $\omega = 2\pi f$ the angular frequency), at the resonant angular frequency $\omega_0 = 2\pi f_0 = 1/\sqrt{LC}$, the impedance of each cell is equal to its intrinsic resistance R. Moreover, as seen in Fig. 2.1, each two adjacent resonators are spaced by the same constant distance and are magnetically coupled with a mutual inductance M, whereas the coupling between nonadjacent resonators is neglected. This assumption is commonly considered for planar arrays of resonators [14, 16, 23] and also for domino resonator arrays, for a certain distance between the resonators [3, 22]. Furthermore, the good agreement between the theoretical and experimental results shown later in this chapter confirms the validity of this assumption. Finally, the $(n+1)$th cell of the array of resonators is connected to a source of voltage $\hat{V}_s$ with an internal resistance R_s and a termination impedance $\hat{Z}_T$ is connected to the first cell of the array. Note that the cells counting is done from the cell connected to the termination impedance to the cell connected to the voltage source. This is done so that the mathematical analysis presented in the next section used to solve the continued fraction and obtain a closed-form expression can be performed.

In the case when there is a receiver above the line, more specifically above the ith cell of the array, with $1 \leq i \leq n$, as shown in Fig. 2.1(a), the receiver will cause a perturbation on the system. This perturbation, caused by the magnetic coupling between the receiver and the ith cell of the resonator array, can be represented by an impedance $\hat{Z}_d$, which is added to the ith cell of the array, as represented in Fig. 2.1(b). The impedance $\hat{Z}_d$ is the impedance of the receiver seen from the ith cell which is below the receiver. Assuming that the receiver has the same resonant frequency as the cells of the array, we can assume that $\hat{Z}_d = R_d$ is real, when working at the resonant frequency f_0.

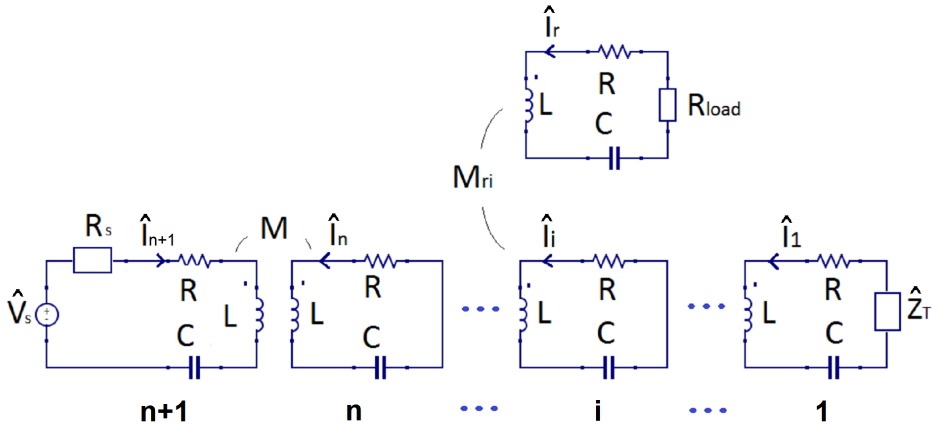

(a)

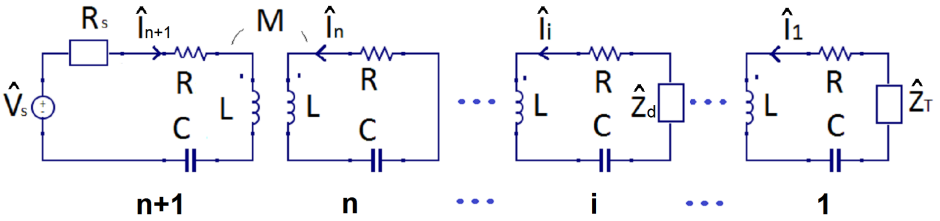

(b)

Figure 2.1: Equivalent circuits of (a) a system composed of $n+1$ cells with a receiver over the ith cell and (b) the same system with the impedance $\hat{Z}_d$ representing the receiver inserted in the ith cell.

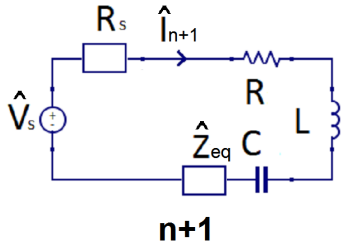

Figure 2.2: Equivalent circuit for the system in Figure 1 with an impedance $\hat{Z}_{eq}$ representing the resonator array (excluding the resonator connected to the source) and the receiver.

The multiple resonator system can be further simplified by introducing an equivalent impedance $\hat{Z}_{eq}$ that represents the impedance of all the resonators after the supplied one and the receivers (if any) connected in series to the impedance of this cell, as depicted in Fig. 2.2. As seen in [14, 16, 22], the equivalent impedance $\hat{Z}_{eq}$ of the nth cells after the one connected to the source, can be represented by a continued fraction and written as:

$$\hat{Z}_{eq} = \cfrac{(\omega M)^2}{\hat{Z} + \cfrac{(\omega M)^2}{\cdots + \cfrac{(\omega M)^2}{\hat{Z} + \cfrac{(\omega M)^2}{\hat{Z} + \hat{Z}'_T}}}} \tag{2.1}$$

with $\hat{Z}'_T = \hat{Z}_T + \hat{Z}_d$ if the receiver is placed above the first cell of the resonator array or with $\hat{Z}'_T = \hat{Z}_T$ in the case there is no receiver.

When the receiver coil is placed above any other cell of the resonator array, the impedance $\hat{Z}_d$ is introduced in the expression of $\hat{Z}_{eq}$ and $\hat{Z}'_T = \hat{Z}_T$:

$$\hat{Z}_{eq} = \cfrac{(\omega M)^2}{\hat{Z} + \cfrac{(\omega M)^2}{\cdots + \cfrac{(\omega M)^2}{\hat{Z}_d + \hat{Z} + \cfrac{(\omega M)^2}{\hat{Z} + \cfrac{(\omega M)^2}{\cdots + \cfrac{(\omega M)^2}{\hat{Z} + \cfrac{(\omega M)^2}{\hat{Z} + \hat{Z}_T}}}}}}}. \tag{2.2}$$

For example, when the receiver is on the $(n-1)$ cell, $\hat{Z}_{eq}$ becomes

$$\hat{Z}_{eq} = \cfrac{(\omega M)^2}{\hat{Z} + \cfrac{(\omega M)^2}{\hat{Z}_d + \hat{Z} + \cfrac{(\omega M)^2}{\hat{Z} + \cfrac{(\omega M)^2}{\cdots + \cfrac{(\omega M)^2}{\hat{Z} + \hat{Z}_T}}}}}. \tag{2.3}$$

In case we are operating at the resonant frequency ω_0, $\hat{Z} = R$ and $\hat{Z}_T = R_T$ and thus (2.1) becomes

$$\hat{Z}_{eq} = \cfrac{(\omega_0 M)^2}{R + \cfrac{(\omega_0 M)^2}{\cdots + \cfrac{(\omega_0 M)^2}{R + \cfrac{(\omega_0 M)^2}{R + \hat{Z}'_T}}}}. \tag{2.4}$$

and (2.3), with $\hat{Z}_d = R_d$, becomes

$$\hat{Z}_{eq} = \cfrac{(\omega_0 M)^2}{R + \cfrac{(\omega_0 M)^2}{\cdots + \cfrac{(\omega_0 M)^2}{R_d + R + \cfrac{(\omega_0 M)^2}{R + \cfrac{(\omega_0 M)^2}{\cdots + \cfrac{(\omega_0 M)^2}{R + \cfrac{(\omega_0 M)^2}{R + R_T}}}}}}}. \tag{2.5}$$

2.3 Mathematical analysis of the continued fraction

After representing the equivalent impedance of a resonator array as a continued fraction, we can perform a mathematical analysis in order to determine its value. We do this by proving that the fraction can be rewritten as a term of a recursive sequence whose general term can be determined using the theory of linear homogeneous difference equations [28]. In this way, we can get an expression for the value of the fraction that depends only on its initial conditions, number of terms and order of the term which is affected by the perturbation. Additionally, using the analytical expressions obtained, we can perform further mathematical analyses on the continued fraction, namely regarding its monotonicity and convergence.

2.3.1 Value of the fraction without a perturbation

The continued fraction (2.1) can be rewritten using generic letters for any number $n+1$ of resonators (with $n \geq 0$) in the form:

$$x_n = \cfrac{a}{b + \cfrac{a}{b + \cfrac{a}{b + \cfrac{a}{\cdots + \cfrac{a}{b + \cfrac{p_0}{q_0}}}}}} \tag{2.6}$$

with a, b, p_0, $q_0 \in \mathbb{C}$ where $q_0 \neq 0$, a and b both not equal to 0. The previous fraction (2.6) is the nth term of the following recursive sequence (with $k \geq 1$):

$$x_k = \frac{a}{b + x_{k-1}} \tag{2.7}$$

with

$$x_0 = \frac{p_0}{q_0}. \tag{2.8}$$

The term x_0 corresponds to the termination impedance of the array connected to the first cell, e.g., $\hat{Z}'_T$ in (2.1) or $\hat{Z}_T$ in (2.2). As referred before and represented in Fig. 2.1, the $(n+1)$ cells of the array are labelled from 1 to $n+1$, with 1 being the cell connected to the termination impedance and $n+1$ is the cell connected to the source. Thus, noting by

$$x_k = \frac{p_k}{q_k}, \tag{2.9}$$

we can verify by induction that $\{p_n\}$ and $\{q_n\}$ are sequences defined by the following recurrence relations:

$$\begin{aligned} p_n &= b p_{n-1} + a p_{n-2} \\ q_n &= b q_{n-1} + a q_{n-2} \end{aligned} \text{ for } n \geq 2, \tag{2.10}$$

being p_0 and q_0 fixed and p_1 and q_1 given by

$$\begin{aligned} p_1 &= a q_0 \\ q_1 &= b q_0 + p_0 \end{aligned}. \tag{2.11}$$

For example, for $n = 2$, from (2.6) we have

$$\frac{p_2}{q_2} = \cfrac{a}{b + \cfrac{a}{b + \cfrac{p_0}{q_0}}} \tag{2.12}$$

and

$$\begin{aligned} p_2 &= abq_0 + ap_0 \\ q_2 &= b^2 q_0 + bp_0 + aq_0 \end{aligned}. \tag{2.13}$$

Introducing (2.11) into (2.13) we get

$$\begin{aligned} p_2 &= b p_1 + a p_0 \\ q_2 &= b q_1 + a q_0 \end{aligned} \tag{2.14}$$

which verifies (2.10) for $n = 2$. Now, supposing that (2.10) is verified for $2 \leq k$:

$$\begin{aligned} p_k &= b p_{k-1} + a p_{k-2} \\ q_k &= b q_{k-1} + a q_{k-2} \end{aligned} \tag{2.15}$$

we want to prove that the same relation is valid for $2 < k+1$:

$$\begin{aligned} p_{k+1} &= bp_k + ap_{k-1} \\ q_{k+1} &= bq_k + aq_{k-1} \end{aligned}. \tag{2.16}$$

Recalling (2.7) and (2.9), we can write

$$x_{k+1} = \frac{a}{b + x_k} \tag{2.17}$$

and

$$\frac{p_{k+1}}{q_{k+1}} = \frac{a}{b + \frac{p_k}{q_k}} = \frac{aq_k}{bq_k + p_k} \tag{2.18}$$

that, under the hypothesis of expression (2.10), with $n = k$, becomes

$$\frac{p_{k+1}}{q_{k+1}} = \frac{a(bq_{k-1} + aq_{k-2})}{b(bq_{k-1} + aq_{k-2}) + bp_{k-1} + ap_{k-2}}. \tag{2.19}$$

Knowing that $p_k = aq_{k-1}$, $q_k = bq_{k-1} + p_{k-1}$, $p_{k-1} = aq_{k-2}$, $q_{k-1} = bq_{k-2} + p_{k-2}$ we have

$$\frac{p_{k+1}}{q_{k+1}} = \frac{bp_k + a^2 q_{k-2}}{b^2 q_{k-1} + bp_{k-1} + bp_{k-1} + ap_{k-2}} = \frac{bp_k + ap_{k-1}}{bq_k + aq_{k-1}}. \tag{2.20}$$

Thus, the sequences $\{p_n\}$ and $\{q_n\}$ are defined by linear homogeneous second order difference equations with constant coefficients which can be solved directly. In fact, the equation in (2.10) given by $p_n - bp_{n-1} - ap_{n-2} = 0$ is a linear homogeneous second order difference equation with constant coefficients. Therefore, from [28] its solution is given by $p_n = m_1\lambda_1^n + m_2\lambda_2^n$ supposing that λ_1 and λ_2 are distinct solutions of the equation $\lambda^2 - b\lambda - a = 0$:

$$\lambda^2 - b\lambda - a = 0 \Leftrightarrow \lambda = \frac{b \pm \sqrt{b^2 + 4a}}{2} \tag{2.21}$$

in which m_1 and m_2 are constants that should be determined using the initial conditions. The same considerations can be done for $\{q_n\}$, considering $q_n = m_3\lambda_1^n + m_4\lambda_2^n$.

In conclusion, the general term of the sequence $\{x_n\} = \{p_n/q_n\}$ is given by

$$x_n = \frac{a_1\left(\frac{b-\sqrt{b^2+4a}}{2}\right)^n + a_2\left(\frac{b+\sqrt{b^2+4a}}{2}\right)^n}{b_1\left(\frac{b-\sqrt{b^2+4a}}{2}\right)^n + b_2\left(\frac{b+\sqrt{b^2+4a}}{2}\right)^n} \tag{2.22}$$

where a_1, a_2, b_1 and b_2 are constants that can be calculated using the initial conditions x_0 and x_1 defined before as:

$$\begin{aligned} x_0 &= \frac{p_0}{q_0} \\ x_1 &= \frac{a}{b + x_0} = \frac{p_1}{q_1} \end{aligned}. \tag{2.23}$$

Then,

$$\begin{aligned} p_n &= a_1\left(\tfrac{b-\sqrt{b^2+4a}}{2}\right)^n + a_2\left(\tfrac{b+\sqrt{b^2+4a}}{2}\right)^n \\ q_n &= b_1\left(\tfrac{b-\sqrt{b^2+4a}}{2}\right)^n + b_2\left(\tfrac{b+\sqrt{b^2+4a}}{2}\right)^n \end{aligned} \tag{2.24}$$

where p_0, q_0 are fixed and $p_1 = aq_0$, $q_1 = bq_0 + p_0$. For simplicity, setting $p_0 = x_0$ and q_0=1, a_1, a_2, b_1 and b_2 can be obtained by solving the following system:

$$\begin{aligned} &a_1 + a_2 = x_0 \\ &b_1 + b_2 = 1 \\ &\frac{a_1}{2}\left(b - \sqrt{b^2+4a}\right) + \frac{a_2}{2}\left(b + \sqrt{b^2+4a}\right) = a \\ &\frac{b_1}{2}\left(b - \sqrt{b^2+4a}\right) + \frac{b_2}{2}\left(b + \sqrt{b^2+4a}\right) = b + x_0 \end{aligned} \quad . \tag{2.25}$$

The expressions of the constants a_1, a_2, b_1 and b_2 obtained are shown in the Appendix A.

2.3.2 Value of the fraction with a perturbation in the i^{th} term

After an expression for the value of the fraction without a perturbation is obtained, we can now calculate the value of the fraction (2.2), which is referred to the equivalent impedance of resonator array with a receiver placed above the ith cell of the array, as represented in Fig. 2.1. To do this, we rewrite the fraction as a generic continued fraction with n terms with a perturbation $b' \neq b$ in the step $i \leq n$ of the recursive sequence:

$$x_n = \cfrac{a}{b + \cfrac{a}{\cdots + \cfrac{a}{b' + \cfrac{a}{b + \cfrac{a}{\cdots + \cfrac{a}{b + \cfrac{p_0}{q_0}}}}}}} \quad \text{with } a, b, b', p_0, q_0 \in \mathbb{C}. \tag{2.26}$$

In order to obtain the value of (2.26), we split the fraction in two continued fractions (one with i terms and the other with $n-i$ terms) and we proceed in three steps: firstly, using (2.22), we calculate x_k for the $(i-1)$th term. Secondly, we identify the ith value x_i using the perturbation b'. Finally, using x_i as an initial value, we are able to determine the value of the fraction, with the last $n-i$ values.

So, as in the previous subsection, we start using (2.22) to determine the term of $(i-1)$th order:

$$x_{i-1} = \frac{a_1\left(b - \sqrt{b^2+4a}\right)^{i-1} + a_2\left(b + \sqrt{b^2+4a}\right)^{i-1}}{b_1\left(b - \sqrt{b^2+4a}\right)^{i-1} + b_2\left(b + \sqrt{b^2+4a}\right)^{i-1}} \tag{2.27}$$

where a_1, a_2, b_1 and b_2 depend on the initial conditions x_0 and x_1 as done before, with (2.25). Afterwards we set,

$$x_i = \frac{a}{b' + x_{i-1}} = y_0 \tag{2.28}$$

and

$$\frac{a}{b + y_0} = y_1 \tag{2.29}$$

with y_0 and y_1 being the initial conditions used for the fraction $y_{n-i} = x_n$:

$$y_{n-i} = x_n = \frac{c_1\left(b - \sqrt{b^2+4a}\right)^{n-i} + c_2\left(b + \sqrt{b^2+4a}\right)^{n-i}}{d_1\left(b - \sqrt{b^2+4a}\right)^{n-i} + d_2\left(b + \sqrt{b^2+4a}\right)^{n-i}}. \tag{2.30}$$

The constants c_1, c_2, d_1 and d_2 (shown in Appendix A) are obtained by the initial conditions y_0 and y_1, as done with (2.24) and (2.25), where it is assumed that $p_0 = y_0$ and $q_0 = 1$, by solving the following system:

$$\begin{aligned} &c_1 + c_2 = y_0 \\ &d_1 + d_2 = 1 \\ &\frac{c_1}{2}\left(b - \sqrt{b^2+4a}\right) + \frac{c_2}{2}\left(b + \sqrt{b^2+4a}\right) = a \\ &\frac{d_1}{2}\left(b - \sqrt{b^2+4a}\right) + \frac{d_2}{2}\left(b + \sqrt{b^2+4a}\right) = b + y_0 \end{aligned} \quad . \tag{2.31}$$

The expression (2.30) represents the value of the fraction (2.2) for $n+1$ resonators with the perturbation in the *i*th term, (receiver facing the *i*th resonator, i.e., *i*=1 corresponds to the resonator connected to the termination impedance and *i*=*n* to the resonator after the one connected to the source).

2.3.3 Convergence of the continued fraction

Following the determination of the value of the continued fraction, we can analyse its convergence by determining its behaviour for an infinite number of terms, in other words, its value for $n \to \infty$.

Supposing that $z^2 - bz - a = 0$ has distinct roots z_1 and z_2, with $|z_1| > |z_2|$, we have

$$\left|\frac{z_2}{z_1}\right| < 1 \tag{2.32}$$

so

$$\lim_{n\to\infty}\left(\frac{z_2}{z_1}\right)^n = 0. \tag{2.33}$$

Now, using these assumptions, we can demonstrate that x_n tends to the quotient of the coefficients of z_1^n. For example, considering that $\left|b - \sqrt{b^2+4a}\right| < \left|b + \sqrt{b^2+4a}\right|$, i.e. $z_1 = b + \sqrt{b^2+4a}$ and $z_2 = b - \sqrt{b^2+4a}$ from (2.22) we rewrite x_n as:

$$x_n = \frac{a_2 z_1^n + a_1 z_2^n}{b_2 z_1^n + b_1 z_2^n} = \frac{a_2 + a_1 \left(\frac{z_2}{z_1}\right)^n}{b_2 + b_1 \left(\frac{z_2}{z_1}\right)^n} \tag{2.34}$$

thus

$$\lim_{n\to\infty} x_n = \lim_{n\to\infty} \frac{a_2 + a_1 \left(\frac{z_2}{z_1}\right)^n}{b_2 + b_1 \left(\frac{z_2}{z_1}\right)^n} = \frac{a_2}{b_2}. \tag{2.35}$$

Calculating a_2/b_2 using the values of the constants a_2 and b_2 described in Appendix A, it is very interesting to note that the value of the limit (2.35) does not depend on the initial conditions x_0 and it is always equal to $\frac{1}{2}\left(\sqrt{4a+b^2}-b\right)$. This proves a very important fact: for fixed $a, b \in \mathbb{C}$, the value of the fraction is always the same when the number of terms is infinite, not depending of the initial condition x_0. So, if we set x_0 equal to this value we can prove that $\{x_n\}$ is a constant sequence, since for $x_0 = \frac{1}{2}\left(\sqrt{4a+b^2}-b\right)$ the constants a_1, a_2, b_1 and b_2, have the following values:

$$\begin{aligned} a_1 &= 0 \\ a_2 &= \tfrac{1}{2}\left(\sqrt{4a+b^2}-b\right) \\ b_1 &= 0 \\ b_2 &= 1 \end{aligned}, \tag{2.36}$$

resulting in

$$x_n = \frac{\frac{1}{2}\left(\sqrt{4a+b^2}-b\right) + 0\left(\frac{z_2}{z_1}\right)^n}{1 + 0\left(\frac{z_2}{z_1}\right)^n} = \frac{1}{2}\left(\sqrt{4a+b^2}-b\right). \tag{2.37}$$

Moreover, it is also important to note that for a finite number of perturbations, the behaviour of the fraction at infinity remains the same, since for example taking (2.30) and setting its limit to infinite, considering the assumptions in (2.32) and (2.33) we have:

$$\lim_{n\to\infty} y_{n-i} = \lim_{n\to\infty} \frac{c_2 + c_1 \left(\frac{z_2}{z_1}\right)^n \left(\frac{z_2}{z_1}\right)^{-i}}{d_2 + d_1 \left(\frac{z_2}{z_1}\right)^n \left(\frac{z_2}{z_1}\right)^{-i}} = \frac{c_2}{d_2} = \frac{1}{2}\left(\sqrt{4a+b^2}-b\right). \tag{2.38}$$

Being $\{x_n\}$ a convergent sequence, $|x_n|$ is bounded, which means that there exists a $M, P \in \mathbb{R}$, so that $M < |x_n| < P$, $\forall n \in \mathbb{N}_0$. In the next subsection we calculate the upper bounds of the set of terms of this sequence for $a, b, b', p_0, q_0 \in \mathbb{R}$.

2.3.4 Monotonicity of the sequence

After the study of the convergence, in order to study monotonicity of the sequence that represents a continued fraction, we take into consideration the particular case in which the constants of the fractions are real (i.e. $a, b, b', p_0, q_0 \in \mathbb{R}$), with $a, b > 0$ and $x_0 \geq 0$. For this case, by studying the monotonicity of the sequence that represents the continued fraction, we can determine if it increases or decreases with the increase of the number of terms.

Rearranging (2.34), we can write:

$$x_n = \frac{a_1}{b_1} + \frac{a_2 b_1 - a_1 b_2}{b_1 \left(b_1 \left(\frac{z_2}{z_1} \right)^n + b_2 \right)}. \tag{2.39}$$

We can start by studying the monotonicity of $\{b_1 w_n + b_2\}$, with $w_n = \left(\frac{z_2}{z_1} \right)^n$. Due to the assumption given by (2.32), $\{w_n\}$ will present an alternating behaviour with positive and negative values, with its subsequences $\{w_{2n}\}$ and $\{w_{2n+1}\}$ having different monotonicities (one is increasing, the other is decreasing) and both convergent to zero. Thus, $\{w_n\}$ yields an analogous behaviour of the sequence $\{b_1 w_n + b_2\}$. Analysing the value of the constants b_1 and b_2 in Appendix A, as b_2 is always positive, the sign of the sequence $\{b_1 w_n + b_2\}$ depends on the sign of b_1 which is negative if $x_0 > \frac{1}{2}\left(\sqrt{4a + b^2} - b \right)$ and positive otherwise. For example, if $x_0 > \frac{1}{2}\left(\sqrt{4a + b^2} - b \right)$, the subsequence $\{b_1 w_{2n} + b_2\}$ is decreasing with values higher than b_2, and the subsequence $\{b_1 w_{2n+1} + b_2\}$ is increasing with values lower than b_2, and both are converging to b_2. On the other hand, in this case, it can be seen the decrease of an even term to its consecutive odd term and an increase of an odd term to its consecutive even term. In case $x_0 < \frac{1}{2}\left(\sqrt{4a + b^2} - b \right)$, the opposite occurs. We can also note that as $|b_1| < |b_2|$, we have, in any case, that $\{b_1 w_n + b_2\}$ is a sequence with positive real terms. Then, considering that

$$(a_2 b_1 - a_1 b_2) = \frac{a - x_0(b + x_0)}{\sqrt{4a + b^2}} \tag{2.40}$$

is negative if $x_0 > \frac{1}{2}\left(\sqrt{4a + b^2} - b \right)$ and positive otherwise, we have that

$$\frac{a_2 b_1 - a_1 b_2}{b_1} = \frac{1}{2}\left(\sqrt{4a + b^2} + b + 2x_0 \right) \tag{2.41}$$

is always positive.

In conclusion, the sequence is not monotonic and it converges to the limit given by (2.35) from lower and higher values, alternatively. Furthermore, all the terms of the sequence are bounded in the range defined by the first two terms, x_0 and x_1, being x_0 the lower bound and x_1 the higher bound if $x_0 < \frac{1}{2}\left(\sqrt{4a + b^2} - b \right)$ and x_0 the higher bound and x_1 the lower bound, otherwise.

2.3.5 Speed of convergence of the sequence

Finally, we can study how fast the fraction converges to its limit. This is done by finding the order of the term such that the absolute value of the difference (δ_n) between the value of the fraction (2.34) and its limit (2.35) is smaller than a given ε. This difference δ_n can be then defined as:

$$\delta_n = \left| x_n - \lim_{n \to \infty} x_n \right| = \left| \frac{a_2 z_1^n + a_1 z_2^n}{b_2 z_1^n + b_1 z_2^n} - \frac{a_2}{b_2} \right|. \tag{2.42}$$

For any $\varepsilon > 0$ there exists an integer number N such that for $n > N$, we have $\delta_n < \varepsilon$. Recalling $w_n = \left(\frac{z_2}{z_1} \right)^n$, which is a sequence that tends to zero because $\left| \frac{z_2}{z_1} \right| < 1$, as assumed before, we get:

$$\begin{aligned}\delta_n &= \left|\frac{a_2+a_1w_n}{b_2+b_1w_n}-\frac{a_2}{b_2}\right| = \left|\frac{(a_1b_2-a_2b_1)\,w_n}{b_2\,(b_1w_n+b_2)}\right| \\ &= \frac{|a_1b_2-a_2b_1|\,|w_n|}{|b_2|\,|b_1w_n+b_2|}.\end{aligned} \tag{2.43}$$

Now, assuming Q a non-zero lower bound of the convergent sequence $|b_1w_n+b_2|$, we have that $|b_1w_n+b_2|>Q$ and thus

$$\delta_n = \frac{|a_1b_2-a_2b_1|\,|w_n|}{|b_2|\,Q} < \varepsilon. \tag{2.44}$$

Solving for n, we can write:

$$N > \log_{\left|\frac{z_2}{z_1}\right|}\left(\frac{|b_2|\,Q}{|a_1b_2-a_2b_1|}\varepsilon\right). \tag{2.45}$$

We can then conclude that for any $\varepsilon>0$, we can define an order N equal to the largest integer contained in $\log_{\left|\frac{z_2}{z_1}\right|}\left(\frac{|b_2|Q}{|a_1b_2-a_2b_1|}\varepsilon\right)$ such that for $n>N$, x_n is in the circle centered in $\frac{1}{2}\left(\sqrt{4a+b^2}-b\right)$ and radius ε. Note that for the case where the constants of the fraction are real, we can set $Q=|b_1w_0+b_2|$ if $x_0>\frac{a_2}{b_2}$, or $Q=|b_1w_1+b_2|$ otherwise.

2.4 Application of the mathematical results - Value and characteristics of the equivalent impedance

The mathematical results obtained in the previous section can now be applied to the equivalent circuit of an array of resonators, as represented in Fig. 2.1, and the expressions (2.1) and (2.2), considered for the cases at the resonant frequency ($\omega=\omega_0$) and at any other frequency ($\omega\neq\omega_0$), are found. Examples of the mathematical results are studied with the software MATLAB using the values for the parameters of the circuit R, L, C and M from the stranded-wire resonator array described in Chapter 5 ($L=12.6\mu$H, $C=93.1n$F, $R=0.11\Omega$, $M=-1.55\mu$H and $f_0=147$kHz), in order to illustrate possible real situations.

2.4.1 Determination of the equivalent impedance

Using the generic values of the fractions (2.22) and (2.30), we can write the expressions for the equivalent impedance $\hat{Z}_{eq}$ in terms of the parameters of the equivalent circuit of the IPT system described previously in section 2.2.

2.4.1.1 Operating frequency different from the resonant frequency, $\omega\neq\omega_0$

In this case, $a=(\omega M)^2$, $b=\hat{Z}$, $x_0=\hat{Z}'_T=\hat{Z}_T+\hat{Z}_d$ (which is reduced to $\hat{Z}_T$ when the receiver is not over the first cell), $b'=\hat{Z}_d+\hat{Z}$.

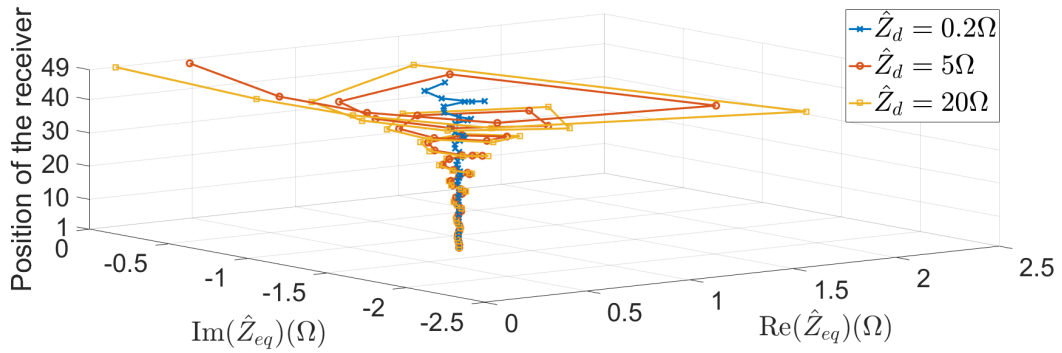

Figure 2.3: Real and imaginary parts of $\hat{Z}_{eq}$ versus the receiver position for different values of $\hat{Z}_d$, for $f = 165$ kHz and for $\hat{Z}_T = 1.5\Omega$. The position of the receiver is 1 when over the first cell and 49 when over the cell next to the one connected to the source.

For a resonator array without a receiver over the resonator line or with the receiver over the first cell of the resonator line

$$\hat{Z}_{eq} = \frac{f^n(2(\omega M)^2 - g\hat{Z}'_T) + g^n(f\hat{Z}'_T - 2(\omega M)^2)}{f^n(f + 2\hat{Z}'_T) - g^n(g + 2\hat{Z}'_T)} \tag{2.46}$$

where $f = \hat{Z} - \sqrt{\hat{Z}^2 + 4(\omega M)^2}$ and $g = \hat{Z} + \sqrt{\hat{Z}^2 + 4(\omega M)^2}$.

For a resonator array with a receiver over the resonator line at any position

$$\hat{Z}_{eq} = \frac{(\omega M)^2\left(e_1 f^n g^{2i} + e_2 f^{2i} g^n - f^i g^i (e_3 f^n + e_4 g^n)\right)}{f^n g^i (e_5 f^i + e_6 g^i) + f^i g^n (e_7 f^i + e_8 g^i)} \tag{2.47}$$

where the constants e_1, e_2, e_3, e_4, e_5, e_6, e_7, and e_8 are described in Appendix A.

Using (2.47) we make an example by plotting the equivalent impedance $\hat{Z}_{eq}$ versus the position of the receiver i and for different values of the receiver impedance $\hat{Z}_d$, for a line of 50 resonators, with the operating frequency equal to $f = 165$kHz and $\hat{Z}'_T = 1.5\Omega$ (Fig. 2.3). Then, by observing Fig. 2.3 we can notice that the equivalent impedance is affected more significantly as the receiver gets closer to the cell next to the one connected to the source and that the effect of the receiver increases with the value of $\hat{Z}_d$.

2.4.1.2 Resonant frequency $\omega = \omega_0$

For this case, $a = (\omega_0 M)^2$, $b = R$, $x_0 = \hat{Z}'_T = R'_T = R_T + R_d$ (which is reduced to R_T when the receiver is not over the first cell), $b' = R_d + R$. Moreover, since all the components of the expression are real, the equivalent impedance is going to be real as well, so $\hat{Z}_{eq} = R_{eq}$.

For a resonator array without a receiver over the resonator line or with the receiver over the first cell of the resonator line

$$\hat{Z}_{eq} = R_{eq} = \frac{f^n(2(\omega_0 M)^2 - gR'_T) + g^n(fR'_T - 2(\omega_0 M)^2)}{f^n(f + 2R'_T) - g^n(g + 2R'_T)}. \tag{2.48}$$

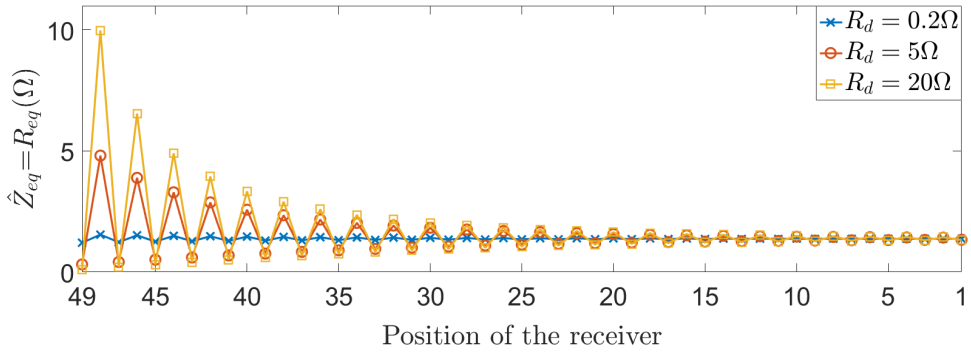

Figure 2.4: $\hat{Z}_{eq} = R_{eq}$ versus the position of the receiver over a line of 50 resonators for different values of R_d, at the resonant frequency f_0 =147 kHz and for $R_T = 1.5\Omega$. The position of the receiver is 1 when over the first cell and 49 when over the cell next to the one connected to the source.

For a resonator array with a receiver over the resonator line at any position

$$\hat{Z}_{eq} = R_{eq} = \frac{(\omega_0 M)^2 \left(e_1 f^n g^{2i} + e_2 f^{2i} g^n - f^i g^i \left(e_3 f^n + e_4 g^n\right)\right)}{f^n g^i \left(e_5 f^i + e_6 g^i\right) + f^i g^n \left(e_7 f^i + e_8 g^i\right)}. \tag{2.49}$$

Then, this time using (2.47), we can show an example by plotting R_{eq} versus the position of the receiver i for different values of the receiver impedance R_d, for an array with 50 resonators, terminated by $R_T = 1.5\Omega$, operating at the resonant frequency $f = 147$kHz. In Fig. 2.4, as already observed in Fig. 2.3, the equivalent impedance is affected more significantly as the receiver gets closer to the cell next to the one connected to the source and for higher values of R_d.

2.4.2 Convergence of the continued fraction - equivalent impedance of an infinite array of resonators

From the value obtained with (2.35), with $a = (\omega M)^2$, $b = \hat{Z}$, we can say that the equivalent impedance $\hat{Z}_{eq}$, for an array with an infinite number of resonators, converges to the following value:

$$\lim_{n\to\infty} \hat{Z}_{eq} = \frac{1}{2}\left(-\hat{Z} + \sqrt{\hat{Z}^2 + 4(\omega M)^2}\right). \tag{2.50}$$

As demonstrated in section 2.3.3, (2.50) does not depend on the initial conditions, i.e., the impedance $\hat{Z}'_T$. The limit depends only on the electrical parameters of the cells, the mutual inductance M and the angular frequency ω. Using the expression (2.1), for a frequency f=165kHz different than the resonant frequency, we can obtain and plot the equivalent impedance $\hat{Z}_{eq}$ for different numbers of resonators $n+1$ and for different values of $\hat{Z}'_T$ (Fig. 2.5). Analogously, for the resonant frequency $f_0 = 147$ kHz, we can plot the equivalent impedance $\hat{Z}_{eq} = R_{eq}$ with (2.4), for different numbers of resonators $n+1$ and for different values of R'_T as shown in Fig. 2.6. It can be noticed that, as we increase the length of the resonator line, even for different values of the impedance $\hat{Z}'_T$ (or resistance R'_T), the equivalent impedance converges always to (2.50). Furthermore, as demonstrated with (2.37), by introducing an impedance $\hat{Z}'_T$ equal to (2.50) into (2.46),

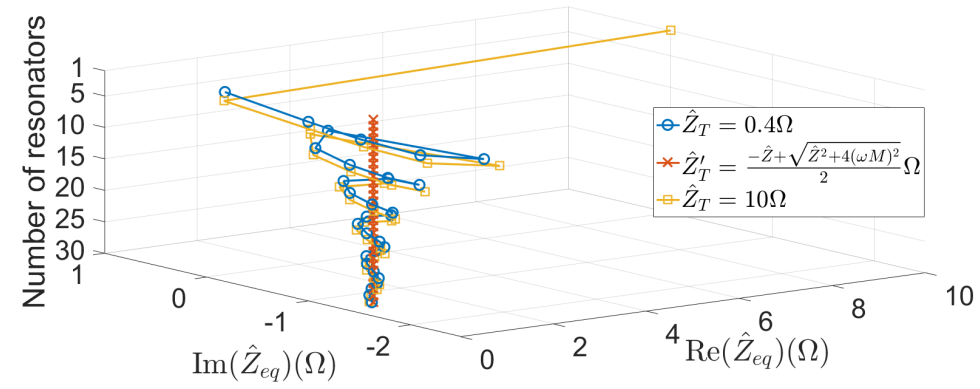

(a)

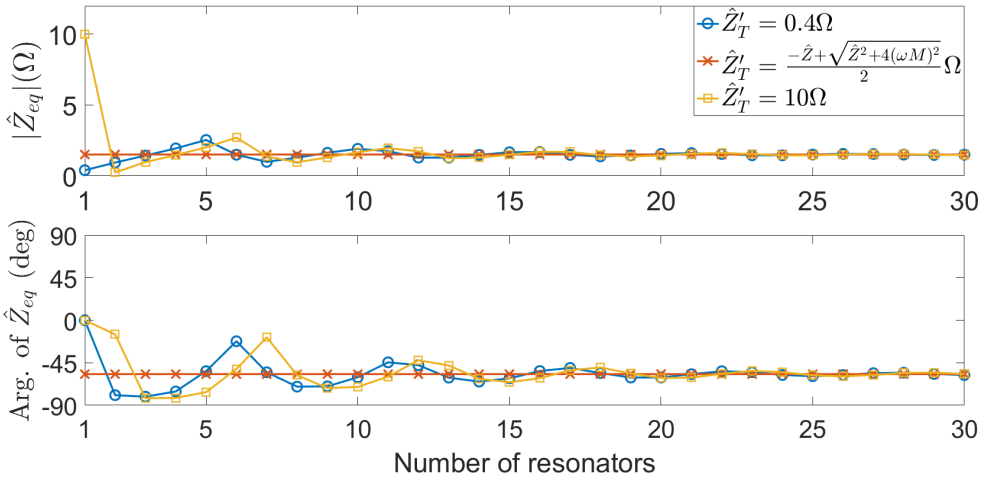

(b)

Figure 2.5: (a) Real and imaginary parts and (b) magnitude and argument of the equivalent impedance $\hat{Z}_{eq}$ versus the number of resonators of the array for $f = 165$kHz and different values of $\hat{Z}'_T$.

the equivalent impedance $\hat{Z}_{eq}$ obtained is constant and equal to $\hat{Z}'_T$ regardless of the number of resonator cells. In this way we can define the expression given by (2.50) as the impedance that perfectly terminates the array, $\hat{Z}_{eq,\infty} = \frac{1}{2}\left(-\hat{Z}+\sqrt{\hat{Z}^2+4(\omega M)^2}\right)$, or at the resonant frequency, $R_{eq,\infty} = \frac{1}{2}\left(-R+\sqrt{R^2+4(\omega_0 M)^2}\right)$. Then, in a line terminated with $R'_T = R_{eq,\infty}$, the impedance seen from the source terminals, for any number of resonators, is given by:

$$R + R_{eq,\infty} = \frac{1}{2}\left(R+\sqrt{R^2+4(\omega_0 M)^2}\right). \tag{2.51}$$

Equation (2.51) coincides with the termination resistance that according to the magnetoinductive wave theory provides matching of the structure [16]. Thus, (2.51) can be considered as the characteristic impedance of the line.

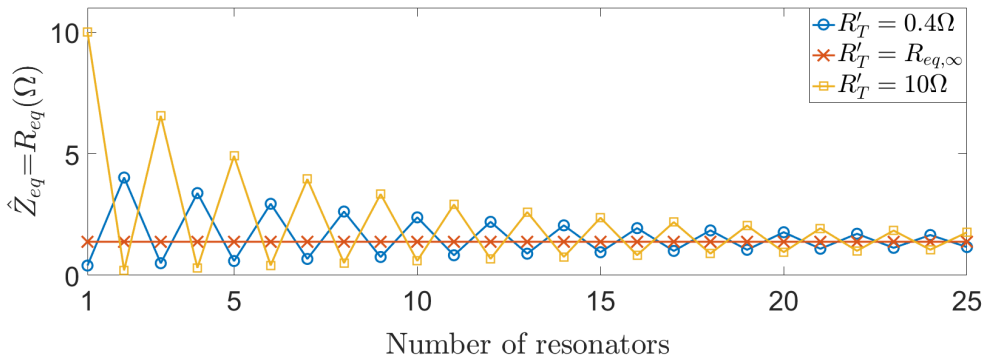

Figure 2.6: $\hat{Z}_{eq} = R_{eq}$ versus the number of resonators of the array at the resonant frequency $f_0 =$ 147 kHz and for different values of R'_T.

This also means that, when a perturbation $\hat{Z}_d$ is present in the $(j+1)$th resonator and the line is terminated with an impedance $\hat{Z}'_T = \hat{Z}_{eq,\infty}$ equal to (2.50), we can determine $\hat{Z}_{eq}$ with (2.46) by replacing $\hat{Z}'_T$ with $\hat{Z}_{eq,\infty} + \hat{Z}_d$ and replacing n with $n - j$.

Furthermore, considering that we are operating at any given frequency, we can plot the impedance $\hat{Z}_{eq,\infty} = \frac{1}{2}\left(-\hat{Z} + \sqrt{\hat{Z}^2 + 4(\omega M)^2}\right)$ versus frequency, as shown in Fig. 2.7.

2.4.3 Monotonicity of the equivalent impedance

As shown in subsection 2.3.4, the monotonicity of the sequence that represents the equivalent impedance of an array of resonator, i.e. the increase or decrease of its odd or even terms, depends on the sign of $a_2 b_1 - a_1 b_2$, that, under the resonance condition, with $a = (\omega_0 M)^2$, $b = R$, $x_0 = R'_T$, becomes

$$\frac{(\omega_0 M)^2 - R_T'^2 - R R'_T}{\sqrt{R^2 + 4(\omega_0 M)^2}}. \tag{2.52}$$

For the circuit parameter values given at the beginning of this section, $a_2 b_1 - a_1 b_2$ and thus (2.52) have the behaviour shown in Fig. 2.8.

We can notice that $a_2 b_1 - a_1 b_2$ is zero for $R'_T = \frac{1}{2}\left(-R + \sqrt{R^2 + 4(\omega_0 M)^2}\right)$ (which for this case is equal to 1.38Ω), negative for $R'_T > \frac{1}{2}\left(-R + \sqrt{R^2 + 4(\omega_0 M)^2}\right)$ and positive otherwise. The constants, as described in Appendix A, a_1, a_2, b_1 and b_2 can also be plotted with respect to R'_T, as Fig. 2.9 shows.

Figures 2.8 and 2.9 illustrate the theoretical results of section 2.3.4. The values of the even and odd terms of the sequence of the continued fraction decrease and increase, respectively, for $R'_T < \frac{1}{2}\left(-R + \sqrt{R^2 + 4(\omega_0 M)^2}\right)$; otherwise, the contrary occurs, i.e., they increase and decrease, respectively, for $R'_T > \frac{1}{2}\left(-R + \sqrt{R^2 + 4(\omega_0 M)^2}\right)$. Therefore, the behaviour of Fig. 2.6 confirms the conclusions obtained regarding the monotonicity of the sequence that represents the equivalent impedance of an array of resonators.

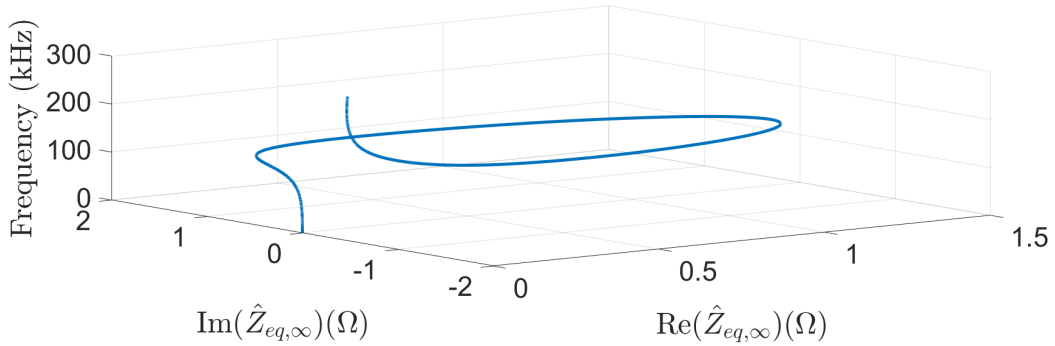

(a)

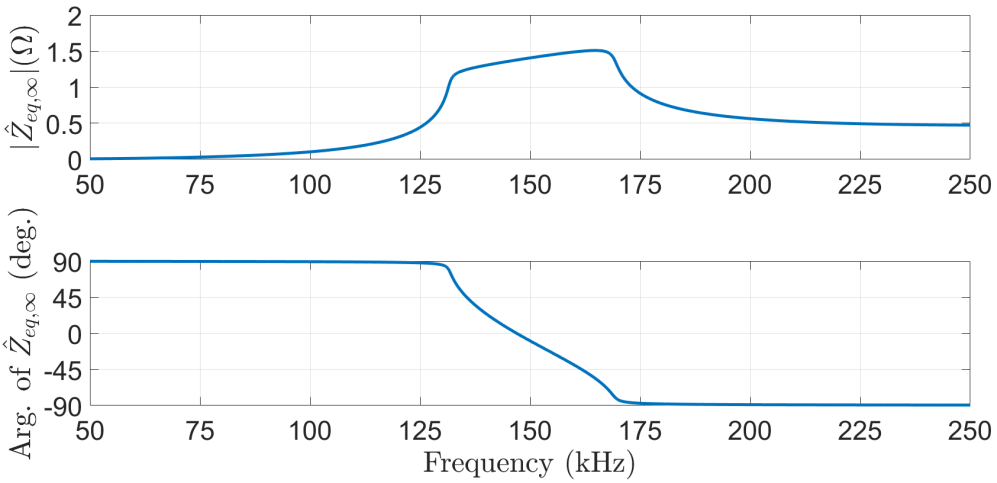

(b)

Figure 2.7: (a) Real and imaginary parts and (b) magnitude and argument of the impedance $\hat{Z}_{eq,\infty}$ versus frequency.

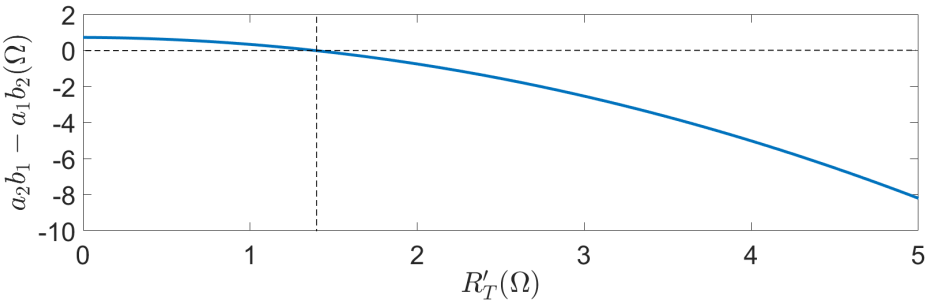

Figure 2.8: Plot of $a_2b_1 - a_1b_2$ versus R'_T.

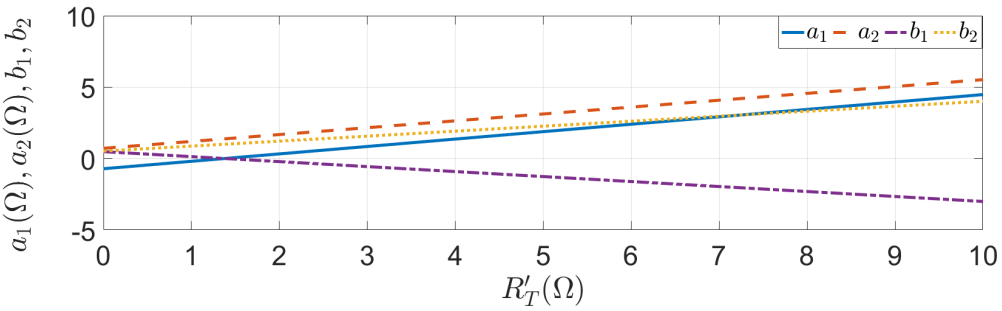

Figure 2.9: Constants a_1, a_2, b_1 and b_2 versus R'_T.

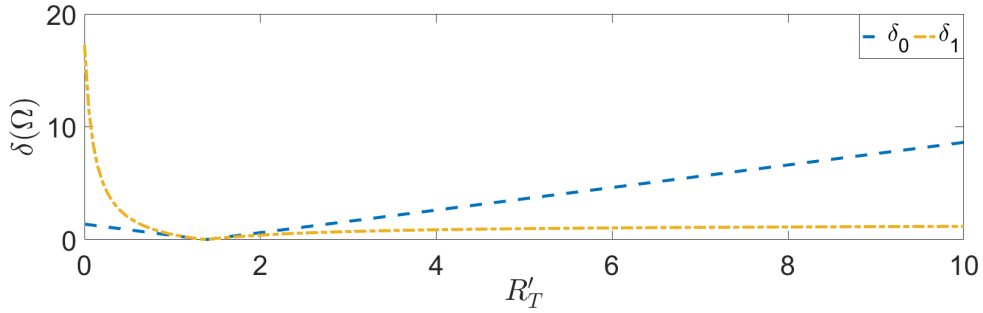

Figure 2.10: Variation of δ with R'_T.

2.4.4 Variation of the speed of convergence with the variation of the circuit parameters

In the same way as done in the previous subsection, we consider the system in a resonance condition, meaning that all the electrical parameters are real. Using (2.42) from the subsection 2.3.5, we have that the difference between $\hat{Z}_{eq} = R_{eq}$ and its limit (2.50), for $n = 0$ (one resonator) and $n = 1$ (two resonators) is given by:

$$\delta_0 = \left| \frac{R + 2R'_T - \sqrt{R^2 + 4(\omega_0 M)^2}}{2} \right| \tag{2.53}$$

and

$$\delta_1 = \left| \frac{R - \sqrt{R^2 + 4(\omega_0 M)^2}}{2} + \frac{(\omega_0 M)^2}{R + R'_T} \right|. \tag{2.54}$$

Firstly, for $R'_T = \frac{1}{2}\left(-R + \sqrt{R^2 + 4(\omega_0 M)^2}\right) = 1.38$, $\delta_0 = 0$ and $\delta_1 = 0$, as expected, since the value of of R_{eq} is constant and equal to is limit. Otherwise, for $R'_T < \frac{1}{2}\left(-R + \sqrt{R^2 + 4(\omega_0 M)^2}\right)$, $\delta_0 < \delta_1$ and for $R'_T > \frac{1}{2}\left(-R + \sqrt{R^2 + 4(\omega_0 M)^2}\right)$ we have that $\delta_0 > \delta_1$, as it can be seen in Fig. 2.10. δ_0 and δ_1 represent the largest differences between the equivalent impedance $\hat{Z}_{eq} = R_{eq}$ and its limit (2.50) for $n \to \infty$, as Fig. 2.6 shows.

Therefore, as referred previously in section 2.3.4, the sequence $\{x_n\}$ is bounded by the first two terms, x_0 and x_1, which means that the maximum and minimum values of the equivalent impedance

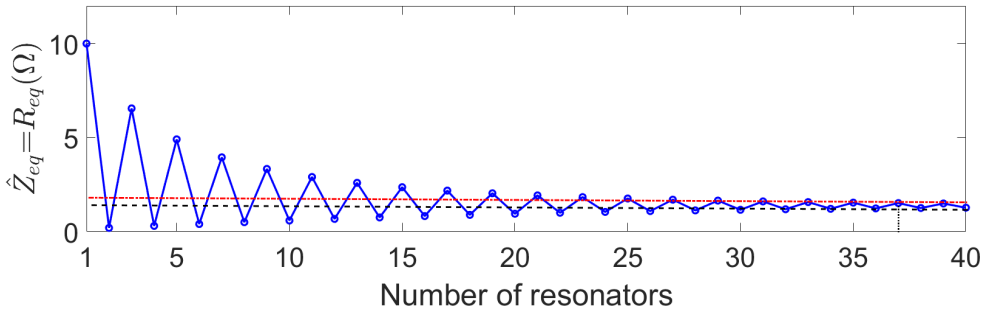

Figure 2.11: $\hat{Z}_{eq} = R_{eq}$ versus the number of resonators, for $R'_T = 10\Omega$ and $\varepsilon = 0.40$. The dashed lines represent the range where $\left|\hat{Z}_{eq} - \lim_{n\to\infty} \hat{Z}_{eq}\right| < \varepsilon$.

for given conditions of the system, are obtained from (2.48) with $n = 0$ (equal to R'_T) and $n = 1$.

From (2.45), for $R'_T > \frac{1}{2}\left(-R + \sqrt{R^2 + 4(\omega_0 M)^2}\right)$, we have

$$N > \log_{\left|\frac{R-\sqrt{R^2+4(\omega_0 M)^2}}{R+\sqrt{R^2+4(\omega_0 M)^2}}\right|} \left(\frac{2}{R - \sqrt{R^2 + 4(\omega_0 M)^2} + 2R'_T}\varepsilon\right) \tag{2.55}$$

or for $R'_T < \frac{1}{2}\left(-R + \sqrt{R^2 + 4(\omega_0 M)^2}\right)$

$$N > \log_{\left|\frac{R-\sqrt{R^2+4(\omega_0 M)^2}}{R+\sqrt{R^2+4(\omega_0 M)^2}}\right|} \left[\frac{2(R + R'_T)}{2(\omega_0 M)^2 - R'_T\left(\sqrt{R^2 + 4(\omega_0 M)^2} + R\right)}\varepsilon\right]. \tag{2.56}$$

The integer number N represents the minimum number of resonators excluding the one connected to the source such that the difference between $\hat{Z}_{eq}$ and $\lim_{n\to\infty} \hat{Z}_{eq}$ is within $\pm\varepsilon$. For example, for $R'_T = 10\Omega$ and $\varepsilon = 0.41$, which represents 30% of $\lim_{n\to\infty} \hat{Z}_{eq}$, then $0.97 < \hat{Z}_{eq} < 1.79$. N is calculated as the smallest integer greater than the logarithm of (2.55), since for this case $R'_T > \frac{1}{2}\left(-R + \sqrt{R^2 + 4(\omega_0 M)^2}\right)$. In this case the value of the logarithm is 35.5 and thus $N = 36$ (i.e., the array has 37 resonators) as Fig. 2.11 shows.

2.4.5 Equivalent impedance of a resonator array with two receivers over it

Previously, by solving the continued fraction, we obtained a closed-form expression for the equivalent impedance of a resonator array, with the receiver over the first cell (or with no receiver) and for a resonator array with a receiver over the ith cell. However, instead of using the expression (2.47), we could use a different method, by splitting the resonator array in two equivalent circuits and thus the continued fraction represented by 2.2 in two different fractions. Then, considering the system represented in Fig. 2.1 but now with the receiver over the $(i+1)$th cell, splitting the resonator array in two parts, using the expression (2.46) for each part, as in Fig. 2.12, we can write as in [29], considering $\hat{Z}_{eq,i}$ the equivalent impedance of the i resonators after the $(i+1)$ cell

$$\hat{Z}_{eq,i} = \frac{f^i(2(\omega M)^2 - g\hat{Z}_T) + g^i(f\hat{Z}_T - 2(\omega M)^2)}{f^i(f + 2\hat{Z}_T) - g^i(g + 2\hat{Z}_T)} \tag{2.57}$$

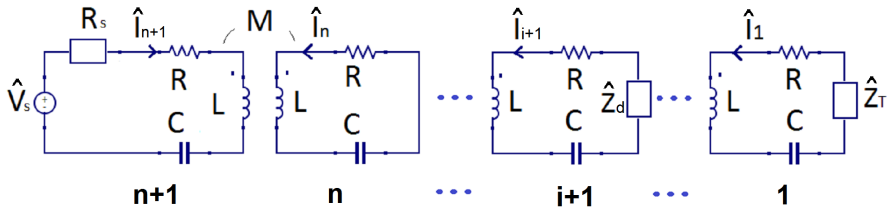

(a)

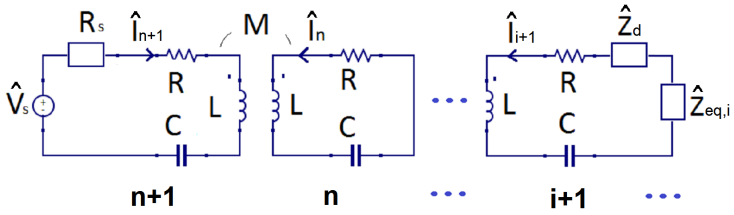

(b)

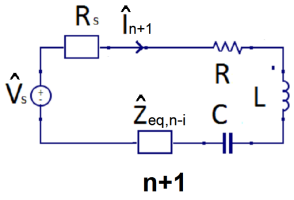

(c)

Figure 2.12: Equivalent circuits of Fig. 2.1 (b), but with the receiver over the $(i+1)$th cell, being (a) the equivalent circuit of the whole resonator array, being (b) $\hat{Z}_{eq,i}$ the equivalent impedance of the i resonators and being (c) $\hat{Z}_{eq,n-i}$ the impedance seen from the supplied cell.

and use as $\hat{Z}_{eq,i}+\hat{Z}_d$ and the new termination impedance for the remaining part of the array, thus:

$$\hat{Z}_{eq,n-i}=\frac{\begin{pmatrix} f^{n-i}(2(\omega M)^2-g(\hat{Z}_d+\hat{Z}_{eq,i})) \\ +g^{n-i}(f(\hat{Z}_d+\hat{Z}_{eq,i})-2(\omega M)^2)\end{pmatrix}}{\begin{pmatrix} f^{n-i}(f+2(\hat{Z}_d+\hat{Z}_{eq,i})) \\ -g^{n-i}(g+2(\hat{Z}_d+\hat{Z}_{eq,i}))\end{pmatrix}}. \tag{2.58}$$

Furthermore, the logic behind (2.57) and (2.58) could also be used to calculate the equivalent impedance for an array of resonators with more than one receiver. Setting the example of an array of $n+1$ resonators with two identical receivers represented by the same equivalent impedance $\hat{Z}_d$ above the $(i+1)$th and $(j+1)$th resonators, with $j>i$, as depicted in Fig. 2.13, we can write:

$$\hat{Z}_{eq,i}=\frac{f^i(2(\omega M)^2-g\hat{Z}_T)+g^i(f\hat{Z}_T-2(\omega M)^2)}{f^i(f+2\hat{Z}_T)-g^i(g+2\hat{Z}_T)}, \tag{2.59}$$

$$\hat{Z}_{eq,j-i}=\frac{\begin{pmatrix} f^{j-i}(2(\omega M)^2-g(\hat{Z}_d+\hat{Z}_{eq,i})) \\ +g^{j-i}(f(\hat{Z}_d+\hat{Z}_{eq,i})-2(\omega M)^2)\end{pmatrix}}{\begin{pmatrix} f^{j-i}(f+2(\hat{Z}_d+\hat{Z}_{eq,i})) \\ -g^{j-i}(g+2(\hat{Z}_d+\hat{Z}_{eq,i}))\end{pmatrix}}, \tag{2.60}$$

and

$$\hat{Z}_{eq,n-j}=\frac{\begin{pmatrix} f^{n-j}(2(\omega M)^2-g(\hat{Z}_d+\hat{Z}_{eq,j-i})) \\ +g^{n-j}(f(\hat{Z}_d+\hat{Z}_{eq,j-i})-2(\omega M)^2)\end{pmatrix}}{\begin{pmatrix} f^{n-j}(f+2(\hat{Z}_d+\hat{Z}_{eq,j-i})) \\ -g^{n-j}(g+2(\hat{Z}_d+\hat{Z}_{eq,j-i}))\end{pmatrix}}. \tag{2.61}$$

Using the same method as in (2.59)-(2.61), it is possible to determine the equivalent impedance if we have more than two receivers over the resonator array. Moreover, it is possible to analyse the case in which the receivers are represented by different impedances, for example, replacing $\hat{Z}_d$ with $\hat{Z}_{d1}$ in (2.60) and $\hat{Z}_d$ with $\hat{Z}_{d2}$ in (2.61), being $\hat{Z}_{d1}\neq\hat{Z}_{d2}$. Note that, as we previously defined in this Chapter that the first cell is the one connected to the termination impedance and the $(n+1)$th is the one connected to the source, we set that the first receiver, represented by $\hat{Z}_{d1}$, is the one nearer to the cell of the array connected to the termination impedance, while the second receiver $\hat{Z}_{d2}$ is the one nearer to the cell of the array connected to the source.

Previously, we considered that the receiver is represented by an impedance $\hat{Z}_d$. However, if we consider that a real receiver is composed by a resonator connected to a given load, we can represent the two receivers, assuming that they are built with identical coils, as different impedances $\hat{Z}_{d1}$ and $\hat{Z}_{d2}$ as in [14, 16, 29]:

$$\hat{Z}_{d1}=\frac{(\omega M_{r,i+1})^2}{\hat{Z}_r+R_{load,1}} \text{ and } \hat{Z}_{d2}=\frac{(\omega M_{r,j+1})^2}{\hat{Z}_r+R_{load,2}} \tag{2.62}$$

where $M_{r,i+1}$ and $M_{r,j+1}$ are the mutual inductances between the two receivers and the cells beneath them, $\hat{Z}_r=R_r+j\omega L_r+1/(j\omega C_r)$ is the impedance of each receiver and R_{load} is a load resistance connected to each receiver, as depicted in Fig. 3.55.

Assuming that the resonant frequency of the receivers is the same of the array cells (i.e. $\omega_{0,r}=$

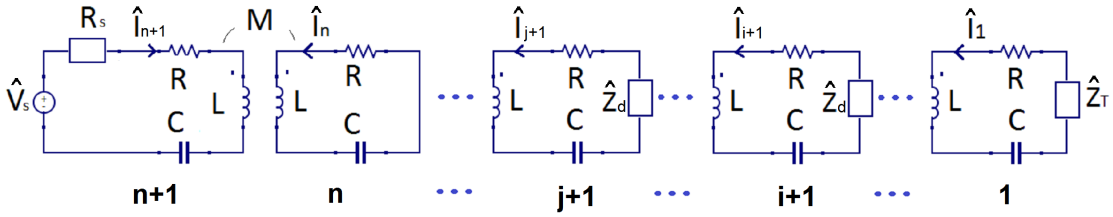

(a)

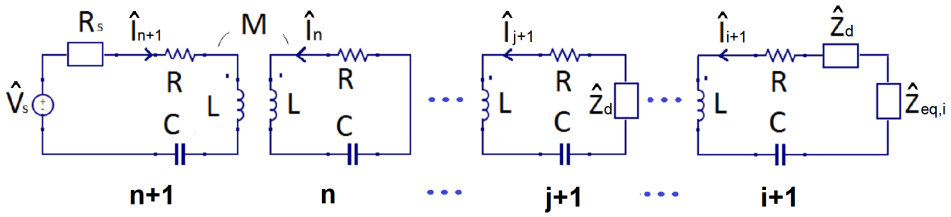

(b)

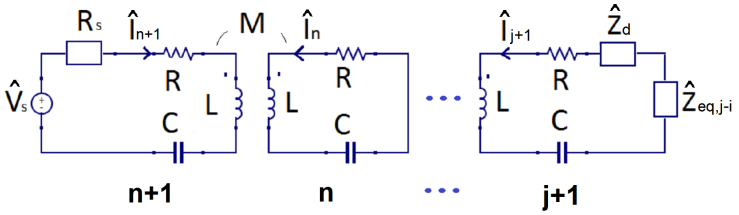

(c)

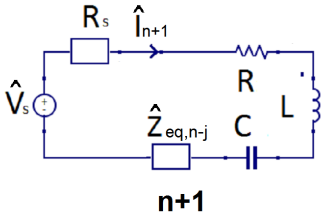

(d)

Figure 2.13: Equivalent circuits of a system composed of n resonators after the cell connected to the voltage source with one receiver over the $(i+1)$th cell and another one over the $(j+1)$th cell.

$1/\sqrt{L_r C_r} = \omega_0 = 1/\sqrt{LC}$), both $\hat{Z}_{d,1}$ and $\hat{Z}_{d,2}$ are real at the resonant frequency of the cells of the array, ω_0 and so their values will depend on the load connected to each receiver and on the mutual inductance between each receiver and the cell below it.

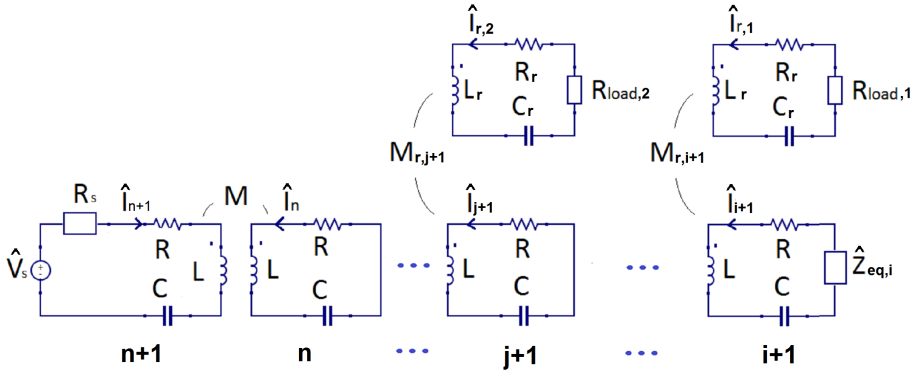

Figure 2.14: Equivalent circuit of Fig. 2.13 (b) including the circuits of the two receivers positioned above the $(i+1)$th and $(j+1)$th cells.

In the following, we perform a numerical example considering a line of 20 resonators with two receivers over the line. Using (2.59)-(2.61), considering that we are operating at the resonator frequency, we can calculate the equivalent impedance seen from the supplied cell of the array, $\hat{Z}_{eq,n-j} = R_{eq,n-j}$, when the receivers are in different positions along the line, for $j > i$, neglecting a possible mutual inductance between the two receivers. In these examples, in order to examine possible real situations, we consider the values acquired through measurements made with the experimental setup referred in Chapter 5 ($L = 12.6\mu$H, $C = 93.1n$F, $R = 0.11\Omega$, $M = -1.55\mu$H and $f_0 = 147$kHz). Supposing that the mutual inductance between the receiver and the cell of the array has the same value as the one between two adjacent cells of the array ($M_{r,i+1} = M_{r,j+1} = 1.55\mu$H) and that the receiver coils are the same as the cells of the array, so ($R_r = R = 0.11\Omega$), the values of $\hat{Z}_{d1}$ and $\hat{Z}_{d2}$ can go from 0Ω (for $R_{load} = \infty$) to 18.6Ω (for $R_{load} = 0\Omega$), depending on the values of $R_{load,1}$ and $R_{load,2}$. Then, we can make an example with $\hat{Z}_T = 1.5\Omega$, assuming different values of $R_{load,1}$ and $R_{load,2}$. For this example we consider three cases, one with $\hat{Z}_{d,1} = \hat{Z}_{d,2} = 5\Omega$, another with $\hat{Z}_{d,1} = \hat{Z}_{d,2} = 10\Omega$ and the last one with $\hat{Z}_{d,1} = 10\Omega$, $\hat{Z}_{d,2} = 5\Omega$ (Figs. 2.15, 2.16 and 2.17).

By examining Figs. 2.15, 2.16 and 2.17 we can note that the equivalent impedance seen from the cell connected to the source has a behaviour similar to that shown in Fig. 2.4, as it oscillates between maximum and minimum values, specially when the receivers are close to the cell connected to the source (position 19). This oscillation becomes more significant when both impedances $\hat{Z}_{d,1}$ and $\hat{Z}_{d,2}$ of the receivers are larger ($\hat{Z}_{d,1} = \hat{Z}_{d,2} = 10\Omega$, Fig. 2.16) and less significant when smaller ($\hat{Z}_{d,1} = \hat{Z}_{d,2} = 5\Omega$, Fig. 2.15), the case depicted in Fig. 2.17 ($\hat{Z}_{d,1} = 10\Omega$, $\hat{Z}_{d,2} = 5\Omega$) being an intermediate case.

It can also be observed that the maximum values of $R_{eq,n-j}$ occur when the second receiver is above the cell connected to the source (position 19) and the first receiver two cells before the last one (position 17), while the minimum values occur when the first and second receivers are in positions 16 and 18, respectively.

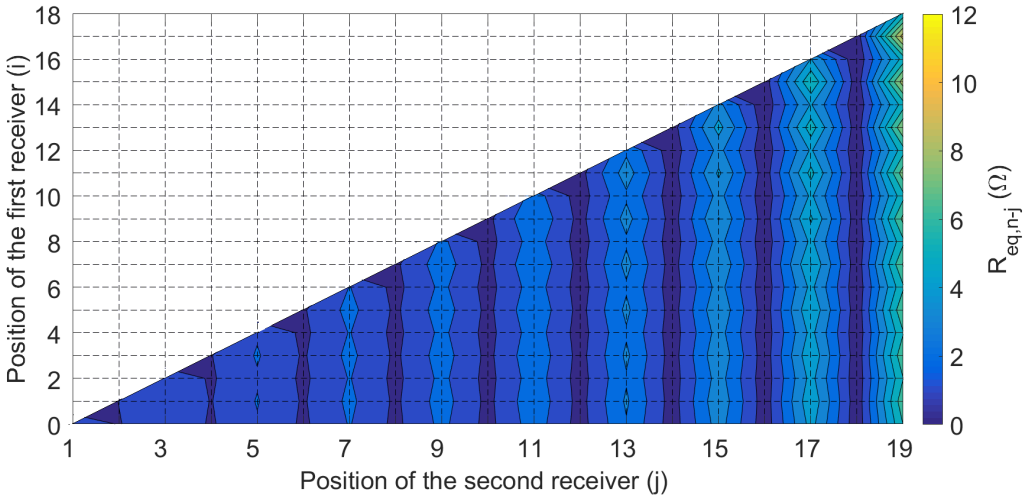

Figure 2.15: $\hat{Z}_{eq,n-j} = R_{eq,n-j}$ for the two receivers in different positions given by i and j (the position 0 being when the receiver is over the first cell and the position 19 when the receiver is over the cell connected to the source) and for $\hat{Z}_{d,1} = \hat{Z}_{d,2} = 5\Omega$.

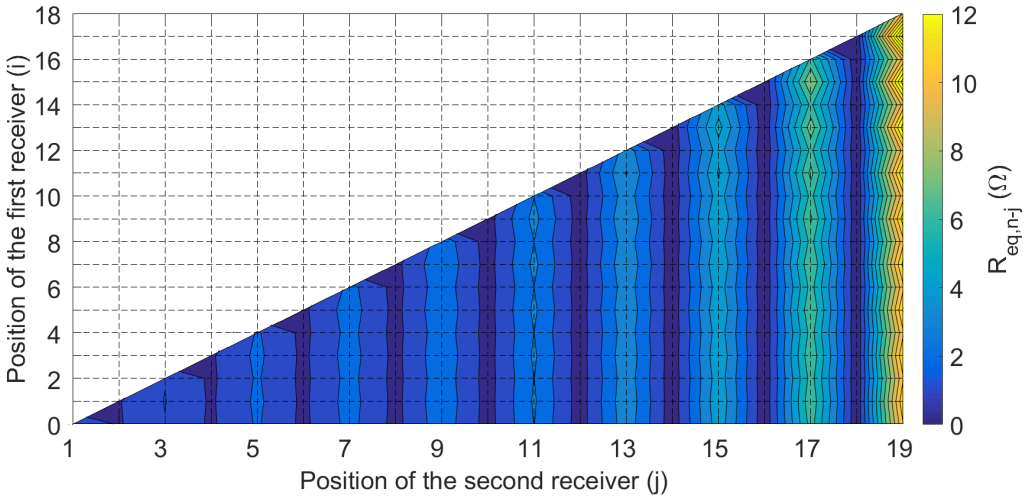

Figure 2.16: $\hat{Z}_{eq,n-j} = R_{eq,n-j}$ for the two receivers in different positions given by i and j (the position 0 being when the receiver is over the first cell and the position 19 when the receiver is over the cell connected to the source) and for $\hat{Z}_{d,1} = \hat{Z}_{d,2} = 10\Omega$.

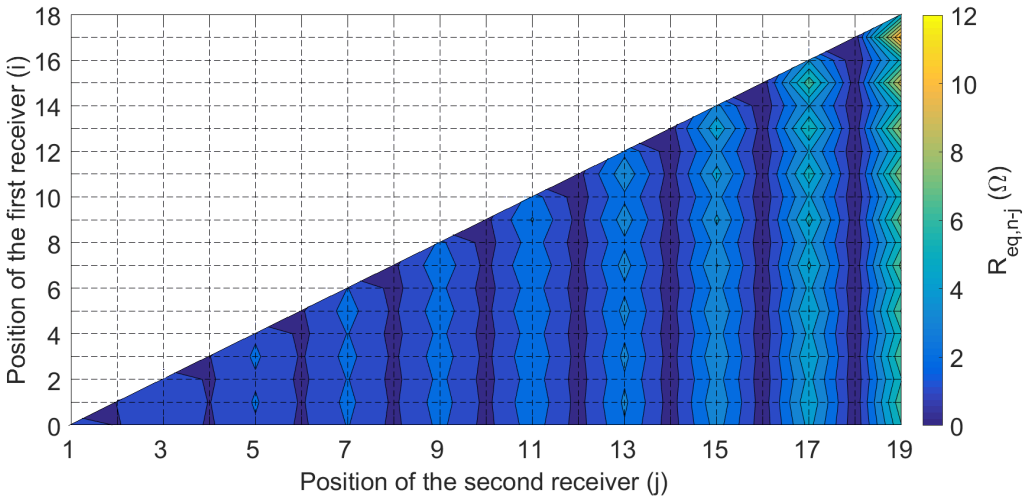

Figure 2.17: $\hat{Z}_{eq,n-j} = R_{eq,n-j}$ for the two receivers in different positions given by i and j (the position 0 being when the receiver is over the first cell and the position 19 when the receiver is over the cell connected to the source) and for $\hat{Z}_{d,1} = 10\Omega$ and $\hat{Z}_{d,2} = 5\Omega$.

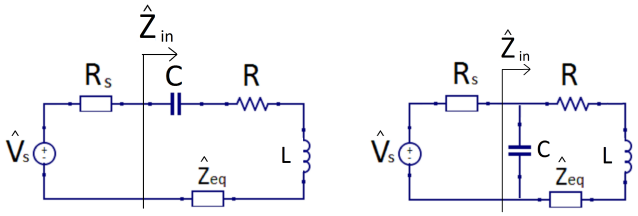

Figure 2.18: Input impedance with the cell connected to the source in (a) series and (b) parallel resonance.

Moreover, for a fixed position of the second receiver, the first receiver in an odd position increases the equivalent impedance and while in an even position it decreases the value of $R_{eq,n-j}$. Also, $R_{eq,n-j}$ will have higher values when the second receiver is on an odd position and low values when in an even position. Generically, we can say that when both receivers are in even positions $R_{eq,n-j}$ has its peak values and when both receivers are in odd positions $R_{eq,n-j}$ has its lower values. On the other hand, by placing the first receiver on a position with different parity of the position of the second receiver (for example, second receiver on an even position, first receiver on an odd position) the oscillation (minima and maxima) of the equivalent impedance is smoothed.

Finally, as both receivers move further away from the source, $R_{eq,n-j}$ tends to be constant and have less variations when the receivers change position. In this case the equivalent impedance $R_{eq,n-j}$ tends to the equivalent impedance of an array with an infinite number of resonators, given by (2.50).

2.4.6 Analysis of the input impedance for series and parallel configuration

As described before, all the resonators of the array are R-L-C circuits which are in series resonance. However, it could be possible for the cell which is connected to the source, to be in series or in parallel resonance, as represented in Fig. 2.18. Then, using the value of $\hat{Z}_{eq}$ obtained in this

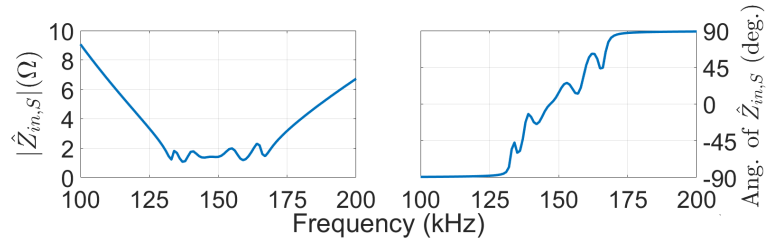

(a)

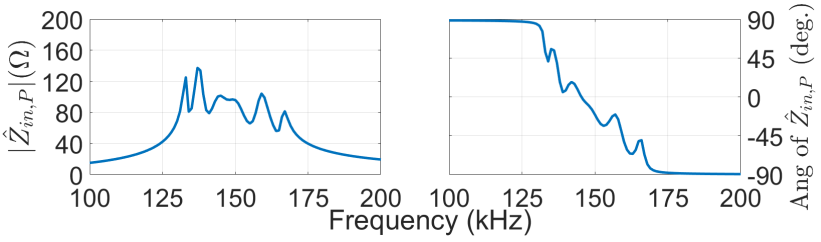

(b)

Figure 2.19: Spectra of the magnitude and phase for the input impedance for (a) series and (b) parallel configurations for a 6-resonator array terminated with $\hat{Z}'_T = 1.5\Omega$.

chapter, we can determine the input impedance $\hat{Z}_{in}$ for the two different resonance topologies as in [19, 30, 31]:

$$\begin{aligned} \hat{Z}_{in,S} &= R + j\omega L + 1/j\omega C + \hat{Z}_{eq} \\ \hat{Z}_{in,P} &= (j\omega C + \tfrac{1}{R+j\omega L+\hat{Z}_{eq}})^{-1} \end{aligned} \tag{2.63}$$

at the angular frequency $\omega = 2\pi f$.

Then, for the two types of resonance, we can plot the amplitude and phase spectra of $\hat{Z}_{in}$ using the values obtained through measurements for the 6-resonator array described in Chapter 5 ($L = 12.6\mu$H, $C = 93.1n$F, $R = 0.11\Omega$, $M = -1.55\mu$H and $f_0 = 147$kHz), considering a termination impedance of $\hat{Z}_T = 1.5\Omega$. The results are presented in Figs. 2.19 and 2.20, for a number of five ($n = 5$) or 7 resonators ($n = 7$) after the supplied cell.

Examining Fig. 2.19, it is possible to observe that the input impedance magnitude is much higher for the parallel configuration, which can be possibly used if the source impedance is large, provided that we want to match the source impedance to the input impedance. Also, that the resonant frequency of the parallel configuration, i.e., the value of the frequency at which the input impedance becomes real, has a slightly lower value than the series resonant frequency.

Moreover, when considering the series configuration, we can note that the magnitude of the input impedance has other minima for frequencies different from the resonant one $f_0 = 147$kHz (approximately 133kHz, 137kHz, 159kHz and 167kHz) and additionally it is limited from about 1.1Ω to 2Ω in the 130kHz to 171kHz range. This frequency range can be related to the bandwidth of transmission referred in [14] and [16], $f_0/\sqrt{1+k} \leq f \leq f_0/\sqrt{1-k}$; for example, in the case considered, having $k = 2M/L = 0.25$, we have a bandwidth $132kHz \leq f \leq 169$kHz.

For the case of an array of 8 resonators, shown in Fig. 2.20, we can see that all the conclusions for the 6-resonators still apply; in this case there are more minima for frequencies different than the resonant one $f_0 = 147$kHz (approximately 136kHz, 141kHz, 154kHz, 161kHz and 168kHz).

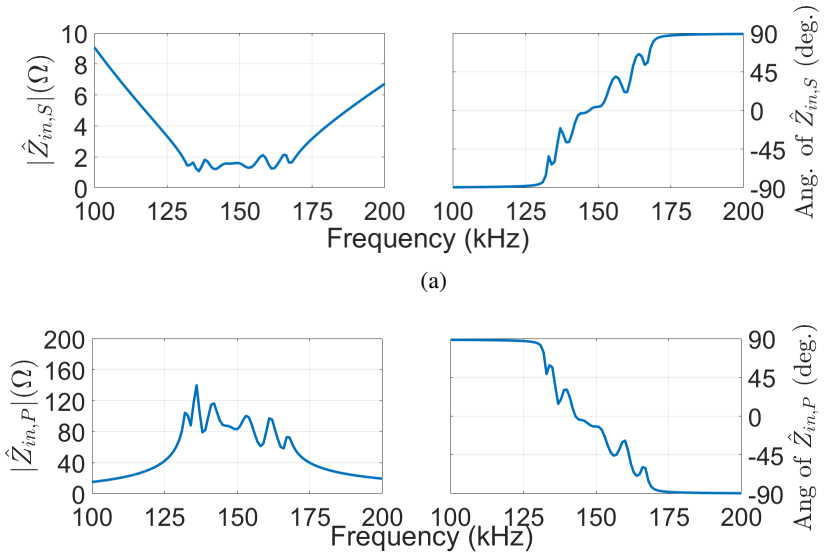

Figure 2.20: Spectra of the magnitude and phase for the input impedance for (a) series and (b) parallel configurations for an 8-resonator array terminated with $\hat{Z}'_T = 1.5\Omega$.

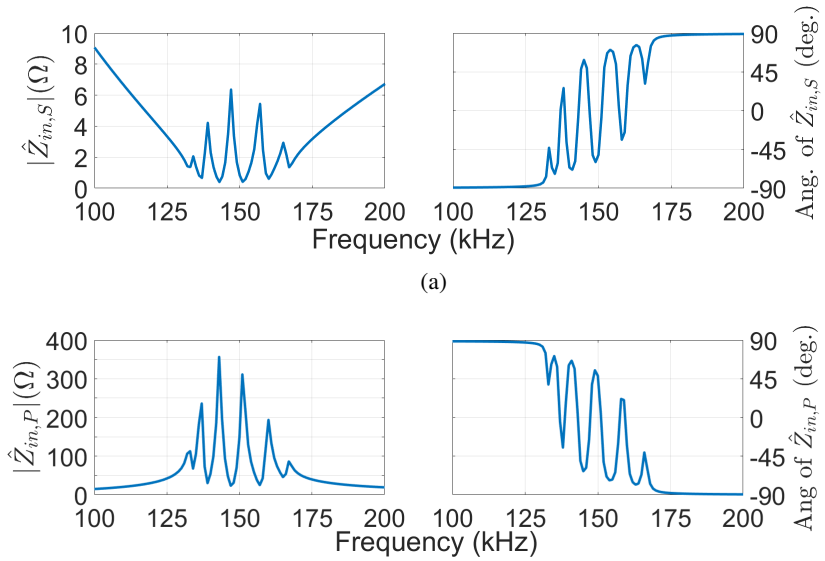

Figure 2.21: Spectra of the magnitude and phase for the input impedance for (a) series and (b) parallel configurations for a 6-resonator array terminated with $\hat{Z}'_T = 0\Omega$.

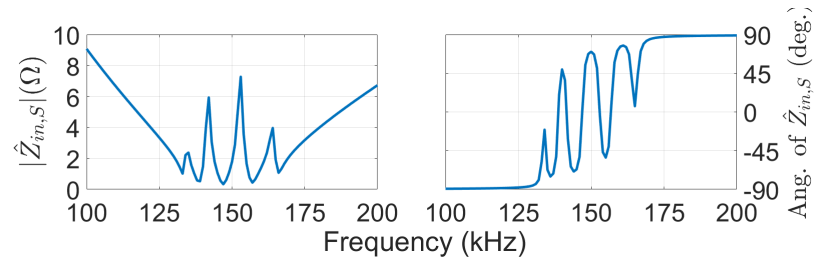

(a)

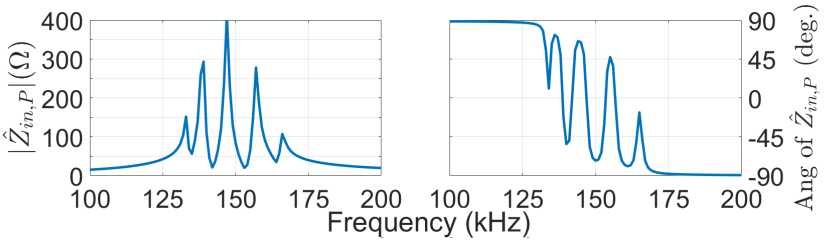

(b)

Figure 2.22: Spectra of the magnitude and phase for the input impedance for (a) series and (b) parallel configurations for an 6-resonator array terminated with $\hat{Z}'_T = 1\text{M}\Omega$.

Still regarding the case of a 6-resonator array, we can further consider the two opposite cases where the array is terminated with $\hat{Z}'_T = 0\Omega$ or $\hat{Z}'_T = 1\text{M}\Omega$ (Figs. 2.21 and 2.22). By comparing the results in Figs. 2.21 and 2.22 with those in Fig. 2.19 we can see that the input impedance has much greater oscillations in both the magnitude and the phase of $\hat{Z}_{in}$, when $\hat{Z}'_T$ gets further away from $\hat{Z}_{eq,\infty}$. Also, due to these larger oscillations on the phase of $\hat{Z}_{in}$ there will be other frequencies for which $\hat{Z}_{in}$ is real.

Eventually, using the theoretical results regarding the convergence of the continued fraction given in subsection 2.4.2, if we want to compare the input impedance for the series or parallel resonance of the cell connected to the source of an array with an infinite number of resonators or an array terminated by $\hat{Z}_{eq,\infty}$ we can write (2.63) replacing $\hat{Z}_{eq}$ by the value given by (2.50):

$$\begin{aligned}\hat{Z}_{in,S,\infty} &= \tfrac{1}{2}\left(R + j\omega L + 1/j\omega C + \sqrt{(R + j\omega L + 1/j\omega C)^2 + 4(\omega M)^2}\right)\\ \hat{Z}_{in,P,\infty} &= \left(j\omega C + \frac{1}{R + j\omega L + \frac{1}{2}\left(-R - j\omega L - 1/j\omega C + \sqrt{(R + j\omega L + 1/j\omega C)^2 + 4(\omega M)^2}\right)}\right)^{-1}\end{aligned} . \tag{2.64}$$

Then, using (2.64), we can plot the amplitude and phase spectra of $\hat{Z}_{in,mat}$ for the series and parallel resonance, using the same electric parameters of the resonator array (Fig. 2.23).

Observing Fig. 2.23, although the conclusions regarding the comparison of the magnitude and the angle for the series and parallel still apply, in this case there will be no oscillations (minima or maxima) in the magnitude and angle of $\hat{Z}_{in}$.

Moreover, rewriting (2.64) at the resonant frequency ω_0 yields:

$$\begin{aligned}\hat{Z}_{in,S,\infty} &= \tfrac{1}{2}\left(R + \sqrt{R^2 + 4(\omega_0 M)^2}\right)\\ \hat{Z}_{in,P,\infty} &= \frac{2L}{C\left(R + \sqrt{4(\omega_0 M)^2 + R^2}\right)} - j\sqrt{\frac{L}{C}}\end{aligned} , \tag{2.65}$$

we can determine the phase angle of $\hat{Z}_{in,P,\infty}$ at f_0, given by:

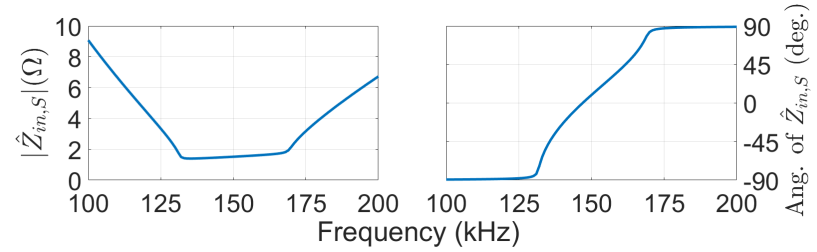

(a)

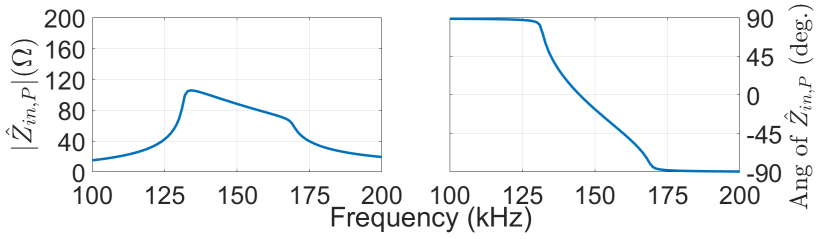

(b)

Figure 2.23: Spectra of the magnitude and phase for the input impedance for (a) series and (b) parallel configurations for array with an infinite number of resonators or terminated by $\hat{Z}'_T = \hat{Z}_{eq,\infty}$.

$$\arg(\hat{Z}_{in,P,\infty}) = \arctan \frac{\left(R + \sqrt{4(\omega_0 M)^2 + R^2}\right)}{2} \sqrt{\frac{C}{L}} \tag{2.66}$$

which for this case is equal to -7.28º.

Furthermore, assuming that the capacitor in the cell connected to the source $(n+1)$ can be different than those in the cells of the array, we can determine its value so that the voltage and the current delivered by the source are in phase, i.e. the imaginary part of the input impedance $\hat{Z}_{in,P,\infty}$ is equal to zero as done in [30] for a two-coil IPT system. Then, by solving

$$\text{Im}\left(\left(j\omega C_{n+1} + \frac{1}{R + j\omega L + \frac{1}{2}\left(-R + \sqrt{R^2 + 4(\omega_0 M)^2}\right)}\right)^{-1}\right) = 0 \tag{2.67}$$

for C_{n+1}, we obtain,

$$C_{n+1} = \frac{2L}{2(\omega_0 L)^2 + R\sqrt{R^2 + 4(\omega_0 M)^2} + 2(\omega_0 M)^2 + R^2}$$

which for this example, becomes $C_{n+1} = 91.2$nF.

2.5 Validation of the theoretical results with Simulink

After the mathematical analysis and the examples performed using the mathematical results, we can verify the validity of the closed-form expressions presented for the equivalent impedance performing simulations using the software Simulink. Then, we can simulate the circuit in Fig. 2.1 of a resonator array with $n+1$ cells considering an ideal voltage source ($R_s = 0$), by building a cir-

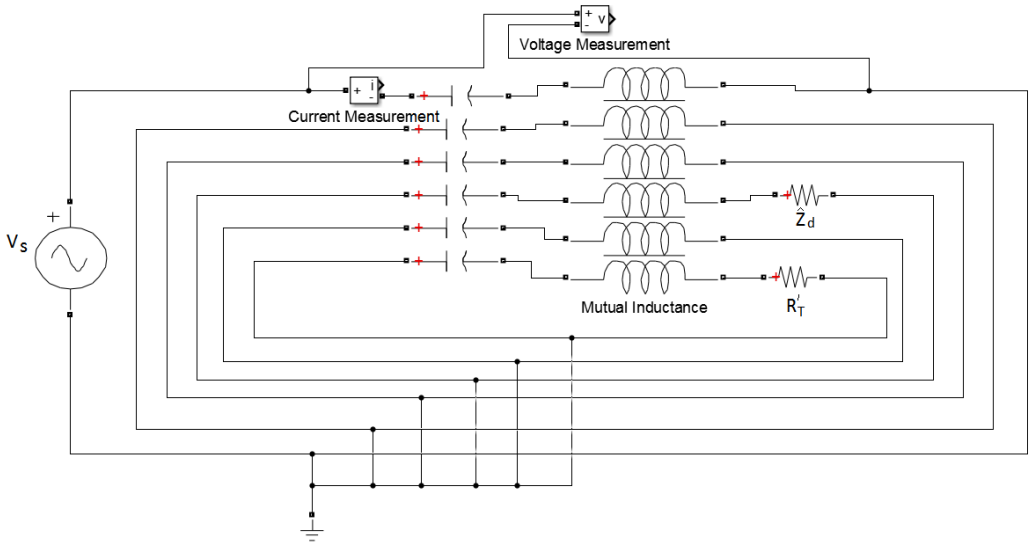

Figure 2.24: Example of a IPT system equivalent circuit simulated with Simulink representing an array with 6 resonators and with the receiver over the 3rd cell.

cuit in Simulink using the Mutual Inductance block. The (n+1)th cell is connected to a sinusoidal voltage source $\hat{V}_s = V_s \angle \theta_v$ at a frequency f. The first cell is connected to a resistance R'_T and an impedance $\hat{Z}_d$ is added to the lth cell in order to represent the effect of the receiver over that cell. An example of the circuit is shown in Fig 2.24. The impedance $\hat{Z}_d$, as in (2.62), is given by:

$$\hat{Z}_d = \frac{(\omega M_{r,l})^2}{\hat{Z} + R_{load}}. \tag{2.68}$$

where $M_{r,l}$ is the mutual inductance between the receiver and the lth cell, R_{load} is a load connected to the receiver which has the same impedance $\hat{Z}$ as the array cells.

Then, by determining with Simulink the current in the cell connected to the given voltage source $\hat{V}_s$, $\hat{I}_{n+1} = I_{n+1} \angle \theta_i$, using the "Current Measurement" block, we can obtain the input impedance $\hat{Z}_{in}$:

$$\hat{Z}_{in} = \frac{\hat{V}_s}{\hat{I}_{n+1}} = \frac{V_s}{I_{n+1}} \angle \theta_v - \theta_i \tag{2.69}$$

and compare this value with the theoretical value for the input impedance calculated using (2.63) for the series resonance case, in which $\hat{Z}_{eq}$ is determined with (2.46)-(2.49):

$$\hat{Z}_{in} = \hat{Z} + \hat{Z}_{eq}. \tag{2.70}$$

In both values of $\hat{Z}_{in}$ presented, obtained with simulations (2.69) and with theoretical results (2.70), the values for R, L, C and M used are the ones obtained through measurements carried out in Chapter 5 ($L = 12.6\mu$H, $C = 93.1n$F, $R = 0.11\Omega$ and $M = -1.55\mu$H).

Table 2.1: Comparison of $\hat{Z}_{in}$ (Ω) at the resonant frequency $f_0 = 147$ kHz obtained through simulations performed with Simulink (2.69) and through developed formulas ((2.70) using (2.48)), for different values of R'_T (0.4Ω, 1.5Ω and 10Ω) and different number of resonators.

Number of resonators $(n+1)$	Equation (2.69)	Equation (2.70)	Equation (2.69)	Equation (2.70)	Equation (2.69)	Equation (2.70)
	$R'_T = 0.4\Omega$		$R'_T = 1.5\Omega$		$R'_T = 10\Omega$	
2	4.1280	4.1287	1.3830	1.3830	0.3128	0.31272
3	0.6066	0.6064	1.5920	1.5920	6.6613	6.6638
4	3.4883	3.4898	1.3974	1.3974	0.4179	0.4176
5	0.6977	0.6973	1.5767	1.5766	5.0141	5.0184
6	3.0471	3.0493	1.4099	1.4010	0.5190	0.5184

Table 2.2: Comparison of $\hat{Z}_{in}$ (Ω) for different frequency values from 135kHz to 165kHz obtained through simulations performed with Simulink (2.69) and through developed formulas ((2.70) using (2.46)) for a 6-resonator array ($n = 5$) terminated with $\hat{Z}'_T = 1.5\Omega$.

f(kHz)	Equation (2.69)	Equation (2.70)
135	1.67$\angle$-59.69	1.67$\angle$-59.69
140	1.75$\angle$-15.60	1.74$\angle$-15.60
145	1.35$\angle$-8.75	1.35$\angle$-8.75
150	1.40$\angle$13.82	1.40$\angle$13.82
155	1.98$\angle$18.79	1.98$\angle$18.78
160	1.25$\angle$47.92	1.25$\angle$47.92
165	2.19$\angle$43.69	2.19$\angle$43.68

2.5.1 Equivalent impedance without a receiver over the resonator line or with a receiver over the first cell of the resonator line

Starting by considering an array with 2 to 6 resonators in which the receiver is over the first cell or is absent, from (2.70) with $\hat{Z}_{eq}$ being calculated from (2.46) (with $n = 1,\ldots,5$) we determine $\hat{Z}_{in}$ for different values of $\hat{Z}'_T$. Then, with Simulink, we use the circuit depicted in Fig. 2.24 where $\hat{Z}_d = 0$. For the case where we operate at the resonant frequency $f_0 = 147$ kHz, we can obtain $\hat{Z}_{in}$ with (2.69) or (2.70) for different values of $\hat{Z}'_T = R'_T$. The results of the comparison are reported in Table 2.1.

Eventually, if we operate at a frequency different than the resonant one, $\hat{Z}_{in}$ becomes a complex quantity. By setting a fixed value of $\hat{Z}'_T = 1.5\Omega$ for an array with 6 resonators ($n = 5$) we can make a comparison of $\hat{Z}_{in}$ obtained with simulations performed with Simulink (2.69) and with developed formulas ((2.70) using (2.48)) and report the results in Table 2.2 for different operating frequencies. As an example, for this case we can represent the voltage and current waveforms obtained with simulations at the frequency of 165kHz (Fig. 2.25).

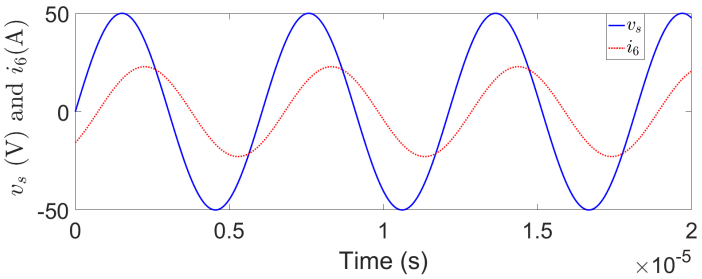

Figure 2.25: Instantaneous values of voltage and current obtained with Simulink for a 6 resonator array terminated with $\hat{Z}'_T = 1.5\Omega$ at $f = 165$kHz.

Table 2.3: Comparison of $\hat{Z}_{in}$ (Ω) determined at the resonant frequency $f_0 = 147$ kHz obtained through simulations performed with Simulink (2.69) and through developed formulas ((2.70) using (2.49)) for different positions of the receiver (i) for a 6-resonator array ($n = 5$) terminated with $R'_T = 1.5\Omega$.

Position of the receiver (ith cell)	Equation (2.69)	Equation (2.70)
1	0.6171	0.6166
2	3.9651	3.9672
3	0.5219	0.5216
4	4.8712	4.8723
5	0.4217	0.4216

2.5.2 Equivalent impedance with a receiver over the resonator line at any position

Next, analysing the case where there is a receiver over the lth cell of the resonator array, in resonance condition, we can calculate $\hat{Z}_{in}$ from (2.70) using (2.49). This is done by using the values of R, L, C and M indicated previously, given an array of 6 resonators ($n = 5$) terminated with $R'_T = 1.5\Omega$ and assuming $M_{r,l} = 1.55\mu$H and $R_{load} = 0.30\Omega$, which from (2.68) makes $\hat{Z}_d = 5\Omega$. The results for different positions of the receiver achieved with (2.70) using (2.49) are compared with the ones determined through simulations (2.69) and shown in Table 2.3. Note that the value of $\hat{Z}_d$ is real at the resonance frequency, because we assumed that the receiver has the same impedance as the cells of the array.

For a frequency different than the resonant one, both $\hat{Z}_{eq}$ (2.47) and $\hat{Z}_d$ (2.68) become complex. Then, terminating the array with a fixed value of $\hat{Z}'_T = 1.5\Omega$ and keeping all the other parameters as in the previous case, we can calculate the equivalent impedance for different values of the operating frequency and for the receiver at a given position. For example, in Table 2.4 the comparison between (2.69) and (2.70) is shown, for a receiver over the third resonator in a 6-resonator array, where (2.70) was calculated from (2.47) with $n = 5$ and $l = 3$.

2.5.3 Convergence of the equivalent impedance

Finally, we can also verify the theoretical results achieved regarding the convergence of the continued fraction that represents the equivalent impedance of a resonator array. As described in

Table 2.4: Comparison of $\hat{Z}_{in}$ (Ω) determined for different frequency values (from 135kHz to 165kHz) obtained through simulations performed with Simulink (2.69) and through developed formulas ((2.70) using (2.47)) when the receiver is over the third cell ($i = 3$) in a 6-resonator array ($n = 5$) terminated with $\hat{Z}'_T = 1.5\Omega$.

f(kHz)	Equation (2.69)	Equation (2.70)
135	1.13∠-68.33	1.14∠-67.94
140	3.03∠-7.01	3.09∠-7.58
145	0.99∠-49.48	0.98∠-49.48
150	1.42∠54.15	1.44∠54.56
155	3.44∠9.31	3.47∠9.16
160	0.78∠29.45	0.78∠29.40
165	1.92∠75.43	1.91∠74.94

Table 2.5: Comparison of $\hat{Z}_{in}$ (Ω) at the operating frequency $f = 165$kHz obtained through simulations performed with Simulink ((2.69)) and through developed formulas ((2.70) using (2.46)) for an array with 10, 20 and 30 resonators ($n = 9$, $n = 19$ and $n = 29$) and for different values of $\hat{Z}'_T$.

	Equation (2.69)		
Number of resonators $(n+1)$	10	20	30
$\hat{Z}'_T = 0.4\Omega$	1.48∠44.55	1.60∠57.10	1.70∠57.92
$\hat{Z}'_T = \frac{-\hat{Z}+\sqrt{\hat{Z}^2+4(\omega M)^2}}{2}$	1.71∠57.03	1.71∠57.04	1.71∠57.03
$\hat{Z}'_T = 10\Omega$	1.31∠59.70	1.65∠60.77	1.73∠58.16
	Equation (2.70)		
Number of resonators $(n+1)$	10	20	30
$\hat{Z}'_T = 0.4\Omega$	1.48∠44.56	1.60∠57.10	1.70∠57.93
$\hat{Z}'_T = \frac{-\hat{Z}+\sqrt{\hat{Z}^2+4(\omega M)^2}}{2}$	1.71∠57.05	1.71∠57.05	1.71∠57.05
$\hat{Z}'_T = 10\Omega$	1.31∠59.68	1.65∠60.78	1.73∠58.16

subsection 2.4.2, setting $\hat{Z}'_T = \hat{Z}_{eq,\infty} = \frac{1}{2}\left(-\hat{Z}+\sqrt{\hat{Z}^2+4(\omega M)^2}\right)$ into (2.46) (for any frequency different than the resonant one) or $R'_T = R_{eq,\infty} = \frac{1}{2}\left(-R+\sqrt{R^2+4(\omega_0 M)^2}\right)$ into (2.48) (for the resonant frequency) the equivalent impedance $\hat{Z}_{eq}$ is constant and equal to $\hat{Z}_{eq,\infty}$ (or $R_{eq,\infty}$) regardless of the number of resonator cells. Then, we can use the Mutual Inductance Simulink block to represent an array with an increasing number of resonators, e.g., 10, 20 and 30 ($n = 9$, $n = 19$ and $n = 29$). Once again, the input impedance (2.70) calculated using (2.46) or (2.48) is compared to the input impedance (2.69) determined with Simulink, for different termination impedances. The results of the comparison for a frequency different than the resonant one ($f = 165$kHz) and for the resonant frequency $f_0 = 147$ kHz are shown in Tables 2.5 and 2.6, respectively.

Moreover, as seen in Tables 2.5 and 2.6, the results confirm what was demonstrated in the theoretical study about the convergence of the continued fraction in subsection 2.3.3, i.e., that $\hat{Z}_{eq}$ tends to $\hat{Z}_{eq,\infty}$ (or $R_{eq,\infty}$) as the number of the resonators increases, meaning that (2.70) tends to $\hat{Z}_{in} = \hat{Z} + \hat{Z}_{eq,\infty}$ at any frequency other than the resonant one and $\hat{Z}_{in} = R + R_{eq,\infty}$ at the resonant frequency.

Table 2.6: Comparison of $\hat{Z}_{in}$ (Ω) at the resonant frequency $f_0 = 147$ kHz obtained through simulations performed with Simulink ((2.69)) with the one obtained through developed formulas ((2.70) using (2.48)) for an array with 10, 20 and 30 ($n = 9$, $n = 19$ and $n = 29$) resonators and for different values of R'_T.

	Equation (2.69)		
Number of resonators $(n+1)$	10	20	30
$R'_T = 0.4\Omega$	2.4885	1.8763	1.6542
$R'_T = \frac{-R+\sqrt{R^2+4(\omega_0 M)^2}}{2}$	1.4876	1.4876	1.4876
$R'_T = 10\Omega$	0.7060	1.0647	1.2762
	Equation (2.70)		
Number of resonators $(n+1)$	10	20	30
$R'_T = 0.4\Omega$	2.4914	1.8797	1.6571
$R'_T = \frac{-R+\sqrt{R^2+4(\omega_0 M)^2}}{2}$	1.4876	1.4876	1.4876
$R'_T = 10\Omega$	0.7048	1.0622	1.2732

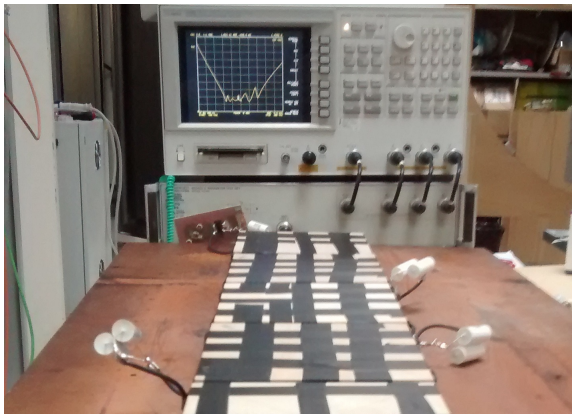

Figure 2.26: Array of resonators connected to a VNA for the measurement of the input impedance.

2.6 Experimental validation of the theoretical results

Following the verification of the theoretical results presented in this chapter through Simulink, we can also perform an experimental verification, with the experimental setup described in Chapter 5 which uses the stranded-wire 6-resonator array. The input impedance of the resonator array is measured by connecting it to an Agilent 4396B 100 kHz - 1.8 GHz Vector Network Analyser (VNA), as shown in Fig. 2.26.

Subsequently, as done as in the previous subsection, the experimental results are then compared with the theoretical values obtained with (2.70).

2.6.1 Equivalent impedance without a receiver over the resonator line or with the receiver over the first cell of the resonator line

Firstly, considering an array with 2 to 6 resonators, from (2.48) with $n = 1,\ldots,5$, and (2.70), we calculate $\hat{Z}_{in}$ at the resonant frequency $f_0 = 147$kHz for different values of R'_T (0.4Ω, 1.5Ω and 10Ω). These results are then compared with the input impedance obtained with measurements with the VNA under the same conditions of the system. The comparison is shown in Fig. 2.27. It can be noticed that the 1.5Ω curve tends to the value $R + R_{eq,\infty}$with much smaller oscillations than

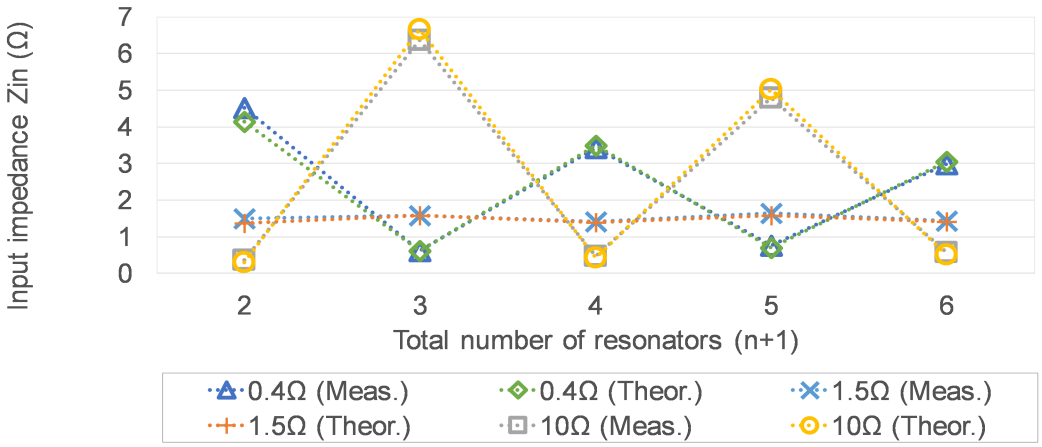

Figure 2.27: Comparison of $\hat{Z}_{in}$ (Ω) measured with the VNA to that calculated through developed formulas ((2.70) using (2.48)) for different values of R'_T (0.4Ω, 1.5Ω and 10Ω) and different number of resonators, at the resonant frequency $f_0 = 147$ kHz.

Table 2.7: Comparison of $\hat{Z}_{in}\,(\Omega)$ measured with the VNA to that calculated through developed formulas (2.70 using (2.48)) for a given value of $\hat{Z}'_T = 1.5\Omega$, for different frequency values from 135kHz to 160kHz.

f(kHz)	Equation (2.73)	Equation (2.70)
135	1.78∠-55	1.67∠-60
140	1.62∠-22	1.74∠-16
145	1.35∠-2	1.35∠-9
150	1.48∠19	1.40∠14
155	2.32∠24	1.98∠19
160	1.26∠36	1.25∠48

the other two cases. In fact, $R'_T = 1.5\Omega$ is the closest value to the resistance value $R_{eq,\infty} = 1.38\Omega$, which makes the equivalent impedance constant, confirming the theoretical results indicated in subsections 2.3.3 and 2.4.2.

At a frequency different than the resonant one, $\hat{Z}_{in}$ is a complex quantity. As an example, the results are reported in Table 2.7 for $\hat{Z}'_T = 1.5\Omega$.

2.6.2 Equivalent impedance with a receiver over the resonator line at any position

In case there is a receiver over the lth cell of resonator array, we can calculate $\hat{Z}_{in}$ in resonance conditions from (2.49) and (2.70). For an array of 6 resonators with the parameter values of R, L, C and M indicated in section 2.5.2, the results for different positions of the receiver are shown in Fig. 2.28. In the experimental setup, we connected a 5Ω resistor to the lth cell to represent the additional impedance $\hat{Z}_d$.

2.6.3 Determination of the input power using the equivalent impedance

As referred in the Introduction of this chapter, the value of equivalent impedance could be used, for a given voltage source, to determine the power delivered from the source to a loaded array. Then,

Figure 2.28: Comparison of $\hat{Z}_{in}$ (Ω) measured with the VNA to that calculated through (2.70) using (2.49) for different positions of the receiver, at the resonant frequency $f_0 = 147$ kHz.

assuming that we are working at the resonant frequency, the power delivered from a sinusoidal voltage source with a given RMS value V_s can be given by:

$$P_{in} = \frac{V_s^2}{R_{eq} + R} \tag{2.71}$$

where R_{eq} is determined with (2.48) or with (2.49). Then, through measurements, the input power is obtained as the average value in a period of the product of the instantaneous voltage and current measured at the terminals of the inverter:

$$P_{in,exp} = (1/T) \int_0^T v_{in}(t)\, i_{in}(t) \mathrm{dt} \tag{2.72}$$

where $T = 1/f_0$ is the period of the waveforms and $v_{in}(t)$ and $i_{in}(t)$ are the measured instantaneous values of the input voltage and current. The product of the instantaneous voltage and current and its average value in a period were calculated with the oscilloscope using the mathematical functions of its internal software.

Finally, setting in (2.71) $V_s = V_{s1} = 4.9V$ with V_{s1}, experimentally determined as in [32] :

$$V_{s1} = \frac{4}{\pi\sqrt{2}} V_{sq} \tag{2.73}$$

where V_{s1} is the RMS of fundamental component of the inverter output square-wave v_{in}, V_{sq} is the measured amplitude value of the square wave, whose duty cycle is assumed to be 0.5.

Then, we can compare the values calculated with theoretical formula (2.71) with the experimental ones obtained with (2.72). This is done first considering an array of 6 resonators terminated with different values of R'_T (0.4Ω, 1.5Ω, 5Ω and 10Ω) and then an array of 6 resonators terminated with $R'_T = 1.5\Omega$ with a receiver in different positions (i). The results of these two comparisons are presented in Figs. 2.29 and 2.30.

Figures 2.29 and 2.30 show that, for a given voltage source, the power delivered by the source increases in an a 6-resonator array for an increasing value of R'_T and that, for a fixed R'_T, the power delivered by the source has large oscillations depending on the position of the receiver. These

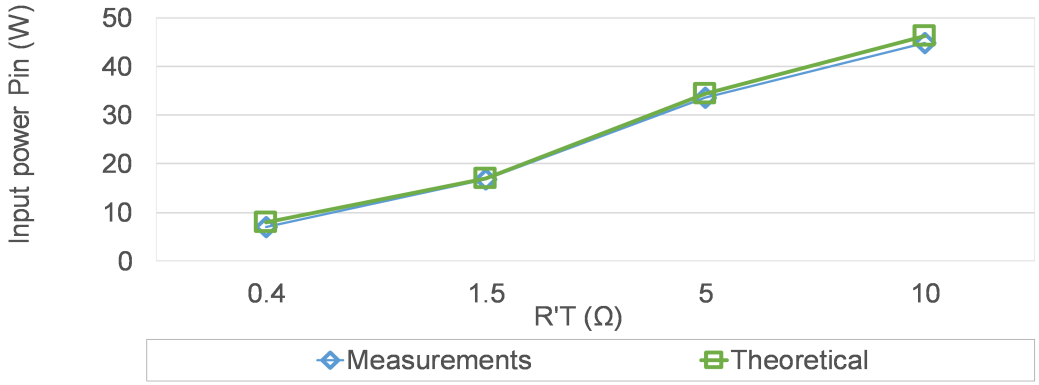

Figure 2.29: Comparison of $P_{in}\ (W)$ at the resonant frequency $f_0 = 147$ kHz obtained with measurements using (2.72) to the one calculated through developed formulas ((2.71) using $V_s = 4.9V$ determined with (2.73) and (2.49)) for different values of R'_T (0.4Ω, 1.5Ω, 5Ω and 10Ω).

Figure 2.30: Comparison of $P_{in}\ (W)$ at the resonant frequency $f_0 = 147$ kHz obtained with measurements using (2.72) to the one calculated through developed formulas ((2.71) using $V_s = 4.9V$ determined with (2.73) and (2.49)) for different positions of the receiver (i).

examples show some of possible practical applications of this study of the equivalent impedance on determining and predicting the input power (and thus the input current) delivered from a given voltage source to the resonator array for varying conditions of the system (variable R'_T or variable position i) which can be useful for the design of the array and its power source.

2.7 Conclusions

In this chapter, a mathematical approach is applied to the study of the equivalent impedance of a resonator array, which is usually represented in literature by a continued fraction, in order to achieve a more complete and rigorous understanding of the behaviour of this type of systems. By applying the theory of linear homogeneous difference equations, the general term of the recursive sequence that represents the continued fraction is obtained. In this way, an explicit closed-form expression for the equivalent impedance is developed, which depends on the characteristics of the system (electrical parameters of the resonator array, termination impedance, number of resonators, position and impedance of receivers). Furthermore, by performing an analysis on convergence of the continued fraction, it is found that for an arbitrarily large number of resonators, the equivalent impedance is given only by the electrical parameters of the resonator array, $\hat{Z}$ and ωM, and that it does not depend on the termination impedance, $\hat{Z}'_T$, and on a finite number of receivers over the line ($\hat{Z}_{eq,\infty} = \frac{1}{2}\left(-\hat{Z} + \sqrt{\hat{Z}^2 + 4\left(\omega M\right)^2}\right)$). Additionally, it is demonstrated that by terminating the resonator array with this impedance $\hat{Z}_{eq,\infty}$, the impedance of the resonator array is constant for any number of resonators. Regarding the monotonicity of the continued fractions, it is also proved that the recursive sequence that describes the system has an oscillating behaviour, having the even and odd terms of the sequence opposite monotonicities (increasing or decreasing), depending on whether the termination impedance is smaller or larger than $\hat{Z}_{eq,\infty}$.

Eventually, in order to illustrate the theoretical results obtained in this chapter, some examples of equivalent impedance calculation for different system configurations are provided, and the calculations are carried out with computing environments such as MATLAB and Mathematica. Besides the examples presented for a resonator array with a receiver over the first cell (or an array without receiver) and for a receiver over the lth cell using the proposed formulas, it is also taken into consideration a resonator array with two receivers over it and it is analysed the case in which the cell connected to the power source is in series or in parallel resonance. Concerning the examples with one receiver or two receivers over the array the effect of the receivers on the equivalent impedance of a resonator array is felt with higher or lower intensity (by increasing or decreasing the equivalent impedance) depending on the position of the receiver and on the value of its impedance; more specifically, for the case with two receivers, the first receiver can further increase or decrease the receivers effect on the equivalent impedance depending on whether it is on the parity of the position of both receivers (even or odd). Regarding the comparison between the input impedance for series or parallel resonance, the parallel resonance produces a higher input impedance but with a phase angle different than zero at the resonant frequency of the cells of the array, while for the series resonance, other minima for the input impedance are found besides the one at the resonant frequency.

In the last part of this chapter, the theoretical formulas are validated with circuit simulations

using the software Simulink and experiments using the setup described in Chapter 5. The comparison of the proposed formulas with simulations and measurements shows a very good agreement. Moreover, by measuring the power delivered from the source to the array and comparing it to the one calculated with the proposed formulas, a possible practical application for this formula is shown.

In summary, the mathematical approach developed in this chapter gives a rigorous theoretical basis that can be used as a powerful tool for designing resonator arrays with given properties and behaviour. More specifically, it can be used to design the power source that supplies the resonator array, since the current and active power delivered by a given voltage source (fixed or variable) can be predicted accurately by knowing the equivalent impedance and its possible variations.

Appendix A

Determination of the constants $a_{1,}$, a_2, b_1, $c_{1,}$, c_2, d_1, d_2 :

$a_1 = \frac{x_0}{2} - \frac{a}{\sqrt{b^2+4a}} + \frac{bx_0}{2\sqrt{b^2+4a}}$; $a_2 = \frac{x_0}{2} + \frac{a}{\sqrt{b^2+4a}} - \frac{bx_0}{2\sqrt{b^2+4a}}$;
$b_1 = \frac{1}{2} - \frac{x_0}{\sqrt{b^2+4a}} - \frac{b}{2\sqrt{b^2+4a}}$; $b_2 = \frac{1}{2} + \frac{x_0}{\sqrt{b^2+4a}} + \frac{b}{2\sqrt{b^2+4a}}$;
$c_1 = \frac{y_0}{2} - \frac{a}{\sqrt{b^2+4a}} + \frac{y_0 b}{2\sqrt{b^2+4a}}$; $c_2 = \frac{y_0}{2} + \frac{a}{\sqrt{b^2+4a}} - \frac{y_0 b}{2\sqrt{b^2+4a}}$;
$d_1 = \frac{1}{2} - \frac{y_0}{\sqrt{b^2+4a}} - \frac{b}{2\sqrt{b^2+4a}}$; $d_2 = \frac{1}{2} + \frac{y_0}{\sqrt{b^2+4a}} + \frac{b}{2\sqrt{b^2+4a}}$.

Constants determined for the value of the fraction:

$e_1 = \hat{Z}_d\left(2(\omega M)^2 - f\hat{Z}_T\right)$;
$e_2 = \hat{Z}_d\left(2(\omega M)^2 - g\hat{Z}_T\right)$;
$e_3 = g\left(\hat{Z} - \hat{Z}_d\right)\hat{Z}_T + 2(\omega M)^2\left(-h + \hat{Z}_d + 2\hat{Z}_T\right)$;
$e_4 = f\left(\hat{Z} - \hat{Z}_d\right)\hat{Z}_T + 2(\omega M)^2\left(h + \hat{Z}_d + 2\hat{Z}_T\right)$;
$e_5 = (\omega M)^2\left(4(\omega M)^2 + f\left(\hat{Z} + \hat{Z}_d\right) + 2\left(-h + \hat{Z}_d\right)\hat{Z}_T\right)$;
$e_6 = \hat{Z}_d\left(f\hat{Z}\hat{Z}_T + (\omega M)^2\left(-f + 2\hat{Z}_T\right)\right)$;
$e_7 = \hat{Z}_d\left(g\hat{Z}\hat{Z}_T - (\omega M)^2\left(g - 2\hat{Z}_T\right)\right)$;
$e_8 = (\omega M)^2\left(4(\omega M)^2 + g\left(\hat{Z} + \hat{Z}_d\right) + 2\left(h + \hat{Z}_d\right)\hat{Z}_T\right)$;
$h = \sqrt{\hat{Z}^2 + 4(\omega M)^2}$.

Note: for (2.48) and (2.49), $\hat{Z}$, $\hat{Z}_T$ and $\hat{Z}_d$ are replaced by R, R_T and R_d, respectively.

3 Mathematical Modelling of the Impedance Matrix

3.1 Introduction

In chapter 2 we performed a study on the equivalent impedance of a resonator array, which is usually expressed by a continued fraction. Expressing the continued fraction as a recursive sequence, we could obtain a closed-form formula using the theory of linear difference equations. The study of the equivalent impedance of a resonator array allows one not only to have a better insight on the behaviour of the system, but also to analyse the power delivered by the source to the array and its variation with the change of the parameters of the system (electrical parameters of the array, total number of resonators of the array, termination impedance, receiver impedance, position of the receiver).

However, the study of the equivalent impedance does not allow one to determine the power absorbed by a load at the end of the array or by a receiver sliding over the array; consequently, it does not allow to calculate the efficiency of the system, taking into account the power delivered by the source to the loaded array of resonators. In literature, the power delivered to a load or a receiver is determined by the use of magnetoinductive wave theory [16] or by obtaining the currents in the resonators through the numerical inversion of the impedance matrix [14]. Methods based on the magnetoinductive wave theory consider the resonator array as a transmission line and thus a clear insight of the behaviour of the resonator array as a circuit cannot be obtained, especially if one tries to predict the behaviour of the system with the changes of its electrical parameters and in the presence of one or two receivers over the coil. Moreover, methods that resort to the numerical inversion of the impedance matrix have the disadvantage of allowing the calculation of the power delivered to a receiver or a load only for specific situations.

In order to obtain a better insight of the system and predict its behaviour even with the variation of its parameters, this chapter presents an analytical analysis of the circuit that represents an array of resonators. Through the mathematical inversion of a tridiagonal matrix, one obtains closed-formulas for the current in each resonator. With the current values, the power supplied by the power source and delivered to a load or receiver, and hence the total efficiency of the system, can be obtained. Moreover, using the formulas obtained in this chapter, the maximum values of efficiency and power absorbed by a load or a receiver for different situations can be obtained. Afterwards, some examples are made with the formulas obtained in this work in order to illustrate the theoretical results obtained. Finally, using Simulink as a circuit simulator and using the experimental setup described in chapter 5, a verification of the obtained formulas is performed along with examples of applications of the theoretical results.

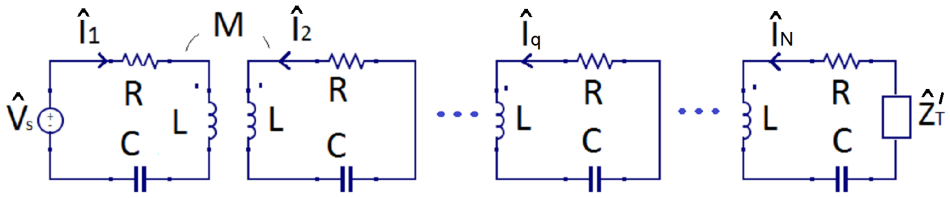

Figure 3.1: Equivalent circuit of an array of resonators represented by (3.5).

3.2 Description of the circuit: cases of study

In this section, we describe the circuit considered and present the relevant cases in order to analyse the power transmission using a resonator array.

Taking as an example a generic circuit composed of a resonator array with N resonators connected to a termination impedance $\hat{Z}'_T$, the equations that describe this system can be written in matrix form as:

$$\hat{\mathbf{V}} = \hat{\mathbf{Z}}_\mathbf{m}\hat{\mathbf{I}} \tag{3.1}$$

with

$$\hat{\mathbf{V}} = [\hat{V}_s, 0..., 0]^T \tag{3.2}$$

being the current vector represented by

$$\hat{\mathbf{I}} = [\hat{I}_1, ..., \hat{I}_q, ..., \hat{I}_N]^T, \tag{3.3}$$

and the impedance matrix [14, 23] by:

$$\hat{\mathbf{Z}}_\mathbf{m} = \begin{bmatrix} \hat{Z}_1 & j\omega M_{12} & ... & j\omega M_{1N} \\ j\omega M_{21} & \hat{Z}_2 & ... & j\omega M_{2N} \\ \vdots & \vdots & \ddots & \vdots \\ j\omega M_{N1} & j\omega M_{N2} & ... & \hat{Z}_N + \hat{Z}'_T \end{bmatrix}. \tag{3.4}$$

Then, as represented in Fig. 3.1, assuming that the mutual inductance between adjacent resonators is given by M whereas the one between non adjacent resonators is neglected, and that all the resonators are identical with impedance given by $\hat{Z} = R + j\omega L + 1/(j\omega C)$, being $\omega = 2\pi f$ the angular frequency, the matrix $\hat{\mathbf{Z}}_\mathbf{m}$ takes the following form:

$$\hat{\mathbf{Z}}_\mathbf{m} = \begin{bmatrix} \hat{Z} & j\omega M & ... & 0 \\ j\omega M & \hat{Z} & ... & 0 \\ \vdots & \vdots & \ddots & j\omega M \\ 0 & 0 & j\omega M & \hat{Z} + \hat{Z}'_T \end{bmatrix}. \tag{3.5}$$

Then, if we want the values of the current vector, i.e. the current flowing in each resonator, we need to determine the inverse matrix $\hat{\mathbf{Z}}_\mathbf{m}^{-1}$:

$$\hat{\mathbf{I}} = \hat{\mathbf{Z}}_{\mathbf{m}}^{-\mathbf{1}}\hat{\mathbf{V}}. \tag{3.6}$$

Considering a fixed voltage vector given by (3.2) we can obtain the values of the currents by knowing the first column of the inverse of the impedance matrix ($\hat{\mathbf{Z}}_{\mathbf{m}(\mathbf{1},\mathbf{1})}^{-\mathbf{1}},...,\hat{\mathbf{Z}}_{\mathbf{m}(\mathbf{N},\mathbf{1})}^{-\mathbf{1}}$). By determining the current in each resonator one can determine also the power transmitted to a certain load or receiver and efficiency of the system, as it will be demonstrated later in this chapter.

Then, as (3.5) shows, the elements of the sub-diagonals of the impedance matrix are identical and equal to $j\omega M$. However, the elements in the main diagonal are not all equal to $\hat{Z}$, as there are one or two elements that are different, depending on whether there is a load, or one or two receivers over the line. In this way, we can consider two different case studies, according to the different mathematical solution of the inverse of the impedance matrix that is described later in this chapter:

- first case: all elements of the impedance matrix main diagonal are identical and equal to $\hat{Z}$ except the last one ($\hat{\mathbf{Z}}_{\mathbf{m}(\mathbf{N},\mathbf{N})}^{-\mathbf{1}} \neq \hat{Z}$);
- second case: all elements of the impedance matrix main diagonal are identical and equal to $\hat{Z}$, except the last one and another element in any given lth position ($\hat{\mathbf{Z}}_{\mathbf{m}(\mathbf{N},\mathbf{N})}^{-\mathbf{1}} \neq \hat{\mathbf{Z}}_{\mathbf{m}(\mathbf{l},\mathbf{l})}^{-\mathbf{1}} = \hat{Z}$, with $l = 1,...,N-1$).

3.2.1 First case

In this case, only the last element of the matrix is different than $\hat{Z}$ and is represented by $\hat{Z}+\hat{Z}'_T$, as in Fig. 3.1. This $\hat{Z}'_T$ could represent a physical load ($\hat{Z}'_T = \hat{Z}_T$, Fig. 3.2(a)) or a receiver (represented by $\hat{Z}_d$) over the Nth cell, in an array terminated with $\hat{Z}_T$ ($\hat{Z}'_T = \hat{Z}_d + \hat{Z}_T$, Fig. 3.2(b)). Moreover, considering an array with N resonators and a receiver over the lth cell (with $N > l$), $\hat{Z}'_T$ could be equal to $\hat{Z}_d + \hat{Z}_{eq,N-l}$ (Fig. 3.2(c)), considering that the matrix (3.2) becomes an lxl matrix and that $\hat{Z}_{eq,N-l}$ represents the equivalent impedance of all the resonators after the lth one ($N-l$ resonators). All these possible variations of the first case are represented in Fig. 3.2.

3.2.2 Second case

In this case, there will be two different elements on the main diagonal of the impedance matrix: the last one and another element in a certain lth position. This element in the lth position will be given by $\hat{Z}+\hat{Z}_{d1}$ and represents a receiver over the lth cell of the resonator array, as represented by (3.7).

$$\hat{\mathbf{Z}}_{\mathbf{m}} = \begin{bmatrix} \hat{Z} & j\omega M & \cdots & 0 & \cdots & 0 & 0 \\ j\omega M & \hat{Z} & \cdots & 0 & \cdots & 0 & 0 \\ \vdots & \vdots & \ddots & \vdots & & \vdots & \vdots \\ 0 & 0 & \cdots & \hat{Z}+\hat{Z}_{d1} & \cdots & 0 & 0 \\ \vdots & \vdots & & \vdots & \ddots & \vdots & \vdots \\ 0 & 0 & \cdots & 0 & \cdots & \hat{Z} & j\omega M \\ 0 & 0 & \cdots & 0 & \cdots & j\omega M & \hat{Z}+\hat{Z}'_T \end{bmatrix} \tag{3.7}$$

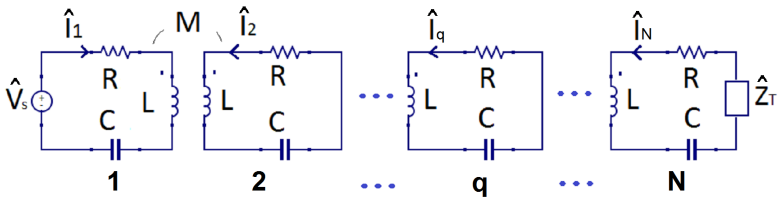

(a)

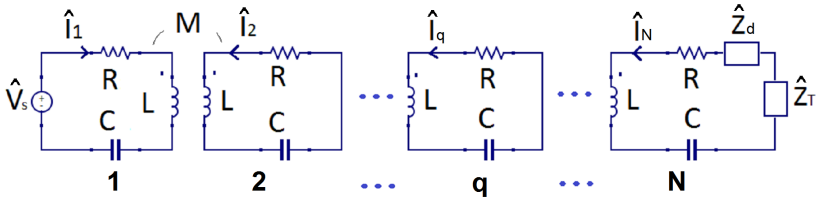

(b)

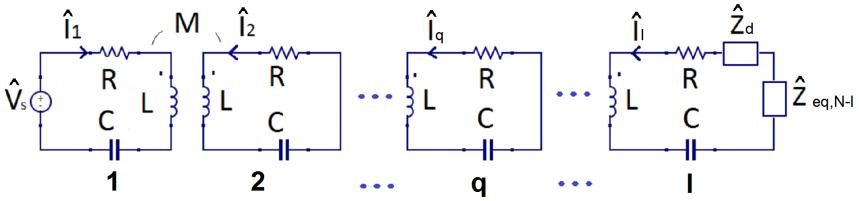

(c)

Figure 3.2: Equivalent circuits of different possible configurations of the system represented by (3.5): (a) physical load (no receiver) on the Nth cell ($\hat{Z}'_T = \hat{Z}_T$); (b) a receiver over the Nth cell ($\hat{Z}'_T = \hat{Z}_d + \hat{Z}_T$); (c) receiver over the lth cell ($\hat{Z}'_T = \hat{Z}_d + \hat{Z}_{eq,N-l}$).

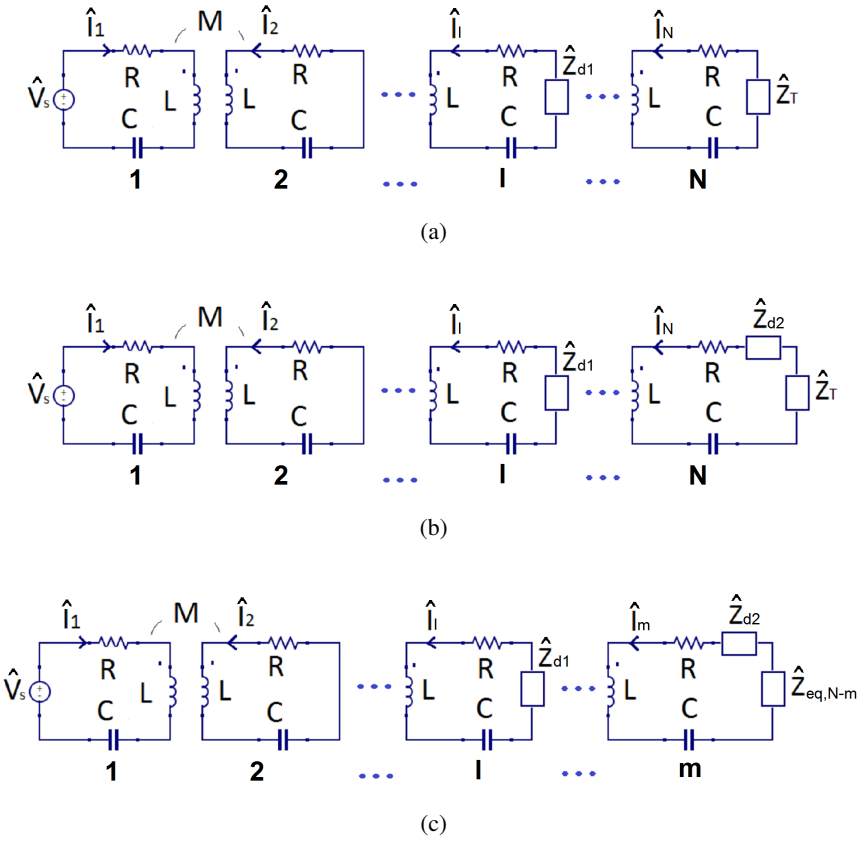

Figure 3.3: Equivalent circuits of different possible configurations of the system represented by (3.7): (a) no second receiver on the Nth cell ($\hat{Z}'_T = \hat{Z}_T$); (b) a second receiver over the Nth cell ($\hat{Z}'_T = \hat{Z}_{d2} + \hat{Z}_T$); (c) a second receiver over the mth cell ($\hat{Z}'_T = \hat{Z}_{d2} + \hat{Z}_{eq,N-m}$).

However, as in the previous case, $\hat{Z}'_T$ can have different values depending on the system that we are representing. Therefore, matrix (3.7) can represent an array of resonators with no second receiver over the Nth resonator ($\hat{Z}'_T$=$\hat{Z}_T$, Fig. 3.3 (a)) or with a second receiver on the Nth resonator ($\hat{Z}'_T$=$\hat{Z}_{d2} + \hat{Z}_T$, Fig. 3.3 (b)). Furthermore, considering an array with N resonators in which the second receiver is over the mth cell (with $N > m > l$), $\hat{Z}'_T$ could be equal to $\hat{Z}_{d2} + \hat{Z}_{eq,N-m}$ (Fig. 3.3(c)), considering that the matrix (3.3) becomes an $m \times m$ matrix and that $\hat{Z}_{eq,N-m}$ represents the equivalent impedance of all the resonators after the mth one ($N - m$ resonators).

3.2.2.1 With a source impedance $\hat{Z}_s$

Finally, in order to consider an array powered by a source with an internal impedance, we can study another specific variation of the second case, performed in order to analyse the effects of the source impedance on the power transmission and efficiency of the system. In this configuration, represented by (3.8), the first and last elements of the matrix are different, such that the first element of the matrix becomes $\hat{Z} + \hat{Z}_s$, being $\hat{Z}_s$ the voltage source impedance, and the Nth element is given, as in the first case, by $\hat{Z} + \hat{Z}'_T$ (Fig. 3.4). Regarding the value of $\hat{Z}'_T$, as in the first case, $\hat{Z}'_T$ could represent a physical load ($\hat{Z}'_T = \hat{Z}_T$), a receiver over the Nth cell in an array terminated with $\hat{Z}_T$ ($\hat{Z}'_T = \hat{Z}_d + \hat{Z}_T$), or a receiver over the lth resonator of the array ($\hat{Z}'_T = \hat{Z}_d + \hat{Z}_{eq,N-l}$), situation

in which (3.8) becomes an lxl cell.

$$\hat{\mathbf{Z}}_{\mathbf{m,3}} = \begin{bmatrix} \hat{Z}+\hat{Z}_s & j\omega M & \dots & 0 \\ j\omega M & \hat{Z} & \dots & 0 \\ \vdots & \vdots & \ddots & j\omega M \\ 0 & 0 & j\omega M & \hat{Z}+\hat{Z}'_T \end{bmatrix} \tag{3.8}$$

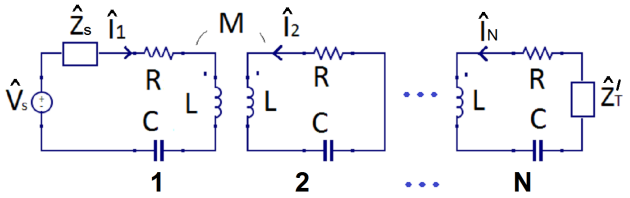

Figure 3.4: Equivalent circuit of an array of resonators represented by (3.8).

Note that if the system is operating at the resonant angular frequency $\omega_0 = 1/\sqrt{LC}$ and assuming that the receivers have the same resonant frequency as the cells of the array, all the values of the diagonals of the matrices presented become real and can be represented by resistances $\hat{Z} = R$, $\hat{Z}'_T = R'_T$, $\hat{Z}_T = R_T$, $\hat{Z}_d = R_d$, $\hat{Z}_{d1} = R_{d1}$, $\hat{Z}_{d2} = R_{d2}$, $\hat{Z}_{eq} = R_{eq}$ and $\hat{Z}_s = R_s$.

3.3 Mathematical determination of the inverse of a tridiagonal matrix

After presenting some interesting practical cases, we determine analytically in this section the inverse of a tridiagonal matrix with the above mentioned particular characteristics. First of all, we assume that all the tridiagonal matrices that we consider are invertible, which means that their determinant is different from zero. Then, we start by considering a generic symmetric tridiagonal matrix $N \times N$, with constant nondiagonal elements α and diagonal elements β_k, with $1 \leq k \leq N$, with $\alpha, \beta_k \in \mathbb{C}$:

$$J = \begin{bmatrix} \beta_1 & \alpha & \cdots & 0 & 0 \\ \alpha & \beta_2 & \cdots & 0 & 0 \\ \vdots & \vdots & \ddots & \vdots & \vdots \\ 0 & 0 & \cdots & \beta_{N-1} & \alpha \\ 0 & 0 & \cdots & \alpha & \beta_N \end{bmatrix}. \tag{3.9}$$

The elements of the inverse of the matrix (3.9), according to [33] and knowing that the inverse of a symmetric matrix is still symmetric, are given by:

$$J^{-1}_{ij} = \frac{(-1)^{i+j}\alpha^{j-i}\theta_{i-1}\phi_{j+1}}{\det J}, \text{ with } 1 \leq i, j \leq N, \tag{3.10}$$

where

$$\theta_{-1} = 0,\ \theta_0 = 1,\ \theta_k = \beta_k\theta_{k-1} - \alpha^2\theta_{k-2},\ k = 1,\ldots,N \tag{3.11}$$

and

$$\phi_{N+2} = 0,\ \phi_{N+1} = 1,\ \phi_k = \beta_k\phi_{k+1} - \alpha^2\phi_{k+2},\ k = N, N-1,\ldots,1. \tag{3.12}$$

Then, as k is decreasing in (3.12), we make a change of variable to obtain an inversion of the order of the index to be able to solve the difference equation defined by (3.12). Then, defining $x_p = \phi_{N-p+1}$, in which the index p increases, we have $x_{-1} = \phi_{N+2}$, $x_0 = \phi_{N+1}$, $x_1 = \phi_N$ and

$$x_p = \beta_{N-p+1}x_{p-1} - \alpha^2 x_{p-2},\ p \geq 2. \tag{3.13}$$

So, the sequence $\{x_n\}$ (and consequently $\{\phi_n\}$) is defined by one homogeneous difference equation with constant coefficients whose general term can be determined by the theory of linear homogeneous difference equations [28] similarly as done in Chapter 2.

As explained in the previous section, we only need to know the values of the elements of the first column of the inverse matrix, $J^{-1}_{i,1}$. However, knowing that the inverse of a symmetric matrix is also symmetric, we can determine the elements of the first row of the inverse matrix, $J^{-1}_{1,j}$ instead. In this way, we get a simplified expression for these elements, as $\theta_0 = 1$:

$$J^{-1}_{1,j} = \frac{(-1)^{1+j}\alpha^{j-1}\phi_{j+1}}{\det J}. \tag{3.14}$$

According to the two cases presented in the previous section, we will consider the following values for the elements of matrix (3.9):

$$\alpha = a,\ \beta_N = c,\ \beta_1 = \beta_2 = ... = \beta_{N-1} = b; \tag{3.15}$$

$$\alpha = a,\ \beta_N = c,\ \beta_1 = \beta_2 = ... = \beta_{l-1} = \beta_{l+1} = ... = \beta_{N-1} = b,\ \beta_l = d; \tag{3.16}$$

being a, b, c and d complex numbers.

3.3.1 First case

For this case, as described in (3.15) we consider the $N \times N$ matrix

$$T = \begin{bmatrix} b & a & 0 & \cdots & 0 & 0 \\ a & b & a & \cdots & 0 & 0 \\ 0 & a & b & \cdots & 0 & 0 \\ \vdots & \vdots & \vdots & \ddots & \vdots & \vdots \\ 0 & 0 & 0 & \cdots & b & a \\ 0 & 0 & 0 & \cdots & a & c \end{bmatrix} \tag{3.17}$$

and $x_0 = \phi_{N+1} = 1$, $x_1 = \phi_N = c$ and $x_p - bx_{p-1} + a^2x_{p-2} = 0$.

Solving this equation similarly as done in Chapter 2, supposing that $b^2 \neq 4a^2$ (that is, the polynomial $x^2 - bx + a^2$ has two distinct roots), we can write:

$$x_p = e_1 \left(\frac{b - \sqrt{b^2 - 4a^2}}{2} \right)^p + e_2 \left(\frac{b + \sqrt{b^2 - 4a^2}}{2} \right)^p \tag{3.18}$$

with e_1 and e_2 being constants to be determined using the initial conditions x_0 and x_1:

$$\begin{aligned} 1 &= e_1 + e_2 \\ 2c &= e_1 \left(b - \sqrt{b^2 - 4a^2} \right) + e_2 \left(b - \sqrt{b^2 - 4a^2} \right) \end{aligned} . \tag{3.19}$$

Referring to the sequence $\{\phi_n\}$, defined as $\phi_{N-p+1} = x_p$, we have

$$\phi_p = e_1 \left(\frac{b - \sqrt{b^2 - 4a^2}}{2} \right)^{N+1-p} + e_2 \left(\frac{b + \sqrt{b^2 - 4a^2}}{2} \right)^{N+1-p} . \tag{3.20}$$

Then, after describing the general term of the sequence $\{\phi_n\}$, we need to calculate the determinant of the matrix T, $\det T$.

So, having the $S \times S$ matrix:

$$X_S = \begin{bmatrix} b & a & \cdots & 0 & 0 \\ a & b & \cdots & 0 & 0 \\ \vdots & \vdots & \ddots & \vdots & \vdots \\ 0 & 0 & \cdots & b & a \\ 0 & 0 & \cdots & a & b \end{bmatrix} \tag{3.21}$$

we know from [34] that:

$$\det X_S = B_S = a^S U_S \left(\frac{b}{2a} \right), \tag{3.22}$$

where U_S is a Chebychev polynomial of second kind, that can be defined as [34]:

$$U_N \left(\frac{b}{2a} \right) = \frac{\left(\frac{b}{2a} + \sqrt{\left(\frac{b}{2a} \right)^2 - 1} \right)^{N+1} - \left(\frac{b}{2a} - \sqrt{\left(\frac{b}{2a} \right)^2 - 1} \right)^{N+1}}{2\sqrt{\left(\frac{b}{2a} \right)^2 - 1}}, \tag{3.23}$$

assuming that $(\frac{b}{2a})^2 \neq 1$.

Thus, by the Laplace Expansion Theorem [35], we have

$$\det T = \det \begin{bmatrix} b & a & \cdots & 0 & 0 \\ a & b & \cdots & 0 & 0 \\ \vdots & \vdots & \ddots & \vdots & \vdots \\ 0 & 0 & \cdots & b & a \\ 0 & 0 & \cdots & a & c \end{bmatrix} = cB_{N-1} - a^2 B_{N-2}. \tag{3.24}$$

Using (3.14) with (3.20) and 3.24, we can calculate the elements $T^{-1}_{1,1}$, $T^{-1}_{q,1}$ and $T^{-1}_{N,1}$:

$$\begin{aligned} T^{-1}_{1,1} &= \frac{\phi_2}{\det T} = \\ &= \frac{e_1 \left(\frac{b - \sqrt{b^2 - 4a^2}}{2} \right)^{N-1} + e_2 \left(\frac{b + \sqrt{b^2 - 4a^2}}{2} \right)^{N-1}}{ca^{N-1} U_{N-1}\left(\frac{b}{2a} \right) - a^N U_{N-2}\left(\frac{b}{2a} \right)}, \end{aligned} \tag{3.25}$$

$$T_{q,1}^{-1} = \quad T_{1,q}^{-1} \quad = \frac{-(-1)^q a^{q-1}\phi_{q+1}}{\det T} \qquad = \\ = \frac{-(-1)^q a^{q-1} e_1 \left(\frac{b-\sqrt{b^2-4a^2}}{2}\right)^{N-q} + e_2 \left(\frac{b+\sqrt{b^2-4a^2}}{2}\right)^{N-q}}{ca^{N-1}U_{N-1}\left(\frac{b}{2a}\right) - a^N U_{N-2}\left(\frac{b}{2a}\right)} \tag{3.26}$$

and

$$T_{N,1}^{-1} = T_{1,N}^{-1} \quad = \quad \frac{(-a)^{N-1}}{\det T} \qquad = \\ = \quad \frac{(-a)^{N-1}}{ca^{N-1}U_{N-1}\left(\frac{b}{2a}\right) - a^N U_{N-2}\left(\frac{b}{2a}\right)} \quad . \tag{3.27}$$

Therefore, determining the constants e_1,e_2 (described in Appendix B) from (3.20), (3.23) and (3.24), and using the software Mathematica to simplify the expressions, we have:

$$T_{1,1}^{-1} = \frac{(\varepsilon_3 - 2c)\,\varepsilon_2^{N-1} - (\varepsilon_2 - 2c)\,\varepsilon_3^{N-1}}{c\left(\varepsilon_3^N - \varepsilon_2^N\right) + 2a^2\left(\varepsilon_2^{N-1} - \varepsilon_3^{N-1}\right)} \tag{3.28}$$

$$T_{q,1}^{-1} = T_{1,q}^{-1} = \frac{(-1)^q (2a)^{q-1}\left((\varepsilon_2 - 2c)\,\varepsilon_3^{N-q} - (\varepsilon_3 - 2c)\,\varepsilon_2^{N-q}\right)}{c\left(\varepsilon_3^N - \varepsilon_2^N\right) + 2a^2\left(\varepsilon_2^{N-1} - \varepsilon_3^{N-1}\right)} \tag{3.29}$$

and

$$T_{N,1}^{-1} = T_{1,N}^{-1} = \frac{2^N \varepsilon_1 (-a)^{N-1}}{c\left(\varepsilon_3^N - \varepsilon_2^N\right) + 2a^2\left(\varepsilon_2^{N-1} - \varepsilon_3^{N-1}\right)} \tag{3.30}$$

with $\varepsilon_1 = \sqrt{b^2-4a^2}$, $\varepsilon_2 = b - \sqrt{b^2-4a^2}$, $\varepsilon_3 = b + \sqrt{b^2-4a^2}$.

3.3.1.1 Second case

Afterwards, as described in (3.16), we consider the $N \times N$ matrix,

$$M = \begin{bmatrix} b & a & \cdots & 0 & \cdots & 0 & 0 \\ a & b & \cdots & 0 & \cdots & 0 & 0 \\ \vdots & \vdots & \ddots & \vdots & & \vdots & \vdots \\ 0 & 0 & \cdots & d & \cdots & 0 & 0 \\ \vdots & \vdots & & \vdots & \ddots & \vdots & \vdots \\ 0 & 0 & \cdots & 0 & \cdots & b & a \\ 0 & 0 & \cdots & 0 & \cdots & a & c \end{bmatrix} \tag{3.31}$$

where the main diagonal element in the lth position is d ($1 \leq l < N$).

Analogously, as done in the previous case, in order to determine the values of the first column of the inverse of the symmetric tridiagonal matrix M, we apply the results presented in (3.10)-(3.12). In this case, according to (3.21) and (3.22) and using the Laplace Expansion Theorem [35] the determinant of M is given by:

$$\det M = \begin{array}{l} (cB_{N-l-1} - a^2 B_{N-l-2})(dB_{l-1} - a^2 B_{l-2}) \\ -a^2 B_{l-1}(cB_{N-l-2} - a^2 B_{N-l-3}) \end{array} . \tag{3.32}$$

Regarding the determination of the first N terms of the sequence $\{\phi_n\}$ we will consider three steps, as done in Chapter 2 where we have defined a perturbation in the continued fraction. The $N-l$ last terms, from $l+1$ to N ($l+1$, $l+2$,...N), are calculated using (3.18), (3.19) and (3.20):

$$\phi_u = e_1\left(\frac{b-\sqrt{b^2-4a^2}}{2}\right)^{N+1-u} + e_2\left(\frac{b+\sqrt{b^2-4a^2}}{2}\right)^{N+1-u},\ l+1 \leq u \leq N \tag{3.33}$$

where the constants e_1 and e_2 are calculated as done in the previous case and their values are presented in Appendix B. The term of order l will be calculated taking into account the element d with the expression:

$$\phi_l = d\phi_{l+1} - a^2\phi_{l+2}, \tag{3.34}$$

where ϕ_{l+1} and ϕ_{l+2} are given by (3.33). Finally, the third step consists in determining the $l-1$ first terms of the sequence $\{\phi_n\}$, from 1 to $l-1$ (1,...,$l-1$). Once again, from (3.18), (3.19) and (3.20) we know that:

$$\phi_f = g_1\left(\frac{b-\sqrt{b^2-4a^2}}{2}\right)^{l+1-f} + g_2\left(\frac{b+\sqrt{b^2-4a^2}}{2}\right)^{l+1-f}, \text{with } f = l-1, l-2, \ldots, 2, 1 \tag{3.35}$$

where g_1 and g_2 are constants that can be calculated by the initial conditions ϕ_l and ϕ_{l+1}, obtained with (3.33) and (3.34):

$$\begin{array}{l} \phi_{l+1} = g_1 + g_2 \\ 2\phi_l = g_1\left(b-\sqrt{b^2-4a^2}\right) + g_2\left(b-\sqrt{b^2-4a^2}\right) \end{array}. \tag{3.36}$$

In conclusion, the elements of the first column of the inverse matrix of M are given by

$$M^{-1}_{t,1} = M^{-1}_{1,t} = \frac{(-a)^{t-1}\phi_{t+1}}{\det M},\ 1 \leq t \leq N \tag{3.37}$$

with ϕ_{t+1} being determined according to the following expression:

$$\phi_h = \begin{cases} e_1\left(\frac{b-\sqrt{b^2-4a^2}}{2}\right)^{N+1-h} + e_2\left(\frac{b+\sqrt{b^2-4a^2}}{2}\right)^{N+1-h},\ l+1 \leq h \leq N+1 \\ d\phi_{l+1} - a^2\phi_{l+2},\ h = l \\ g_1\left(\frac{b-\sqrt{b^2-4a^2}}{2}\right)^{l+1-h} + g_2\left(\frac{b+\sqrt{b^2-4a^2}}{2}\right)^{l+1-h},\ 1 \leq h \leq l-1 \end{cases}. \tag{3.38}$$

Thus, knowing the values of the constants e_1, e_2, g_1 and g_2 (described in Appendix B), determining $\det M$ using (3.22) and (3.32), using Mathematica software to simplify the expressions we can write (3.37) as:

$$M_{1,1}^{-1}=\begin{cases}\dfrac{2^{-n-1}(\varepsilon_2\varepsilon_3)^{-l-2}\left(\begin{array}{c}-32a^4\varepsilon_3^{l+1}\varepsilon_2^{l+n}+\\ 4a^2\left(\varepsilon_2^n\varepsilon_3^{l+1}\left(2\varepsilon_2^l\left(2b^2-b(2c+d-2\varepsilon_1)-\varepsilon_1(2c+d)+2cd\right)-\varepsilon_2(\varepsilon_3-2c)\varepsilon_3^l\right)\right)\\ -(\varepsilon_2-2c)\varepsilon_2^l\varepsilon_3^n\left(2\varepsilon_3(b-d)\varepsilon_2^l-\varepsilon_2^2\varepsilon_3^l\right)\\ +\varepsilon_2^2(2d-\varepsilon_2)\varepsilon_3^{l+1}\left((\varepsilon_3-2c)\varepsilon_2^n\varepsilon_3^l-(\varepsilon_2-2c)\varepsilon_2^l\varepsilon_3^n\right)\end{array}\right)}{\varepsilon_1^2\det M}, & l\geq 3\\ \dfrac{2^{-n+1}\left((\varepsilon_3-2c)\left(d\varepsilon_2-2a^2\right)\varepsilon_2^{n-3}+(2c-\varepsilon_2)\left(d\varepsilon_3-2a^2\right)\varepsilon_3^{n-3}\right)}{\varepsilon_1\det M}, & l=2\\ \dfrac{2^{-n}\left((\varepsilon_3-2c)\varepsilon_2{}^{n-1}+(2c-\varepsilon_2)\varepsilon_3{}^{n-1}\right)}{\varepsilon_1\det M}, & l=1\end{cases} \tag{3.39}$$

$$M_{l,1}^{-1}=M_{1,l}^{-1}=\frac{2^{-N}(-2a)^{l-1}\left((\varepsilon_3-2c)\varepsilon_2{}^{N-l}+(2c-\varepsilon_2)\varepsilon_3{}^{N-l}\right)}{\varepsilon_1\det M},\ 2\leq l\leq N-1 \tag{3.40}$$

$$M_{N,1}^{-1}=M_{1,N}^{-1}=\frac{(-a)^{N-1}}{\det M} \tag{3.41}$$

with $\varepsilon_1=\sqrt{b^2-4a^2}$, $\varepsilon_2=b-\sqrt{b^2-4a^2}$, $\varepsilon_3=b+\sqrt{b^2-4a^2}$. Note that in (3.39), the particular cases where the element d is on the first or second position of the main diagonal ($l=1$ or $l=2$) are separated, since the expressions obtained for these two cases are much simpler than the expressions for other positions.

3.4 Application of the mathematical results

In this section, we apply the mathematical results obtained in the previous section, by replacing the generic mathematical constants (a, b, c and d) by the circuit parameters. In this way, we can obtain expressions for the currents in each resonator for the cases presented before, and consequently expressions for the power delivered to a load or receiver and the efficiency of the system. Moreover, with these expressions, one can determine analytically the maximum values of power delivered and efficiency for the different cases. The expressions presented were simplified using the software Mathematica. Finally, some examples are made in order to illustrate the results obtained. The examples are performed using the values of R, L, C and M acquired through measurements made on the experimental setup illustrated in Chapter 5 ($L=12.6\mu$H, $C=93.1n$F, $R=0.11\Omega$, $M=-1.55\mu$H and $f_0=147$kHz).

3.4.1 First case

3.4.1.1 Values of the currents in the resonators

We start by considering the first case represented by (3.5), by replacing $a=j\omega M$, $b=\hat{Z}$ and $c=\hat{Z}_T'$ in (3.28)-(3.30). Then, we can write the expressions for the currents in the resonators:

$$\hat{I}_1=\hat{V}_s\frac{\left(\iota_3+2\hat{Z}_T'\right)\iota_3^{N-1}-\left(\iota_2+2\hat{Z}_T'\right)\iota_2^{N-1}}{\left(\hat{Z}+\hat{Z}_T'\right)\left(\iota_3^N-\iota_2^N\right)+2\left(\omega M\right)^2\left(\iota_3^{N-1}-\iota_2^{N-1}\right)} \tag{3.42}$$

$$\hat{I}_q = \hat{V}_s \frac{(-1)^q 2^{q-1} (j\omega M)^{q-1} \left(\left(\iota_2 + 2\hat{Z}'_T\right) \iota_2^{N-q} - \left(\iota_3 + 2\hat{Z}'_T\right) \iota_3^{N-q} \right)}{\left(\hat{Z} + \hat{Z}'_T\right) \left(\iota_3^N - \iota_2^N\right) + 2 (\omega M)^2 \left(\iota_3^{N-1} - \iota_2^{N-1}\right)} \tag{3.43}$$

and

$$\hat{I}_N = \hat{V}_s \frac{2^N (-j\omega M)^{N-1} \iota_1}{\left(\hat{Z} + \hat{Z}'_T\right) \left(\iota_3^N - \iota_2^N\right) + 2 (\omega M)^2 \left(\iota_3^{N-1} - \iota_2^{N-1}\right)} \tag{3.44}$$

with $\iota_1 = \sqrt{4(\omega M)^2 + \hat{Z}^2}$, $\iota_2 = \hat{Z} - \sqrt{4(\omega M)^2 + \hat{Z}^2}$, $\iota_3 = \hat{Z} + \sqrt{4(\omega M)^2 + \hat{Z}^2}$. Note that $\hat{I}_1$ and $\hat{I}_N$ are particular cases of $\hat{I}_q$, since $q = 1, ..., N$.

Then, we can perform an example, considering that we are operating at resonant frequency, taking as a reference a voltage source with $\hat{V}_s = 1\angle 0^{\circ}$V. Then, using the expression of $\hat{I}_q$ given by (3.43), we can obtain the values of the currents for an example of an array of 8 resonators (with $N = 8$, and q from 1 to 8), terminated with different values of R'_T.Thus, for $R'_T = 0.4\Omega$; $R'_T = R_{eq,\infty} = \left(-R + \sqrt{4(\omega_0 M)^2 + R^2}\right)/2$ and $R'_T = 10\Omega$, we have the currents shown in Fig. 3.5. Then, keeping the same values considered before, we consider now that the resonator intrinsic AC resistance is 3 times higher, $R = 0.33\Omega$, and calculated $\hat{I}_q$ for the same different values of R'_T. The results are shown in Fig. 3.6.

Firstly, we can see that the currents have a phase difference of 90º due to the $j\omega_0 M$ factor. Furthermore, when the resonator array is perfectly terminated ($R'_T = R_{eq,\infty}$, as in Fig. 3.5 (b) and Fig. 3.6 (b)), the absolute value of the currents decreases smoothly from the first to the last resonator, while with different values of R'_T there are bigger oscillations regarding the absolute values of the currents, which are also represented in Fig. 3.7. The peaks of the absolute value of the currents on the resonators will occur on even or odd resonators, depending on whether the array is terminated by $R'_T < \left(-R + \sqrt{4(\omega_0 M)^2 + R^2}\right)/2$ or by $R'_T > \left(-R + \sqrt{4(\omega_0 M)^2 + R^2}\right)/2$, respectively. Moreover, regarding the case when the resistance had a higher value, we can see that the absolute value of the current has a higher decrease, but smoother oscillation.

For the perfectly terminated case, using (3.43) and setting $R'_T = R_{eq,\infty} = \left(-R + \sqrt{4(\omega_0 M)^2 + R^2}\right)/2$, the value of I_{q+1}/I_q is equal to j, meaning that all the currents would have the same absolute value.

Note that, for these examples, we considered a negative mutual inductance M which is the case of the planar resonators. Regarding situations where the mutual inductance is considered positive (domino-resonators, for example [3]), the previous conclusions and results concerning the absolute values of the currents still apply. The only difference would be that the phase difference between the currents will be -90º instead of 90º.

$$\frac{\hat{I}_{q+1}}{\hat{I}_q} = \frac{-2j\omega_0 M}{R + \sqrt{4(\omega_0 M)^2 + R^2}} \tag{3.45}$$

whose value is $0.9562j$ for the case represented in Fig. 3.5 and $0.8746j$ for the case depicted in Fig. 3.6. As seen in (3.45), for the perfect termination, the ratio between the currents in two consecutive resonators will be constant and does not depend on the value of R'_T, but only on the electrical parameters of the line. For a low-loss line, i.e. $R \ll \omega_0 M$, (3.45) becomes equal to j, meaning that all the currents would have the same absolute value.

Note that, for these examples, we considered a negative mutual inductance M which is the case

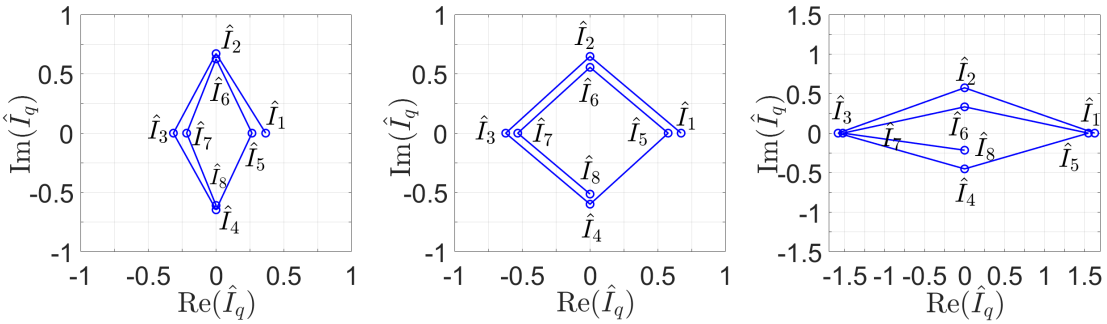

(a) (b) (c)

Figure 3.5: Real and imaginary parts for the current in each resonator, $\hat{I}_q$, with $1 \leq q \leq 8$, for an array of 8 resonators, for different values of R'_T: (a) R'_T=0.4Ω, (b) $R'_T = R_{eq,\infty}$ and (c) R'_T=10Ω.

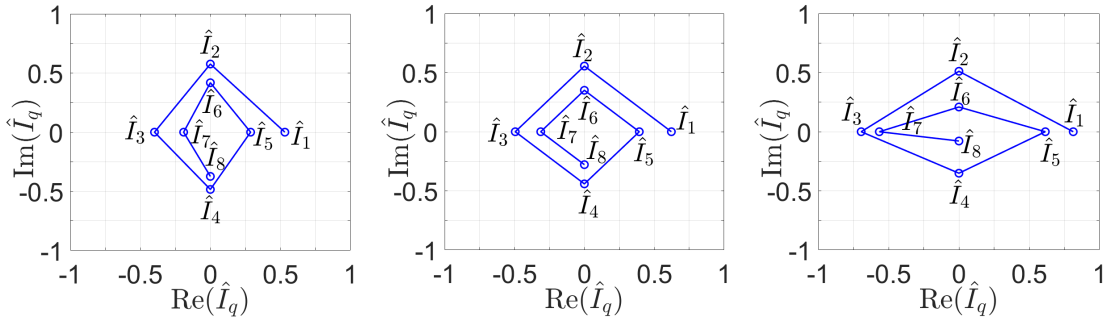

(a) (b) (c)

Figure 3.6: Real and imaginary parts for the current in each resonator, $\hat{I}_q$, with $1 \leq q \leq 8$, for an array of 8 resonators, for $R = 0.33\Omega$ and for different values of R'_T: (a) R'_T=0.4Ω, (b) $R'_T = R_{eq,\infty}$ and (c) R'_T=10Ω

of the planar resonators. Regarding situations where the mutual inductance is considered positive (domino-resonators, for example [3]), the previous conclusions and results concerning the absolute values of the currents still apply. The only difference would be that the phase difference between the currents will be -90º instead of 90º.

3.4.1.2 Efficiency and power delivered to a load or a receiver over the last cell represented by R_T

Now considering that we want do determine the efficiency of the power delivered to a physical load, or a receiver over the last cell (Fig. 3.2 (a)) represented by $\hat{Z}_T$ ($\hat{Z}'_T = \hat{Z}_T$), and supposing that we are working at the resonant frequency, so $\hat{Z} = R$, $\omega M = \omega_0 M$ and $\hat{Z}'_T = R'_T = R_T$, we can define the efficiency as the ratio between the power absorbed by R_T and the input power:

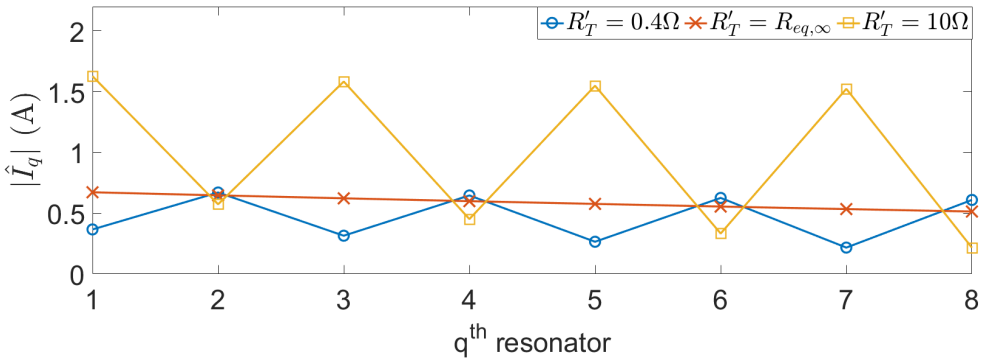

(a)

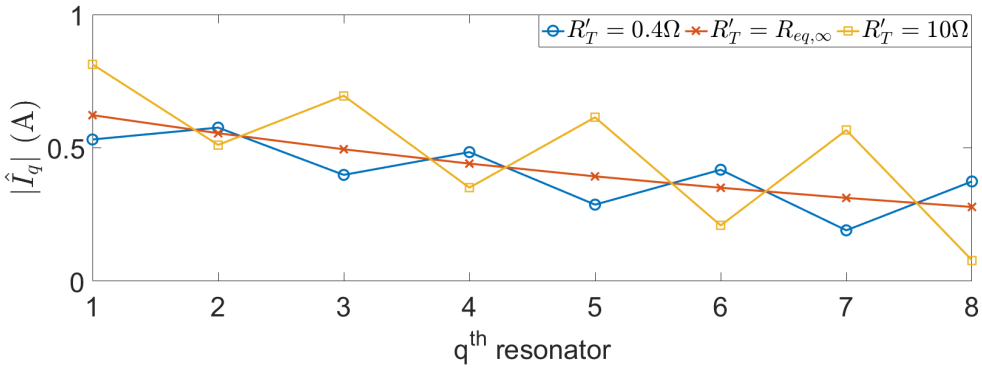

(b)

Figure 3.7: Absolute values of the current in each resonator, $\hat{I}_q$, with $1 \leq q \leq 8$, for an array of 8 resonators, for different values of R'_T=0.4Ω, (b) $R'_T = R_{eq,\infty}$ and (c) R'_T=10Ω and for different values of R: (a) $R = 0.11\Omega$ and (b) $R = 0.33\Omega$.

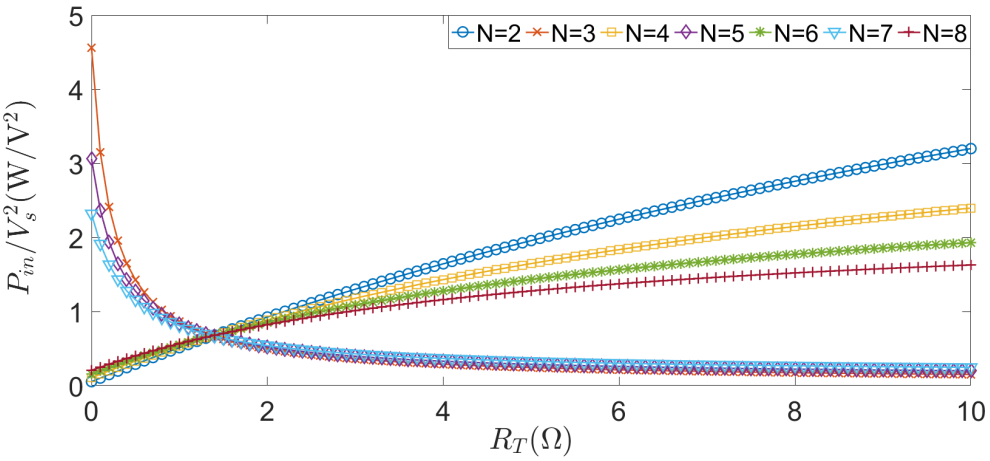

Figure 3.8: Input power P_{in} (3.47) for different values of R_T and different number of resonators N.

$$\eta = \frac{P_{R_T}}{P_{in}} = \frac{{I_N}^2 R_T}{V_s I_1} \tag{3.46}$$

in which I_1, I_N and V_s are the RMS values of the current in the first and Nth resonator and of the voltage source, respectively.

Then, using the expressions obtained for the currents, (3.42) and (3.44) we can rewrite the expressions for the input power, the power delivered to a load R_T and the efficiency as defined by (3.46):

$$P_{in} = \frac{V_s^2\left(-\iota_2^{N-1}\left(\iota_2+2R_T\right)+\iota_3^{N-1}\left(\iota_3+2R_T\right)\right)}{2\left(\omega_0 M\right)^2\left(\iota_3^{N-1}-\iota_2^{N-1}\right)-\left(R+R_T\right)\left(\iota_2^N-\iota_3^N\right)} \tag{3.47}$$

$$P_{R_T} = \frac{4^N V_s^2 R_T \left(\omega_0 M\right)^{2N-2}\iota_1^2}{\left(\left(R+R_T\right)\left(\iota_3^N-\iota_2^N\right)+2\left(\omega_0 M\right)^2\left(\iota_3^{N-1}-\iota_2^{N-1}\right)\right)^2} \tag{3.48}$$

$$\eta = \frac{4^{N+1} R_T \left(\omega_0 M\right)^{2N}\iota_1^2}{\left(\begin{array}{c}\left(\iota_2^N\left(\iota_3 R_T-2\left(\omega_0 M\right)^2\right)+\iota_3^N\left(2\left(\omega_0 M\right)^2-\iota_2 R_T\right)\right)\\ \left(\iota_1\left(\iota_2^N+\iota_3^N\right)-\left(R+2R_T\right)\left(\iota_2^N-\iota_3^N\right)\right)\end{array}\right)} \tag{3.49}$$

with $\iota_1 = \sqrt{4(\omega_0 M)^2+R^2}$, $\iota_2 = R-\sqrt{4(\omega_0 M)^2+R^2}$, $\iota_3 = R+\sqrt{4(\omega_0 M)^2+R^2}$.

First of all, it is interesting to notice that the value of the efficiency does not depend on the RMS value of the voltage source V_s; it depends only on the electrical parameters of the array and the load R_T. However, the values P_{R_T} and P_{in} depend on V_s. So, for a simpler illustration of the formulas obtained, considering that the resonator array is fed by a voltage source with a fixed RMS value, V_s, in the examples we consider the values of the power per square of the RMS value of the voltage source, i.e. P_{R_T}/V_s^2. So, we can calculate the input power, output power for different number of resonators N and values of R_T using (3.47), (3.48) and (3.49), respectively. The results are shown in Figs. 3.8 to 3.10.

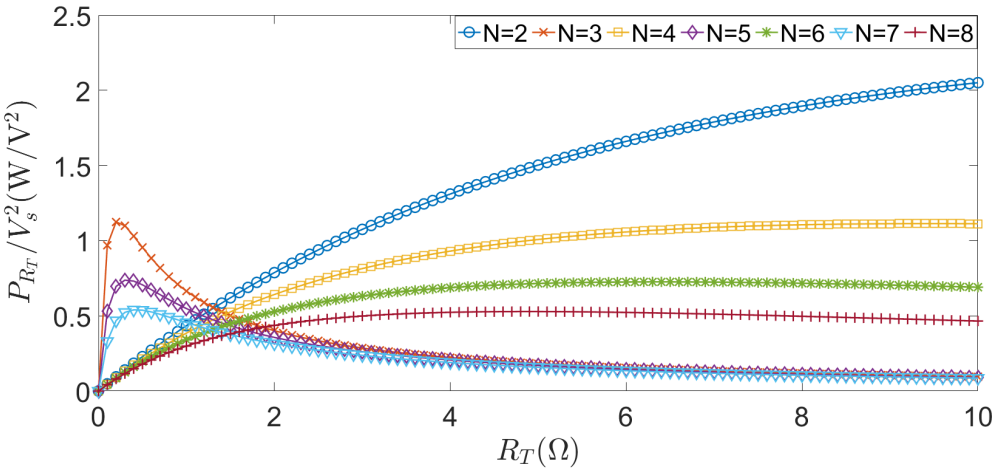

Figure 3.9: Power absorbed by R_T (3.48) for different values of R_T and different number of resonators N.

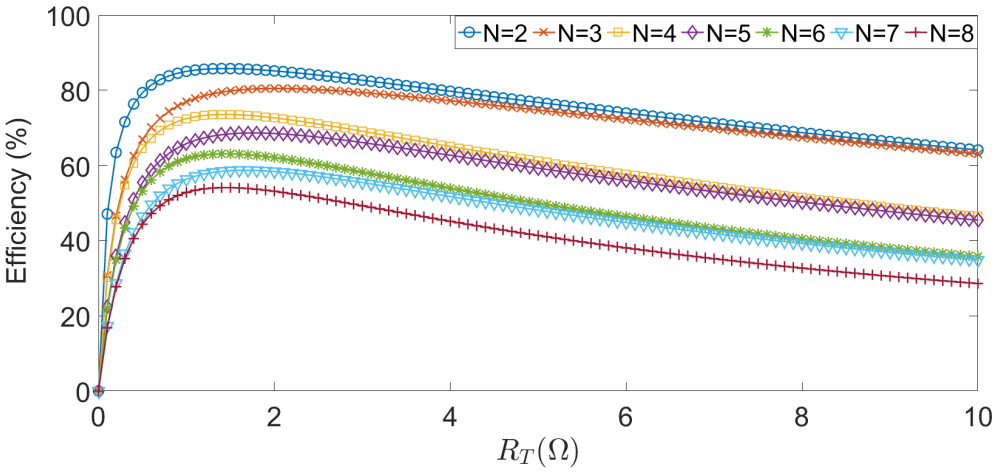

Figure 3.10: Efficiency (%) for different values of R_T and different number of resonators N.

Observing Figs. 3.8 to 3.10, we can draw some conclusions. First, the input power has the same value for any number of resonators, if R_T has a certain value. This value confirms what was demonstrated in Chapter 2, i.e., if the line is terminated with $R_T = R_{eq,\infty} = \left(-R + \sqrt{4(\omega_0 M)^2 + R^2}\right)/2$ (in this case $R_T = 1.38\Omega$), the input impedance remains constant for any number of resonators, meaning that for $R_T = R_{eq,\infty}$ and a fixed voltage source we have constant input power. Secondly, regarding P_{in} and P_{R_T}, we can see that both curves have different behaviour for even or odd numbers of cells: for a given voltage source and for a fixed value of R_T we obtain higher or lower values of power depending on whether we are considering odd or even numbers of cells. For example, for $R_T = 5\Omega$, we have higher values of power with an even number of cells ($N = 2$, 4, 6 and 8). Finally, this alternating behaviour regarding even or odd numbers of cells does not affect the value of the efficiency. Instead, for the same value of R_T, the efficiency drops with the increase of

the total number of resonators N. However, as we can observe in Fig. 3.10 there is a value of R_T that results in the maximum efficiency for every number of resonators. We can obtain this value of R_T by determining analytically the maximum efficiency with

$$\frac{d\eta}{dR_T} = 0 \tag{3.50}$$

and solving (3.50) for R_T:

$$R_{T,\eta max} = \pm \frac{\omega_0 M \sqrt{R\left(\iota_3^N - \iota_2^N\right) + \iota_1\left(\iota_2^N + \iota_3^N\right)}}{\sqrt{R\left(\iota_2^N - \iota_3^N\right) + \iota_1\left(\iota_2^N + \iota_3^N\right)}}. \tag{3.51}$$

Considering a very long line, and assuming that $|\iota_2| < |\iota_3|$, we get:

$$\lim_{N\to\infty} R_T, \eta_{max} = \frac{R + \sqrt{4\left(\omega_0 M\right)^2 + R^2}}{2}. \tag{3.52}$$

Using the value obtained with (3.51) in (3.49), we can obtain the maximum possible efficiency that we can achieve for an array with certain electrical parameters, for a given number of resonators, as

$$\eta_{max} = \frac{\iota_1^2 4^N \left(\omega_0 M\right)^{2N} \sqrt{\iota_3 \iota_2^N - \iota_2 \iota_3^N} \sqrt{\iota_3^{N+1} - \iota_2^{N+1}}}{\left(\begin{array}{c} -4\left(\omega_0 M\right)^3 \left(\iota_2^N - \iota_3^N\right)\left(\iota_2^N + \iota_3^N\right)^2 - 2\left(\omega_0 M\right) R^2 \left(\left(\iota_2^N - 2\iota_3^N\right)\left(\iota_2 \iota_3\right)^N + 4^N \left(-\iota_2 \left(\omega_0 M\right)^2\right)^N\right) \\ + \left((-4)^N R^2 \left(\omega_0 M\right)^{2N} + 2\left(\omega_0 M\right)^2 \left(\iota_2^{2N} + \iota_3^{2N}\right)\right) \sqrt{\iota_3 \iota_2^N - \iota_2 \iota_3^N} \sqrt{\iota_3^{N+1} - \iota_2^{N+1}} \end{array}\right)}. \tag{3.53}$$

Regarding the value of P_{R_T}, we can see in Fig. 3.9 that there is, for a given number of resonators, a value of R_T which gives the maximum power transfer to R_T. As done previously, we can obtain this value of R_T through the determination the maximum value of P_{R_T} with

$$\frac{dP_{R_T}}{dR_T} = 0. \tag{3.54}$$

and (3.54) for R_T :

$$R_{T,P_{R_T} max} = \frac{R\iota_2^N - \iota_1 \iota_2^N - R\iota_3^N - \iota_1 \iota_3^N}{2\iota_2^N - 2\iota_3^N}. \tag{3.55}$$

The value obtained in (3.55), if we consider a very long line, becomes:

$$\lim_{N\to\infty} R_{T,P_{R_T} max} = \frac{R + \sqrt{4(\omega_0 M)^2 + R^2}}{2}. \tag{3.56}$$

Once again, if we want to determine the maximum power that it is possible to deliver to R_T, for certain electrical parameters of the array, voltage source with RMS value V_s and number of resonators, we can use the value of (3.55) in (3.48) and obtain:

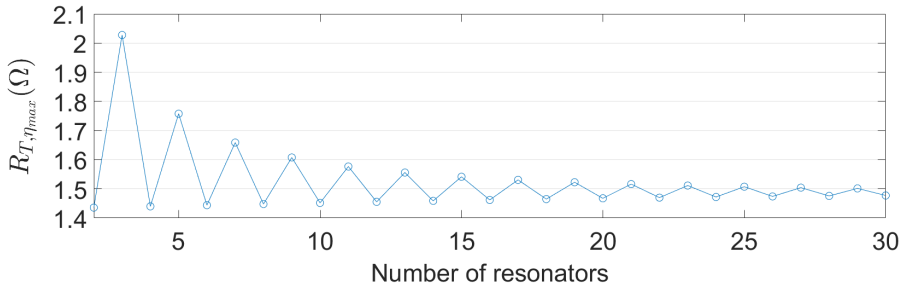

Figure 3.11: Value of R_T, η_{max} for different numbers of resonators (N).

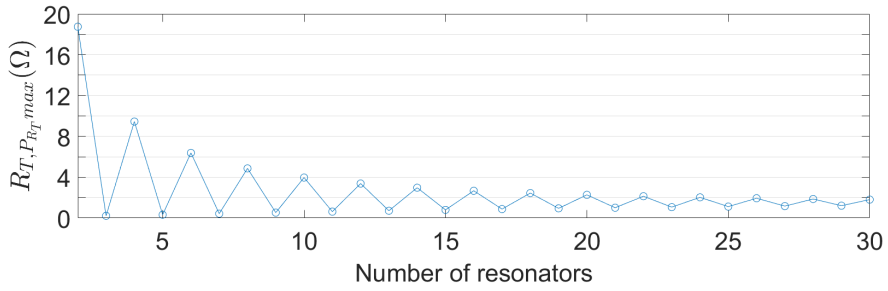

Figure 3.12: Value of $R_T, P_{R_T}max$ for different numbers of resonators (N).

$$P_{R_T,max} = -\frac{2^{2N-1}V_s^2(\omega_0 M)^{2N-2}\iota_1^2}{\left(\iota_2^N-\iota_3^N\right)\left(\iota_1\left(\iota_2^N+\iota_3^N\right)+R\left(\iota_3^N-\iota_2^N\right)\right)}. \tag{3.57}$$

Then, using (3.51) and (3.55) we can plot the value of the value of R_T for different numbers of resonators (N), as Figs. 3.11 and 3.12 show.

We can see from Figs. 3.11 and 3.12 that, although the values of R_T that guarantee maximum efficiency and power delivered tend both to the same value for a large number of resonators ($R_T = 1.49$ from (3.52) and (3.56)), e.g., $R_T, P_{R_T}max$ has larger oscillations from maximum to minimum values. Moreover, it is interesting to note that the values given by (3.52) and (3.56) tend to $\omega_0 M$ for a low-loss line ($R \ll \omega_0 M$), which is considered to be the matching impedance of a long low-loss line according to the magnetoinductive wave theory [14, 16]. Then, in order to evaluate the maximum possible values of efficiency and power delivered to R_T, we can define a parameter r as

$$r = R/(2\omega_0|M|). \tag{3.58}$$

The higher this ratio, the higher the losses of the resonator array and so r tends to zero for a low-loss line. This ratio r is simply the factor $1/|kQ|$ that, according to the magnetoinductive wave theory, increases the attenuation in each cell [14, 16].Then, for different values of r, using (3.53) and (3.57) we can plot the maximum efficiency and the maximum power transfer using (3.53) and (3.57) that is possible to deliver to a load R_T given by (3.51) and (3.55), for a resonator array with for a determinate number of resonator and different values of r (Figs. 3.13 and 3.14).

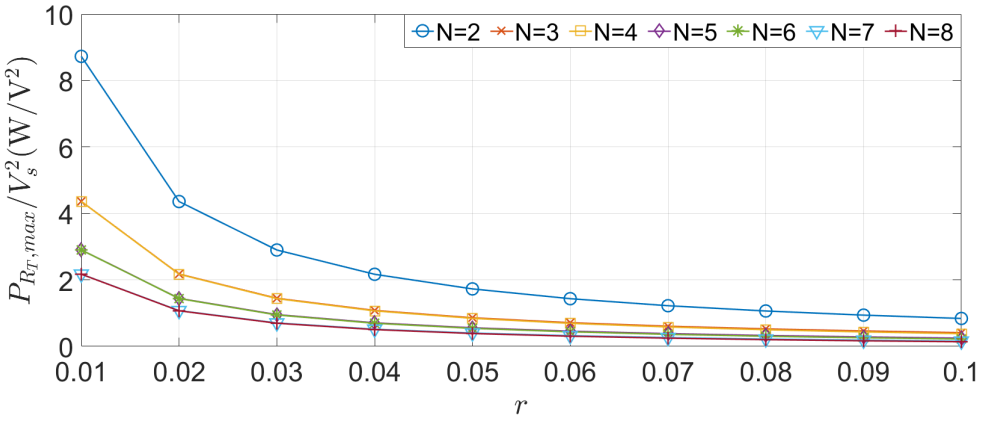

Figure 3.13: Maximum power transfer to a determinate load R_T that is possible to obtain with a resonator array with N resonators and given values of r.

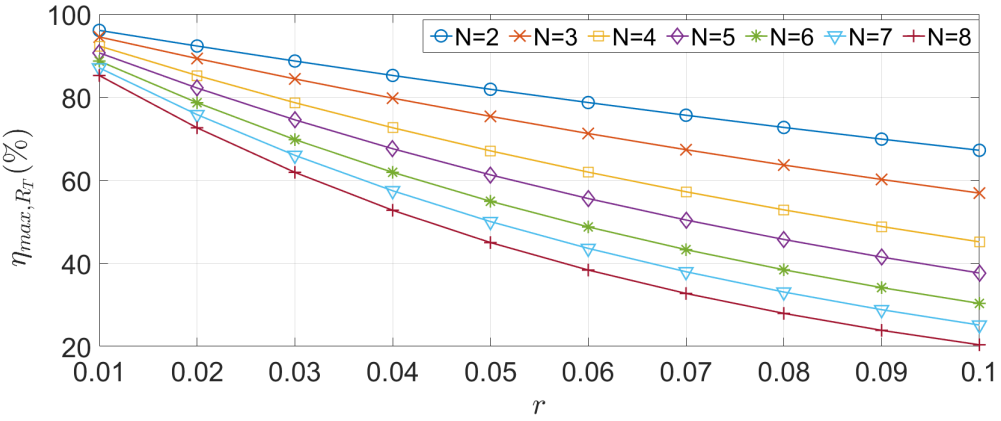

Figure 3.14: Maximum efficiency that is possible to obtain with a resonator array with N resonators and given values of r.

As expected, both efficiency and power delivered to R_T decrease with the increase of the ratio r (i. e. with the decrease of $|kQ|$) due to higher losses and attenuation in the array and decreases with the number of resonators N, too.

3.4.1.3 Efficiency and power transmitted to a receiver R_d over the lth cell

Eventually, considering a receiver represented by $\hat{Z}_d$ over the lth cell (Fig. 3.2 (c)), $\hat{Z}'_T = \hat{Z}_d + \hat{Z}_{eq,N-l}$, and assuming that we are working at the resonant frequency, so $\hat{Z} = R$, $\omega M = \omega_0 M$, $\hat{Z}'_T = R'_T = R_d + R_{eq,N-l}$, we can define the efficiency as the ratio between the power absorbed by R_d and the input power as:

$$\eta = \frac{P_{R_d}}{P_{in}} = \frac{I_l^2 R_d}{V_s I_1} \tag{3.59}$$

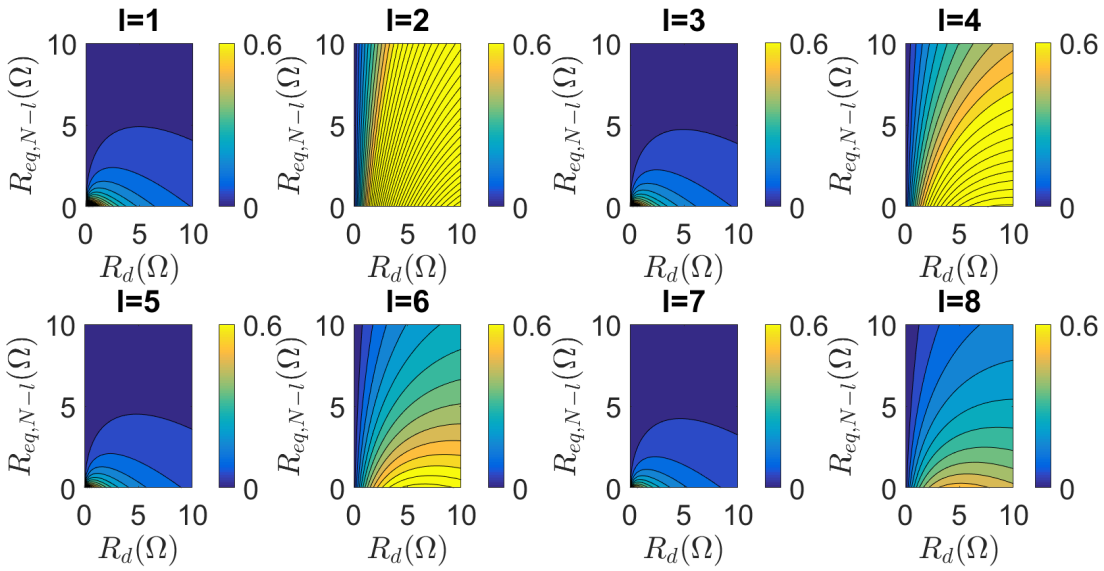

Figure 3.15: Power delivered to R_d, P_{R_d}/V_s^2 (W/V^2), determined with (3.60) for different values of $R_{eq,N-l}$ and R_d and for different positions of the receiver l.

where I_1, I_l and V_s are the RMS values of the current in the first and lth resonators and of the voltage source.Then, using the expressions obtained for the currents, (3.42) and (3.44), replacing N with l, we can rewrite the expressions of the power delivered to receiver represented by R_d over the lth position and the relevant efficiency as defined by (3.46):

$$P_{R_d} = \frac{4^l V_s^2 R_d (\omega_0 M)^{2l-2} \iota_1^2}{\left(\left(R+R_d+R_{eq,N-l}\right)\left(\iota_3^l-\iota_2^l\right)+2\left(\omega_0 M\right)^2\left(\iota_3^{l-1}-\iota_2^{l-1}\right)\right)^2}, \tag{3.60}$$

$$\eta = \frac{4^{l+1} R_d (\omega_0 M)^{2l} \iota_1^2}{\left(\begin{array}{c}\left(\iota_1\left(\iota_2^l+\iota_3^l\right)+\left(\iota_3^l-\iota_2^l\right)\left(R+2\left(R_d+R_{eq,N-l}\right)\right)\right) \\ \left(\left(R_d+R_{eq,N-l}\right)\left(\iota_1\left(\iota_2^l+\iota_3^l\right)+R\left(\iota_2^l-\iota_3^l\right)\right)-2(\omega_0 M)^2\left(\iota_2^l-\iota_3^l\right)\right)\end{array}\right)}. \tag{3.61}$$

Note that the expressions (3.60) and (3.61) can be used for the particular situation represented in Fig. 3.2 (b), where there is a receiver over the Nth cell and the line is terminated by R_T, replacing in (3.60) and (3.61) l with N and $R_{eq,N-l}$ with R_T.Then, for different values of R_d and $R_{eq,N-l}$ and for distinct positions of the receiver we can plot the power delivered to the receiver R_d using (3.60) and the efficiency using (3.61) . The results are shown in Figs. 3.15 and 3.16, respectively.

It can be observed in Fig. 3.15 that, similarly as observed in Figs. 3.8 and 3.9, the value of the power delivered to R_d has opposite behavior for odd and even values of l. For example, for $R_d = R_{eq} = 5\Omega$, P_{R_d} has highest values when the receiver is on an even position ($l = 2$, 4 and 8) and lowest values for odd positions ($l = 1$, 3, 5 and 7). Moreover, as it can be noticed in Fig. 3.16, both the efficiency and power delivered to a receiver get higher as $R_{eq,N-l}$ goes to zero. However, as we saw in Chapter 2, $R_{eq,N-l}$ can only be equal to zero if the receiver is over the last cell and

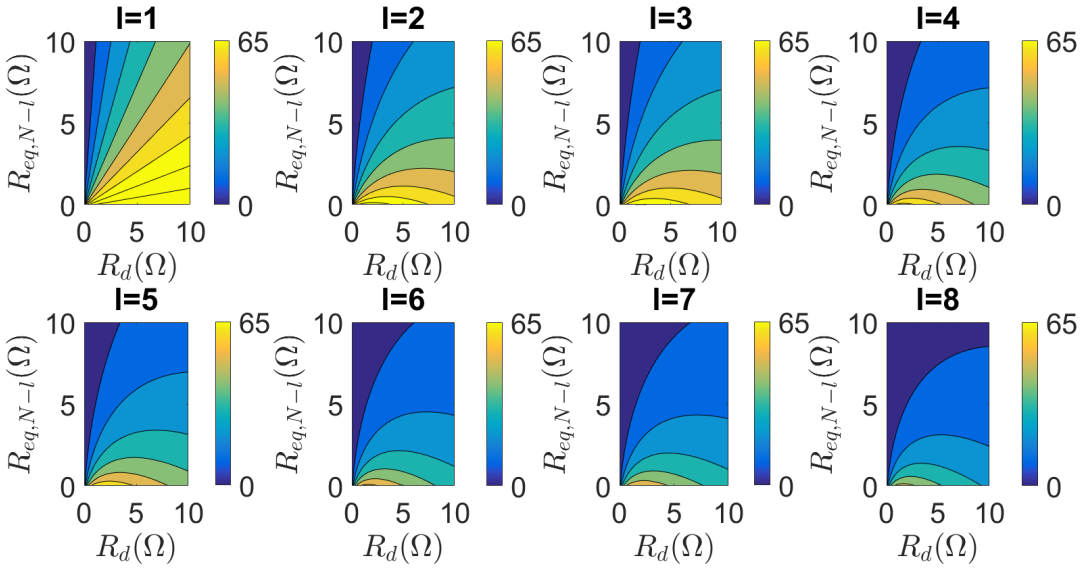

Figure 3.16: Efficiency (%) determined with (3.61) for different values of $R_{eq,N-l}$ and R_d and for different positions of the receiver l.

$R_{eq,N-l} = R_T = 0$ (which represents the situation already studied and analysed in Figs. 3.8 to 3.10). Otherwise, $R_{eq,N-l}$ has a value that oscillates between low and high values as seen in Fig. 2.6, depending on the number of resonators after the receiver, the termination impedance at the end of the line and the electrical parameters of the system. The only way to guarantee that $R_{eq,N-l}$ is constant for any number of resonators after the receiver is to terminate the line with a resistance $R_T = R_{eq,\infty} = \left(-R + \sqrt{4(\omega_0 M)^2 + R^2}\right)/2$, so the equivalent impedance of all the resonators after the lth one ($R_{eq,N-l}$) is always equal to $\left(-R + \sqrt{4(\omega_0 M)^2 + R^2}\right)/2$. Then, for this particular case we can replace $R_{eq,N-l}$ by $R_{eq,\infty} = \left(-R + \sqrt{4(\omega_0 M)^2 + R^2}\right)/2$ in (3.60) and (3.61) and have

$$P_{R_d}(R_{eq,N-l} = R_{eq,\infty}) = \frac{4^l V_s^2 R_d (\omega_0 M)^{2l-2} \iota_1^2}{\left(R_d \left(\iota_3^l - \iota_2^l\right) + \iota_1 \iota_3^l\right)^2} \tag{3.62}$$

and

$$\eta_{R_d}(R_{eq,N-l} = R_{eq,\infty}) = \frac{2^{2l+1} R_d (\omega_0 M)^{2l} \left(4(\omega_0 M)^2 + R^2\right)}{\left(\begin{array}{c} \left(\iota_1 \iota_3^l + R_d \left(\iota_3^l - \iota_2^l\right)\right)\left(-R\left(\iota_1 \iota_3^l - R_d \iota_2^l + R_d \iota_3^l\right)\right) \\ +\iota_1 R_d \left(\iota_2^l + \iota_3^l\right) + 4(\omega_0 M)^2 \iota_3^l + R^2 \iota_3^l \end{array}\right)} \tag{3.63}$$

Then, using (3.62) and (3.63), we can plot again the efficiency and power, for different values of R_d and different positions of the receiver l (Figs. 3.17 and 3.18).

Again, as seen before, the power delivered to a receiver represented by a given R_d has high or low values depending on the parity of the position of the receiver l, while the efficiency decreases

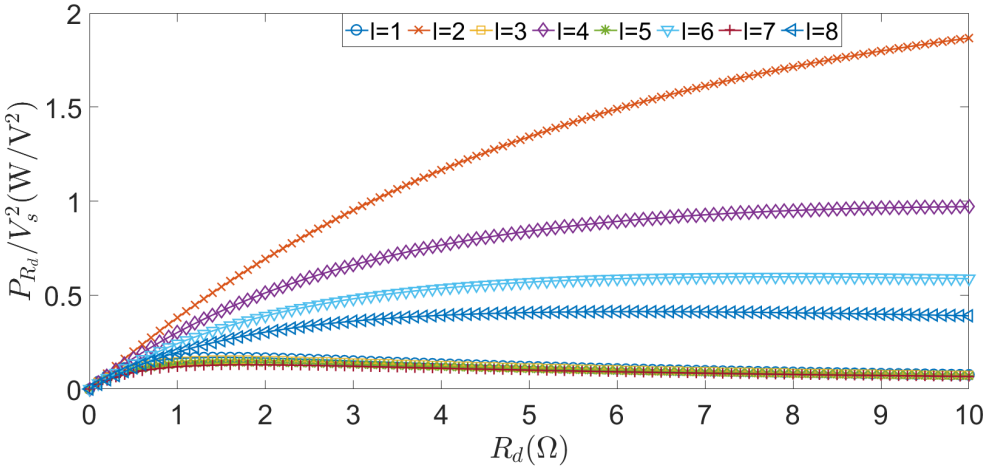

Figure 3.17: Power delivered to R_d for different values of R_d and for different positions of the receiver l for an array terminated with $R_{eq,\infty}$.

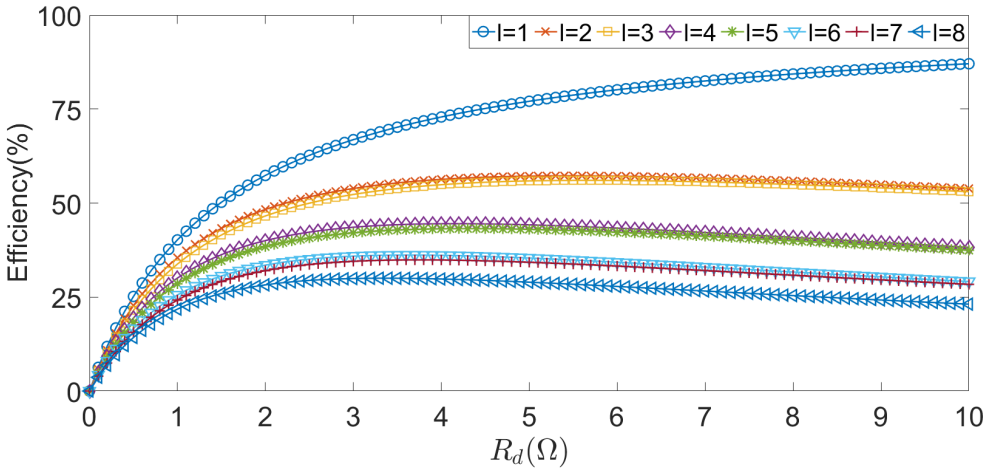

Figure 3.18: Efficiency (%) for different values of R_d and for different positions of the receiver l for an array terminated with $R_{eq,\infty}$.

as the position of the receiver increases. Another interesting thing to note is that for a fixed position l of the receiver, the variation of the power delivered to R_d and the efficiency with R_d is more limited than the one observed in Figs. 3.9 and 3.10.

Nevertheless, to obtain the maximum efficiency possible, we need to determine the value or R_d that guarantees the maximum efficiency for a certain position l of the receiver, which can be calculated by solving

$$\frac{d\eta_{R_d}(R_{eq,N-l} = R_{eq,\infty})}{dR_d} = 0 \tag{3.64}$$

for R_d . Equation (3.64) gives

$$R_d, \eta_{max.(R_{eq,N-l}=R_{eq,\infty})} = \frac{\sqrt{\iota_1^2(-\iota_2)\iota_3^{2l}}}{\sqrt{\left(\iota_3^l - \iota_2^l\right)\left(R\left(\iota_2^l - \iota_3^l\right) + \iota_1\left(\iota_2^l + \iota_3^l\right)\right)}}. \tag{3.65}$$

Finally, if the receiver is in a position which is very distant from the source, R_d, η_{max} tends to the value given by:

$$\lim_{l\to\infty} R_d, \eta_{max.(R_{eq,N-l}=R_{eq,\infty})} = \sqrt{4(\omega_0 M)^2 + R^2}. \tag{3.66}$$

Using (3.65) in (3.63) we can write the expression for the maximum possible value for the efficiency of an array terminated with $R_{eq,\infty}$, with a receiver on the lth position, for given electrical parameters of the array:

$$\eta_{max.(R_{eq,N-l}=R_{eq,\infty})} = \frac{\iota_1 4^l (\omega_0 M)^{2l}}{\left(\begin{array}{c} \iota_1\iota_3^{2l} - \sqrt{\iota_2\iota_3^{2l}}\sqrt{\iota_3\iota_2^{2l} + \iota_2\iota_3^{2l} + (-1)^{l+1}2^{2l+1}R(\omega_0 M)^{2l}} \\ -R\iota_3^{2l} + (-4)^l R(\omega_0 M)^{2l} \end{array}\right)}. \tag{3.67}$$

In the same way, the value of R_d that guarantees the maximum power transfer to the load is given by solving

$$\frac{dP_{R_d}(R_{eq,N-l} = R_{eq,\infty})}{dR_d} = 0 \tag{3.68}$$

for R_d, resulting in the following expression:

$$R_{d,P_{R_d}max.(R_{eq,N-l}=R_{eq,\infty})} = -\frac{\iota_1\iota_3^l}{\iota_2^l - \iota_3^l}. \tag{3.69}$$

Again, by substituting (3.69) in (3.62), we can write the expression for the maximum possible value of the power that can be delivered to a receiver represented by R_d on the lth position, over an array terminated with $R_{eq,\infty}$, with a given voltage source with RMS value V_s and given electrical parameters of the array:

$$P_{R_d max.(R_{eq,N-l}=R_{eq,\infty})} = \frac{4^{l-1}V_s^2(\omega_0 M)^{2l-2}\iota_1\iota_3^{-l}}{\iota_3^l - \iota_2^l} \tag{3.70}$$

If the receiver is very distant from the source, $R_{d,P_{R_d}max}$ tends to the value given by:

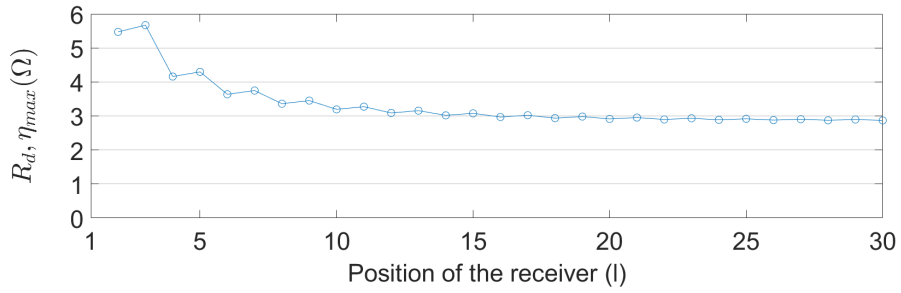

Figure 3.19: Value of $R_d, \eta_{max.(R_{eq,N-l}=R_{eq,\infty}}$ for different positions of the receiver.

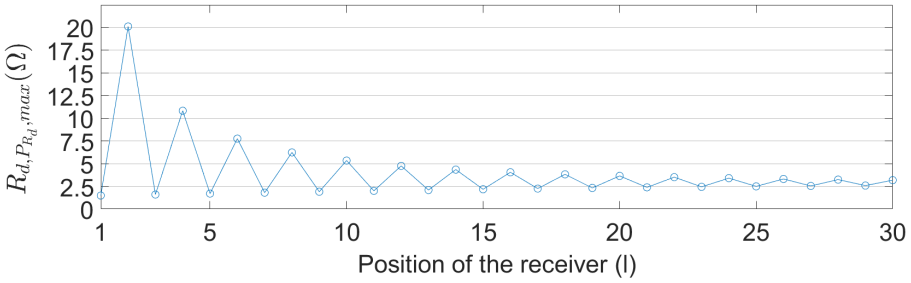

Figure 3.20: Value of $R_{d,P_{R_d}max.(R_{eq,N-l}=R_{eq,\infty}}$ for different positions of the receiver.

$$\lim_{l\to\infty} R_{d,P_{R_d}max.(R_{eq,N-l}=R_{eq,\infty})} = \sqrt{4(\omega_0 M)^2+R^2} \tag{3.71}$$

Then, using (3.65) and (3.69) we can plot the values of R_d that guarantee the maximum efficiency and maximum power transferred, respectively (Figs. 3.19 and 3.20).

As shown in (3.66) and (3.71), the value of the receiver impedance R_d that guarantees the maximum efficiency and power tends to $\sqrt{4(\omega_0 M)^2+R^2} = 2.87$; in the case of a very low loss line ($R \ll \omega_0 M$) R_d tends to $2\omega_0 M$. However, as seen in Figs 3.19 and 3.20, the value of R_d that guarantees the maximum efficiency has less oscillations and gets closer to $\sqrt{4(\omega_0 M)^2+R^2}$ for a smaller number of resonators than the value of R_d for the maximum power delivered.

If we want to know what is the maximum theoretical power and efficiency that we can obtain for particular circuit conditions, we can use r defined in (3.58) in equations (3.67) and (3.70) and plot the values for different values of r and different positions of the receiver l in an array terminated with $R_{eq,\infty}$ (Figs. 3.21 and 3.22).

As seen in Fig. 3.22, the maximum efficiency values decrease with r and with the position of the receiver l. On the other hand, as it can be observed in Fig. 3.21, the values for the maximum power that can be delivered to R_d decrease with r; for the same value of r, higher values are found

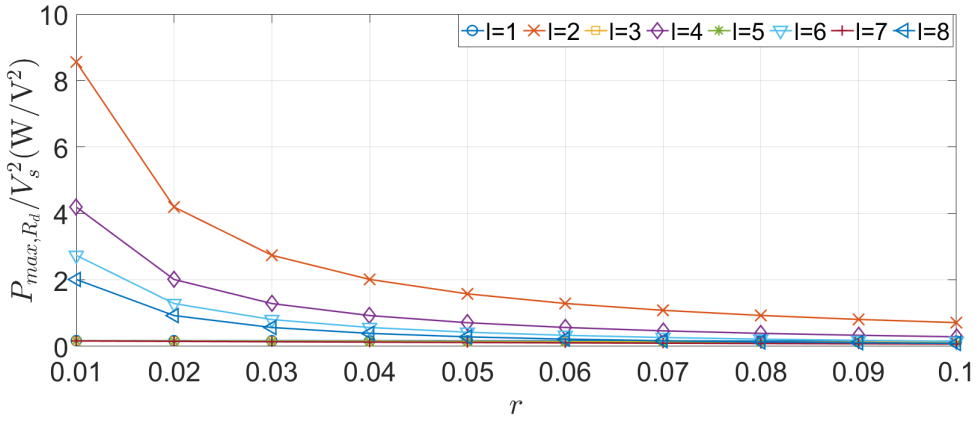

Figure 3.21: Maximum power transfer to a determinate receiver R_d in the lth position that is possible to obtain for different values of r.

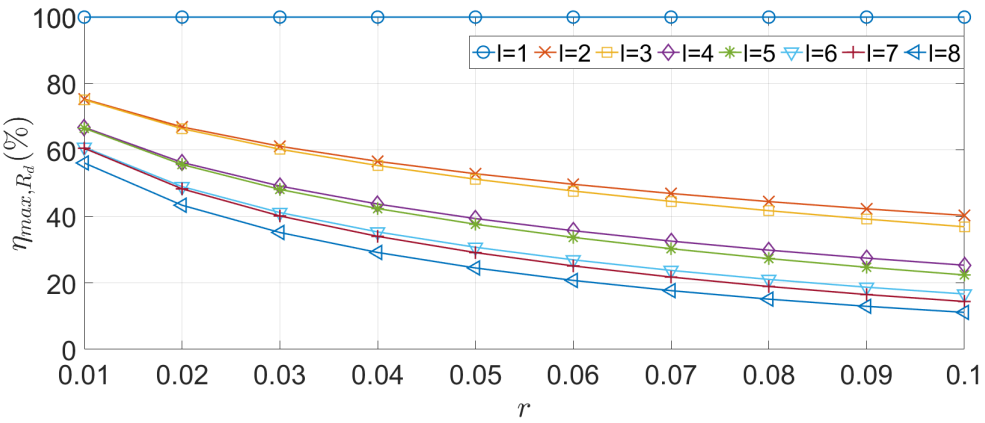

Figure 3.22: Maximum efficiency that is possible to obtain with a receiver R_d in the lth position for different values of r.

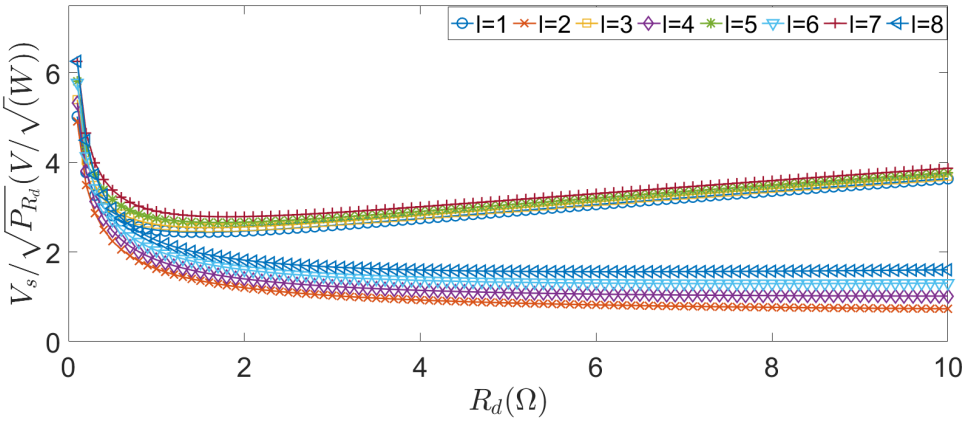

Figure 3.23: Voltage source RMS values V_s considering a fixed power P_{R_d}, for different values of R_d and for different positions of the receiver l for an array terminated with $R_{eq,\infty}$.

for an even position ($l = 2$, 4, 6 and 8) than for an odd position ($l = 1$, 3, 5 and 7). Moreover, the values shown in Figs. and 3.22 and 3.21 are lower than the ones in Figs. 3.13 and 3.14, since now we are considering that the resonator array continues after the cell under the receiver, which leads to extra losses.

So far, we have determined the power delivered to R_d, P_{R_d} for a constant voltage source. Instead, for a variable voltage source, we can calculate the RMS value of the voltage source V_s needed to keep the power P_{R_d} constant for different positions of the receiver (Fig. 3.23).

3.4.2 Second case

3.4.2.1 Values of the currents on the resonators

After the analysis and examples provided for the first case, we now consider a second case, represented by (3.7). Then replacing $a = j\omega M$; $b = \hat{Z}$; $c = \hat{Z} + \hat{Z}_T''$ $d = \hat{Z} + \hat{Z}_{d1}$, in (3.39)-(3.41) we can write the expressions for the currents in the resonators:

$$\hat{I}_1 = \begin{cases} \dfrac{2^{-2l-N-1}(\omega M)^{-2(l+1)}\hat{V}_s \begin{pmatrix} \iota_1\left(-4^l\right)(\omega M)^{2l}\left(\iota_2^N-\iota_3^N\right)\left(2(\omega M)^2+\hat{Z}_T'(\hat{Z}_{d1}-Z)\right) \\ +4^l(\omega M)^{2l}\left(\iota_2^N+\iota_3^N\right)\left(2(\omega M)^2(\hat{Z}_{d1}+2\hat{Z}_T')+Z\hat{Z}_T'(Z-\hat{Z}_{d1})\right) \\ +(-1)^l\hat{Z}_{d2}\left(\iota_2^{2l}\iota_3^N\left(\iota_3(Z+\hat{Z}_T')+2(\omega M)^2\right)+\iota_2^N\iota_3^{2l}\left(\iota_2(Z+\hat{Z}_T')+2(\omega M)^2\right)\right) \end{pmatrix}}{\iota_1^2\det\hat{\mathbf{Z}}_\mathbf{m}}, & l \geq 3 \\ \dfrac{2^{1-N}\hat{V}_s\left(\iota_2^{N-3}(\iota_3-2(\hat{Z}+\hat{Z}_T'))\left(\iota_2(Z+\hat{Z}_{d1})+2(\omega M)^2\right)+\iota_3^{N-3}(\iota_3+2\hat{Z}_T')\left(\iota_3(\hat{Z}+\hat{Z}_{d1})+2(\omega M)^2\right)\right)}{\iota_1\det\hat{\mathbf{Z}}_\mathbf{m}}, & l = 2 \\ \dfrac{2^{-N}\hat{V}_s\left((\iota_3-2\hat{Z}_T')\iota_2^{N-1}+(2\hat{Z}_T'-\iota_2)\iota_3^{N-1}\right)}{\iota_1\det\hat{\mathbf{Z}}_\mathbf{m}}, & l = 1 \end{cases} \tag{3.72}$$

$$\hat{I}_l = \hat{V}_s\frac{2^{l-N-1}(-j(\omega M))^{l-1}\left(\iota_2^{N-l}(\iota_2+2\hat{Z}_T'))+\iota_3^{N-l}(\iota_3+2\hat{Z}_T')\right)}{\iota_1\det\hat{\mathbf{Z}}_\mathbf{m}}, \text{ for } 2 \leq l \leq N-1 \tag{3.73}$$

and

$$\hat{I}_N = \hat{V}_s \frac{(-j\omega M)^{N-1}}{\det \hat{\mathbf{Z}}_\mathbf{m}} \tag{3.74}$$

with

$$\det\hat{\mathbf{Z}}_\mathbf{m} = \frac{2^{-2l-N-1}(\omega M)^{-2l}\begin{pmatrix} 4^l(\omega M)^{2l}\left((\iota_1-\hat{Z}_{d1})\iota_2^N(\iota_2-2\hat{Z}'_T)+(\iota_1+\hat{Z}_{d1})\iota_3^N(\iota_3+2\hat{Z}'_T)\right) \\ +(-1)^l\hat{Z}_{d1}\left(\iota_2^{2l}\left(-\iota_3^N\right)(\iota_3+2\hat{Z}'_T)-\iota_2^N\iota_3^{2l}(\iota_2+2\hat{Z}'_T)\right)\end{pmatrix}}{\iota_1^2} \tag{3.75}$$

where $\iota_1 = \sqrt{4(\omega M)^2+\hat{Z}^2}$, $\iota_2 = \hat{Z}-\sqrt{4(\omega M)^2+\hat{Z}^2}$, and $\iota_3 = \hat{Z}+\sqrt{4(\omega M)^2+\hat{Z}^2}$

3.4.2.2 Efficiency and power delivered to a receiver R_{d1} over the lth resonator

First of all, we analyse the particular situation where there is a receiver represented by $\hat{Z}_{d1}$ over the lth cell, in a line with N resonators, terminated by $\hat{Z}'_T = \hat{Z}_T$, as represented in Fig. 3.3 (a). Then, considering that we are operating at the resonant frequency, so that $\hat{Z} = R$, $\omega M = \omega_0 M$, $\hat{Z}_{d1} = R_{d1}$ and $\hat{Z}_T = R_T$, we can define the efficiency as the ratio between the power absorbed by R_{d1} and the input power as:

$$\eta_{R_{d1}} = \frac{P_{R_{d1}}}{P_{in}} = \frac{{I_l}^2 R_{d1}}{V_s I_1} \tag{3.76}$$

where I_1, I_l and V_s are the RMS values of the currents in the first and lth resonators and of the voltage source, respectively.Then, using the expression obtained for the current (3.72), we can rewrite the expressions for the power delivered to a receiver R_{d1}:

$$P_{R_{d1}} = \frac{V_s^2 4^{l-N-1}(\omega_0 M)^{-2l-2}\left(\iota_2^N\iota_3^l(\iota_3-2(R+R_T))+\iota_2^l\iota_3^N(\iota_3+2R_T)\right)^2}{\iota_1^2\left(\det\hat{\mathbf{Z}}_\mathbf{m}\right)^2}R_{d1}. \tag{3.77}$$

Note that this case was already analysed in subsection 3.4.1.3, using the simplification in which the $N-l$ resonators after the lth one were reduced to an equivalent impedance $R_{eq,N-l}$. However, using the results obtained for the currents, we can study this case with more detail, taking into account the termination impedance R_T at the end of the line.

As an example, we can start considering a receiver over an array of 7 ($N = 7$) or 8 resonators ($N = 8$). Then, using (3.76) and (3.77) we can plot the efficiency and the power delivered to the receiver R_{d1} in the lth position for different values of R_{d1} and R_T, for arrays of 7 or 8 resonators. The results are presented in Figs. 3.24 to 3.27.

Comparing the results displayed in Figs. 3.24 and 3.25, we can observe that for the 7-resonator array the peaks of efficiency and power transferred to R_{d1} occur for low values of R_T when the

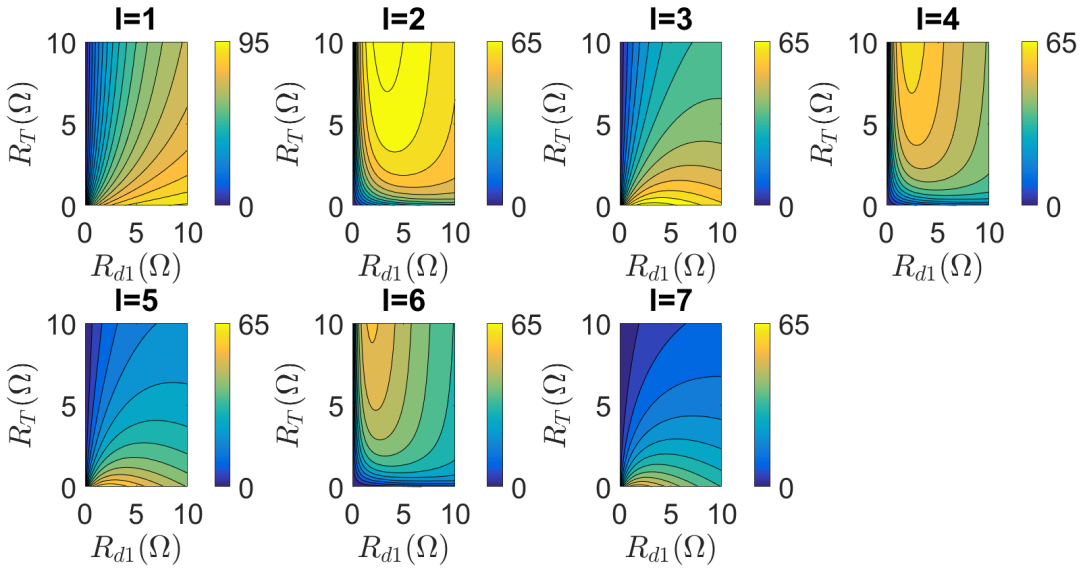

Figure 3.24: Efficiency (%) determined with (3.76), for different values of R_T and R_{d1} and for different positions of the receiver (l) for a 7-resonator array.

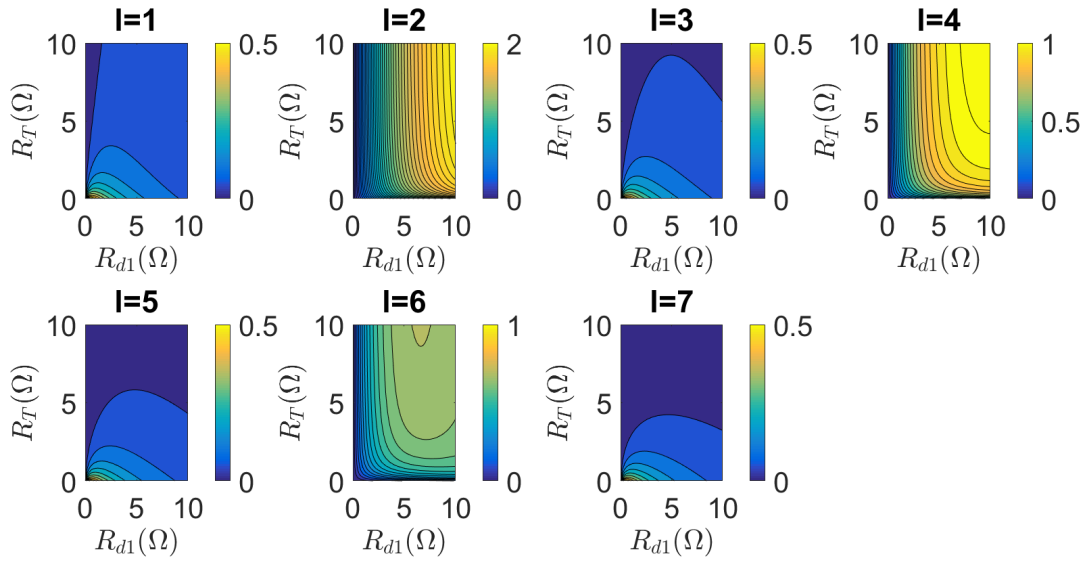

Figure 3.25: Power delivered to R_{d1}, $P_{R_{d1}}/V_s^2$ (W/V^2), determined with (3.77) for different values of R_T and R_{d1} for different positions of the receiver (l) for a 7-resonator array.

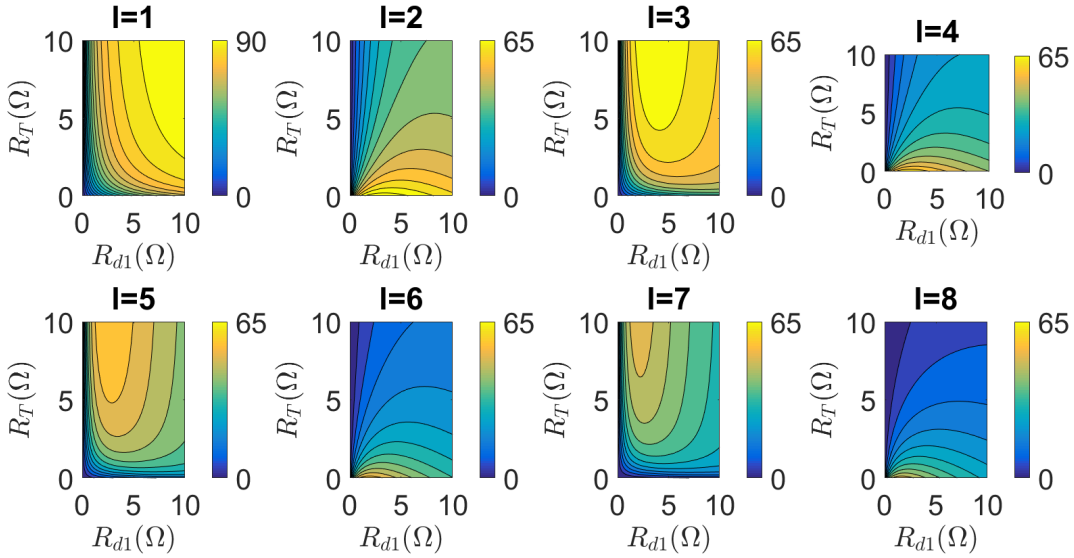

Figure 3.26: Efficiency (%) determined with (3.76), for different values of R_T and R_{d1} and for different positions of the receiver (l) for a 8-resonator array.

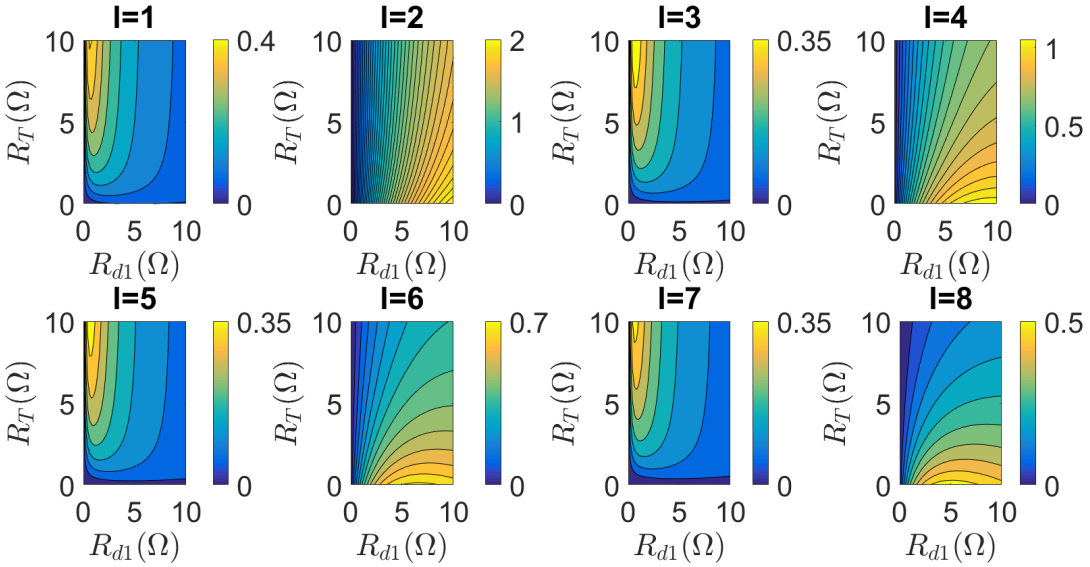

Figure 3.27: Power delivered to R_{d1}, $P_{R_{d1}}/V_s^2$ (W/V^2), determined with (3.77) for different values of R_T and R_{d1} for different positions of the receiver (l) for a 8-resonator array.

receiver is in an odd position ($l = 1$, 3, 5 and 7) and for high values of R_T when the receiver is in an even position ($l = 2$, 4 and 6); contrarily, regarding the 8-resonator array, as seen in Figs. 3.26 and 3.27, the peaks of efficiency and $P_{R_{d1}}$ occur for low values of R_T when the receiver is in an even position ($l = 2$, 4, 6 and 8) and for high values of R_T when the receiver is in an odd position ($l = 1$, 3, 5 and 7). Therefore, in a more generic way, we can say that the peaks of efficiency and delivered power $P_{R_{d1}}$ occur for low values of R_T when the difference $N-l$ between the total number of resonators N and the receiver's position l is an even number and for high values of R_T when $N-l$ is an odd number, also confirming what shown in [14, 16].

Furthermore, the results obtained in Figs. 3.24 to 3.27 confirm what was shown previously in Figs. 3.16 and 3.15, i.e., the efficiency and power transfer are maxima when $R_{eq,N-l}$ is close to zero. $R_{eq,N-l}$ represents the $N-l$ cells after the resonator below the receiver (lth one). In order to obtain a low value of $R_{eq,N-l}$ we need a high value of R_T when $N-l$ is odd and a low value of R_T when $N-l$ is an even number. This oscillation of $R_{eq,N-l}$ caused by higher or lower values of R_T, also demonstrated in Chapter 2, can only be smoothed by setting $R_T = R_{eq,\infty} = \left(-R+\sqrt{4(\omega_0 M)^2+R^2}\right)/2$, which was already analysed with the results being shown in Figs. 3.17 and 3.18. In fact, if we replace $R_T = R_{eq,\infty} = \left(-R+\sqrt{4(\omega_0 M)^2+R^2}\right)/2$ in (3.77) and (3.76), we obtain equivalent expressions to (3.70) and (3.63) (with $R_{d1} = R_d$).

3.4.2.3 Efficiency and power delivered to two receivers R_{d1} and R_{d2}, with the receiver R_{d1} over the lth resonator and the receiver R_{d2} over the last cell

Now, we analyse a receiver represented by $\hat{Z}_{d1}$ over the lth cell ($1 \leq l < N$) and another one over the Nth cell, as represented by (3.3) (b), meaning that $\hat{Z}'_T = \hat{Z}_{d2} + \hat{Z}_T$. Assuming that we are operating at the resonant frequency, so that $\hat{Z} = R$, $\omega M = \omega_0 M$, $\hat{Z}_{d1} = R_{d1}$, $\hat{Z}_{d2} = R_{d2}$ and $\hat{Z}_T = R_T$, we can define the total efficiency of the system as the ratio between the sum of the powers absorbed by R_{d1} and R_{d2} and the input power as:

$$\eta_{total} = \eta_{R_{d1}} + \eta_{R_{d2}} = \frac{P_{R_{d1}} + P_{R_{d2}}}{P_{in}} = \frac{{I_l}^2 R_{d1} + {I_N}^2 R_{d2}}{V_s I_1}. \tag{3.78}$$

in which I_1, I_l , I_N and V_s are the RMS values of the current in the first, lth, Nth resonators and of the voltage source, respectively.Then, using the expressions obtained for the currents (3.72), (3.73) and (3.74) we can rewrite the expressions for the powers delivered to receivers R_{d1} and R_{d2}:

$$P_{R_{d1}} = \frac{V_s^2 4^{l-N-1} (\omega_0 M)^{-2l-2} \left(\iota_2^N \iota_3^l (\iota_3 - 2(R+R_{d2}+R_T)) + \iota_2^l \iota_3^N (\iota_3 + 2(R_{d2}+R_T))\right)^2}{\iota_1^2 \left(\det \hat{\mathbf{Z}}_\mathbf{m}\right)^2} R_{d1} \tag{3.79}$$

and

$$P_{R_{d2}} = V_s^2 \frac{(\omega_0 M)^{2N-2}}{\left(\det \hat{\mathbf{Z}}_\mathbf{m}\right)^2} R_{d2}. \tag{3.80}$$

Considering that $R_T = 0$, which means that the Nth cell is not connected to any termination impedance, using (3.78), (3.79) and (3.80) we can plot the power delivered to each receiver and also the total efficiency of the system for arrays of 7 or 8 resonators (Figs. Figs. 3.28–3.30 and

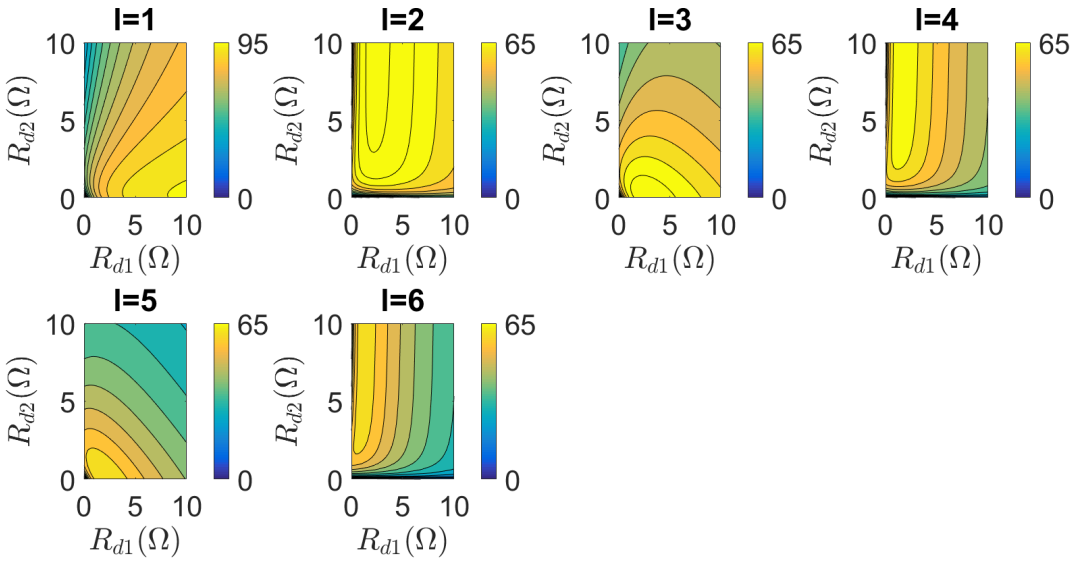

Figure 3.28: Total efficiency (%) determined with (3.78) (with $R_T = 0$) for different values of R_{d1} and R_{d2} and for different positions of the first receiver R_{d1} (l) for a 7-resonator array ($N = 7$) with the second receiver R_{d2} over the Nth cell.

3.32– 3.31, respectively).

Again, the behaviour of the efficiency and power delivered to the receivers R_{d1} and R_{d2} repeats itself for odd or even positions of the first receiver depending on the total number of resonators. Starting by analysing the values of the total efficiency (Figs. 3.28 and 3.31), we have peak values for low values of R_{d2} when $N-l$ is even ($l = 1$, 3 and 5 for the 7 resonator case and $l = 2$, 4 and 6 for the 8 resonator case) and for high values of R_{d2} when $N-l$ is odd ($l = 2$, 5 and 6 for the 7 resonator case and $l = 1$, 3, 5 and 7 for the 8 resonator case). Moreover, for the cases with an odd $N-l$, when R_{d1} is between approximately 1Ω and 4Ω, there is a large range of values of R_{d2} which guarantee the maximum efficiency. Regarding the power delivered to R_{d1} (Figs. 3.29 and 3.32), as expected, the values obtained are the same ones obtained in the previous case, see Figs. 3.25 and 3.27. Finally, analysing the value of the power delivered to the second receiver $P_{R_{d2}}$ (Figs. 3.30 and 3.33), the highest values occur for $R_{d1} = 0$ (i.e., no first receiver), meaning that all the power delivered to the array is absorbed by the second receiver R_{d2}, which is the same result obtained in section 3.4.1.2. However, for the same values of R_{d1} and R_{d2} the values of $P_{R_{d2}}$ are higher when $N-l$ is an even number than when $N-l$ is an odd one.

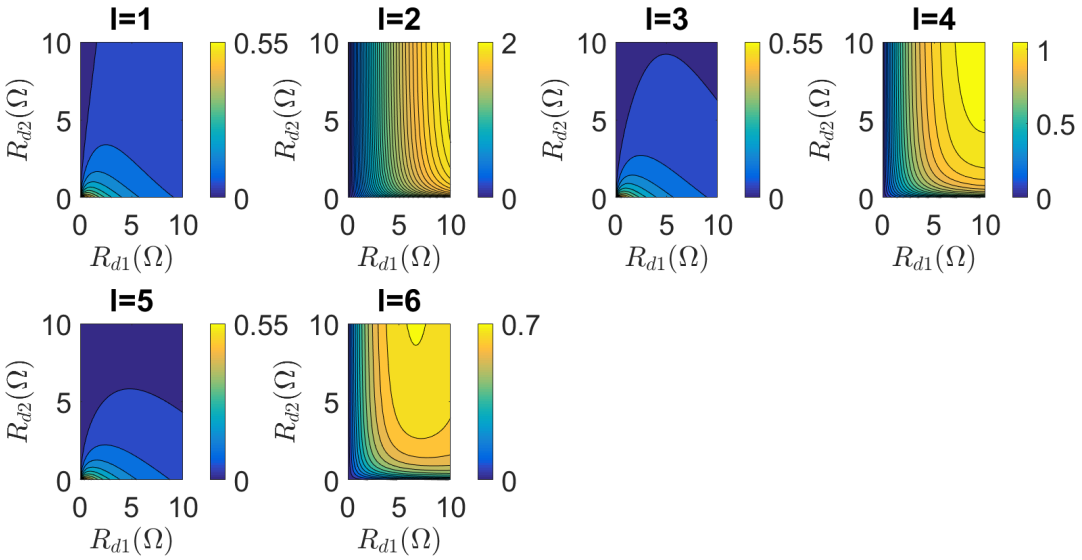

Figure 3.29: Power delivered to R_{d1}, $P_{R_{d1}}/V_s^2$ (W/V^2) determined with (3.79) (with $R_T = 0$) for different values of R_{d1} and R_{d2} and for different positions of the receiver R_{d1} (l) for a 7-resonator array ($N = 7$) with the second receiver R_{d2} over the Nth cell.

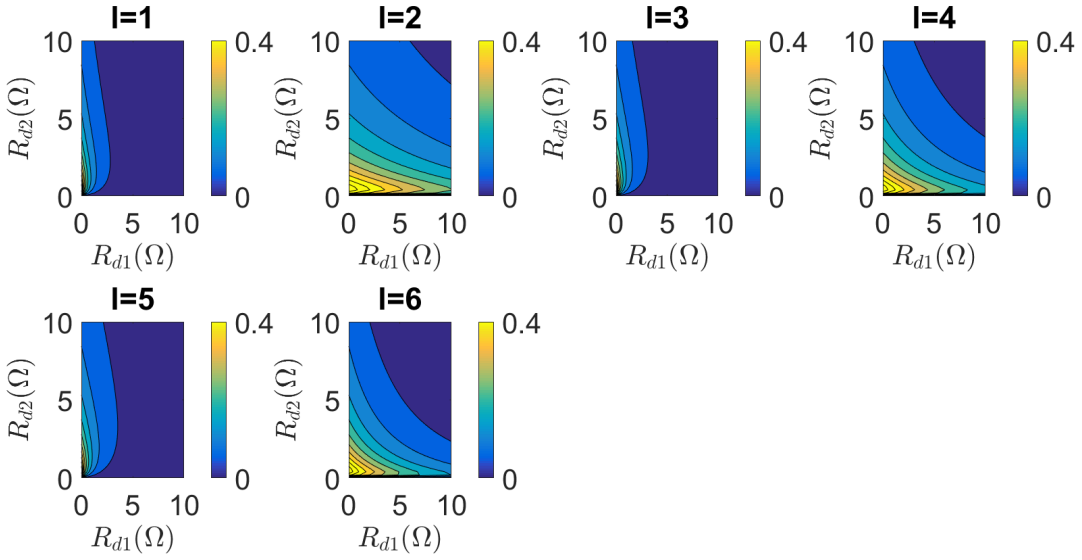

Figure 3.30: Power delivered to R_{d2} , $P_{R_{d2}}/V_s^2$ (W/V^2) determined with (3.80) (with $R_T = 0$) for different values of R_{d1} and R_{d2} and for different positions of the receiver R_{d1} (l) for a 7-resonator array ($N = 7$) with the second receiver R_{d2} over the Nth cell.

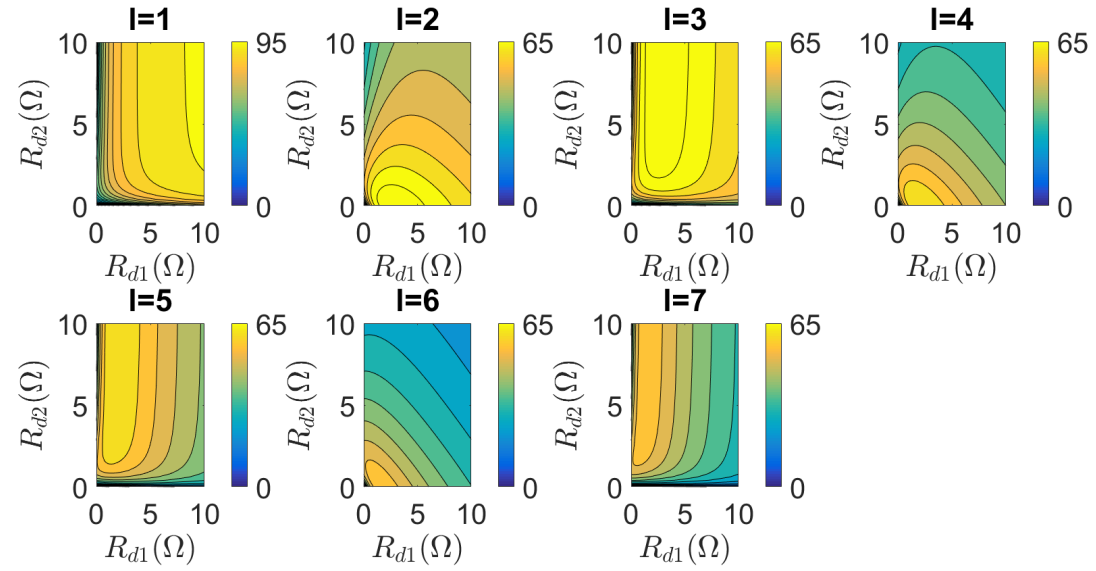

Figure 3.31: Total efficiency (%) determined with (3.78) (with $R_T = 0$) for different values of R_{d1} and R_{d2} and for different positions of the first receiver R_{d1} (l) for a 8-resonator array $(N = 8)$ with the second receiver R_{d2} over the Nth cell.

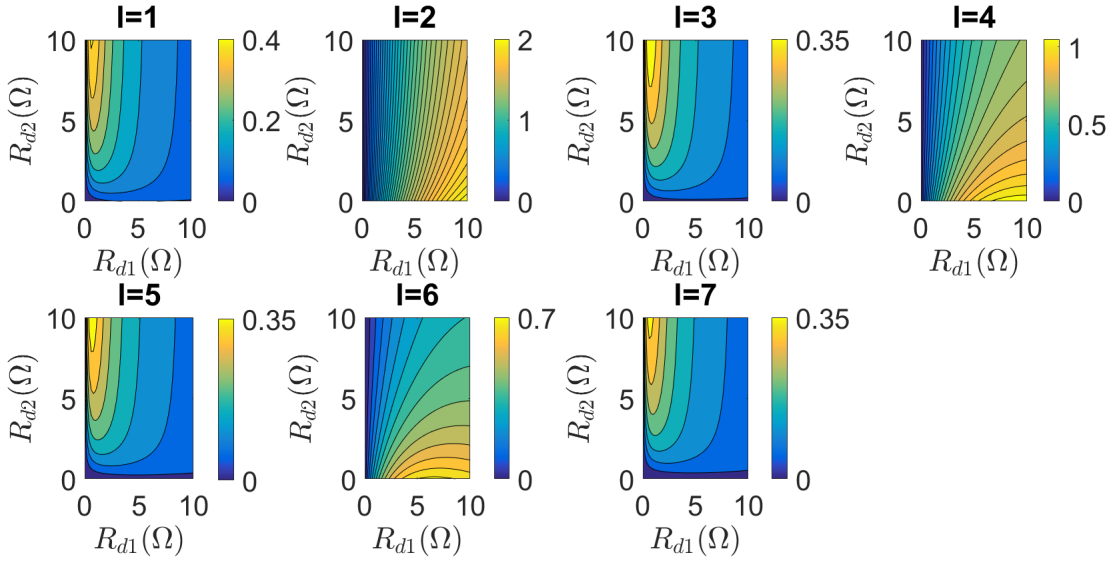

Figure 3.32: Power delivered to R_{d1}, $P_{R_{d1}}/V_s^2$ (W/V^2) determined with (3.79) (with $R_T = 0$) for different values of R_{d1} and R_{d2} and for different positions of the receiver R_{d1} (l) for a 8-resonator array $(N = 8)$ with the second receiver R_{d2} over the Nth cell.

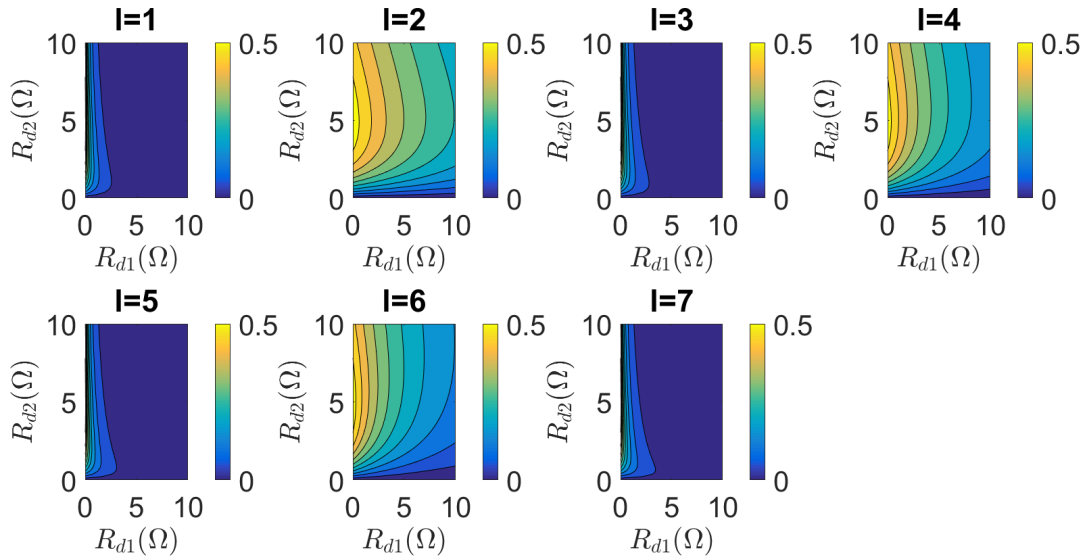

Figure 3.33: Power delivered to R_{d2} , $P_{R_{d2}}/V_s^2$ (W/V^2) determined with (3.80) (with $R_T = 0$) for different values of R_{d1} and R_{d2} and for different positions of the receiver R_{d1} (l) for a 8-resonator array ($N = 8$) with the second receiver R_{d2} over the Nth cell.

We consider now another example where the difference $P_{R_{d2}} - P_{R_{d1}}$ between the power delivered to each receiver is plotted in order to examine the conditions of the system under which the power delivered to each resonator is the same (i.e. $P_{R_{d2}} - P_{R_{d1}} = 0$). The results are shown in Figs. 3.34 and 3.35 for 7-resonator and 8-resonator arrays ($N = 7$ and $N = 8$), respectively.

Then, from the plots in Figs. 3.34 and 3.35, using the expressions of $P_{R_{d1}}$ and $P_{R_{d2}}$, (3.79) and (3.80), and solving the equation $P_{R_{d2}} - P_{R_{d1}} = 0$ for R_{d1}, we can determine the values of R_{d1} and R_{d2} which make the power delivered to both receivers equal. We can plot these values of R_{d1} and R_{d2} for different positions of the first receiver l in for arrays of 7 or 8 resonators ($N = 7$ and $N = 8$) (Figs. 3.36 and 3.36).

Observing Figs. 3.34 to 3.37 it is possible to see that the difference $P_{R_{d2}} - P_{R_{d1}}$ depends on the value of $N - l$ being even or odd. For example, for a $R_{d2} = 5\Omega$, we need higher values of R_{d1} to keep the power constant if $N - l$ is even and lower values of R_{d1} otherwise. Considering that the first receiver is represented by a fixed value of R_{d1}, we can adjust the value of receiver R_{d2} on the last cell, depending on the position l of the first receiver, in order to keep the power delivered to both resonators equal. For example, as observed in Figs. 3.36 and 3.37, if R_{d1} is equal to 0.9Ω, we can adjust R_{d2} from 2Ω to 4Ω, depending on the position of the first receiver in order to make that the same power is delivered to both receivers.

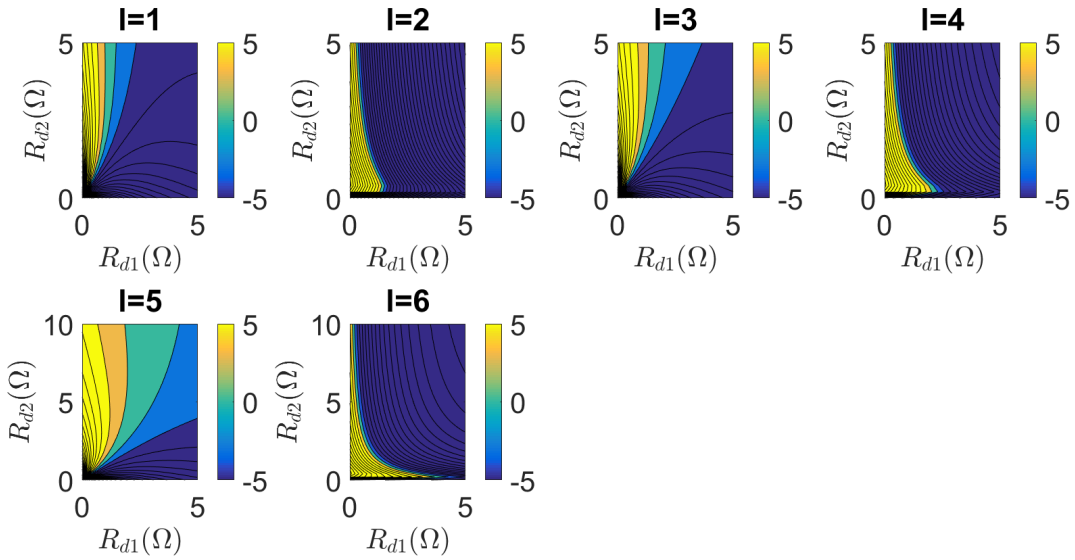

Figure 3.34: Difference between the powers delivered to each receiver $P_{R_{d2}} - P_{R_{d1}}$(in W/V)^2 (determined with (3.79) and (3.80), with $R_T = 0$) for different values of R_{d1} and R_{d2} and for different positions of the first receiver (l) for a 7-resonator array ($N = 7$).

3.4.2.4 Efficiency and power delivered to two receivers R_{d1} and R_{d2} over the array

We consider now the situation represented in Fig. 3.3 (c), i.e., two receivers over different positions, e.g., over the lth resonator and mth resonator, in a resonator array with N resonators (with $1 \leq l < m < N$) terminated by a resistance $R_T = R_{eq,\infty} = \left(-R + \sqrt{4(\omega_0 M)^2 + R^2}\right)/2$. Then, we can use (3.78) –(3.80) with $R_T = R_{eq,N-m} = \left(-R + \sqrt{4(\omega_0 M)^2 + R^2}\right)/2$ to calculate the total efficiency of the system and the power delivered to each receiver depending on its position. Since in this case there are too many variablesto consider in order to make a simple analysis, we consider that the receivers are equivalent, and are in different positions on the resonator array. Thus, for $R_{d1} = R_{d2} = 5\Omega$ and $R_{d1} = R_{d2} = 1.5\Omega$ we can plot $P_{R_{d1}}$, $P_{R_{d2}}$ and η_{total} (Figs. 3.38– 3.40 and 3.41–3.43, respectively).

By comparing Figs. 3.38, 3.39 and 3.40 with Figs. 3.41, 3.42 and 3.43 we observe that we can achieve higher peak values for $P_{R_{d1}}$, $P_{R_{d2}}$ and η_{total} for higher values of R_{d1} and R_{d2} (5Ω), but also lower minimum values. In other words, for smaller values of R_{d1} and R_{d2} (1.5Ω), there is a smaller variation of $P_{R_{d1}}$, $P_{R_{d2}}$ and η_{total} with the change of the position of the receivers,

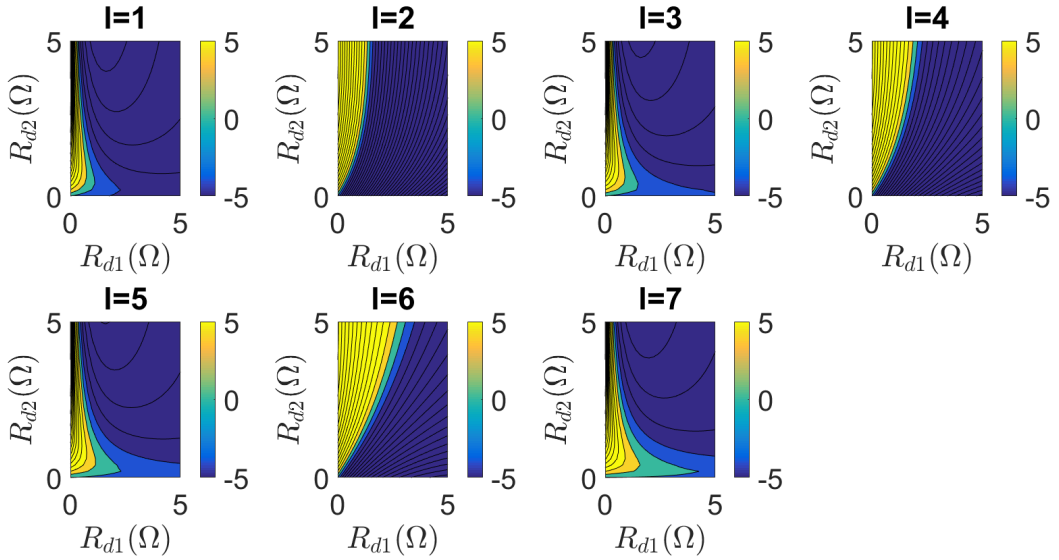

Figure 3.35: Difference between the powers delivered to each receiver $P_{R_{d2}} - P_{R_{d1}}$(in W/V)^2 (determined with (3.79) and (3.80), with $R_T = 0$) for different values of R_{d1} and R_{d2} and for different positions of the first receiver (l) for a 8-resonator array $(N = 8)$.

although the maximum values of the power delivered to each receiver and total efficiency are lower. Moreover, regarding the power delivered to R_{d1}, we can see that it has its maximum values for even values of l and minimum values for odd values of l, which is in agreement with what was shown in Figs. 3.15 and 3.17, and also that the position of the second receiver has little influence on $P_{R_{d1}}$ when it is far away from the first one ($m \gg l$). Finally, regarding the power delivered to R_{d2}, we can see that its maximum values are obtained when both receivers are in even positions (e.g., $l = 2$ and $m = 4$).

3.4.2.5 Efficiency and power delivered to a load or a receiver over the last cell represented by R_T, considering the effect of a source impedance R_s

Using the mathematical results obtained for the second case, we can also analyse the effect of a source with an internal resistance in the efficiency and power transfer of the system, situation which is represented in Fig. 3.4 and in (3.8). For simplicity, we consider the situation where there is a receiver or a physical load over the last cell ($\hat{Z}'_T = \hat{Z}_T$) using the expressions of the currents determined in the second case considered (3.72) to (3.74), with $\hat{Z}_{d1} = \hat{Z}_s$ and $l = 1$. Assuming that we are operating at the resonant frequency, so that $\hat{Z} = R$, $\omega M = \omega_0 M$, $\hat{Z}_s = R_s$, $\hat{Z}_T = R_T$, we can write the expression for the efficiency, considering that the input power is determined at the terminals of the voltage source, including the internal source resistance R_s:

$$\eta_{R_T,w/R_s} = \frac{P_{R_T,w/R_s}}{P_{in,w/R_s}} = \frac{I_N^2 R_T}{(V_s - R_s I_1) I_1} \tag{3.81}$$

where I_1, I_N and V_s are the RMS values of the currents in the first and Nth resonators and of the voltage source.Then, using the expressions obtained for the currents (3.72) and (3.74) we can rewrite the expressions for the efficiency and power delivered to a load or a receiver on the last

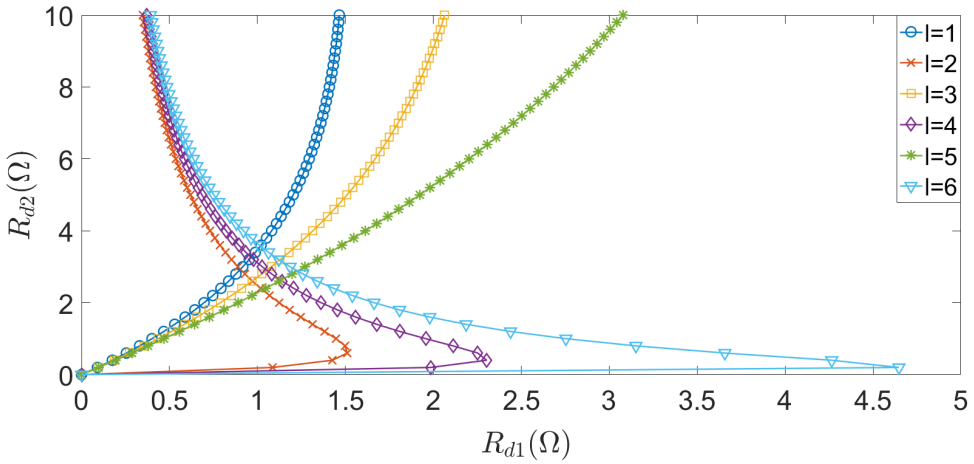

Figure 3.36: Values of R_{d1} and R_{d2} that make the power delivered to both receivers equal, ($P_{R_{d2}} - P_{R_{d1}}$=0) (determined with (3.79) and (3.80), with $R_T = 0$) for different positions of the first receiver l for a 7-resonator array ($N = 7$).

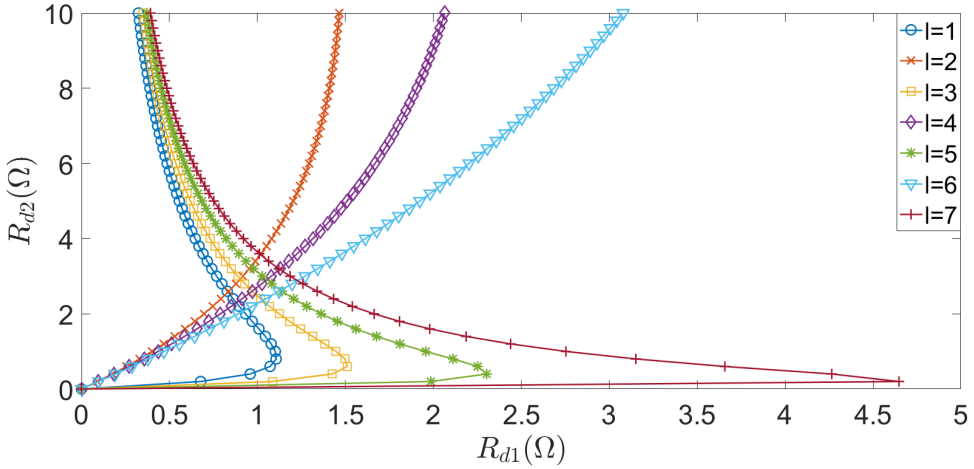

Figure 3.37: Values of R_{d1} and R_{d2} that make the power delivered to both receivers equal, ($P_{R_{d2}} - P_{R_{d1}}$=0) (determined with (3.79) and (3.80), with $R_T = 0$) for different positions of the first receiver l for a 8-resonator array ($N = 8$).

cell represented by R_T:

$$\eta_{R_T,w/R_s} = \frac{2^{2N+1} R_T (\omega_0 M)^{2N} \iota_1^2}{\left(\begin{array}{c} -\iota_1 \left((\omega_0 M)^2 + R_T^2 \right) \left(\iota_2^{2N} - \iota_3^{2N} \right) + R R_T \left(2R \iota_2^N \iota_3^N - R_T \left(\iota_2^N - \iota_3^N \right)^2 \right) \\ + (\omega_0 M)^2 \left(4R_T \left(\iota_2^{2N} + \iota_3^{2N} \right) + R \left(\iota_2^N - \iota_3^N \right)^2 \right) \end{array} \right)} \tag{3.82}$$

and

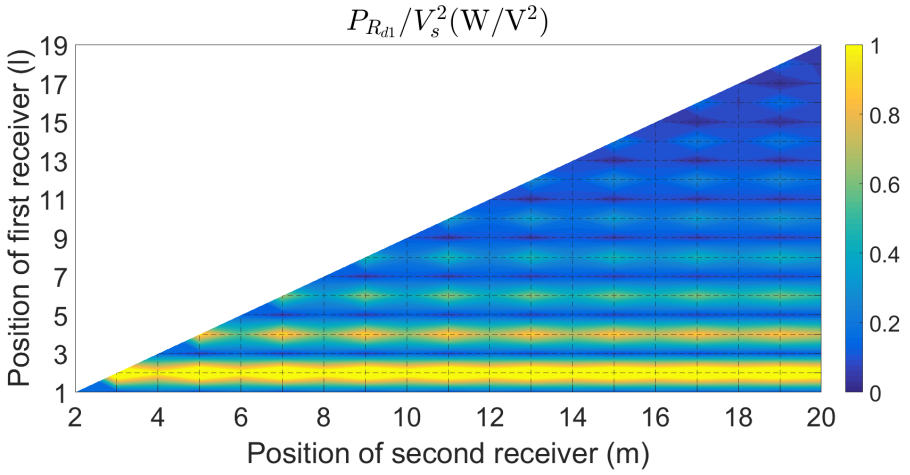

Figure 3.38: Power delivered to R_{d1} for $R_{d1} = R_{d2} = 5\Omega$ and for different positions of the first and second receiver m (1 refers to the resonator connected to the power source and 20 to the resonator connected to the termination impedance).

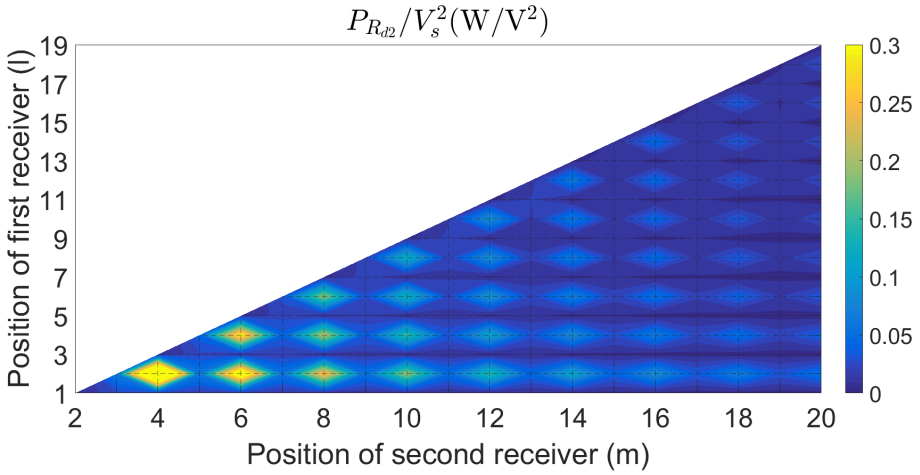

Figure 3.39: Power delivered to R_{d2} for $R_{d1} = R_{d2} = 5\Omega$ and for different positions of the first l and second receiver m (1 refers to the resonator connected to the power source and 20 to the resonator connected to the termination impedance).

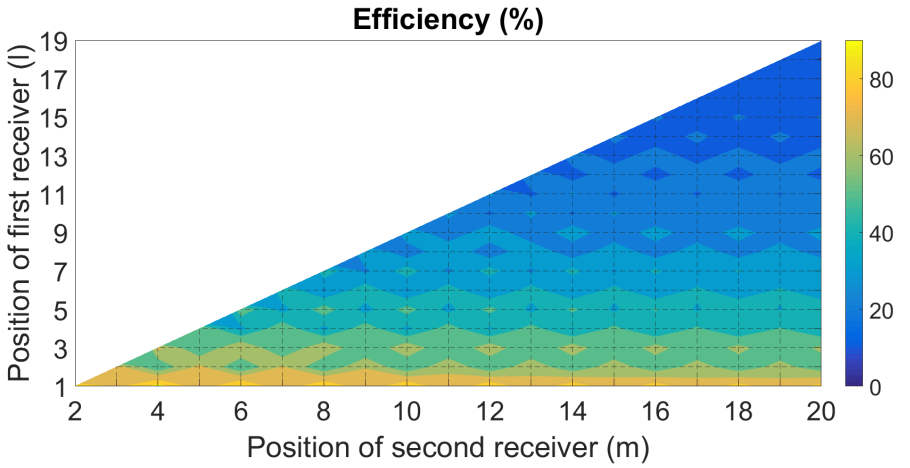

Figure 3.40: Total efficiency (η_{total}) for $R_{d1} = R_{d2} = 5\Omega$ and for different positions of the first l and second receiver m (1 refers to the resonator connected to the power source and 20 to the resonator connected to the termination impedance).

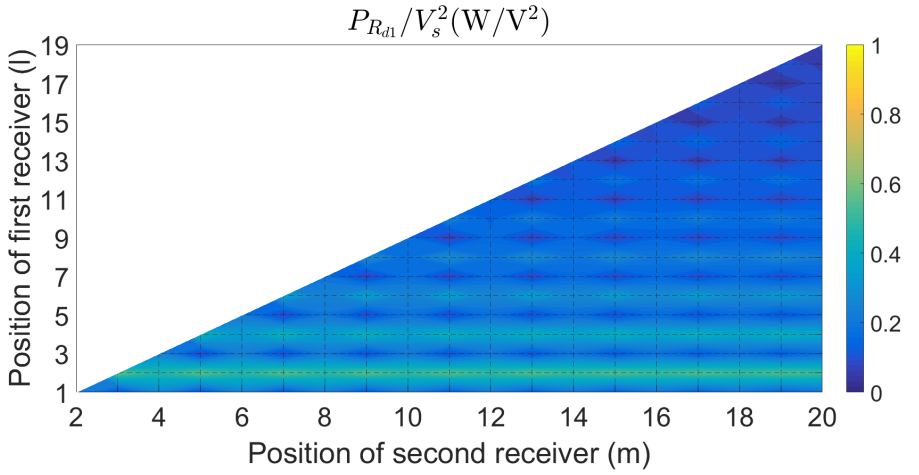

Figure 3.41: Power delivered to R_{d1} for $R_{d1} = R_{d2} = 1.5\Omega$ and for different positions of the first l and second receiver m (1 refers to the resonator connected to the power source and 20 to the resonator connected to the termination impedance).

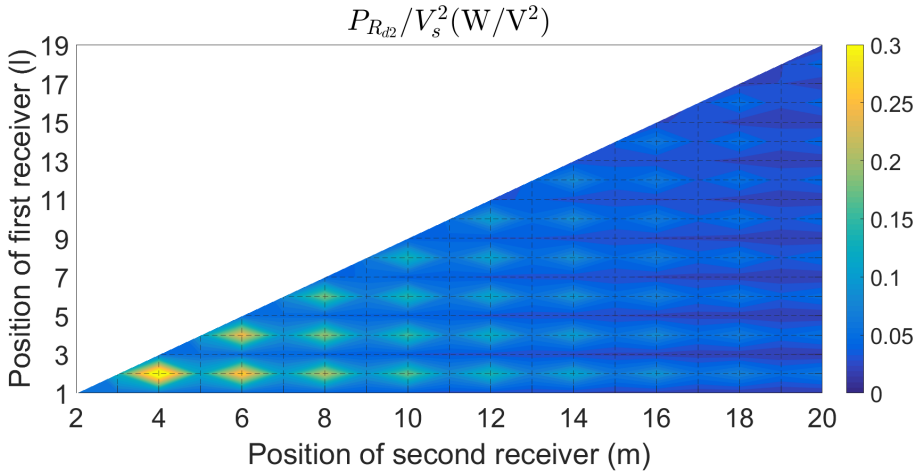

Figure 3.42: Power delivered to R_{d2} for $R_{d1} = R_{d2} = 1.5\Omega$ and for different positions of the first l and second receiver m (1 refers to the resonator connected to the power source and 20 to the resonator connected to the termination impedance).

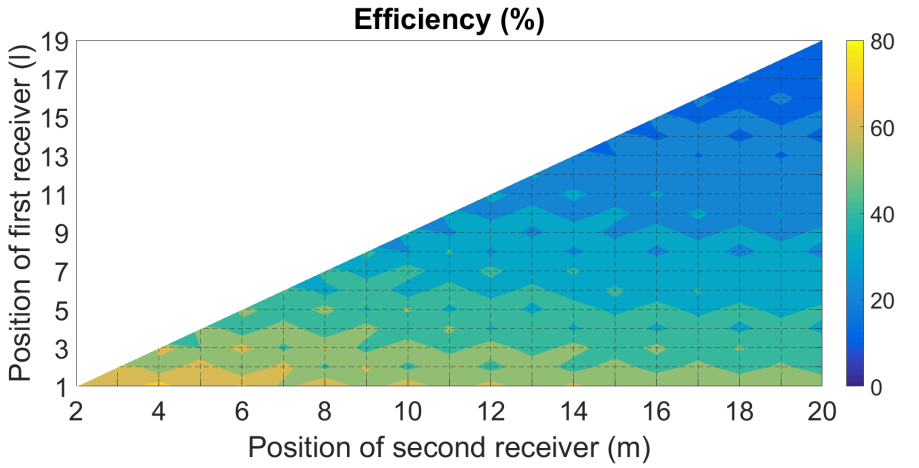

Figure 3.43: Total efficiency (η_{total}) for $R_{d1} = R_{d2} = 1.5\Omega$ and for different positions of the first l and second receiver m (1 refers to the resonator connected to the power source and 20 to the resonator connected to the termination impedance).

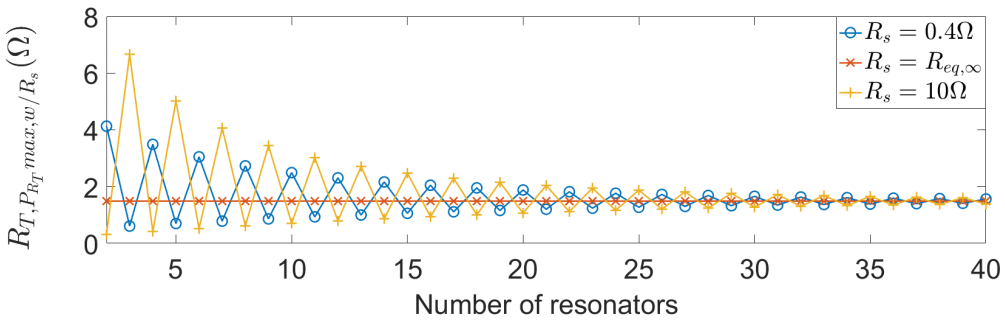

Figure 3.44: Value of $R_{T,P_{R_{T,w/R_s}}max}$ versus the total number of resonators for different values of R_s ($R_s = 0.4$, $R_s = R_{eq,\infty} = \left(-R + \sqrt{4(\omega_0 M)^2 + R^2}\right)/2$ and $R_s = 10\Omega$).

$$P_{R_T,w/R_s} = \frac{\iota_1^2 4^{N-1} V_s^2 R_T (\omega_0 M)^{2N-2}}{\left(\begin{array}{c} 2(\omega_0 M)^2 \iota_2^{N-2}(R_s + 2R + R_T) + \iota_2^{N-1}(R_s + R)(R + R_T) \\ +4(\omega_0 M)^4 \iota_2^{N-3} - \iota_3^{N-3}\left(\iota_3(R_s + R) + 2(\omega_0 M)^2\right)\left(\iota_3(R + R_T) + 2(\omega_0 M)^2\right) \end{array} \right)^2}. \tag{3.83}$$

It is interesting to notice that the expression for the efficiency calculated at the terminals of the voltage source does not depend on the internal voltage source resistance R_s. One can then conclude that all the findings regarding the efficiency values for the previous cases are also valid for the situation where there is an internal source impedance different than zero, and that expressions (3.49) and (3.81) are equivalent. On the other hand, the expression of the power delivered to the load depends on R_s, considering a voltage source with a given RMS value V_s.

As seen before, we can obtain the value of R_T which guarantees the maximum power transfer by letting:

$$\frac{dP_{R_T,w/R_s}}{dR_T} = 0, \tag{3.84}$$

which, by solving it for R_T, yields:

$$R_{T,P_{R_T,w/R_s}max} = -\frac{(\omega_0 M)^2\left(\iota_1\left(\iota_2^N + \iota_3^N\right) - (2R_s + R)\left(\iota_2^N - \iota_3^N\right)\right)}{\left(\iota_2^N - \iota_3^N\right)\left(2(\omega_0 M)^2 - R_s R\right) - \iota_1 R_s\left(\iota_2^N + \iota_3^N\right)} \tag{3.85}$$

which in this case depends on the value of R_s. Then we can plot $R_{T,P_{R_T,w/R_s}max}$ versus the number of resonators of the array, assuming for example the following values for the internal source impedance, $R_s = 0.4\Omega$, $R_s = R_{eq,\infty} = \left(-R + \sqrt{4(\omega_0 M)^2 + R^2}\right)/2$ and $R_s = 10\Omega$. The plots of $R_{T,P_{R_T,w/R_s}max}$ are shown in Fig. 3.44.

In order to match the source to the line of resonators, we set $R_s = R_{eq,\infty} = \left(-R + \sqrt{4(\omega_0 M)^2 + R^2}\right)/2$. For this case, $R_{T,P_{R_T,w/R_s}max}$ becomes constant and does not depend on the total number of resonators:

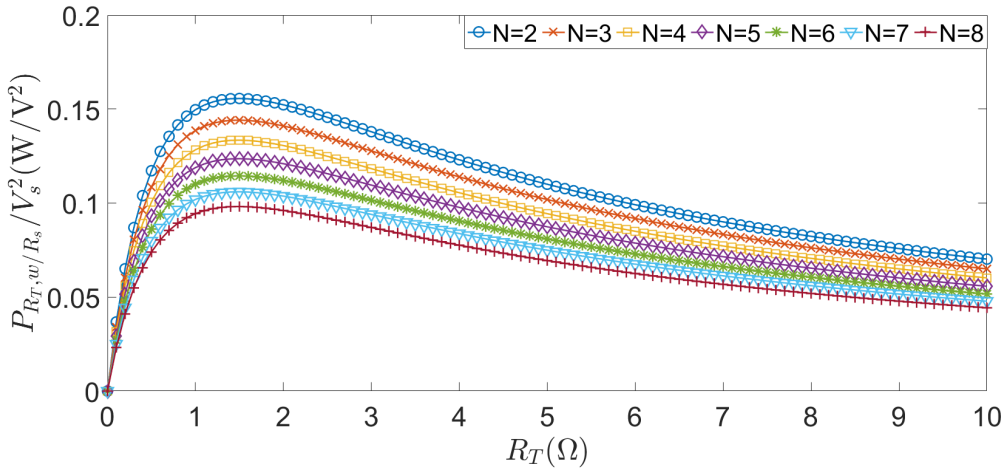

Figure 3.45: $P_{R_T,w/R_s}$ (W/V^2) obtained with (3.83) for $R_s = R_{eq,\infty} = \left(-R + \sqrt{4(\omega_0 M)^2 + R^2}\right)/2$ versus R_T and for different numbers of resonators.

$$R_{T,P_{R_T,w/R_s}max} = \left(R + \sqrt{4(\omega_0 M)^2 + R^2}\right)/2. \tag{3.86}$$

Plotting $P_{R_T,w/R_s}$ using (3.83), letting $R_s = R_{eq,\infty} = \left(-R + \sqrt{4(\omega_0 M)^2 + R^2}\right)/2$ and for different numbers of resonators, we can see in Fig. 3.45 that the peaks of the power delivered to the load R_T all occur for $R_T = \left(R + \sqrt{4(\omega_0 M)^2 + R^2}\right)/2 = 1.48\Omega$ for any total number of resonators N.

3.5 Validation with Simulink

In order to validate the formulas proposed in this chapter, we built a circuit in Simulink and computed the currents in each resonator, the power delivered to a certain load and the efficiency of the system for the cases presented before. In both the calculations with Simulink and with the theoretical expressions, the values of R, L, C and M are the ones used in the numerical examples presented in the previous section.

As done in the previous Chapter 2, we used the Simulink block Mutual inductance to represent the array. This block contains the parameters of the intrinsic resistance of the coils, R, the self-inductance of the coils, L and the mutual inductance between two adjacent coils, M. Then feeding an array with a sinusoidal voltage source $\hat{V}_s$, adding a capacitor with a capacitance value C to each resonator circuit and adding two resistors R_d and R_T as shown in Fig. 3.46, we can simulate an array of resonators whose circuit is depicted in Fig. 3.3 (b) (considering $\hat{Z}_d = R_d$ and $\hat{Z}_T = R_T$). The currents in the resonators are determined using the block "Current measurement" and then the RMS values of each current and the phase difference between the currents in different resonators are calculated. Then, we can calculate the input power and the power absorbed by R_d and R_T, by determining the voltage and current with the Simulink blocks "Voltage Measurement" (in Fig. 3.46 labelled V_IN, V_RD, V_RT) and "Current Measurement" (in Fig. 3.46 labelled I_in, I_Rd, I_RT), respectively, and use the outputs of these blocks to calculate the active power with the

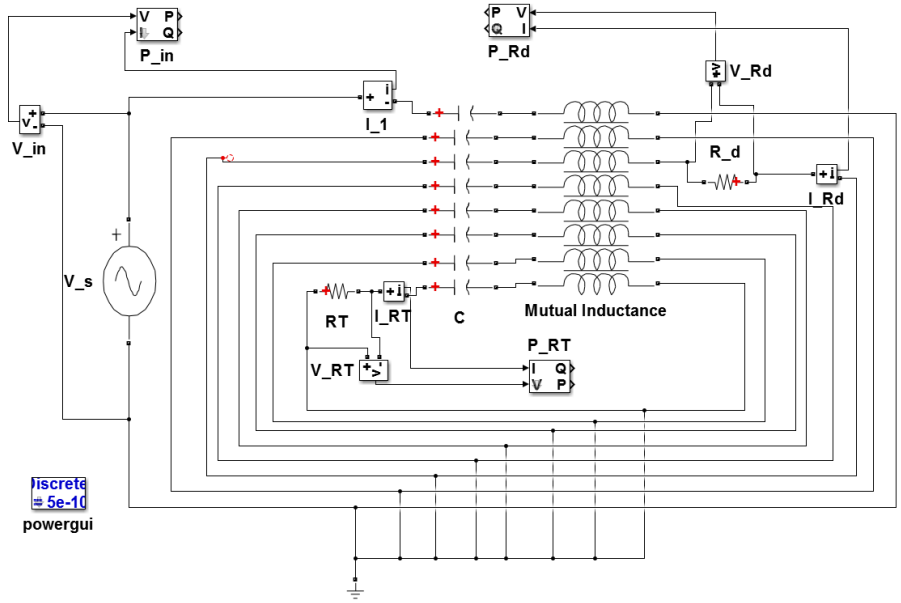

Figure 3.46: Example of a Simulink circuit representing an array of 8 resonators with the receiver represented by a resistance R_d in the 3rd position.

"Power" block (in Fig. 3.46 labelled P_in, P_Rd, P_RT).

In all the examples presented in the next subsections, the RMS value of the sinusoidal voltage source is set to V_s=10V and the operating frequency of the voltage source is set to the resonant frequency $f_0 = 147$kHz.

3.5.1 First case

3.5.1.1 Currents in the resonators

Letting $R_d = 0\Omega$, we obtain the waveforms of the currents in each resonator in Simulink for different values of R_T (0.4Ω, $R_T = R_{eq,\infty}$, $R_T = 10\Omega$). The waveforms of the currents in each resonator obtained with Simulink are represented in Fig. 3.47.

As seen in the examples of Section 3.4.1, the currents in adjacent resonators have a -90º of phase difference between them, such that after four resonators the currents are in phase again (i_5 is again in phase with i_1, i_6 with i_2, etc.) and also the peak values of currents decrease gradually from the first to the last one when $R_T = R_{eq,\infty}$ and oscillate when R_T is lower or higher than this value.

3.5.1.2 Efficiency and power delivered to a load or a receiver over the last cell represented by R_T

Regarding the first case, we can first obtain in Simulink the power delivered to R_T in a 8-resonator array, setting $R_d = 0\Omega$, and using the block P_RT to obtain the efficiency of the system η dividing the values obtained with this block by the ones obtained with the block P_in (Fig. 3.46). Then, for different values of R_T we can compare the values obtained with Simulink and the ones obtained with (3.48) and (3.49) for $N = 8$. The values are compared in Table 3.1.

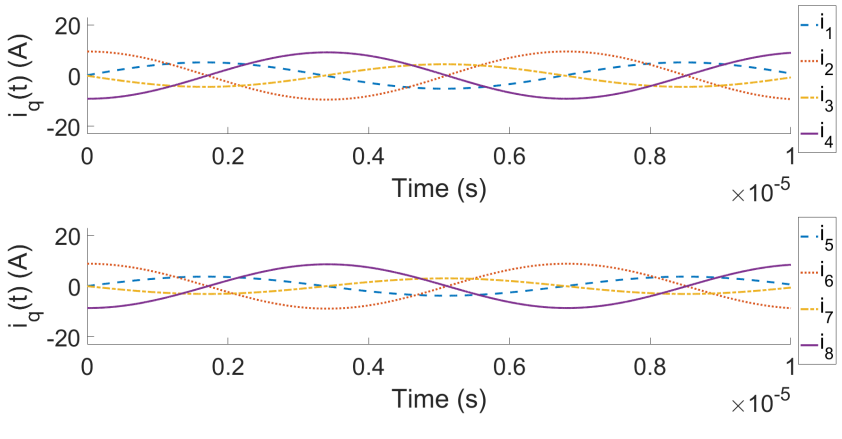

(a)

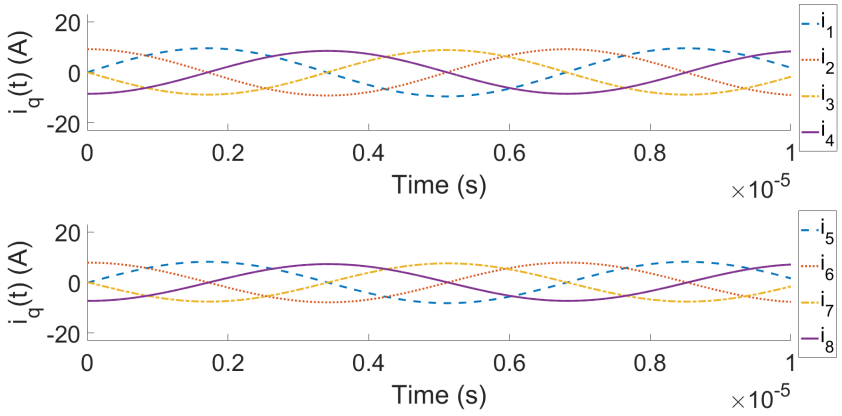

(b)

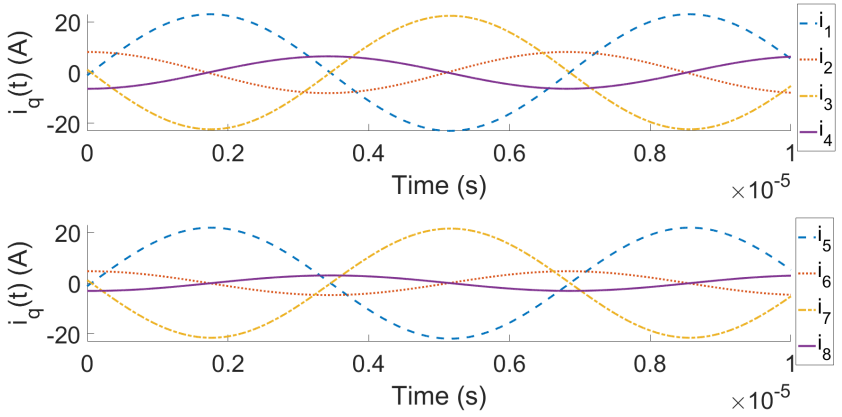

(c)

Figure 3.47: Waveforms of the current in each resonator, for an array of 8 resonators, for different values of R_T: (a) R_T=0.4Ω, (b) $R_T = R_{eq,\infty}$ and (c) R_T=10Ω

Table 3.1: Comparison of the values of P_{R_T} and η obtained with Simulink to those obtained with the developed formulas.

	Simulink		Values obtained with (3.48) and (3.49)	
$R_T(\Omega)$	P_{R_T}(W)	$\eta(\%)$	P_{R_T}(W)	$\eta(\%)$
0.4	14.85	40.52	14.84	40.52
1.5	38.08	54.10	38.08	54.10
10	46.41	28.59	46.53	28.59

Table 3.2: Comparison of the values of P_{R_T} and η obtained with Simulink to those obtained with the developed formulas.

	Simulink		Values obtained with (3.60) and (3.61)	
$R_d(\Omega)$	P_{R_d}(W)	$\eta(\%)$	P_{R_d}(W)	$\eta(\%)$
0.4	9.93	18.10	9.91	18.08
5	11.36	55.90	11.35	55.89
10	7.35	53.04	7.35	53.03

3.5.1.3 Efficiency and power transmitted to a receiver R_d over the lth cell

Letting $R_T = R_{eq,\infty} = \left(-R + \sqrt{4(\omega_0 M)^2 + R^2}\right)/2$ and for different values of R_d, which is added to the 3rd resonator ($l = 3$), we can compare the values obtained with Simulink for P_{R_d} and the efficiency $\eta = P_{R_d}/P_{in}$, with the values obtained using (3.60) and (3.61). The comparison is presented in Table 3.2.

3.5.2 Second case

3.5.2.1 Efficiency and power delivered to a receiver over the lth position R_{d1}

Regarding the second case, we consider the circuit represented in Fig. 3.46 and obtain with Simulink the power $P_{R_{d1}}$ delivered to a receiver represented with R_{d1}, as well as the efficiency $\eta = P_{R_{d1}}/P_{in}$ for different values of R_{d1} and R_T. Then we compare the values obtained with the simulations to the values determined with (3.77) and (3.79). The receiver R_{d1} is on the 3rd resonator and the resonator array has a total of 8 resonators ($l = 3$ and $N = 8$). The results are show in Table 3.3.

3.5.2.2 Efficiency and power delivered to two receivers R_{d1} and R_{d2}, with the receiver R_{d2} in a fixed position

We consider now the case with the second receiver R_{d2} over the last cell, thus replacing in the scheme of Fig. 3.46 R_T by R_{d2} and P_{R_T} by $P_{R_{d2}}$, and keeping the receiver R_{d1} in the 3rd position ($l = 3$) in a 8-resonator array ($N = 8$). After obtaining with Simulink the values for $P_{R_{d1}}$, $P_{R_{d2}}$ and $\eta_{total} = (P_{R_{d1}} + P_{R_{d2}})/P_{in}$, we can compare them with the values calculated with (3.79), (3.80) and (3.78) (with $R_T = 0$), respectively. The comparison is presented in Table 3.4.

Table 3.3: Comparison of the values of $P_{R_{d1}}$ and η obtained with Simulink and those obtained with the developed formulas.

	Simulink			Values obtained with (3.77)		
	$P_{R_{d1}}$(W)			$P_{R_{d1}}$(W)		
	R_{d1}=0.4Ω	$R_{d1}=5\Omega$	$R_{d1}=10\Omega$	R_{d1}=0.4Ω	$R_{d1}=5\Omega$	$R_{d1}=10\Omega$
R_T= 0.4Ω	3.13	7.43	5.71	3.12	7.42	5.71
$R_T = R_{eq,\infty}$	9.93	11.36	7.35	9.93	11.36	7.35
R_T= 10Ω	37.38	15.60	8.75	37.42	15.60	8.75
	Simulink			Values obtained with (3.76)		
	$\eta = P_{R_{d1}}/P_{in}$ (%)			$\eta = P_{R_{d1}}/P_{in}$ (%)		
	R_{d1}=0.4Ω	$R_{d1}=5\Omega$	$R_{d1}=10\Omega$	R_{d1}=0.4Ω	$R_{d1}=5\Omega$	$R_{d1}=10\Omega$
R_T= 0.4Ω	9.44	42.56	44.45	9.43	42.54	44.43
$R_T = R_{eq,\infty}$	18.10	55.90	53.04	18.10	55.90	53.04
R_T= 10Ω	36.87	68.14	59.79	36.87	68.14	59.79

Table 3.4: Comparison between the values of $P_{R_{d1}}$, $P_{R_{d2}}$ and η_{total} obtained with Simulink and the ones obtained with the developed formulas for the first receiver in the 3rd position ($l = 3$) and the second receiver over the last cell of a 8-resonator array ($N = 8$).

	Simulink			Values obtained with (3.79)		
	$P_{R_{d1}}$(W)			$P_{R_{d1}}$(W)		
	R_{d1}=0.4Ω	$R_{d1}=5\Omega$	$R_{d1}=10\Omega$	R_{d1}=0.4Ω	$R_{d1}=5\Omega$	$R_{d1}=10\Omega$
R_{d2}= 0.4Ω	3.69	7.94	5.94	3.68	7.94	5.93
R_{d2}= 5Ω	24.87	14.33	8.34	24.90	14.33	8.34
R_{d2}= 10Ω	32.96	15.17	8.60	33.01	15.17	8.60
	Simulink			Values obtained with (3.80)		
	$P_{R_{d2}}$(W)			$P_{R_{d2}}$(W)		
	R_{d1}=0.4Ω	$R_{d1}=5\Omega$	$R_{d1}=10\Omega$	R_{d1}=0.4Ω	$R_{d1}=5\Omega$	$R_{d1}=10\Omega$
R_{d2}= 0.4Ω	11.05	1.90	0.71	11.05	1.91	0.71
R_{d2}= 5Ω	19.82	0.91	0.26	19.84	0.91	0.26
R_{d2}= 10Ω	14.12	0.52	0.15	14.14	0.52	0.15
	Simulink			Values obtained with (3.78)		
	$\eta_{total} = (P_{R_{d1}} + P_{R_{d2}})/P_{in}$ (%)			$\eta_{total} = (P_{R_{d1}} + P_{R_{d2}})/P_{in}$ (%)		
	R_{d1}=0.4Ω	$R_{d1}=5\Omega$	$R_{d1}=10\Omega$	R_{d1}=0.4Ω	$R_{d1}=5\Omega$	$R_{d1}=10\Omega$
R_{d2}= 0.4Ω	40.14	51.51	46.62	40.14	51.50	46.61
R_{d2}= 5Ω	52.73	65.11	54.88	52.73	65.11	54.89
R_{d2}= 10Ω	48.76	65.67	55.29	48.77	65.67	55.29

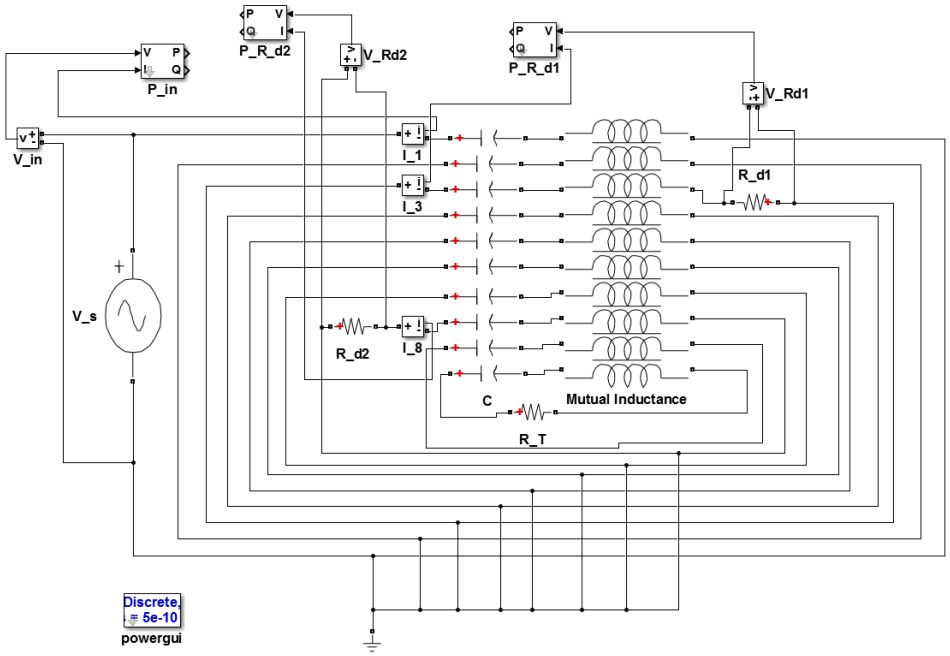

Figure 3.48: Simulink circuit built for simulations representing an array of 10 resonators terminated by a termination resistance R_T and with the first and second receivers represented by R_{d1} and R_{d2} in the 3rd and 8th positions, respectively.

3.5.2.3 Efficiency and power delivered to two receivers R_{d1} and R_{d2} over the array

Now we consider the second receiver receiver in a given mth position of a resonator array with N resonators terminated with $R_{eq,\infty} = \left(-R + \sqrt{4(\omega_0 M)^2 + R^2}\right)/2$. For example, arranging the first receiver R_{d1} in the 3rd position ($l = 3$) and the second receiver R_{d2} in the 8th position ($m = 8$), we can calculate the power delivered to each receiver, and then calculate the total efficiency of the system. In order to simulate this situation a different circuit was designed in Simulink, considering an array with 10 resonators terminated by a load $R_T = R_{eq,\infty} = \left(-R + \sqrt{4(\omega_0 M)^2 + R^2}\right)/2$, with the first receiver in the 3rd position and the second in the 8th position, as shown in Fig. 3.48. The results obtained with Simulink are then compared with the ones obtained using (3.79), (3.80) and (3.78) with $R_T = R_{eq,N-m} = R_{eq,\infty} = \left(-R + \sqrt{4(\omega_0 M)^2 + R^2}\right)/2$, and shown in Table 3.5.

3.5.2.4 Efficiency and power delivered to a load or a receiver over the last cell represented by R_T, considering the effect of a source impedance R_s

Finally, in order to compare the effect of an internal source resistance R_s , we built a different circuit in Simulink, adding the resistances R_s to the first cell and R_T to the last one, as represented in Fig. 3.49. Then, for a 8-resonator array and $R_T = 1.5\Omega$ we can determine with Simulink the power delivered to the load R_T and the efficiency $\eta = P_{R_T}/P_{in}$, the input power being calculated at the terminals of the voltage source as described in (3.81) and as represented in Fig. 3.49. The efficiency and power delivered to R_T are determined in Simulink for different values of R_s and then compared with the values obtained with (3.83) and (3.81). The results of the comparison are shown in Table 3.6.

We can see, as already shown before, that the value of the efficiency does not depend on the

Table 3.5: Comparison between the values of $P_{R_{d1}}$, $P_{R_{d2}}$and η_{total} obtained with Simulink and the ones obtained with the developed formulas for the first receiver R_{d1} in the 3rd position ($l = 3$) and the second receiver in the 8th position ($m = 8$) in a line terminated by $R_{eq,\infty}$.

	Simulink			Values obtained with (3.79)		
	$P_{R_{d1}}$(W)			$P_{R_{d1}}$(W)		
	R_{d1}=0.4Ω	$R_{d1} = 5\Omega$	$R_{d1} = 10\Omega$	R_{d1}=0.4Ω	$R_{d1} = 5\Omega$	$R_{d1} = 10\Omega$
R_{d2}= 0.4Ω	3.13	7.43	5.71	3.12	7.42	5.71
R_{d2}= 5Ω	27.09	14.65	8.46	27.11	14.65	8.46
R_{d2}= 10Ω	37.38	15.60	8.75	37.42	15.60	8.75
	Simulink			Values obtained with (3.80)		
	$P_{R_{d2}}$(W)			$P_{R_{d2}}$(W)		
	R_{d1}=0.4Ω	$R_{d1} = 5\Omega$	$R_{d1} = 10\Omega$	R_{d1}=0.4Ω	$R_{d1} = 5\Omega$	$R_{d1} = 10\Omega$
R_{d2}= 0.4Ω	11.70	2.22	0.85	11.69	2.22	0.86
R_{d2}= 5Ω	23.62	1.02	0.30	23.63	1.02	0.30
R_{d2}= 10Ω	17.34	0.58	0.16	17.36	0.58	0.16
	Simulink			Values obtained with (3.78)		
	$\eta_{total} = (P_{R_{d1}} + P_{R_{d2}})/P_{in}$ (%)			$\eta_{total} = (P_{R_{d1}} + P_{R_{d2}})/P_{in}$ (%)		
	R_{d1}=0.4Ω	$R_{d1} = 5\Omega$	$R_{d1} = 10\Omega$	R_{d1}=0.4Ω	$R_{d1} = 5\Omega$	$R_{d1} = 10\Omega$
R_{d2}= 0.4Ω	44.75	55.31	51.10	44.75	55.30	51.09
R_{d2}= 5Ω	58.20	70.11	60.47	58.20	70.11	60.47
R_{d2}= 10Ω	53.98	70.67	60.90	53.98	70.67	60.90

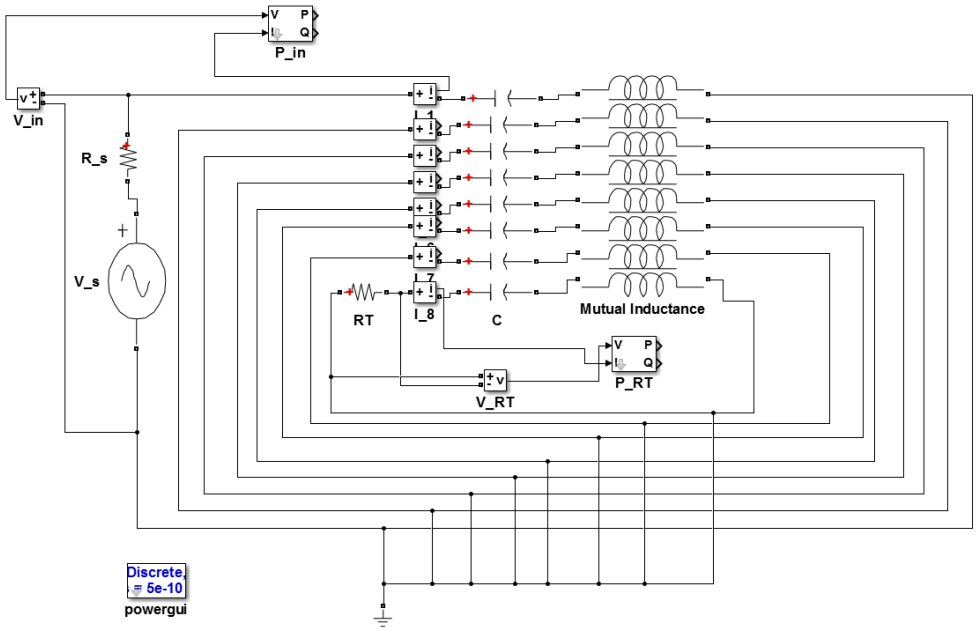

Figure 3.49: Simulink circuit built for simulations representing an array of 8 resonators with a voltage source resistance R_s and terminated by a resistive load R_T.

Table 3.6: Comparison between the values of P_{R_T} and η obtained with Simulink and the ones obtained with the developed formulas.

	Simulink		Values obtained with (3.83) and (3.81).	
$R_s(\Omega)$	P_{R_T}(W)	$\eta(\%)$	P_{R_T}(W)	$\eta(\%)$
0	38.08	54.10	38.08	54.10
5	1.86	54.10	1.86	54.10
50	0.03	54.10	0.03	54.10

value of R_s. However, for a given voltage source, the power delivered to R_T decreases with the increase of R_s, due to the losses in the source. We can observe a very good agreement between the values obtained with the formulas presented in Section 3.4 and those obtained with Simulink. In this way, it is verified that the formulas are correct and accurate and that these formulas can be used for the design of a resonator array, since they can save time compared to numerical simulations with Simulink, specially when we want to quickly predict the behaviour of the system regarding variations in the conditions of the system (as total number of resonators, position of the receiver or value of the receiver impedance).

3.6 Experimental verification

After the numerical simulations, the experimental setup described in the Chapter 5 was used in order to verify experimentally the results obtained in this chapter, first using the planar multilayer coils and afterwards the stranded-wire, wooden core coils. Regarding the results obtained in this section, the voltages were measured with a 500 MHz Agilent Infiniium 54825A digital oscilloscope using a TESTEC TT-SI 9002 voltage differential probe connected to the oscilloscope and the currents were measured with the same oscilloscope and a Tektronix TCP305 DC to 50 MHz current probe. The value of V_s used in the developed formulas was experimentally determined using (2.73).

3.6.1 Measuring the power and efficiency

The measured values for the efficiency and power transmission were obtained by measuring the input power ($P_{in,exp}$) and the power delivered to a resistive load ($P_{R_T,exp}$) or to a load that represents a receiver ($P_{R_{d1},exp}$ or $P_{R_{d2},exp}$) were obtained from measurements. The input power was determined calculating the average value over a period of the product of the instantaneous voltage and current measured at the terminals of the inverter:

$$P_{in,exp} = (1/T) \int_0^T v_{in}(t)\, i_{in}(t) \mathrm{dt} \tag{3.87}$$

where $T = 1/f_0$ is the period of the waveforms and $v_{in}(t)$ and $i_{in}(t)$ are the measured instantaneous values of the input voltage and current. The product of the instantaneous voltage and current and its average value in a period were calculated with the oscilloscope using the mathematical functions of its internal software. The power delivered to a given load was calculated measuring the RMS

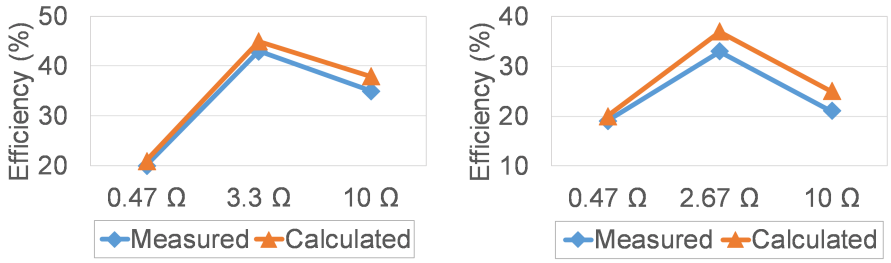

(a) (b)

Figure 3.50: Efficiency for different values of R_T at the resonant frequency of (a) 294kHz and (b) 192 kHz calculated with (3.49) and obtained through measurements with (3.89).

value of the voltage at the terminals of the load (V_T, V_{d1} or V_{d2}) and dividing its squared value by the value of the load (R_T, R_{d1} and R_{d2}):

$$P_{R_T,exp} = V_T^2/R_T;\ P_{R_{d1},exp} = V_{d1}^2/R_{d1};\ P_{R_{d2},exp} = V_{d2}^2/R_{d2}. \tag{3.88}$$

Then, using the previous values, we can calculate the experimental efficiency of the system considering a load R_T, one or two receivers:

$$\eta_{exp,R_T} = P_{R_T,exp}/P_{in,exp};\ \eta_{R_{d1},exp} = P_{R_{d1},exp}/P_{in,exp};\ \eta_{total,exp} = (P_{R_{d1},exp}+P_{R_{d2},exp})/P_{in,exp}. \tag{3.89}$$

3.6.1.1 First case

Efficiency and power delivered to a load or a receiver over the last cell represented by R_T

Efficiency of the power delivered to R_T using multilayer planar resonators

Considering the experimental setup composed of the 4-resonator array with multilayer planar resonators, the values of R, L, C and M and f_0 as described in Chapter 5 were used to determine the efficiency of the system with (3.49). Then, these results were compared to the values obtained through measurements with (3.89) . The comparison between these results was then carried out for different values of R_T and is shown in Fig. 3.50. For this experimental setup, using (3.51), the values of R_T that guarantee the maximum efficiency are $R_T, \eta_{max} = 3.6\Omega$ for $f_0 = 294$ kHz and $R_T, \eta_{max} = 2.4\,\Omega$ for $f_0 = 192$ kHz.

Efficiency and power delivered to R_T using stranded-wire resonators

Using the 6-resonator array with stranded-wire and wooden core, the efficiency of the system and the power delivered to the load were calculated with (3.49) and (3.48), respectively and obtained with (3.88) and (3.87) through measurements. For this array, using (3.51) and (3.55), the values of R_T that guarantee the maximum efficiency and maximum power transfer are $R_{T,\eta_{max}} = 1.44\Omega$ and $R_{T,P_{R_T,max}} = 6.4\,\Omega$, respectively.

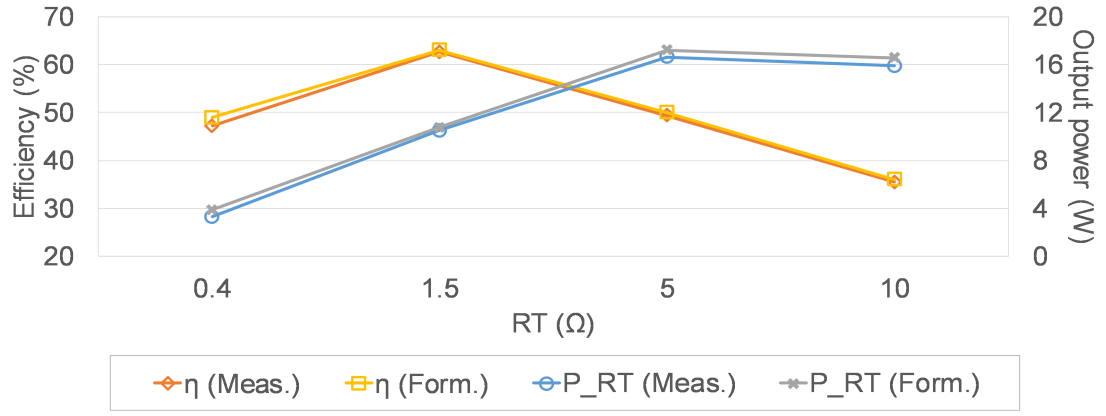

Figure 3.51: Comparison between the values of P_{R_T} and η obtained with measurements (using (3.88) and (3.89)) and the ones obtained with the developed formulas (3.48) and (3.49) for a 6-resonator array with stranded-wire resonators and for different values of R_T.

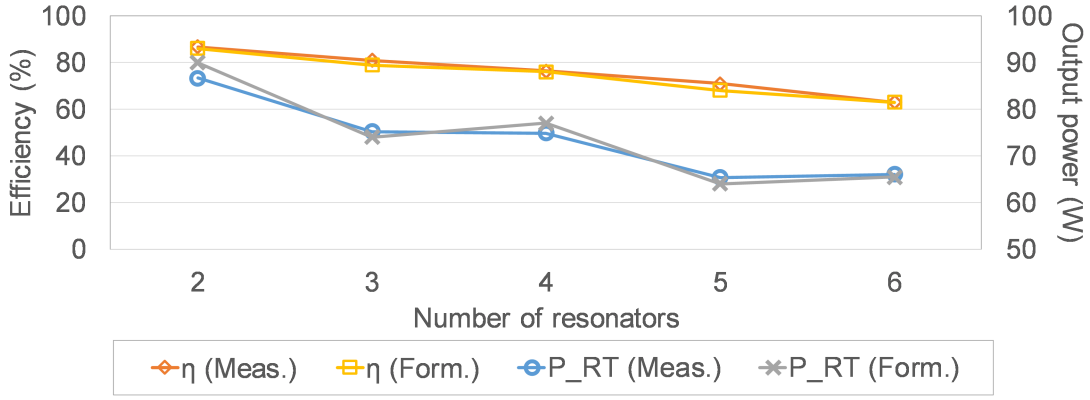

Figure 3.52: Comparison between the values of P_{R_T} and η obtained with measurements (using (3.88) and (3.89)) and the ones obtained with the developed formulas (3.48) and (3.49) for an array with different number of resonators terminated by $R_T = 1.5\Omega$.

The comparison between these results was then carried out versus different values of R_T,as shown in Fig. 3.51, assuming $V_s = 4.9$, and versus different number of resonators (N), as shown in Fig. 3.52, assuming $V_s = 12.1$.

It can be noticed that for both resonant frequencies and for the different types of coils the efficiency is higher when R_T is close to the value of $R_{T,\eta_{max}}$, and lower otherwise, as seen in Figs. 3.50 and 3.51. The same is verified regarding the maximum power transfer to a load: the maximum power transfer occurs when R_T is near $R_{T,P_{R_T,max}}$, as observed in Fig. 3.51.

Regarding the measurements done with the multilayer planar resonators, when the operating frequency lowers the resistance decreases approximately with the square-root of the frequency, and the quality factor $Q = \omega L/R$ decreases with the square-root of the frequency as well. Then, for a given value of $|k| = 2|M|/L$, assuming that the cells of the array are in fixed positions, the product $|kQ| = 2\omega_0|M|/R$ decreases approximately with $\sqrt{f}$, thus increasing the losses in each cell. Moreover, for the stranded-wire coils, the values of the efficiency are higher, due to the higher values of $1/r = |kQ| = 2\omega_0|M|/R$. The multilayer and the stranded-wire resonator arrays

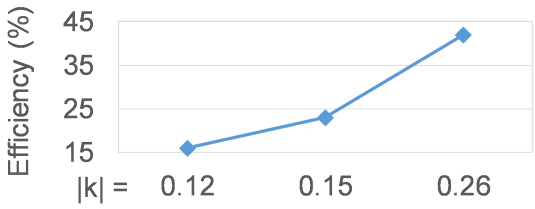

Figure 3.53: Measured efficiency versus the values of the coupling coefficient k.

have similar values of $|k|$ (0.26 and 0.24, respectively); however, the multilayer resonators have much smaller values of Q, comparing to the stranded wire resonators (39 to 106), resulting in different maximum efficiencies measured for an array of 4 resonators: 42% to 71%.

We further consider the system with the multilayer planar resonators with a fixed termination impedance (3.3Ω) and the same resonators and resonant frequency (f=294kHz). If we set the side by side distance between the coils to 5mm and 10mm, we measure $|k|$ values of $|k| = 0.12$ and $|k| = 0.15$, respectively. The reduction of the coupling coefficient $|k|$ for a fixed Q decreases the product $|kQ|$ and thus increases the attenuation in each cell. Then, if we measure the efficiency for these lower values of k, we get lower values of efficiency, as shown in Fig. 3.53.

3.6.1.2 Second case

Efficiency and power delivered to a receiver over the lth position R_{d1}

In order to verify experimentally the power delivered to a receiver represented by R_{d1}, we used the stranded-wire 6-resonator array ($N = 6$), terminated by a resistance R_T, and used a resistive load to represent the receiver R_{d1}. Then, for the receiver R_{d1} in the 3rd position, we calculate the values of power transmitted to the receiver R_{d1} and efficiency $\eta_{R_{d1}}$ using (3.79) and (3.78) with $R_{d2} = 0$ and $l = 3$. We then make a comparison with the values obtained through measurements with (3.88) and (3.89). This comparison is done for different values of R_{d1} and R_T, assuming $V_s = 5.0V$ and is shown in Table 3.7.

Furthermore, we consider another example where we set $R_{d1} = 5\Omega$ and $R_T = 1.5\Omega$, assuming the receiver in different positions and $V_s = 4.9V$. Then, we compare the values of power absorbed by the receiver and efficiency of the system obtained using (3.79) and (3.78) (with $R_{d2} = 0$ and $l = 2$ to $l = 5$) with the ones obtained through measurements with (3.88) and (3.89). The results are presented in Fig. 3.54.

Efficiency and power delivered to two receivers R_{d1} and R_{d2}, with the receiver R_{d2} in a given position

Finally, analysing the situation where we want to deliver power to two receivers, being one is in a given position, we consider an example with the first receiver R_{d1} on the 3rd position ($l = 3$) and the second one R_{d2} on the 6th cell, for a 6-resonator array, using resistive loads to represent the receivers. Then, we obtain the values of the total efficiency of the system and the power delivered to each receiver using (3.79), (3.80) and (3.78) (with $l = 3$, $R_T = 0$ and $N = 6$) and compare them with the values obtained trough measurements with (3.88) and (3.89), considering $V_s = 5.0V$. The

Table 3.7: Comparison between the values of $P_{R_{d1}}$ and $\eta_{R_{d1}}$ obtained with measurements (using (3.88) and (3.89)) and the ones obtained with the developed formulas (3.79) and (3.78), for a 6-resonator array for different values of R_{d1} and R_T.

	Values obtained through measurements with (3.88)			Values obtained with (3.79)		
	$P_{R_{d1},exp}$(W)			$P_{R_{d1}}$(W)		
	R_{d1}=0.4Ω	$R_{d1}=5\Omega$	$R_{d1}=10\Omega$	R_{d1}=0.4Ω	$R_{d1}=5\Omega$	$R_{d1}=10\Omega$
$R_T=0.4\Omega$	-	1.9	1.5	-	1.7	1.3
$R_T=1.5$	3.0	3.1	2.1	2.7	2.9	1.9
$R_T=10\Omega$	10.0	4.1	-	11.5	4.0	-
	Values obtained through measurements with (3.89)			Values obtained with (3.78)		
	$\eta_{R_{d1},exp}$ (%)			$\eta_{R_{d1}}$(%)		
	R_{d1}=0.4Ω	$R_{d1}=5\Omega$	$R_{d1}=10\Omega$	R_{d1}=0.4Ω	$R_{d1}=5\Omega$	$R_{d1}=10\Omega$
$R_T=0.4\Omega$	-	38.6	40.1	-	39.7	42.4
$R_T=1.5\Omega$	21.2	55.2	49.8	19.0	56.9	53.6
$R_T=10\Omega$	42.6	65.9	-	41.1	69.7	-

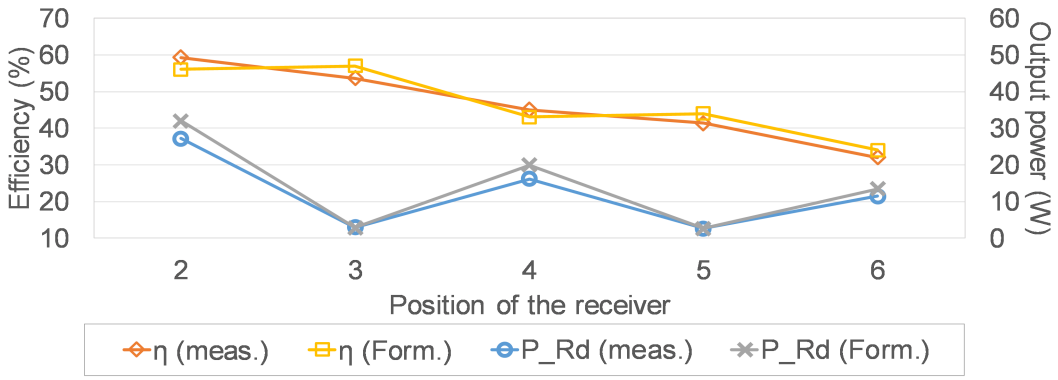

Figure 3.54: Comparison between the values of $P_{R_{d1}}$ and $\eta_{R_{d1}}$ obtained with measurements (using (3.88) and (3.89)) and the ones obtained with the developed formulas ((3.79) and (3.78)), for a 6-resonator terminated $R_T = 1.5\Omega$ array for $R_{d1} = 5\Omega$ in different positions.

Table 3.8: Comparison between the values of $P_{R_{d1}}$, $P_{R_{d2}}$ and η_{total} obtained with measurements (using (3.88) and (3.89)) and the ones obtained with the developed formulas (3.79), (3.80) and (3.78), for a 6-resonator array with the first receiver on the 3rd position ($l = 3$) and the second receiver over the last cell of a 6-resonator array ($N = 6$).

	Values obtained through measurements with (3.88)			Values obtained with (3.79)		
	$P_{R_{d1},exp}$(W)			$P_{R_{d1}}$(W)		
	R_{d1}=0.4Ω	$R_{d1} = 5\Omega$	$R_{d1} = 10\Omega$	R_{d1}=0.4Ω	$R_{d1} = 5\Omega$	$R_{d1} = 10\Omega$
R_{d2}= 0.4Ω		1.9	1.5	-	1.7	1.3
R_{d2}= 1.5Ω	3.0	3.1	2.1	2.7	2.9	1.9
R_{d2}= 10Ω	10.0	4.1		11.5	4.0	-
	Values obtained through measurements with (3.88)			Values obtained with (3.80)		
	$P_{R_{d2},exp}$(W)			$P_{R_{d2}}$(W)		
	R_{d1}=0.4Ω	$R_{d1} = 5\Omega$	$R_{d1} = 10\Omega$	R_{d1}=0.4Ω	$R_{d1} = 5\Omega$	$R_{d1} = 10\Omega$
R_{d2}= 0.4Ω		0.7	0.3	-	0.7	0.3
R_{d2}= 1.5Ω	6.4	0.6	0.2	7.0	0.6	0.2
R_{d2}= 10Ω	4.6	0.2		5.6	0.2	-
	Values obtained through measurements with (3.89)			Values obtained with (3.78)		
	$\eta_{total,exp}$ (%)			$\eta_{total} = (P_{R_{d1}} + P_{R_{d2}})/P_{in}$ (%)		
	R_{d1}=0.4Ω	$R_{d1} = 5\Omega$	$R_{d1} = 10\Omega$	R_{d1}=0.4Ω	$R_{d1} = 5\Omega$	$R_{d1} = 10\Omega$
R_{d2}= 0.4Ω	-	52.4	48.1	-	56.5	51.4
R_{d2}= 1.5Ω	66.3	65.6	54.9	67.9	68.6	59.1
R_{d2}= 10Ω	62.3	68.3	-	61.0	72.4	-

comparison was made for different values of R_{d1} and R_{d2} and is shown in Table 3.8.

We observe a good agreement between the values calculated with the formulas developed in Section 3.4 and the values obtained through measurements. The differences found could be due to measurement errors and to imperfections in the manufacturing of the coils, which can lead to slightly different values of self-inductance and intrinsic resistance of the coils and extra resistance caused by soldering of the capacitors to the coils. However, the changes in the general behaviour of the power and efficiency with the variations of the parameters verified in Section 3.4 are also observed from the measurements. For example, as observed in Fig. 3.51 the efficiency and power peaks are achieved for different values of R_T, as it was already been noticed before in subsection 3.4.1.2.

3.7 Power transmitted to a real receiver

In this chapter, in order to simplify the analysis and examples performed in Section (3.4), we have considered so far that the receiver is represented by an impedance R_d, R_{d1} or R_{d2}. However, in the case where there is a receiver with a load R_{load} connected to it, we have to consider the power delivered to R_{load} in order to determine the whole efficiency of the system.

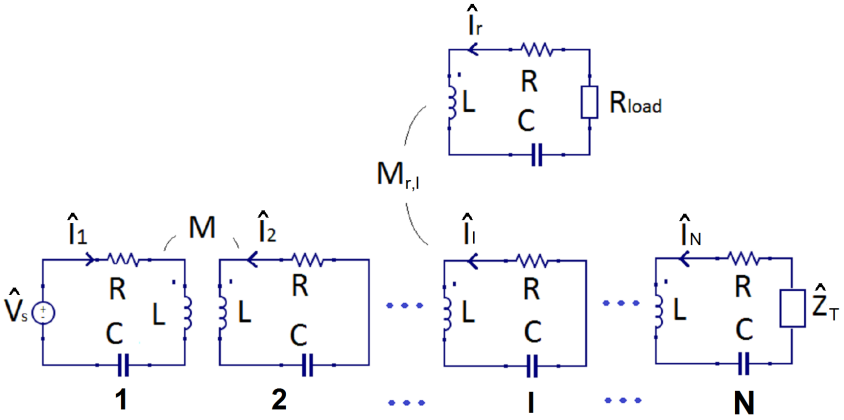

Figure 3.55: Equivalent circuit of the array with N resonators, including the circuit of the receiver that is over the lth cell.

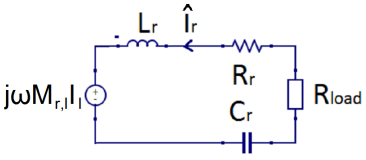

Figure 3.56: Equivalent circuit of the receiver that is over the lth cell.

The equivalent circuit of the array with the detailed circuit of the receiver is shown in Fig. 3.55. The impedance that represents the receiver R_d, assuming that the receiver has the same resonant frequency than the one of the cells of the array ($1/\sqrt{L_r C_r} = 1/\sqrt{LC} = \omega_0$), is given by [14]:

$$R_d = \frac{(\omega_0 M_{r,l})^2}{R_r + R_{load}}, \tag{3.90}$$

where $M_{r,l}$ is the mutual inductance between the receiver and the cell beneath it, R_r is the intrinsic AC resistance of the receiver and R_{load} is a certain load connected to the receiver.

In this way, the power delivered to a load connected to a receiver is given by:

$$P_{R_{load}} = I_r^2 R_{load} \tag{3.91}$$

where I_r is the RMS value of the current of the receiver, which can be rewritten in terms of the RMS value of the current I_l on the lth resonator of the array according to the circuit represented in Fig. 3.56 as seen in [14, 30]:

$$I_r = \frac{\omega_0 M_{r,l} I_l}{R_r + R_{load}}. \tag{3.92}$$

If we want to write the relation between $P_{R_d} = I_l^2 R_d$ and $P_{R_{load}}$ we can now rewrite:

$$\frac{P_{R_{load}}}{P_{R_d}} = \frac{R_{load}}{R_r + R_{load}}. \tag{3.93}$$

Thus, in order to have minimum losses in the receiver, R_{load} should be much larger than the resistance of the receiver R_r. This, however, could imply a lower value of R_d if $M_{r,l}$ is not high enough. Then, for a desired value of R_d, $M_{r,l}$ and R_{load} should be higher as possible in order to suppress the effect of the resistance of the receiver, so that the power and efficiency calculated with the formulas provided in Section 3.4 can be approximately the same as the ones for a load connected to the receiver. Otherwise, if we want to determine the value of the power delivered to a load connected to the receiver R_{load} we just have to multiply (3.93) for the values P_{R_d},$P_{R_{d1}}$ or $P_{R_{d2}}$ obtained through the formulas presented in Section 3.4.

3.7.1 Experimental verification

In order to verify the theoretical considerations made in this section, we can use one of the stranded-wire resonators (thus $R_r = R$ in (3.93)) and place it over different positions of the array. We consider an example where the array is terminated by $R_T = 1.5\Omega$, a 5Ω load is connected to the receiver resonator ($R_{load} = 5\Omega$) and the mutual inductance between the receiver coil and the cell below has the measured value $M_{r,l} = 4.8\mu H$. We can obtain the power delivered to the load connected to the receiver by measuring the voltage at the terminals of the load,

$$P_{R_{load},exp} = V_{load}^2/R_{load}, \tag{3.94}$$

the efficiency being given by:

$$\eta_{R_{load},exp} = P_{R_{load},exp}/P_{in}, \tag{3.95}$$

where P_{in} was determined as in (3.87).

Then, we can perform a comparison between between the values of $P_{R_{load},exp}$ and $\eta_{R_{load},exp}$ obtained with measurements (using (3.94) and (3.95)) and the ones obtained with the developed formulas (3.77), (3.76) multiplying them by the factor (3.93) (equal to 0.98 in this example):

$$P_{R_{load}} = \frac{P_{R_{d1}} R_{load}}{R_r + R_{load}} \tag{3.96}$$

and

$$\eta_{R_{load}} = \frac{\eta_{R_{d1}} R_{load}}{R_r + R_{load}} \tag{3.97}$$

for a 6-resonator ($N = 6$) array terminated with $R_T = 1.5\Omega$ with $R_{d1} = 3.8\Omega$ and $R_r = R$, consdering $V_s = 4.6V$. The results of the comparison are shown in Fig. 3.57.

We can see by the good agreement between the calculations and the results obtained through measurements that all the formulas developed and all the conclusions achieved through the analysis of those formulas in Section (3.4) can also by applied to the case of a real receiver just by taking into account the factor given by (3.93).

Finally, if we want to study the relation between the distance of the receiver from the array and the power transfer in efficiency in different positions, we can consider distances from the array of 4cm and 9cm. The mutual coupling values between the receiver and the cell below it are then $M_{r,l} = 2.7\mu H$ and $M_{r,l} = 1.2\mu H$, respectively. Then, considering a value of $R_{load} = 3.33\Omega$, we

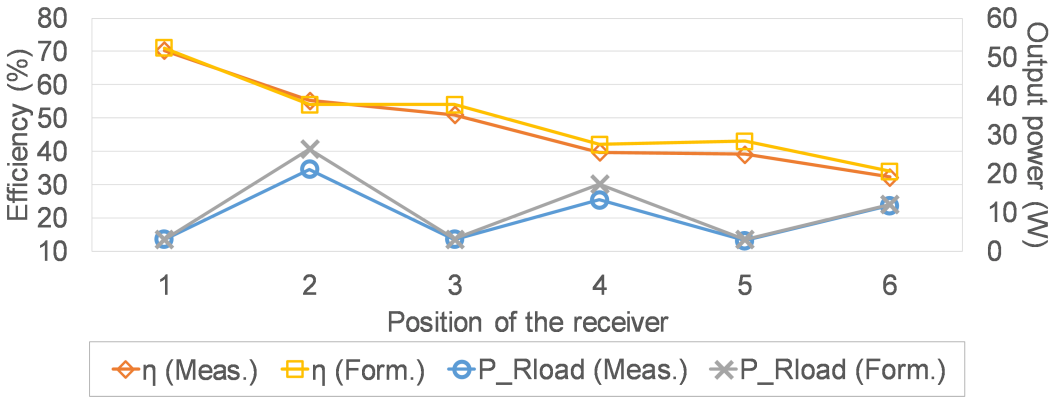

Figure 3.57: Comparison between the values of $P_{R_{load}}$ and $\eta_{R_{load}}$ obtained with measurements (using (3.88) and (3.89)) and the ones obtained with the developed formulas ((3.79), (3.78) and 3.93), for a 6-resonator array terminated by $R_T = 1.5\Omega$ for a receiver with a connected load of $R_{load} = 5\Omega$, the mutual inductance between the receiver and the cell beneath it being $M_{r,l} = 4.8\mu H$, versus the receiver position.

have, according to (3.90), a corresponding value of R_d of 5.7Ω, 1.8Ω and 0.4Ω for the distances of 1, 4 and 9cm, respectively. The measurements of the power delivered to R_{load} and efficiency determined with (3.94) and (3.95) are shown in Fig. (3.58), for different distances between the receiver and the cell of the array below it, considering a voltage source with a constant RMS value.

It is possible to notice by observing Fig. 3.58 that the efficiency, for the distances of 1cm ($R_d = 5.7\Omega$) and 4cm ($R_d = 1.8\Omega$), remains approximately the same from positions 2 to 6. Moreover, regarding the power delivered to R_{load}, increasing the distance from the receiver to the cell of the array below it, the variation of $P_{R_{load}}$ with the receiver position decreases. However, the power delivered to R_{load} and the efficiency decrease with the increase of the distance.

3.8 Conclusions

In this chapter, the impedance matrix which represents a resonator array was analysed. The study of the inverse of the impedance matrix allows one to obtain the current in each resonator and thus calculate the power delivered to a given load or to one or two receivers over the array and to determine the efficiency of the system.

By performing a mathematical study on the inverse of a tridiagonal matrix, which is the structure of the impedance matrix, analytical expressions of the currents were obtained, for two different cases and respective subcases, which represent several possible IPT systems used to transfer power wirelessly to a load, or to one or two receivers. For each case, using the expressions of the currents in the resonators developed in this chapter, the expressions of the power delivered to a load or a receiver were obtained along with the expressions for the efficiency of the system. Using these expressions, studies and comparisons were performed, regarding the values of the delivered power and efficiency for different conditions and parameters of the system, which allowed a better under-

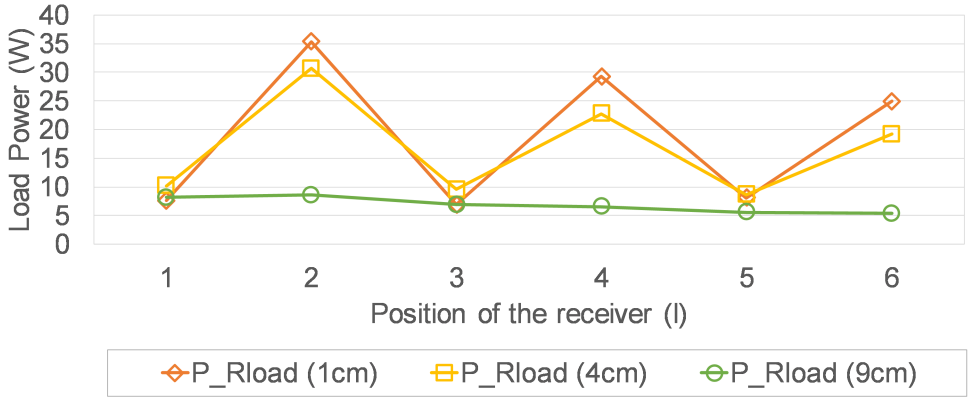

(a)

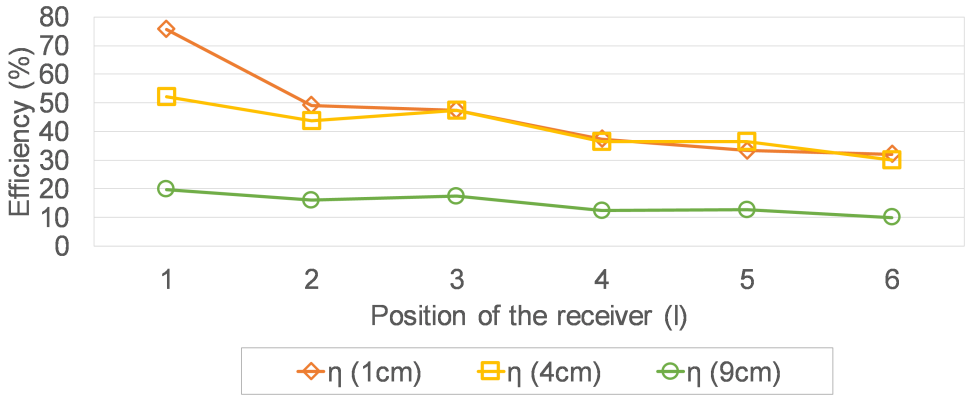

(b)

Figure 3.58: (a) Power delivered to $R_{load} = 3.3\Omega$ calculated with (3.94) and (b) efficiency of the system calculated with (3.95) versus the position of the receiver and for different distances between the receiver coil and the array cell below it .

standing of the behaviour of power transmission using resonator arrays to be achieved. Moreover, using the developed expressions one can determine analytically the maximum possible values of efficiency and power transfer for given conditions and also which conditions and parameters lead to maximum efficiency and power transfer.

To start with, regarding the values of the currents, it was found that the values of the currents can oscillate between higher and lower values when the array is not perfectly terminated. The analyses carried out on several examples that represent a different possible IPT system, show that the values of the maximum power transfer and efficiency changed substantially for each case, depending on the electrical parameters of the array, value of the impedance of the load or the receiver or receivers, position of the receiver, number of resonators, etc. However, in several particular situations it was found that values of the transferred power have opposite behaviour for odd or even numbers of resonators N or for the difference between the number of resonators and position of the receiver, $N-l$. Moreover, it was shown that the matching of the voltage source to the array of resonators does not affect the efficiency of the system, but it does, however, affect the delivered power, for a given voltage source. Afterwards, using at first Simulink as a circuit simulator and then performing measurements using the experimental setup described in Chapter 5, the expressions and formulas developed in this chapter were validated, thus showing their practical applicability for the design of an IPT system composed of a resonator array. Finally, it was taken into account that the receiver that is over the resonator array is not a physical impedance but instead another resonator coil with a load connected, and the losses in the receiver coil when calculating the whole efficiency of the system.

In conclusion, the expressions of the currents of the resonators, obtained through the analytical determination of the inverse of the impedance matrix, allow one to determine accurately the values of the power delivered to a load or to one or two receivers, and the efficiency of the system for fixed (i.e., the electrical parameters) or variable (i.e., receiver position) parameters of the system. The expressions developed are a powerful tool for the design of a resonator array, since one can easily predict the behaviour of the system, for given electrical parametrs of the system and different positions of the receiver and save time in comparison to numerical calculations or simulations. So, depending on the application desired for the resonator array, one can use the expressions obtained to optimize the IPT system regarding maximum power transfer, maximum efficiency or constant power delivered.

Appendix B

Constants determined in Section 3.3:

$$e_1 = \frac{\sqrt{b^2-4a^2}+b-2c}{2\sqrt{b^2-4a^2}};$$

$$e_2 = \frac{\sqrt{b^2-4a^2}-b+2c}{2\sqrt{b^2-4a^2}};$$

$$g_1 = \frac{2^{l-n-1}\left((b-d)(-b+2c+\varepsilon_1)\varepsilon_3{}^{n-l}-\varepsilon_2{}^{n-l}\left(4a^2-2b^2+b(2c+d-2\varepsilon_1)-2cd+2c\varepsilon_1+d\varepsilon_1\right)\right)}{\varepsilon_1{}^2};$$

$$g_2 = \frac{2^{l-n-1}\left(\varepsilon_3{}^{n-l}\left(-4a^2+2b^2-b(2c+d+2\varepsilon_1)+2c(d+\varepsilon_1)+d\varepsilon_1\right)+(d-b)(\varepsilon_3-2c)\varepsilon_2{}^{n-l}\right)}{\varepsilon_1{}^2}.$$

4 Magnetic near field generated from an array of resonators

4.1 Introduction

In literature, the studies performed on arrays of resonators have been made typically with the aim of analysing the efficiency and power transmission of these arrays [3, 5, 14, 16]; other important aspects of such systems, such as their electromagnetic compatibility or generated magnetic near field, have not been considered in depth. Papers concerning the electromagnetic compatibility [36, 37], human exposure [38, 39] or shielding of the magnetic near field generated [40, 41] refer to traditional two-coil IPT systems. Usually these studies use the IEEE [42] or ICNIRP [43] Standards as a reference for the limits of magnetic near field exposure. One of the reasons for which the magnetic field generated by resonator arrays has not been considered so far, is that usually the systems presented have a low transmitted power (from mW to a few Watts [3, 44]). However, if we take into account resonator arrays that are capable to deliver higher amounts of power, possibly to be used in applications as powering electronic devices or charging electrical vehicles, we definitely have to consider the magnetic field generated by a resonator array in order to analyse other aspects as the IPT system electromagnetic compatibility and limitation of human exposure [45].

For these reasons, in this chapter the magnetic near field generated by an IPT system which uses an array of coupled resonators as represented in Fig. 3.2 is assessed. First, using the Finite-Element software FEMM, an analysis on the magnetic field generated by a 6-resonator array is performed examining its spatial distribution and peak values, for a voltage source of fixed RMS value, or for a constant power delivered to R_T, for different values of R_T. Afterwards, considering the 4-multilayer resonator array described in Chapter 5, the difference between the field generated near and at a distance from the resonator array is examined along with its variation with different values of R_T. A circular magnetic near-field probe was used in order to measure the value of the average magnetic flux density normal component incident on the probe area. Finally, the measurements made with the circular probe are compared with the simulations carried out using a finite-element software.

4.2 Magnetic near field simulations

In this section, we assess the magnetic near field generated from an array of resonators arranged in a plane along a line and connected to a termination resistance R_T, as represented in Fig. 3.2, using the Finite-Element Software FEMM. As an example, we consider the stranded-wire 6-resonator array described in Chapter 5. Then, in order to study the spatial distribution of the magnetic flux

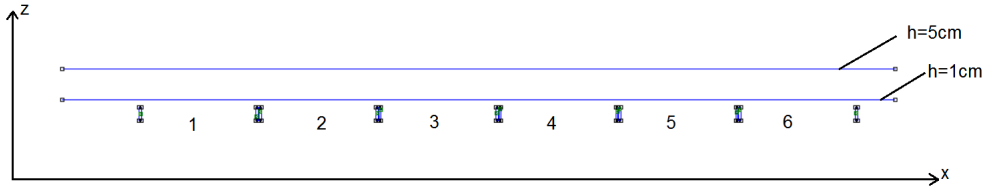

Figure 4.1: Scheme of the 6-resonator array cut by a transversal plane, used in FEMM for magnetic near field simulations.

density mangnitude, we considered a transversal plane that cuts the array in half, as represented in Fig. 4.1.

Eventually, we can perform the simulations calculating the value of the current in each resonator with the expression (3.43) developed in Chapter 3, using the values for the stranded-wire resonator array ($L = 12.6\mu$H, $C = 93.1n$F, $R = 0.11\Omega$, $M = -1.55\mu$H and $f_0 = 147$kHz) and for different values of R_T (0.4Ω, $R_{eq,\infty}$ and 10Ω).

Then, for the study of the spatial distribution of the magnetic flux density magnitude $|B|$, we considered two situations: one in which the power delivered to the load R_T, calculated with (3.48), is constant and equal to $P_{R_T} = 10W$ (which implies a variable RMS value of the voltage source V_s), and the other where we considering a given voltage source, with its RMS value V_s constant and equal to 5V. For these two situations, the spatial distribution of $|B|$ along the x and z axes, is represented in Figs. 4.2 and 4.4; the distribution of $|B|$ along a line parallel to the x axis at different heights from the array ($h = 1$cm and $h = 5$cm, as shown in Fig. 4.1) is shown in Figs. 4.3 and 4.5.

By analysing Fig. 4.3, it is possible to observe that the oscillation in the magnitude of the currents in consecutive resonators for values of R_T different than $R_{eq,\infty}$ (as seen in Fig. 3.5 in the previous Chapter 3), is also reflected in the magnetic flux density magnitude $|B|$. This means that when the array is terminated with $R_T = R_{eq,\infty}$, there are less variations in the magnetic flux density magnitude along a line parallel to x axis, as it can be clearly observed in Fig. 4.3. Moreover, by observing Figs. 4.2 and 4.3 (a) at a close distance from the array of resonators (for example h=1cm), higher values of the magnetic flux density near the edges of the resonators can be noticed. Finally, in the case where P_{R_T} is assumed constant, the magnetic flux density magnitude $|B|$ considered at points over a line parallel to the x axis (Fig. 4.3) has higher values when the value of R_T is different than $R_{eq,\infty} = 1.38\Omega$ ($R_T = 0.4\Omega$ and $R_T = 10\Omega$), while the lowest peak values of $|B|$ are obtained for $R_T = R_{eq,\infty}$; in particular, the highest values of $|B|$ are achieved for $R_T = 10\Omega$.

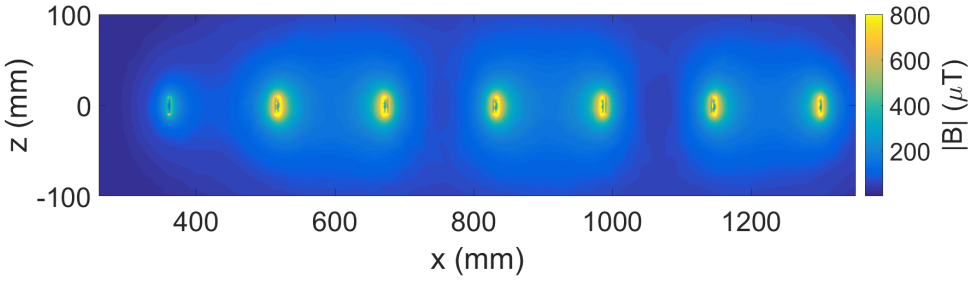

(a)

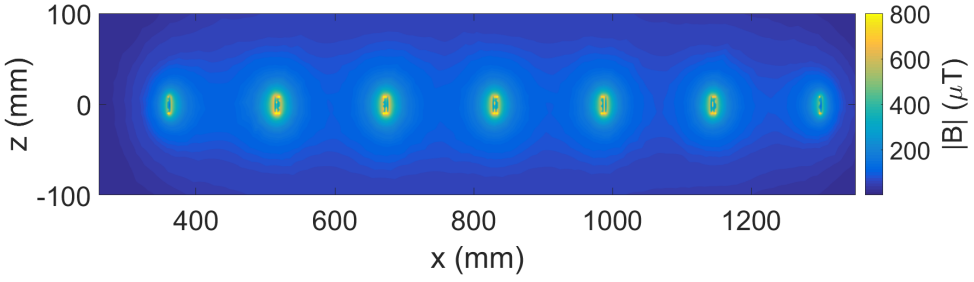

(b)

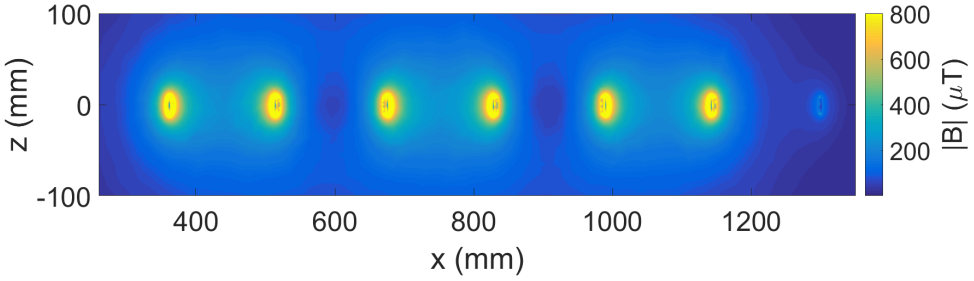

(c)

Figure 4.2: Spatial distribution of the magnetic flux density magnitude $|B|$ generated by a 6-resonator array along the x and z axes, for a constant power $P_{R_T} = 10W$ and for different values of R_T: (a) R_T=0.4Ω, (b) $R_T = R_{eq,\infty}$ and (c) R_T=10Ω .

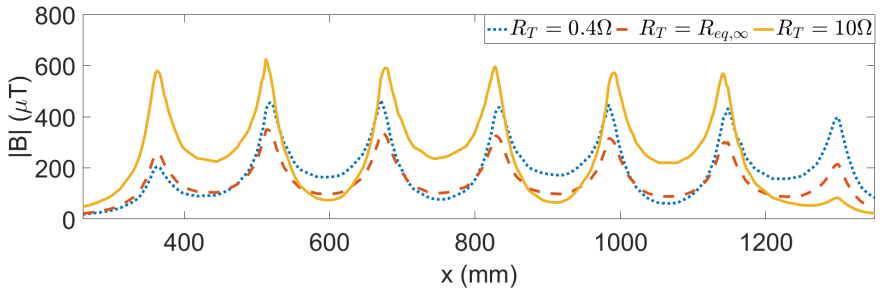

(a)

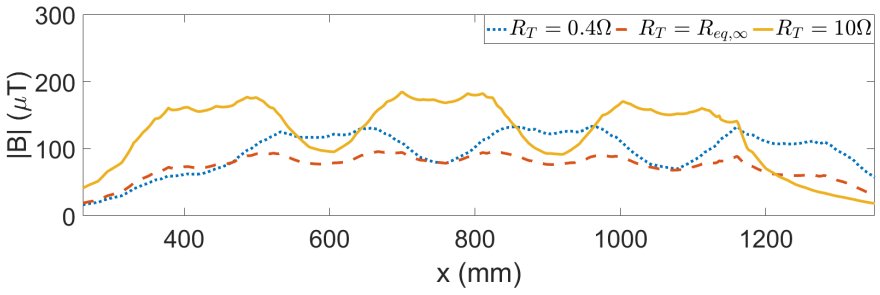

(b)

Figure 4.3: Magnetic flux density $|B|$ along a line parallel to the x axis at height h from the array (a) $h = 1cm$, (b) $h = 5cm$.

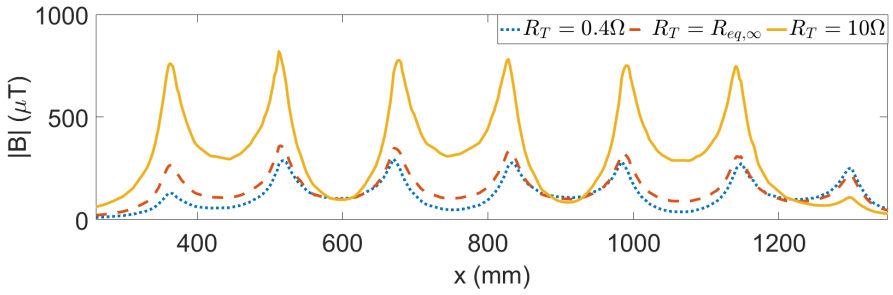

(a)

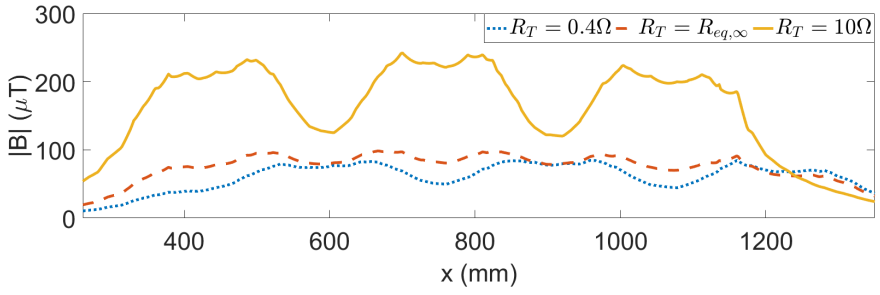

(b)

Figure 4.5: Magnetic flux density $|B|$ along a line parallel to the x axis at height h from the array (a) $h = 1cm$, (b) $h = 5cm$.

Afterwards, considering a voltage source with a constant RMS value $V_s = 5V$, we can note in Figs. 4.4 and 4.5 a smoother variation of the magnetic flux density magnitude over the resonator

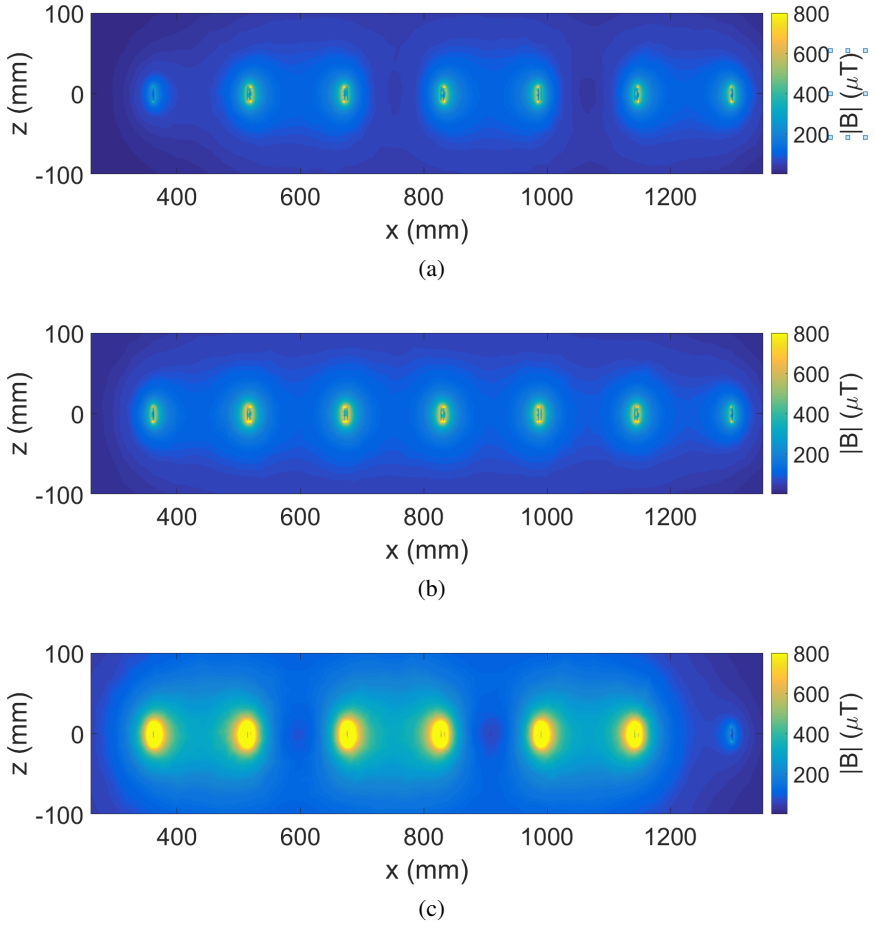

Figure 4.4: Spatial distribution of the magnetic flux density magnitude $|B|$ generated by a 6-resonator array along the x and z axes, for a voltage source with a constant RMS value $V_s = 5V$ and for different values of R'_T: (a) R'_T=0.4Ω, (b) $R'_T = R_{eq,\infty}$ and (c) R'_T=10Ω.

array, as seen in the previous case for $R_T = R_{eq,\infty}$, as the currents in adjacent resonators have similar magnitudes. However, in this case, even though the highest peak values for $|B|$ are still found for $R_T = 10\Omega$, the lowest peak values occur for $R_T = 0.4\Omega$. Still, we need to take into consideration that the power absorbed by the load, P_{R_T}, and the power delivered by the voltage source to the array, P_{in}, are different for each case: P_{R_T} has the values of 4.0W, 10.6W and 17.3W, P_{in} has values of 8.2W, 16.8W and 48.2W for $R_T = 0.4\Omega$, $R_{eq,\infty}$ and 10Ω, respectively. In conclusion, for a voltage source with a constant RMS value, although for $R_T = 0.4\Omega$ the lowest peak values of $|B|$ are noted, both the power delivered to R_T, P_{R_T}, and the efficiency, P_{R_T}/P_{in}, are smaller than those obtained when $R_T = R_{eq,\infty}$.

4.3 Magnetic near field measurement

In order to measure the magnetic near field generated by an array of resonators and verify the results regarding its variation with different values of R_T, a self-constructed circular magnetic near-field probe of a 4cm diameter (built from a coaxial cable, as shown in Fig. 4.6, was used. This probe was then connected to an Agilent 4396B Spectrum Analyzer (2 Hz-1.8 GHz). The electromotive force (e.m.f.) ε at the terminals of the probe produced by the time-varying mag-

Figure 4.6: Magnetic near field circular probe used for the e.m.f. measurements.

netic field generated by the resonator array was then measured. According to Faraday's law and supposing that B is uniform over the area A, it is given by:

$$\varepsilon = -N\frac{d}{dt}(BA\cos\theta) \tag{4.1}$$

where N is the number of turns of the inductor and θ is the angle between the vector of the magnetic flux density and the normal vector to the area considered. From (4.1), considering that the magnetic flux density B is a sinusoidal quantity with frequency $f = \omega/2\pi$, and that the probe has one single turn ($N = 1$), it is possible to determine the average value B_p of the RMS value of the magnetic flux density normal component ($\theta = 0^o$) incident on the probe area, at the resonant frequency ω_0, as

$$B_p = \frac{V_p}{A_p\omega_0} \tag{4.2}$$

where V_p is the RMS value of the voltage measured at the probe terminals and A_p is the area of the probe.

Eventually, using the 4-resonator array with planar multilayer coils, whose equivalent circuit is depicted in Fig. 3.2 (as described in Chapter 5), V_p was measured at points at different distances from the resonators. Measurements were made along a semicircular line of 1.82 m of diameter (along the edge of a circular wooden table, as shown in Fig. 4.7) centred on the array structure. Another set of measurements were performed along the horizontal symmetry axis of the array structure at a height of 2.5 cm above it. In order to avoid the possible influence of the inverter on the measurements, these are performed with the inverter outside the circular table, as seen in Fig. 4.7. Two different capacities (20nF and 47nF) are connected to the coils in order to make the system resonant at 294kHz and 192kHz, respectively. For the resonance frequency of 294kHz the magnetic near field is assessed using the values for R_T 0.47Ω, 3.3Ω and 10Ω, while for the resonance frequency of 192kHz the termination impedances of 0.47Ω, 2.67Ω and 10Ω are used. In both cases, the power delivered to the load is kept constant and equal to 5W.

The magnetic flux density is found from V_p with (4.2), i.e., as the average normal component of the magnetic flux density incident on the probe area. By aligning the probe axis with each

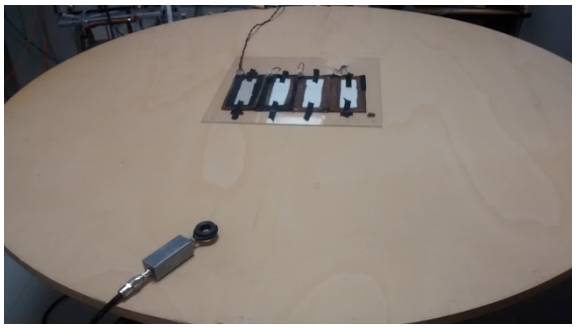

Figure 4.7: Resonator array on the circular table and magnetic near field probe used in the measurement.

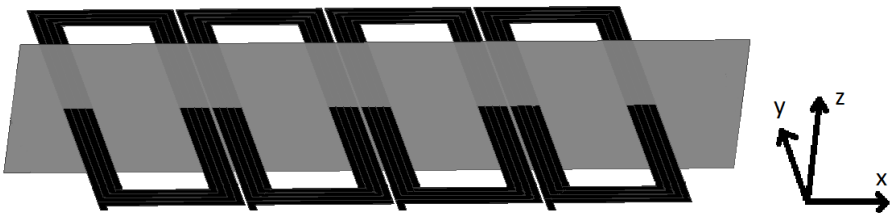

Figure 4.8: Resonator array representation with transversal cross-section used in the finite element simulations.

coordinate axis (as represented in Fig. 4.8), we can then obtain the corresponding average RMS normal components $B_{p,x}$, $B_{p.y}$, $B_{p,z}$ of the magnetic flux density, which lead to:

$$B_{meas} = \sqrt{B_{p,x}^2 + B_{p,y}^2 + B_{p,z}^2}. \tag{4.3}$$

Then, an analysis was made of the variation of the RMS values of the magnetic flux density magnitude at points both near and at a distance from the resonator array. Using the value of the current measured in each resonator, simulations were performed with a Finite Element software and the simulated values were then compared with the ones obtained through measurements using (4.2) and (4.3). This was done for both 294 kHz (Figs. 4.9 and 4.10) and 192 kHz (Figs. 4.11 and 4.12) resonant frequencies.

By analysing Figs. 4.9-4.12 we can observe that, as seen in the previous section with the simulations made on the 6-resonator array, when R_T is close to $R_{eq,\infty}$ (which is equal to 3.2Ω and 2.0Ω

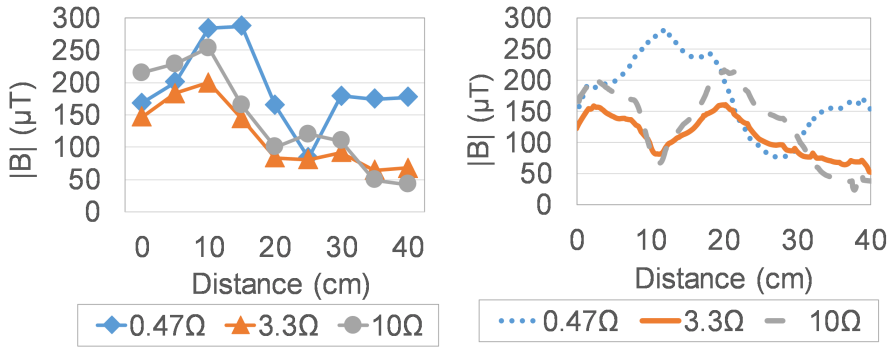

Figure 4.9: Comparison between the magnetic flux density magnitude (RMS value) obtained with (a) measurements and (b) simulations along a line above the resonators at 294kHz and for different values of R_T.

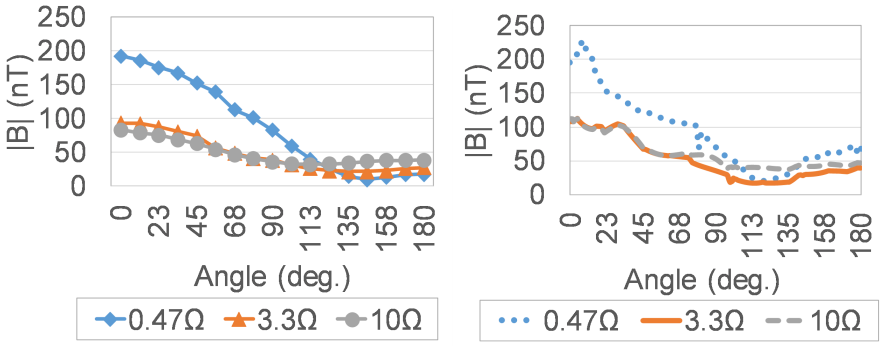

Figure 4.10: Comparison between the magnetic flux density magnitude (RMS value) obtained with (a) measurements and (b) simulations along a semicircular line around the resonators at 294kHz and for different values of R_T.

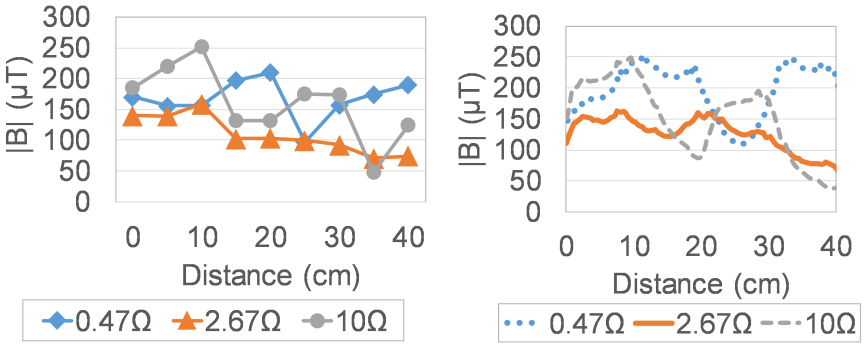

Figure 4.11: Comparison between themagnetic flux density magnitude (RMS value) obtained with (a) measurements and (b) simulations along a line above the resonators at 192kHz and for different values of R_T.

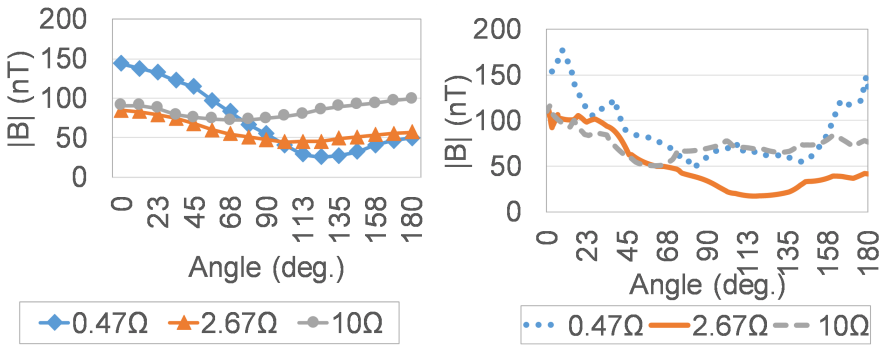

Figure 4.12: Comparison between the magnetic flux density magnitude (RMS value) obtained with (a) measurements and (b) simulations along a semicircular line around the resonators at 192kHz and for different values of R_T.

for the 294kHz and 192kHz cases, respectively), the peak values of the magnetic flux density are never the highest ones and their values vary less along the lines considered. Moreover, the peak values of the magnetic flux density magnitude at a distance from the array are much smaller than the ones at points close to the resonator array (from hundred of nT to hundred of μT). However, this means that not all the magnetic flux density is confined into the array of resonators and that the field at a distance from the system has to be considered.

4.4 Conclusion

In this chapter the magnetic near field generated by an IPT system composed of an array of resonators is examined.

To start with, using the software FEMM, the spatial distribution of the magnetic flux density is analysed considering a 6-resonator array with stranded-wire resonators as an example. Two cases are considered: one in which the power delivered to R_T, P_{R_T}, is considered constant and equal to 10W and another where the voltage source that supplies the resonator array has a constant RMS value $V_s = 5$V. For different values of R_T it is possible to observe that the oscillation in the magnitude of the current in each resonator (already noticed in Chapter 3 for R_T different than $R_{eq,\infty}$) is also reflected on the values of the magnitude of the magnetic flux density. This means that, if we consider a line parallel to the symmetry axis of the array at a given height, the values of the magnetic flux density magnitude vary less along that line when $R_T = R_{eq,\infty}$. Moreover, in the case with a constant delivered power P_{R_T} and $R_T = R_{eq,\infty}$, the peak values of the magnetic flux density magnitude are never the highest ones along the lines considered, while in the case for a voltage source with fixed RMS value this happens for $R_T = 0.4\Omega$; in both cases, the highest peak values are observed for $R_T = 10\Omega$. Additionally, at a small distance from the resonator array, the magnetic flux density magnitude is higher near the edges of the resonators.

Regarding the measurements made on the multilayer 4-resonator array using a circular magnetic near-field probe, it is found that, as expected from the precedent section, when the value of R_T is closer to $R_{eq,\infty}$ the peak values of the magnetic flux density are never the highest ones, at points both near the array and at a distance from the array. This is observed when the system is

operating both at 294kHz and at 192kHz resonant frequencies. Moreover, although the magnetic flux density measured at a distance from the resonator array is much lower than the one measured close to the array, not all the magnetic flux density is confined into the array of resonators. This implies that this magnetic flux density detected at a distance from the array of resonators should to be considered specially with systems capable of delivering higher power. In the same way, the magnetic near field measured at points a close to the array should also be limited according to the limits defined by IEEE and ICNIRP Standards for human exposure. Finally, the good agreement between the values obtained with experiments and simulations indicates that the circular magnetic near-field probe can be used to measure the magnetic near flux density with a good accuracy.

5 Experimental Setup

5.1 Introduction

In inductive wireless power transfer systems and prototypes presented in literature, the type of coils and power source used usually depends on the operating frequency and power delivered by these systems. When operating at high frequencies (usually up to a few tens of MHz) and low power (up to a few Watts) usually the coils are single or multilayered flat resonators, printed on PCB boards, [8, 11, 14, 16]. Concerning the power and efficiency analyses of the IPT systems, signal generators driving RF power amplifiers [8, 13, 44, 46] or vector network analysers (VNA) [14, 16] are mainly used.

On the other hand, in order to be able to transmit larger power with IPT systems, power converters are used to supply the inductors. By using AC-DC-AC converters as in [2, 4] or just a DC-AC converter, as in [47, 48], it is possible to feed the coils with a high frequency voltage (for higher power applications, around a few tens of kHz). Although the high frequency voltage generated by the DC-AC stage is a square wave, the current circulating in the coils is sinusoidal, as the resonant circuit behaves as a filter (considering that the coils have a high quality factor Q, as referred in [32]). Regarding the type of switches used in the converters, many high power prototypes presented in literature use inverters with IGBT switches [4, 47] as they have higher rated voltages. However, these converters with IGBTs usually operate up to a few tens of kHz. Converters with higher switching frequencies, as in [48, 49], use MOSFET switches.

When we work at kHz frequencies, the quality factor of the coils ($Q = \omega L/R$) is much lower in comparison to that at frequencies of the MHz level because, despite the fact that the resistance decreases approximately with the square-root of frequency ($\sqrt{f}$) due to the skin-effect, ωL decreases with the frequency. As the value of the inductance L depends mainly on the geometry of the wire and coils, a way to increase the quality factor of the coils and reduce the losses in the resonators is the utilization of Litz wire, as in [4, 13, 31].

In this chapter we describe the experimental setup used in this thesis for the experimental verification of the theoretical results obtained. The experimental setup uses an inverter with MOSFET switches as the power source and two types of resonator arrays: one with rectangular planar multilayer coils and the other with square stranded-wire coils.

5.2 Power source - resonant inverter

As referred in the introduction of this chapter, many high power vehicle charging applications, as in [2, 4], use a two-stage AC-DC-AC converter to power IPT systems in which the former AC-DC stage rectifies the AC current from the grid and the latter DC-AC stage produces the AC current at the desired high frequency, as in Fig. 5.1.

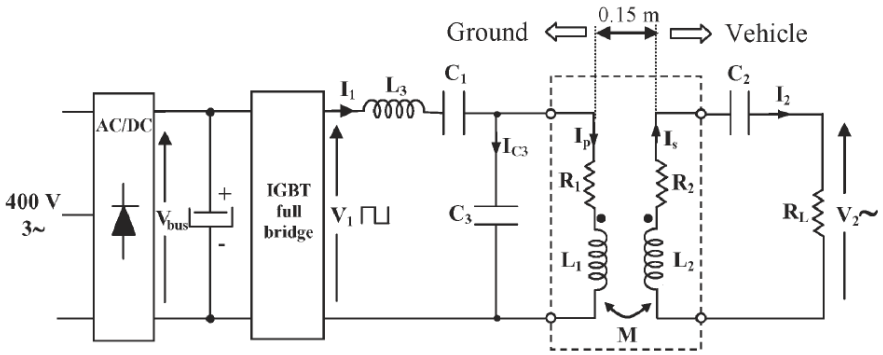

Figure 5.1: Example of an AC-DC-AC converter for a inductive power transfer system for electric vehicle charging [4].

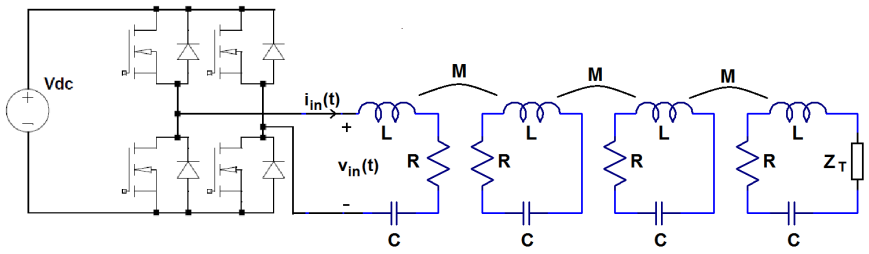

Figure 5.2: Example of the circuit of a full-bridge inverter fed by a DC voltage source V_{dc} connected to an array of 4 resonators.

In the experimental setup used in this thesis we use just the final DC-AC stage, using a resonant inverter powered by a DC voltage source. As in this thesis we operate at frequencies from 150kHz to 300kHz, a Class D voltage-switching inverter with MOSFETs, as in [32], is used. The layout of the circuit of the inverter feeding an array of 4-resonators is represented in Fig. 5.2. The inverter was built using a Fairchild FSB44104A Motion SPM® 45 LV Series module that has integrated a three-phase MOSFET inverter and the MOSFET drive circuit (HVIC and LVIC), as represented in Fig. 5.3.

The circuit shown in Fig. 5.3 was then implemented by using an Elind 3232 DC voltage source to power the MOSFET drive circuit to 15V and an Arduino Due microprocessor board to set the switching frequency of the MOSFETs. The Arduino Due board was connected to ports “Gating WH” to “Gating UL” (represented by MCU (MicroController Unit) in Fig. 5.3). Furthermore, in order to build the circuit shown in Fig. 5.3 all the other components (capacitors, resistors and diodes) were connected to each other using a PCB board, as shown in Fig. 5.4. The values used for the resistors, capacitors and diodes, as recommended by the manufacturer, were the following:

- $R_s = 100\Omega$; $R_{BS} = 56\Omega$;
- $C_{PS} = 1nF$; $C_{BS} = 100\mu F$; $C_{BSF} = 1\mu F$; $C_{SP15F} = 100\mu F$; $C_{DCS} = 200\mu F$
- Diode D_{BS} was a Schottky 60V /1A diode, while the Diodes connected between pins 22 and 21, 20 and 21 and 18 and 17 were 24V, 3W Zener Diodes.

Finally, the inverter DC bus was connected to an AIM-TTI Instruments QPX1200SP 1200W DC

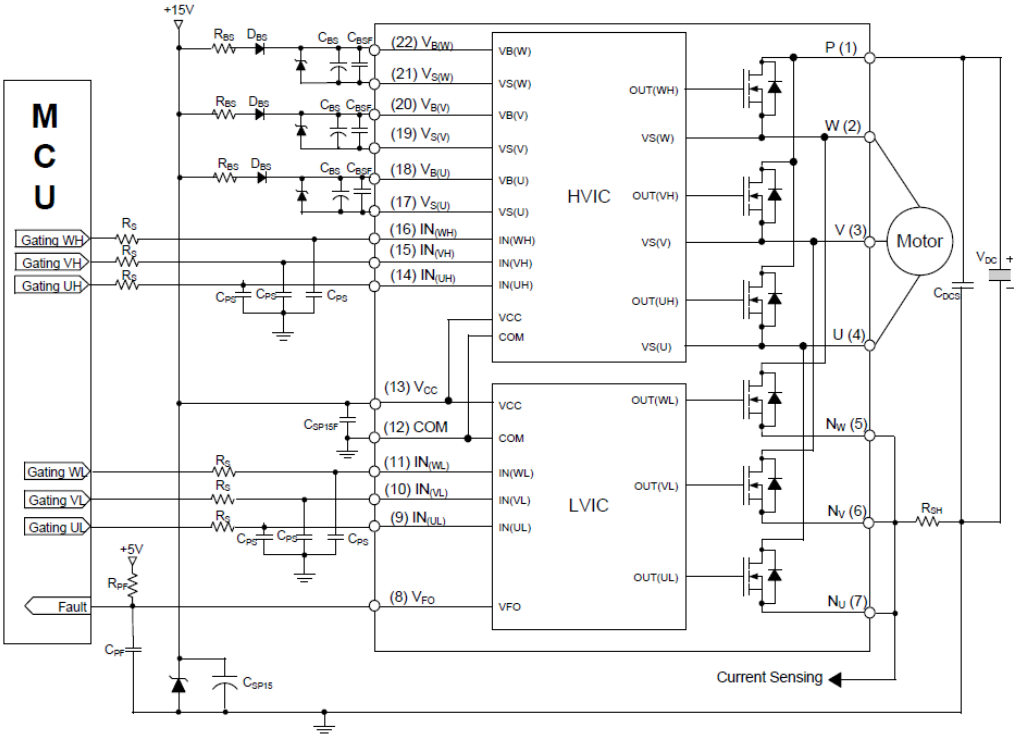

Figure 5.3: Typical application circuit and internal equivalent circuit of the FSB44104A Motion SPM® 45 LV Series. .

Power Supply.

It is important to note that, although the FSB44104A module has a three-phase inverter integrated, in order to obtain an equivalent circuit as in Fig. 5.2, we only need two phases of the inverter. In our case, only the phases U and V were used. Eventually, as referred before, the frequency of the square wave voltage generated by the inverter is determined by the Arduino Due microcontroller. Then, by setting the Arduino Due to switch the MOSFETS in phase U and V alternatively, we can obtain a full-square wave between the phases U and V at a determined frequency, as shown in Fig. 5.5.

5.3 Array with multilayer planar coils

In this section we describe the design and manufacturing of the array composed of four rectangular multilayer flat spiral resonators, as shown in Fig. 5.6, with the dimensions reported in Tab. 5.1.

Concerning the calculation of the resonators electrical parameters, the self-inductance L of each resonator is found through the partial inductance method [50, 51]. This method consists in the calculation of the self-inductance of the resonator by adding the partial self- and mutual inductances of the smaller elements in which the resonators can be subdivided. The partial self-inductances are determined with the finite element simulation programme FEMM [52] while the partial mutual

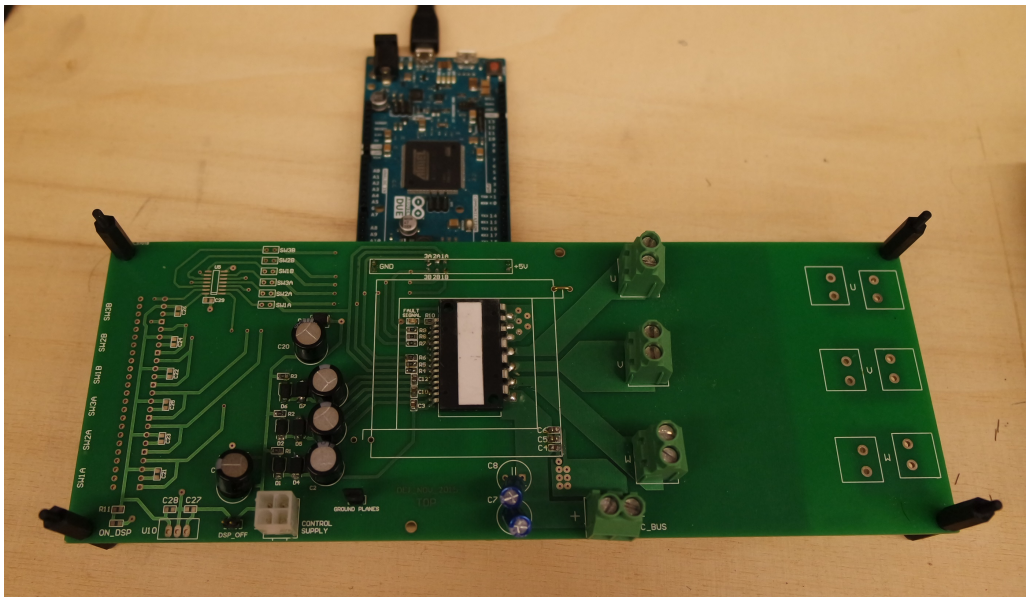

Figure 5.4: PCB board with the FSB44104A module and Arduino Due microprocessor, built for implementing the inverter circuit used in this thesis.

Table 5.1: Dimensions of the designed resonators represented in Fig. 5.6.

Dimensions	[mm]
l	250
lm	100
Thickness of the resonator track (t)	0.1
Width of the resonator track (w)	5
Space between turns (st)	0.1
Space between layers (sl)	0.25

inductances are found with the calculation method proposed in [53]. Regarding the AC resistance of the resonators, it is calculated using the value of the resistance per unit length obtained with FEMM, so that the skin effect, proximity effects and crowding current density effects on the AC resistance are taken into consideration. The stray capacitance associated to the parasitic capacitances between turns and layers is neglected in this thesis. This because as we operate at a resonant frequency much lower than the self-resonant frequency of the coils, the stray capacitance is much smaller than the additional capacitance used to tune the resonators to a particular resonant frequency.

Considering that we want to reduce the losses in each resonator, from [14, 16] we know that the attenuation in each cell decreases with the increase of the product $|kQ|$, which is referred in this thesis as the inverse of factor $r = R/2\omega_0|M|$ (3.58). In order to analyse the variation of $|kQ|$ with the number of turns and layers, in Fig. 5.7 the quality factor Q, the coupling coefficient magnitude $|k|$ and the $|kQ|$ product are plotted versus the number of turns and for different layer numbers n, considering two resonators placed side-by-side at a distance of 5 mm and an operating frequency of $f = 300$ kHz [5]. As it can be observed in Fig. 5.7 (a), the quality factor has a maximum for $n = 1$ for about 7 turns ($Q \cong 55$) and for $n = 2$ for about 5 turns ($Q \cong 69$). Conversely, Fig. 5.7 (b) shows that the coupling coefficient magnitude $|k|$ decreases with the number of turns, with similar

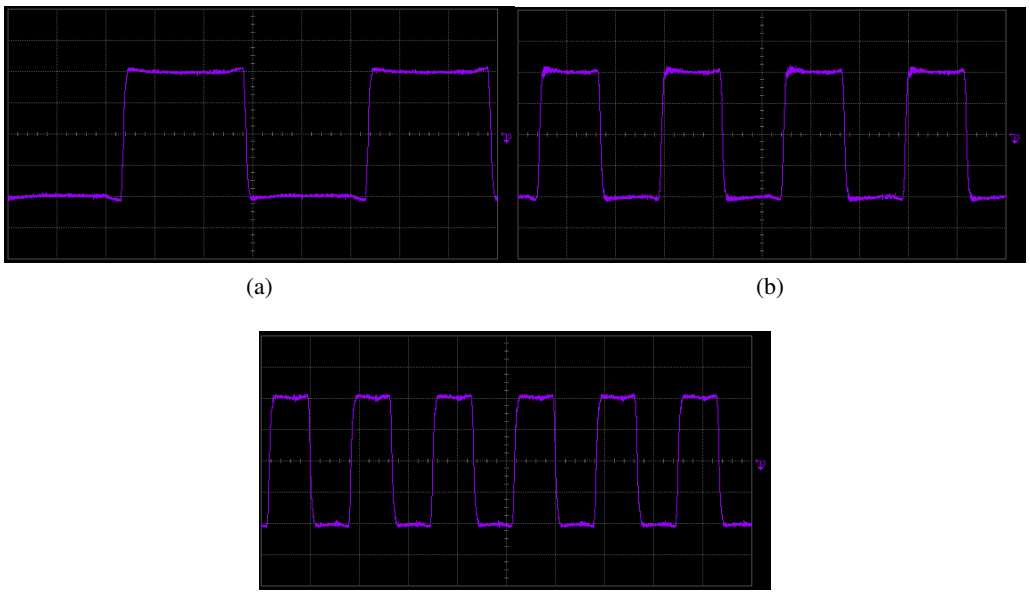

(a) (b)

(c)

Figure 5.5: Voltage between phases U and V, as in Fig. 5.3 for an operating frequency of (a) $f = 100$kHz, (b) $f = 200$kHz and (c) $f = 300$kHz. Horizontal scale $2\mu s$/div; vertical scale $5V$/div.

values for $n = 1$ and $n = 2$. However as we want to maximize the product $|kQ|$ it is important to notice that, as seen in Fig. 5.7 (c), $|kQ|$ reaches a maximum for $n = 1$ for 4 turns ($|kQ| = 7$) and for $n = 2$ for 3 turns ($|kQ| = 9$).

As a result of the conclusions drawn from Fig. 5.7, the multilayer resonators were built with 2 layers and 3 turns, according to the scheme of Fig. 5.6 and with the dimensions of Table 5.1. The resonators were fabricated in laboratory by cutting a copper sheet and two identical layers were manufactured and welded together, using electrical tape as insulator between the layers and cardboard as resonator substrate (Fig. 5.8). In the calculations presented in Fig. 5.7 the coils were designed to resonate at 300 kHz. However, for this resonator array, by using two different commercially available capacitors of 20nF and 47nF, the experimental system was set to resonate at 294kHz and 192kHz, respectively

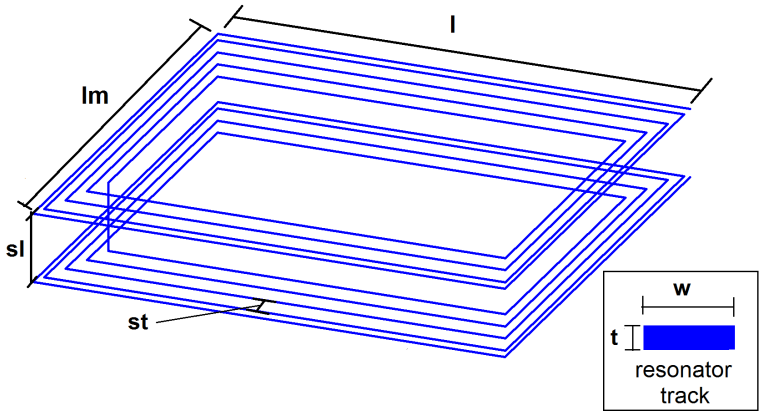

Figure 5.6: Representation of a multilayer flat spiral resonator and its dimensions.

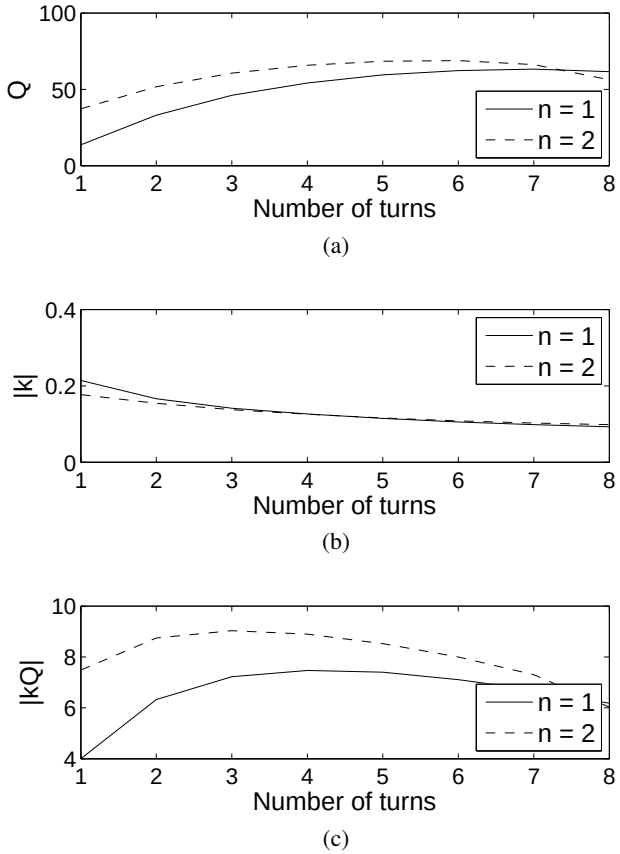

Figure 5.7: Values of Q (a), $|k|$ (b) and $|kQ|$ (c) versus the number of turns for one and two layers [5].

Table 5.2: Measured and calculated values of the resonator parameters.

Parameters	Measured	Calculated	
Frequency (kHz)	100	192	294
L(μH)	14.8	14.8	14.8
R(Ω)	0.42	0.58	0.72
Q	22	31	38

Using the methods described previously, the resonators were designed to have a value of self-inductance of 14.8μH. The self-inductance was then measured using an Agilent 4263B LCR Meter at 100kHz. The mutual inductance M between any pair of adjacent resonators was empirically calculated using the following:

$$V_2 = \omega M I_1 \tag{5.1}$$

where V_2 is the RMS value of the measured voltage at the terminals of the second resonator of the pair, I_1 is the RMS value of the sinusoidal current injected in the first resonator. From (5.1), the mutual inductance M obtained through measurements is 1.9μH.

The measured and calculated self-inductance, resistance, and relevant quality factor of a cell are reported in Table 5.2. The value of the self-inductance of the resonators was measured with an Agilent 4263B LCR Meter at 100 kHz. As the value of the resistance was measured at 100kHz, for other frequencies the value is estimated to increase with the square-root of the frequency $\sqrt{f}$, due to the skin-effect while the inductance is estimated to remain approximately the same value. The equivalent series resistance (ESR) of the capacitor was measured and was found to be negligible compared to the coil resistance. The quality factor and the resistance are calculated for $f = 294$ kHz and $f = 192$ kHz. Note that the value obtained for the quality factor at 294 kHz, $Q = 38$, is smaller that the one predicted in Fig. 5.7(a), probably because of a higher value of the resistance of the coils due to the soldering of the two layers. The value of the coupling coefficient magnitude, $|k| = 0.26$, is higher that the one predicted in Fig 5.7(b), due to the smaller side-by-side distance set between the resonators in the experimental setup with respect to the one used for calculations in Fig. 5.7 (5mm). This was done in order to increase the performance of the system and compensate the lower value of Q experimentally obtained, thus making the product $|kQ|$ equal to 9.9, similar to the value predicted in Fig. 5.7(c).

The experimental setup of the array of four multilayer planar resonators connected to the inverter and a termination impedance Z_T as represented in Fig. 5.2 is shown in Fig. 5.8.

5.4 Stranded wire coils

The second array presented in this thesis uses square coils made with stranded wire, as a cheap alternative to Litz wire. The wire used was a Alpha Wire PPE Hook Up Wire, 3.31 mm², 600 V 12 AWG. The stranded wire was composed of 65 tinned copper strands of 0.25 diameter each, making a conductor area of 3.31mm^2. Each wire was insulated with PPE (Polyphenylene Ether) and had a total diameter of 2.97mm. For the fabrication of the coils a wood block of 153x153x29 mm with a channel 1.5mm deep and 18mm wide was used , as shown in Fig. 5.9(a). Then, the

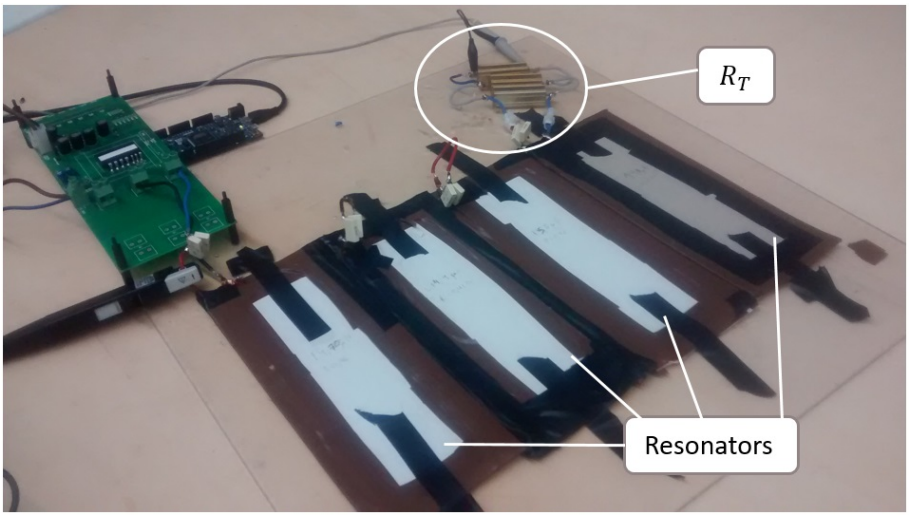

Figure 5.8: Array of four multilayer planar coils connected to the inverter.

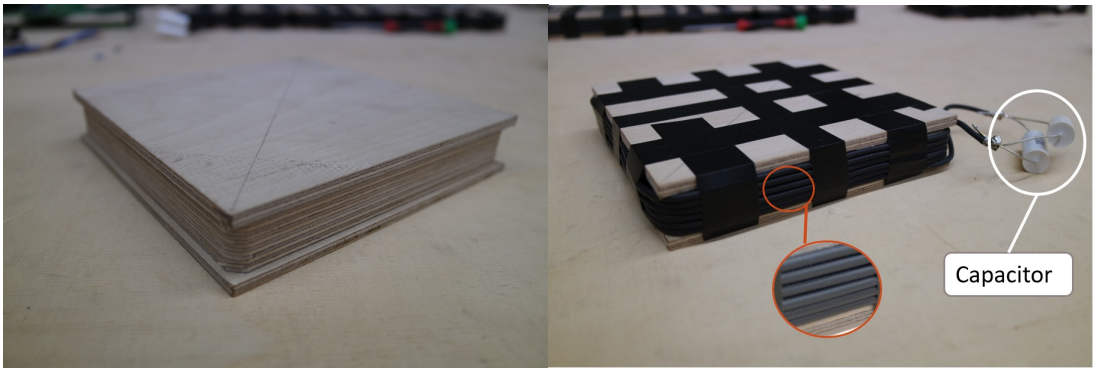

(a) (b)

Figure 5.9: Wooden core used for the fabrication of the coils (a) and complete manufactured coil (b).

wire was wrapped around the channel with 6 turns, and kept tight around the wood block with electrical tape, as shown in Fig. 5.9 (b).

Then, as seen in 5.9 (b), two capacitors of 47nF were connected to each resonator, making a total capacity of 94nF. The resonators were then placed side-by-side as close as possible, with just 0.6 mm of separation between the wires due to the insulation of the wires (0.3mm thickness). An example of the experimental setup used in this thesis for an array of 6 resonators is represented in Fig. 5.10, with the first resonator connected to the inverter described in section 5.2 and the last one to a resistance.

The inductance of the resonators was predicted using the formula for a rectangular solenoid as in [54] and a value of $L = 12.6\mu$H was obtained. The experimental values of the self-inductance, intrinsic AC resistance, added capacitance and resonant frequency of each resonator were determined through measurements using a Vector Network Analyser (VNA). The mutual inductance M between any pair of adjacent resonators was also determined with the VNA from (5.2):

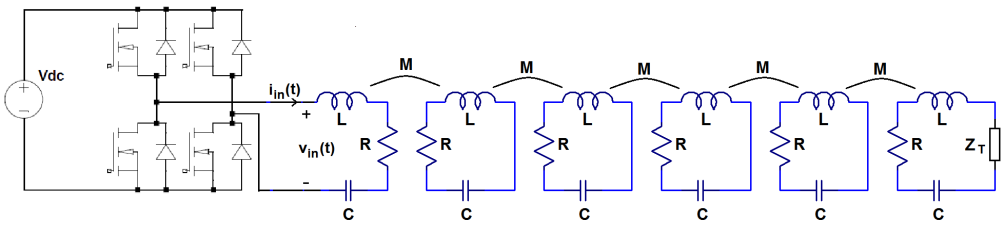

(a)

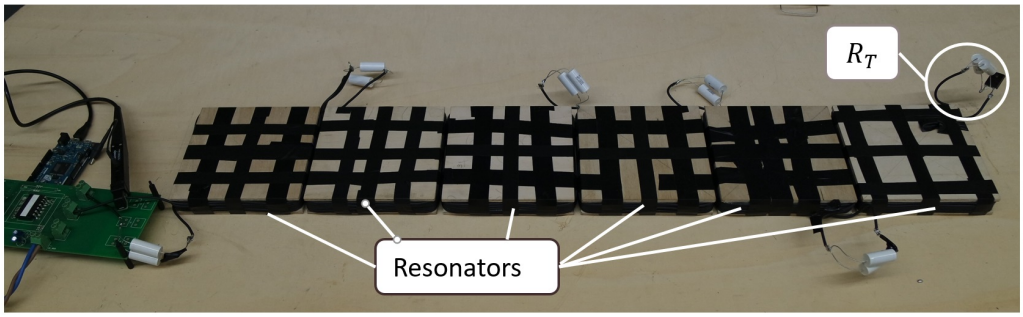

(b)

Figure 5.10: Equivalent circuit of the experimental setup using 6 coils (a) and complete experimental setup used in laboratory (b).

Table 5.3: Average measured circuit parametervalues of the resonator array.

Parameter	L(μH)	C(nF)	R(Ω)	M(μH)	$f_0 = 1/\left(2\pi\sqrt{LC}\right)$(kHz)
Measured values	12.6±0.1	93.1±0.2	0.11±0.01	-1.55±0.05	147.0±0.5

$$\hat{Z}_{in} = R + \frac{(\omega_0 M)^2}{R} \tag{5.2}$$

After performing measurements in all the inductors, the average values between the maximum and minimum measured values for each parameter are given in Table 5.3.

Note that for these coils, although we are operating at a lower frequency, due to the larger section of the conductor, we obtained a larger value of Q, equal to 108. Moreover, having a similar value of $|k| = 0.25$, we have a product $|kQ| = 27$, much higher than the value of 9.9 obtained for the planar multilayer coils. This leads to a lower attenuation, which is clearly observed in the efficiency measurements made in Chapter 3, where for an array of 4 resonators larger values are obtained for the array with stranded wire.

For the cases presented in Chapters 2 and 3, where we considered a receiver over the array, we used a resistance to represent the receiver (Fig. 5.11 (b)) or a real receiver (Fig. 5.11(c)), using one of the resonators of the array. Regarding the real receiver, as seen in Fig. 5.11(c), the resonator is placed directly over the array, meaning that the distance between the faced resonators is 1 cm due to the wooden substrate. For this distance, the mutual inductance measured between the receiver and the resonator below it was measured using the VNA with (5.2) and a value of $M_{r,l}$ =4.8μH was obtained. Moreover, the receiver was distanced 4cm and 9cm from the cells of the array, which gives a measured mutual inductance between the receiver and the cell beneath it of $M_{r,l} = 2.7\mu H$

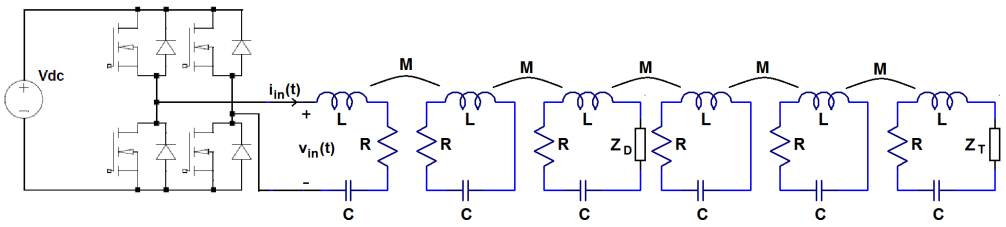

(a)

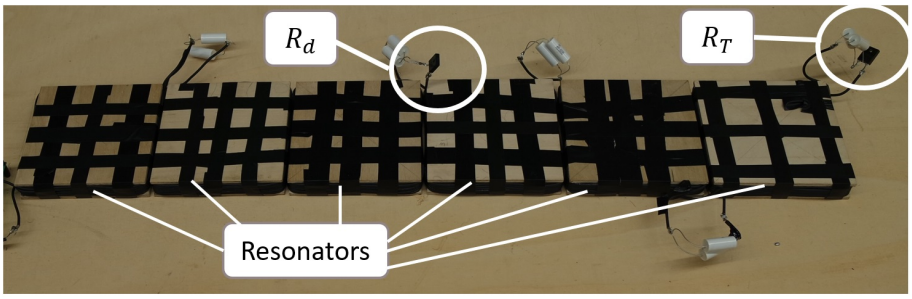

(b)

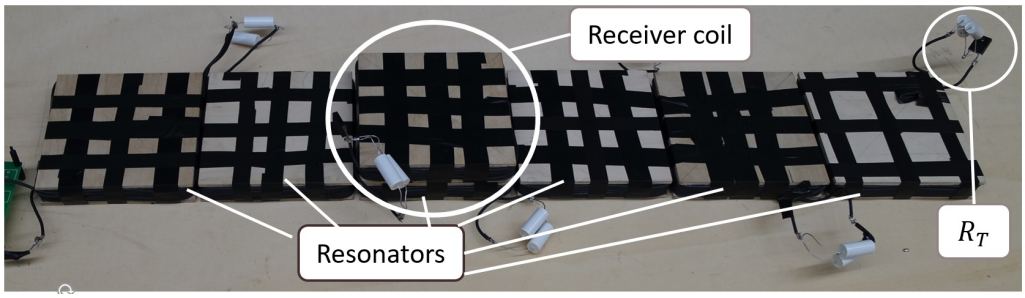

(c)

Figure 5.11: (a) Equivalent circuit of the experimental setup using 6 coils with a receiver over the 3rd resonator and (b) complete experimental setup used in laboratory, using a resistance to represent the receiver or (c) with a real receiver (resonator).

and $M_{r,l} = 1.2\mu H$, respectively.

The resistors used in the experiments were Thick Film resistors, with a rated maximum dissipated power of 100W.

An example of the waveforms of the input voltage and current $v_{in}(t)$, $i_{in}(t)$ and the voltage at the terminals of the termination resistance $v_T(t)$ (using the setup shown in Fig. 5.10) is shown in Fig. 5.12. The voltage $v_T(t)$ leads the input voltage $v_{in}(t)$ by 90º. This happens because the current in the 6th resonator leads the first resonator current by 90º, as seen in Chapter 3.

Another example with the voltage $v_d(t)$ at the terminals of the resistance that represents the receiver, when it is in the 3rd position ($l = 3$) (Fig. 5.11(b)), is shown on Fig. 5.13. In this case the voltage $v_d(t)$ is in phase opposition with respect to the input voltage $v_{in}(t)$ because the resistance R_d is connected to the 3rd receiver of the array whose current is in phase opposition with respect to the first resonator current, as seen in Chapter 3.

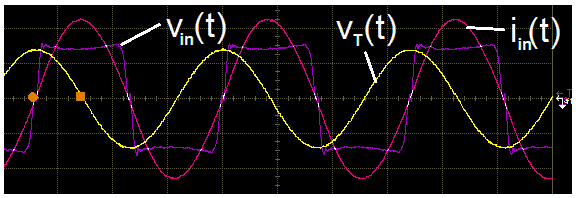

Figure 5.12: Example of the waveforms of the input voltage and current $v_{in}(t)$, $i_{in}(t)$ and of the voltage $v_T(t)$ at the terminals of $R_T = 1.5\Omega$, $v_T(t)$ obtained with the oscilloscope. Horizontal scale: $2\mu s$/div. Vertical scale 10V/div. and 5A/div.

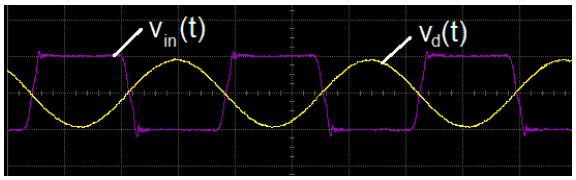

Figure 5.13: Example of the waveforms of the input voltage $v_{in}(t)$, of the voltage at the terminals of the resistance $R_d = 5\Omega$ that represents the receiver over the 3rd resonator of the array ($l = 3$) $v_d(t)$ of obtained with the oscilloscope. Horizontal scale: $2\mu s$/div. Vertical scale 10V/div.

5.5 Conclusion

In this chapter we describe the manufacturing of the experimental setup used in this thesis. First, the power source of the resonator arrays was build using the inverter integrated in the Fairchild FSB44104A module composed of a full-bridge inverter. The FSB44104A was integrated in a PCB board together with the circuit that powered the MOSFET drive, which was controlled by the microprocessor Arduino Due. Regarding the type of resonator arrays, two types of resonator arrays were used. The first one used four rectangular planar coils with two layers and three turns per layer fabricated with a 0.1mm thickness coil sheet in a substrate of cardboard and it was operated at resonant frequencies of 192kHz and 294kHz. Then, in order to build an array with a higher quality factor, seven resonators with 6 turns were fabricated in laboratory using a stranded wire with a cross section of 3.31mm^2, wound around a square wooden substrate of 153x153x29mm. This new array was then operated at a resonant frequency of 147kHz. Finally, regarding the array with stranded-wire resonators, in order to represent a receiver over a given resonator, an additional resistance was added to a given resonator of the array or, alternatively, one of the resonators was placed over the array and used as a receiver.

6 Conclusions

6.1 Discussion of the results

In this thesis a mathematical approach is used in order to obtain an accurate solution of the circuit model of a resonator array used for inductive power transfer.

Assuming that the equivalent impedance of a resonator array is represented by a continued fraction, it is possible, by using the theory of linear homogeneous equations, to obtain the general term of the recursive sequence that represents that same fraction in a closed-form expression, which allows one to quickly determine the value of the equivalent impedance for different characteristics of the system (different electrical parameters, number of resonator arrays and of receivers) and predict its behaviour with the variation of its parameters. Moreover, using the analytical expression obtained, one can study the convergence and the monotonicity of the continued fraction. With this study it is found that the recursive sequence converges to a determinate value, which represents the equivalent impedance of a resonator array with an infinite number of resonators, $\hat{Z}_{eq,\infty}$. By terminating the array with an impedance of this value, the value of the equivalent impedance remains constant for any number of resonators. Furthermore, regarding the monotonicity of the recursive sequence, it is shown that the sequence has an oscillating behaviour depending on whether the array is terminated with an impedance whose value is larger or smaller than $\hat{Z}_{eq,\infty}$. Furthermore, the closed-form expressions for the equivalent impedance developed can be used as a tool for the design of the array, but more specifically for the design of the power source that feeds the array: for a given voltage source, by knowing the equivalent impedance and its possible variations, the power delivered from the source to the array can be calculated and predicted.

Afterwards, a mathematical analysis is made on the inversion of the impedance matrix of the circuit model of the resonator array in order to determine the current in each resonator. By assuming the impedance matrix as a tridiagonal matrix, two cases are considered: the former where all the elements in the main diagonal are equal except for the last one, and the latter where all the elements of the main diagonal are equal except for two elements (the last one and another in any position). In this way, by analytically performing the inversion of a tridiagonal matrix, it is possible to develop the expressions needed to calculate the current in each resonator for several cases: the array terminated in a load, the array with one or two receivers and an IPT system with a source with an internal impedance. Eventually, using the expressions for the currents one can determine the power delivered from the source to the array and the power delivered to a load, or to one or two receivers placed over the array and, consequently, the efficiency of the system. Then, after developing the expressions for the currents, the input power and the power delivered to a load or to a receiver, in order to illustrate the results obtained a few numerical examples are made for the different types of resonator arrays presented. It is found out that, if the array is not terminated with $\hat{Z}_{eq,\infty}$, the absolute values of the currents in two adjacent resonators oscillate, whereas if it

is terminated with $\hat{Z}_{eq,\infty}$, the current absolute value decreases gradually from the first to the last resonator. Additionally, it is observed that the load or the impedance of the receiver at the end of the array that guarantees the maximum power transfer or maximum efficiency changes with the number of resonators of the array tending eventually to a constant value. Likewise, the value of the equivalent impedance of the receiver, $\hat{Z}_d$, that guarantees the maximum power transfer or maximum efficiency in an array terminated with $\hat{Z}_{eq,\infty}$ changes with the position of the receiver but eventually tends to a constant value. Moreover, it is noticed that the power delivered to a load or a receiver for different values of the load or receiver equivalent impedance follows a pattern depending on the parity of the difference between the value of the total number of resonators and the position of the receiver, $N-l$: the curves of the power with odd or even values of $N-l$ have similar shapes. Then, it is demonstrated that the value of the source impedance does not influence the efficiency of the system but, for a voltage source with a constant RMS value, it influences the power delivered to a load or receiver at the end of the array. Besides, by matching the source to the loaded array, the value of the impedance that guarantees the maximum power transfer becomes constant. These theoretical results can help one to achieve a better understanding of how the power transfer occurs in a resonator array, but also can be a powerful tool for the design of a resonator array with given characteristics.

After the mathematical analysis made on the circuit model of a resonator array, an assessment of the magnetic near field generated by an array is carried out, along with its variation with the value of the termination impedance. By performing simulations and measurements, it is observed that the oscillation of the currents in adjacent resonators when the termination impedance is different than $\hat{Z}_{eq,\infty}$ is also reflected on the magnetic field generated. Furthermore, for a constant power delivered to the termination impedance, the peak values of the magnetic flux density determined are larger when the termination impedance is well different than $\hat{Z}_{eq,\infty}$. This means that, by using $\hat{Z}_{eq,\infty}$ as the termination impedance, not only we have smoother variations of the spatial distribution of the magnetic flux density, but also lower peak values of the magnetic flux density.

Finally, it is important to note that the theoretical results obtained with the mathematical approach are verified not only with circuit simulations but also with the experimental setup described in the forth chapter of this thesis. The good match between the theoretical results, simulations and measurements validates the expressions developed and shows a practical applicability of the results on the design of resonator arrays. Also, in the experimental verifications it is shown that the arrays of resonators can transfer higher amounts of power and operate at hundred kHz frequency levels.

6.2 Original contribution

The analytical approach for the solution of the circuit model of a resonator array presented in this thesis is an original contribution to the ongoing research about the utilization of resonator arrays for inductive power transfer, compared to other methods presented in literature (as magnetoinductive wave (MIW) theory or numerical circuit analysis). The results presented in this thesis are in agreement with those obtained with the magnetoinductive wave theory for one receiver over the array. Moreover, this approach allows a broader analysis of these systems, as several different

types of arrays and configurations of array/receiver can be considered (e.g., arrays with even two receivers), electrical parameters or operating conditions. Then, the developed closed-form expressions can be used by designers as calculation tools, as they allow one to save time in comparison with numerical methods or simulations. The expressions can give guidelines to those who want to obtain maximum efficiency or maximum power transfer to a load, or to one or two receivers, for arrays with known electrical parameters. Finally, as the expressions concern the solution of the circuit model and refer to electrical parameters, they can be used for arrays with different types of power source, and different components of the circuit (resonators, capacitors or loads) regarding the materials used for the construction of the resonators.

Furthermore, the analysis presented on the magnetic field generated by a resonator array is an original work, as the studies available in literature about the magnetic field generated by IPT systems refer to two-coil systems.

Ultimately, the experimental setup presented in this work, composed of a power inverter operating at hundred kHz level which supplies a resonator array capable to deliver a power to a load or a receiver up to about 90W, differs from most of the arrays seen in literature, which operate at a few MHz and deliver only a few Watts of power. This shows new possible future applications for IPT systems with arrays of resonators for powering small electronic or domestic devices.

6.3 Future work

There is further work that can be done considering the results presented in this thesis.

Regarding the mathematical analysis of the inversion of the impedance matrix, the cases where the voltage source is not connected to the first resonator, but to any other resonator of the array can also be taken into consideration. Moreover, the pattern of the values of the currents and equivalent impedances observed for odd and even values of the resonator number (or position of the receiver) can be further studied by considering each case individually and analysing the formulas and results for each case.

In addition, the magnetic field generated by a resonator array can be further investigated in the case where there is a real receiver over the array in different positions or in the case that the resonators are placed in a domino configuration.

Then, concerning future experimental work, it has to be remembered that the stranded-wire was chosen as an economic alternative to the Litz wire, which is usually recommended for resonator operating at this low frequency level. Indeed, the utilization of Litz wire would decrease the losses of the system and increase its efficiency and maximum power transferred, also making it possible to use more resonators, keeping the efficiency at the same level as that with stranded wire coils. Finally, using power converters of new technology, capable of operating at higher frequencies (MHz level) can further increase the efficiency, along with the use of ferrite cores for the coils. Moreover, connecting a rectifier to the receiver instead of a resistor, it is possible to study the possible application of a resonator array for battery charging.

Bibliography

[1] G. A. Covic and J. T. Boys, "Inductive power transfer," *Proceedings of the IEEE*, vol. 101, no. 6, pp. 1276–1289, 2013.

[2] S. Li and C. C. Mi, "Wireless power transfer for electric vehicle applications," *IEEE Journal of Emerging and Selected Topics in Power Electronics*, vol. 3, no. 1, pp. 4–17, March 2015.

[3] W. Zhong, C. K. Lee, and S. Y. R. Hui, "General analysis on the use of tesla's resonators in domino forms for wireless power transfer," *IEEE Transactions on Industrial Electronics*, vol. 60, no. 1, pp. 261–270, Jan. 2013.

[4] J. L. Villa, J. Sallan, J. F. S. Osorio, and A. Llombart, "High-misalignment tolerant compensation topology for icpt systems," *IEEE Transactions on Industrial Electronics*, vol. 59, no. 2, pp. 945–951, 2012.

[5] J. Alberto, G. Puccetti, G. Grandi, U. Reggiani, and L. Sandrolini, "Experimental study on the termination impedance effects of a resonator array for inductive power transfer in the hundred kHz range," in *Proc. 2015 IEEE Wireless Power Transfer Conference (WPTC 2015)*, Boulder, CO, USA, May 2015, pp. 1–4.

[6] N. Tesla, "Apparatus for transmitting electrical energy." Dec. 1 1914, uS Patent 1,119,732. [Online]. Available: https://www.google.com/patents/US1119732

[7] ——, "Experiments with alternate currents of very high frequency and their application to methods of artificial illumination," *Transactions of the American Institute of Electrical Engineers*, vol. VIII, no. 1, pp. 266–319, Jan 1891.

[8] R. F. Xue, K. W. Cheng, and M. Je, "High-efficiency wireless power transfer for biomedical implants by optimal resonant load transformation," *IEEE Transactions on Circuits and Systems I: Regular Papers*, vol. 60, no. 4, pp. 867–874, April 2013.

[9] A. Kurs, A. Karalis, R. Moffatt, J. D. Joannopoulos, P. Fisher, and M. Soljačić, "Wireless power transfer via strongly coupled magnetic resonances," *science*, vol. 317, no. 5834, pp. 83–86, 2007.

[10] A. P. Sample, D. A. Meyer, and J. R. Smith, "Analysis, experimental results, and range adaptation of magnetically coupled resonators for wireless power transfer," *IEEE Transactions on Industrial Electronics*, vol. 58, no. 2, pp. 544–554, Feb. 2011.

[11] B. T. Ranum, N. W. D. E. Rahayu, and A. Munir, "Development of wireless power transfer receiver for mobile device charging," in *The 2nd IEEE Conference on Power Engineering and Renewable Energy (ICPERE) 2014*, Dec 2014, pp. 48–51.

[12] S. Y. R. Hui, W. Zhong, and C. K. Lee, "A critical review of recent progress in mid-range wireless power transfer," *IEEE Transactions on Power Electronics*, vol. 29, no. 9, pp. 4500–4511, Sept. 2014.

[13] L. Sun, H. Tang, and Y. Zhang, "Determining the frequency for load-independent output current in three-coil wireless power transfer system," *Energies*, vol. 8, no. 9, p. 9719, 2015. [Online]. Available: http://www.mdpi.com/1996-1073/8/9/9719

[14] G. Puccetti, C. J. Stevens, U. Reggiani, and L. Sandrolini, "Experimental and numerical investigation of termination impedance effects in wireless power transfer via metamaterial," *Energies*, vol. 8, no. 3, pp. 1882–1895, 2015.

[15] X. Zhang, S. L. Ho, and W. N. Fu, "Quantitative design and analysis of relay resonators in wireless power transfer system," *IEEE Transactions on Magnetics*, vol. 48, no. 11, pp. 4026–4029, Nov 2012.

[16] C. J. Stevens, "Magnetoinductive waves and wireless power transfer," *IEEE Transactions on Power Electronics*, vol. 30, no. 11, pp. 6182–6190, Nov. 2015.

[17] S. A. Mirbozorgi, H. Bahrami, M. Sawan, and B. Gosselin, "A smart multicoil inductively coupled array for wireless power transmission," *IEEE Transactions on Industrial Electronics*, vol. 61, no. 11, pp. 6061–6070, Nov 2014.

[18] Z. Liu, Z. Chen, Y. Guo, and Y. Yu, "A novel multi-coil magnetically-coupled resonance array for wireless power transfer system," in *2016 IEEE Wireless Power Transfer Conference (WPTC)*, May 2016, pp. 1–3.

[19] C. J. Stevens, "A magneto-inductive wave wireless power transfer device," *Wireless Power Transfer*, vol. 2, no. 01, pp. 51–59, 2015.

[20] B. Wang, W. Yerazunis, and K. H. Teo, "Wireless power transfer: Metamaterials and array of coupled resonators," *Proceedings of the IEEE*, vol. 101, no. 6, pp. 1359–1368, June 2013.

[21] E. Shamonina, V. A. Kalinin, K. H. Ringhofer, and L. Solymar, "Magnetoinductive waves in one, two, and three dimensions," *Journal of Applied Physics*, vol. 92, no. 10, pp. 6252–6261, 2002. [Online]. Available: http://scitation.aip.org/content/aip/journal/jap/92/10/10.1063/1.1510945

[22] Y. Zhang, Z. Zhao, and K. Chen, "Frequency-splitting analysis of four-coil resonant wireless power transfer," *IEEE Transactions on Industry Applications*, vol. 50, no. 4, pp. 2436–2445, July 2014.

[23] L. Solymar and E. Shamonina, *Waves in Metamaterials*. OUP Oxford, 2009.

[24] C. D. Olds, A. Rockett, and P. Szusze, *Continued fractions*. Mathematical Association of America (MAA), 1992.

[25] J. Beato-Lopez, C. de la Cruz Blas, A. Mitra, and C. Gomez-Polo, "Electrical model of giant magnetoimpedance sensors based on continued fractions," *Sensors and Actuators A: Physical*, vol. 242, pp. 73 – 78, 2016.

[26] Z. Gong, Z. Tang, S. Mukamel, J. Cao, and J. Wu, "A continued fraction resummation form of bath relaxation effect in the spin-boson model," *The Journal of chemical physics*, vol. 142, no. 8, p. 084103, 2015.

[27] G. Puccetti, U. Reggiani, and L. Sandrolini, "Experimental analysis of wireless power transmission with spiral resonators," *Energies*, vol. 6, no. 11, pp. 5887–5896, 2013.

[28] S. Elaydi, *An introduction to difference equations*. Springer Science & Business Media, 2005.

[29] J. Alberto, L. Sandrolini, and U. Reggiani, "Circuit model of a resonator array for a WPT system by means of a continued fraction," in *2016 IEEE 2nd International Forum on Research and Technologies for Society and Industry Leveraging a better tomorrow (RTSI) (IEEE RTSI 2016)*, Bologna, Italy, Sep. 2016, pp. 38–43.

[30] C.-S. Wang, O. H. Stielau, and G. A. Covic, "Design considerations for a contactless electric vehicle battery charger," *IEEE Transactions on Industrial Electronics*, vol. 52, no. 5, pp. 1308–1314, Oct 2005.

[31] J. L. Villa, J. Sallán, A. Llombart, and J. F. Sanz, "Design of a high frequency inductively coupled power transfer system for electric vehicle battery charge," *Applied Energy*, vol. 86, no. 3, pp. 355 – 363, 2009.

[32] M. K. Kazimierczuk, "Class d voltage-switching mosfet power amplifier," in *IEE Proceedings B-Electric Power Applications*, vol. 138, no. 6. IET, 1991, pp. 285–296.

[33] C. d. Fonseca and J. Petronilho, "Explicit inverse of a tridiagonal k- toeplitz matrix," *Numerische Mathematik*, vol. 100, no. 3, pp. 457–482, 2005. [Online]. Available: http://dx.doi.org/10.1007/s00211-005-0596-3

[34] C. da Fonseca and J. Petronilho, "Explicit inverses of some tridiagonal matrices," *Linear Algebra and its Applications*, vol. 325, no. 1, pp. 7 – 21, 2001. [Online]. Available: http://www.sciencedirect.com/science/article/pii/S0024379500002895

[35] F. R. Gantmakher, *The theory of matrices*. American Mathematical Soc., 1998, vol. 131.

[36] H. Qi, W. Chen, Y. Sha, Y. Han, H. Li, and X. Yang, "A study of electromagnetic emission from two-coil wpt system using resonant magnetic field coupling," in *2016 Asia-Pacific International Symposium on Electromagnetic Compatibility (APEMC)*, vol. 01, May 2016, pp. 484–487.

[37] Q. Zhu, Y. Zhang, C. Liao, Y. Guo, L. Wang, and L. WANG, "Null-coupled electromagnetic field cancelling coil for wireless power transfer system," *IEEE Transactions on Transportation Electrification*, vol. PP, no. 99, pp. 1–1, 2016.

[38] W.-G. Kang, H.-Y. Jun, Y.-H. Park, and J.-K. Pack, "Investigation of the assessment method for human exposure from a wireless power transfer system," in *2013 Asia-Pacific Microwave Conference Proceedings (APMC)*, Seoul, South Korea, Nov. 5-8 2013, pp. 836–838.

[39] X. L. Chen, A. Umenei, D. Baarman, N. Chavannes, V. De Santis, J. Mosig, and N. Kuster, "Human exposure to close-range resonant wireless power transfer systems as a function of design parameters," *IEEE Transactions on Electromagnetic Compatibility*, vol. 56, no. 5, pp. 1027–1034, Oct. 2014.

[40] H. Kim, C. Song, J. Kim, D. Jung, E. Song, S. Kim, and J. Kim, "Design of magnetic shielding for reduction of magnetic near field from wireless power transfer system for electric vehicle," in *Proc. 2014 International Symposium on Electromagnetic Compatibility (EMC Europe)*, Sept 2014, pp. 53–58.

[41] H. Kim, C. Song, D. H. Kim, D. H. Jung, I. M. Kim, Y. I. Kim, J. Kim, S. Ahn, and J. Kim, "Coil design and measurements of automotive magnetic resonant wireless charging system for high-efficiency and low magnetic field leakage," *IEEE Transactions on Microwave Theory and Techniques*, vol. 64, no. 2, pp. 383–400, Feb 2016.

[42] "Ieee standard for safety levels with respect to human exposure to radio frequency electromagnetic fields, 3 khz to 300 ghz," *IEEE Std C95.1-2005 (Revision of IEEE Std C95.1-1991)*, pp. 1–238, April 2006.

[43] I. C. on Non-Ionizing Radiation Protection *et al.*, "Guidelines for limiting exposure to time-varying electric and magnetic fields (1 hz to 100 khz)," *Health Physics*, vol. 99, no. 6, pp. 818–836, 2010.

[44] W. X. Zhong, C. K. Lee, and S. Y. Hui, "Wireless power domino-resonator systems with noncoaxial axes and circular structures," *IEEE Transactions on Power Electronics*, vol. 27, no. 11, pp. 4750–4762, Nov 2012.

[45] J. Alberto, L. Sandrolini, and U. Reggiani, "Magnetic near field from an inductive power transfer system using an array of coupled resonators," in *Proc. 2016 Asia-Pacific International Symposium on Electromagnetic Compatibility (APEMC 2016)*, Shenzhen, China, May 2016.

[46] E. M. Thomas, J. D. Heebl, C. Pfeiffer, and A. Grbic, "A power link study of wireless non-radiative power transfer systems using resonant shielded loops," *IEEE Transactions on Circuits and Systems I: Regular Papers*, vol. 59, no. 9, pp. 2125–2136, Sept. 2012.

[47] D. J. Thrimawithana and U. K. Madawala, "A generalized steady-state model for bidirectional ipt systems," *IEEE Transactions on Power Electronics*, vol. 28, no. 10, pp. 4681–4689, Oct 2013.

[48] G. D. Capua, N. Femia, G. Petrone, G. Lisi, D. Du, and R. Subramonian, "Power and efficiency analysis of high-frequency wireless power transfer systems," *International Journal of Electrical Power & Energy Systems*, vol. 84, pp. 124 – 134, 2017. [Online]. Available: http://www.sciencedirect.com/science/article/pii/S014206151630062X

[49] T. Nagashima, X. Wei, E. Bou, E. Alarcón, M. K. Kazimierczuk, and H. Sekiya, "Analysis and design of loosely inductive coupled wireless power transfer system based on class-E^2

dc-dc converter for efficiency enhancement," *IEEE Transactions on Circuits and Systems I: Regular Papers*, vol. 62, no. 11, pp. 2781–2791, Nov. 2015.

[50] A. Ruehli, "Inductance calculations in a complex integrated circuit environment," *IBM Journal of Research and Development*, vol. 16, no. 5, pp. 470–481, Sept 1972.

[51] C. Paul, *Inductance: Loop and Partial*. Wiley, 2010.

[52] D. C. Meeker, "Finite Element Method Magnetics," http://www.femm.info, version 4.2 (09Nov2010 Build).

[53] C. Sonntag, E. Lomonova, and J. Duarte, "Implementation of the neumann formula for calculating the mutual inductance between planar pcb inductors," in *18th International Conference on Electrical Machines, 2008. ICEM 2008.* IEEE, 2008, pp. 1–6.

[54] F. W. Grover, *Inductance calculations: working formulas and tables*. Courier Corporation, 2004.